

Defining the functional role of microRNA-128-3p in neurons as it pertains to prion disease

by

AMRIT SINGH BOESE

A Thesis submitted to the Faculty of Graduate Studies of

The University of Manitoba

in partial fulfilment of the requirements of the degree of

DOCTOR OF PHILOSOPHY

Department of Medical Microbiology and Infectious Diseases

Max Rady College of Medicine, Rady Faculty of Health Sciences

University of Manitoba

Winnipeg, Manitoba

Copyright © 2017 by Amrit Singh Boese

Abstract

Central Nervous System neurodegenerative diseases include prion, Alzheimer's, Huntington's, and Parkinson's, all characterized by accumulating aggregates of misfolded host protein. With disease progression, neuronal degeneration results in cognitive and physical symptoms leading to fatality. There are no cures for these diseases. In the brains of patients and animal models, changes in miR-128-3p levels have been described in the literature albeit at terminal disease in a mixed cell population. I hypothesized that miR-128-3p is altered in neurons at early stages of prion induced neurodegeneration, when synaptic dysfunction is commencing, and that miR-128-3p regulates gene targets vital to synaptic function. To determine this, miR-128-3p was detected in the CA1 of the hippocampus, a neuronal subpopulation affected by misfolded prions, during a timecourse of RML scrapie infection in mice. CA1 neuronal cell bodies were isolated using laser capture microdissection and miR-128-3p levels were determined using RT-qPCR. Subsequently, the 3' UTR targets for miR-128-3p were predicted using the TargetScan Human algorithm and a few with prion disease relevance were validated using Luciferase Reporter assays. Next, miR-128-3p levels were determined by RT-qPCR of RNA from synaptoneurosome fractions isolated from the hippocampi and forebrains of RML scrapie prion infected mice and mock infected controls at an early and late stage of disease. As a number of miR-128-3p targets were glutamate receptor subunits, which are found in synapses and integral to their function, the role of miR-128-3p in glutamate signaling pathways was explored. Hippocampal neurons were cultured from embryonic CD1 mice and used as a model to induce glutamate signaling and miR-128-3p response was quantified by RT-qPCR. Lastly, miR-128-3p gain of and loss of function experiments were performed in cultured hippocampal neurons to delineate global proteome changes using mass spectrometry. Results show that miR-128-3p had a trend towards deregulation

in the CA1 throughout prion infection and was increased in hippocampal synapses during early disease. The validated gene targets included *GRM5*, *GRIN2B*, and *GRIN2D*. Prolonged synaptic glutamate signaling and toxic levels of glutamate reduced miR-128-3p levels in hippocampal neurons. No changes to glutamate receptor proteins were detected in miR-128-3p gain of function experiments. However, three proteins were downregulated significantly, *SLIT3*, *KCC2A*, and *SF3A3*. This is the first neuronal report of miR-128-3p alterations during early neurodegeneration in an animal model. It provides the basis for future work into therapeutic modulation of miR-128-3p in a region within which the reversal of synapse loss restored cognitive ability in prion infected mice.

Acknowledgements

First of all, I would like to thank my advisor, Dr. Stephanie Booth, who has provided me with unyielding support over the years, without which the completion of my PhD would not have been possible. She has shown a kindness and depth that will never be forgotten, and is a role model for women in STEM. My cherished memories will always be the PrioNet conference in Vancouver in 2010 and the adventures of the fleece jacket, such good laughs were had. I would also like to acknowledge my thesis committee of Dr. Chris Anderson, Dr. Yvonne Myal, and Dr. Joanne Embree who have all provided support and guidance during my long journey. In addition, Dr. Archie McNicol was a friendly face during my time on the Health Sciences Graduate Students Association and his presence is sorely missed. I also appreciated the help from Angela Nelson and Sharon Tardi who provided me with many administrative answers.

This work would not have been possible without the help of others. For Chapter 1, the animal work and histology were performed by Sarah Medina, Kathy Frost, and Yulian Niu. The LCM and RNA work was performed by Dr. Anna Majer, Sarah Medina, and Kathy Manguiat while I performed the RT-qPCR analysis. Kathy Manguiat also provided technical support on some of the gene expression assays in other chapters. I would like to thank Aileen Patterson for conducting the *GRM5* luciferase assay. For the synaptoneurosome work, it was a group effort with the conceptualization by Dr. Reuben Saba with Kristyn Burak performing the TaqMan validations. I would like to thank Dr. Patrick Chong and Stuart McCorrister from the Proteomics core at the National Microbiology Laboratory for help with mass spectrometry. The members of the Booth lab provided support in many forms and include Bernard Abrenica, Deborah Sorensen, Clark Philipson, and Rhiannon Huzarewich.

I cannot forget to thank those that were in the rat race with me, fellow graduate students Kristyn Burak, Kyle Caligiuri, Shantel Gushue, Dr. Michael Stobart, Melissa Rabb, Andrew McDermid, Kamilla Gale, and Dr. Jessica Forbes. Dr. Anna Majer provided a lot of social support with our Parlour coffee breaks that helped me through some very difficult times. I will never forget all our ‘laugh at our pain’ jokes a la Seinfeld and the political talk! It was a significant friendship that I hope lasts for a long time beyond graduate school.

For funding, I would like to thank Research Manitoba for a PhD studentship and the University of Manitoba for selecting me for the McCrorie-West Family Fellowship. For travel awards, I am grateful to the Faculty of Graduate Studies at the University of Manitoba, and the now defunct but so useful, PrioNet Canada, for funding to attend conferences. Finally, the funds I received through various presentation awards were encouraging, from Manitoba Neuroscience Network, Manitoba Medical Service Foundation, Public Health Agency of Canada, and PrioNet Canada.

I found a lot of thesis writing support online, particularly for time management from Dr. Hugh Kearns from the @ithinkwellHugh twitter handle, which helped enormously as well as @PhDForum for thesis writing sympathy, and @SUWTNA which provided a much needed kick to start off the writing process. In addition, Dr. Kathryn Ritchot provided me with support during thesis writing, I could not have achieved this goal without her help.

The most important acknowledgement is saved for last, my beautiful family. Firstly, my husband, Darren Boese, whose endless support is the main reason I completed my PhD. I think out of the both of us he may be the one most glad I am done my thesis! Not only the social support and printing so many draft copies of my thesis but in taking care of our two amazing boys, Tristan and Oliver. Tristan is particularly excited for mom to be done typing ‘so many words’, and Oliver

who could care less but loves to smash the keyboard when I'm trying to work! I cannot go without thanking the village that helped with our children throughout my studies including Grandma and Grandpa Boese, Auntie Krista, Simi Chib, and the numerous daycare providers. At the end of this doctoral journey, which I liken to the metamorphosis and perhaps migration of a Monarch butterfly, *Danaus plexippus*, I cannot wait to emerge a butterfly, spread my wings and fly!!!

Dedication

This thesis is dedicated to my parents, *Paramjeet Kaur Singh* and *Kuldip Singh*.

*I am grateful for the opportunities that you have bestowed upon me
and dad, I miss you every single day.*

Table of Contents

| | |
|---|-------------|
| Abstract..... | II |
| Acknowledgements | IV |
| Dedication | VII |
| Table of Contents | VIII |
| List of Tables | XV |
| List of Figures..... | XVII |
| List of Copyrighted Material for which Permission was Obtained | XXII |
| Abbreviations | XXIV |
| 1. Introduction..... | 1 |
| 1.1 Neurodegenerative diseases..... | 1 |
| 1.2 Prion diseases | 3 |
| 1.2.1 Prion strains | 3 |
| 1.2.2 Prion diseases in animals | 4 |
| 1.2.3 Human Prion diseases | 5 |
| 1.3 Related proteinopathies..... | 13 |
| 1.4 Characteristics and Functions of PrP^C | 16 |
| 1.4.1 Metal Ion Homeostasis | 19 |
| 1.4.2 Glutamate Receptors..... | 21 |
| 1.4.3 Other PrP ^C functions..... | 23 |
| 1.5 PrP^{Sc} | 23 |

| | | |
|-------------|--|-----------|
| 1.6 | PrP^C to PrP^{Sc} conversion, propagation, and accumulation | 26 |
| 1.7 | Mouse model of RML scrapie prion disease..... | 28 |
| 1.8 | The involvement of glutamate receptors in neurodegenerative disease | 29 |
| 1.9 | microRNAs and their role in neurodegenerative disease | 33 |
| 1.9.1 | miR-128-3p..... | 35 |
| 1.9.2 | miR-128-3p role in Central Nervous System..... | 35 |
| 1.9.3 | miR-128-3p involvement in CNS neurodegenerative disease | 38 |
| 1.10 | Use of Laser Capture Microdissection as a means of isolating neuron specific miR-128-3p deregulation <i>in vivo</i> | 41 |
| 1.11 | miR Target prediction and validation..... | 42 |
| 1.12 | Synaptic Loss and miR detection in Prion Disease | 45 |
| 1.13 | Protein target determination strategies | 49 |
| 2. | Hypothesis and Objectives | 54 |
| 2.1 | Overall Hypothesis..... | 54 |
| 2.2 | Objectives..... | 54 |
| 3. | Methods..... | 55 |
| 3.1 | Ethics statement | 55 |
| 3.2 | RML scrapie Mouse Model..... | 55 |
| 3.3 | LCM mediated isolation of neuronal cell bodies from the CA1 region of the hippocampus and total RNA extraction | 56 |
| 3.4 | Immunohistochemistry of brain sections for PrP ^{Sc} and anti-Ionized calcium binding adaptor molecule 1..... | 57 |

| | | |
|-------------|--|-----------|
| 3.5 | Immunofluorescence of brain sections with Fluoro-Jade C and for Glial Fibrillary Acidic Protein | 58 |
| 3.6 | RT-qPCR with miR TaqMan probe assays..... | 59 |
| 3.7 | Fold change determination using the delta delta Ct method | 60 |
| 3.8 | <i>In silico</i> prediction of miR-128-3p targets | 60 |
| 3.9 | Experimental Validation of 3` UTR targets using Luciferase Reporter Assay..... | 61 |
| 3.9.1 | Luciferase reporter plasmid constructs | 61 |
| 3.9.2 | 3` UTR plasmid stock preparation | 61 |
| 3.9.3 | 3` UTR Sequence confirmation | 62 |
| 3.9.4 | Luciferase Reporter Assay | 63 |
| 3.9.5 | Luciferase Data analysis | 64 |
| 3.10 | Synaptoneurosome experiments | 64 |
| 3.10.1 | Synaptoneurosome isolation | 64 |
| 3.10.2 | Total RNA and protein extraction from Synaptoneurosomes..... | 67 |
| 3.10.3 | Electron Microscopy of Synaptoneurosomes | 68 |
| 3.10.4 | Western Blot analysis | 69 |
| 3.10.5 | miR Microarray Analysis of Synaptoneurosome derived RNA | 70 |
| 3.10.6 | RT-qPCR using miR PCR Array Rodent Panel I | 70 |
| 3.10.7 | Protein Preparation for Mass spectrometry..... | 71 |
| 3.10.8 | RT-qPCR with the TaqMan Gene Expression Assay for mRNA detection | 74 |
| 3.11 | Primary Hippocampal Experiments | 76 |
| 3.11.1 | Cultured mouse primary hippocampal neurons: dissection, culture, and maintenance | 76 |

| | | |
|-------------|--|------------|
| 3.11.2 | Immunostaining of primary neuronal cells | 78 |
| 3.11.3 | Total RNA extraction from primary cell cultures | 79 |
| 3.11.4 | RT-qPCR with Locked Nucleic Acid primers for miR detection..... | 80 |
| 3.11.5 | RT-qPCR for TaqMan gene expression assays | 81 |
| 3.11.6 | Action potential bursting experiment using 4-aminopyridine and (+)-bicuculline ... | 81 |
| 3.11.7 | Induction of glutamate excitotoxicity | 82 |
| 3.12 | Gain of function and Loss of function experiments | 82 |
| 3.12.1 | Lipofectamine 2000 transfection of pre-miRs or anti-miRs | 82 |
| 3.12.2 | Global proteome detection of miR-128-3p gain of function in primary hippocampal neurons | 83 |
| 3.12.3 | TMT Labeling of proteins for Mass spectrometry..... | 84 |
| 3.12.4 | Peptide Fractionation | 85 |
| 3.12.5 | Mass spectrometry | 85 |
| 3.12.6 | Global proteome data processing and analysis | 86 |
| 4. | Results | 88 |
| 4.1 | miR-128-3p is temporally dysregulated in neurons of prion infected mice..... | 88 |
| 4.1.1 | Rationale | 88 |
| 4.1.2 | Hypothesis..... | 98 |
| 4.1.3 | miR-128-3p is increased during preclinical disease in micro-dissected neuronal cell bodies from the CA1 region of the hippocampus | 98 |
| 4.2 | Bioinformatic prediction of miR-128-3p targets | 104 |
| 4.2.1 | Rationale | 104 |
| 4.2.2 | Hypothesis..... | 104 |

| | | |
|------------|---|------------|
| 4.2.3 | TargetScan predicted 3` UTR sites for miR-128-3p seed sequence binding..... | 104 |
| 4.2.4 | Selection of genes for glutamate receptors NMDAR and mGluR5 as targets for further validation | 113 |
| 4.2.5 | Luciferase Reporter Assays confirms miR-128-3p binding to 3` UTR of <i>GRIN2B</i> , <i>GRIN2D</i> , and <i>GRM5</i> | 116 |
| 4.3 | Enrichment of miR-128-3p within the synaptoneuroosomes prepared from forebrain and hippocampus | 123 |
| 4.3.1 | Rationale | 123 |
| 4.3.2 | Hypothesis..... | 123 |
| 4.3.3 | Validation of isolated synaptoneuroosomes reveals synaptoneurosome defining features | 124 |
| 4.3.4 | Synaptoneuroosomes in RML scrapie prion infected forebrain and hippocampus are not contaminated with astrocytes..... | 128 |
| 4.3.5 | miRs were detected in synaptoneuroosomes from RML scrapie prion infected samples by PCR Arrays | 132 |
| 4.3.6 | Hippocampal synaptoneurosome miR levels are changed during early stages of RML scrapie prion infection | 135 |
| 4.3.7 | Forebrain synaptoneuroosomes demonstrate a temporal profile during RML scrapie prion infection..... | 140 |
| 4.3.8 | The synaptoneurosome proteome contains predicted miR-128-3p targets..... | 145 |
| 4.3.9 | NMDAR and mGluR5 mRNA transcripts are present at the synapse | 151 |
| 4.4 | miR-128-3p is involved in excitotoxic glutamate signaling in hippocampal neurons | 155 |

| | | |
|------------|--|------------|
| 4.4.1 | Rationale | 155 |
| 4.4.2 | Hypothesis..... | 156 |
| 4.4.3 | Establishment of Primary Hippocampal Neuron Culture | 156 |
| 4.4.4 | Expression of <i>GRIN2B</i> , <i>GRIN2D</i> , and <i>GRM5</i> genes increases during the maturation and growth of primary hippocampal neurons | 159 |
| 4.4.5 | The expression of miR-128-3p increases as murine hippocampal neurons mature in culture | 161 |
| 4.4.6 | Action potential bursting model in cultured hippocampal neurons elicits the downregulation of miR-128-3p and related mRNA transcripts during chronic activation..... | 163 |
| 4.4.7 | Chronic excitotoxic levels of glutamate lead to a reduction in miR-128-3p in primary hippocampal neurons | 169 |
| 4.5 | A proteomics approach to determine novel miR-128-3p targets..... | 176 |
| 4.5.1 | Rationale | 176 |
| 4.5.2 | Hypothesis..... | 176 |
| 4.5.3 | Increasing miR-128-3p levels in primary hippocampal neurons decreases <i>GRM5</i> and <i>GRIN2D</i> levels | 177 |
| 4.5.4 | The knockdown of miR-128-3p does not change <i>GRIN2B</i> or <i>GRIN2D</i> levels in primary hippocampal neurons | 179 |
| 4.5.5 | Mass spectrometry of cultured hippocampal neurons detects many proteins..... | 179 |
| 4.5.6 | Slit homolog 3 protein was downregulated when miR-128-3p was increased in primary hippocampal neurons | 187 |
| 5. | Discussion..... | 195 |

| | | |
|------|--|-----|
| 5.1 | Summary..... | 195 |
| 5.2 | RML scrapie prion mouse model | 197 |
| 5.3 | CA1 profile of miR-128-3p | 198 |
| 5.4 | Targets of miR-128-3p found through computational biology | 204 |
| 5.5 | Validation of glutamate receptor subunit genes as miR-128-3p targets | 206 |
| 5.6 | Synaptoneurosome profiling of miRs in RML scrapie | 210 |
| 5.7 | Primary hippocampal culture..... | 216 |
| 5.8 | Glutamate signaling relationship to miR-128-3p..... | 218 |
| 5.9 | Increased levels and knockdown of miR-128-3p in primary hippocampal neurons 221 | |
| 5.10 | Protein targets of miR-128-3p..... | 224 |
| 6. | Conclusions..... | 231 |
| 7. | Future Directions | 233 |
| 8. | Appendices..... | 237 |
| | Appendix 1. pMirTarget plasmid map. | 237 |
| | Appendix 2. pmirGLO plasmid map. | 238 |
| | Appendix 3. Copyright permissions | 239 |
| 9. | References | 246 |

List of Tables

| | |
|--|-----|
| Table 1. The proteins involved in a select subset of CNS neurodegenerative diseases. | 2 |
| Table 2. Human Prion disease types and nomenclature..... | 7 |
| Table 3. A select list of functions attributed to PrP ^C in neurons. | 20 |
| Table 4. Characteristics of PrP ^C and PrP ^{Sc} | 24 |
| Table 5. Specifics for miR-128-3p deregulation in the CNS neurodegenerative conditions..... | 39 |
| Table 6. The TargetScan predicted targets for miR-128-3p in Human and Mouse..... | 107 |
| Table 7. Top 32 miR-128-3p TargetScan predicted 3` UTR targets in common between human and mouse..... | 111 |
| Table 8. Glutamate receptor subunit 3` UTR target sites assessed by TargetScan..... | 115 |
| Table 9. The 3` UTR sequences inserted in the Luciferase reporter plasmid..... | 117 |
| Table 10. Summary of treatments for each Luciferase Reporter Assay performed..... | 119 |
| Table 11. 29 miRs that were detected through microarray analysis at the synaptoneurosome compartment of adult wild-type CD1 mice in common with rats..... | 126 |
| Table 12. Total number of mice used to isolate synaptoneuroosomes at asymptomatic (105 dpi) and late, symptomatic (165 dpi) stages of infection..... | 131 |
| Table 13. The miRs detected in hippocampal synaptoneuroosomes at the early timepoint of RML scrapie prion infection in mice that were increased or decreased by ≥ 2 fold..... | 138 |
| Table 14. The miRs at early stages of RML scrapie prion infection that were increased ≥ 2 fold in forebrain synaptoneuroosomes..... | 143 |
| Table 15. The miRs that were increased or decreased ≥ 2 fold at late stages of RML scrapie prion infection in forebrain synaptoneuroosomes..... | 144 |

| | |
|--|-----|
| Table 16. Synaptic neuronal proteins detected by mass spectrometry in the wild-type CD1 derived forebrain synaptoneurosomes..... | 148 |
| Table 17. Synaptic proteins derived from wild-type mouse forebrain whose genes contain TargetScan predicted 3` UTR binding sites for miR-128-3p..... | 152 |
| Table 18. The concentrations and volumes used to TMT label each protein sample from the miR-128-3p proteomic experiment in primary hippocampal neurons..... | 183 |
| Table 19. A select list of neuronal proteins found in the miR-128-3p gain of function protein lysates from primary hippocampal neurons as detected by mass spectrometry..... | 188 |

List of Figures

| | |
|--|-----|
| Figure 1. The domain organization and tertiary protein structure of PrP ^C | 17 |
| Figure 2. The recruitment and propagation of PrP ^{Sc} from the normal host cellular PrP ^C | 27 |
| Figure 3. The synaptic response to glutamate in neurons..... | 31 |
| Figure 4. The production of miR from transcription to processing and mode of action. | 34 |
| Figure 5. Mature and Primary microRNA-128-3p sequences..... | 36 |
| Figure 6. The Luciferase Reporter Assay for miR binding to 3` UTR..... | 46 |
| Figure 7. The neuronal synapse contains miRs, mRNA, RISC complex proteins, ribosomes, and protein..... | 48 |
| Figure 8. Flow chart for synaptoneurosomes preparation..... | 66 |
| Figure 9. Detection of PrP ^{Sc} in the hypothalamus of RML scrapie prion infected mice. | 90 |
| Figure 10. Detection of PrP ^{Sc} in the thalamus of RML scrapie prion infected mice. | 91 |
| Figure 11. Detection of PrP ^{Sc} in the forebrain of RML scrapie prion infected mice. | 92 |
| Figure 12. Detection of PrP ^{Sc} in the hippocampus of RML scrapie prion infected mice. | 93 |
| Figure 13. Fluoro-Jade C staining of coronal hippocampal sections from mock infected and RML scrapie prion infected mice to detect neurodegeneration..... | 94 |
| Figure 14. Detection of astrocytes within the CA1 region of the hippocampus in coronal brain sections from RML scrapie prion infected mice..... | 96 |
| Figure 15. Detection of microglia in the CA1 region using immunohistochemistry during RML scrapie prion infection in mice..... | 97 |
| Figure 16. Capture of the CA1 neuronal cell bodies using LCM technology..... | 99 |
| Figure 17. RNA integrity determination of total RNA from LCM captured CA1 neuronal cell bodies..... | 100 |

| | |
|---|-----|
| Figure 18. Fold change in mature miR-128-3p from total RNA derived from <i>CA1</i> neuronal cell bodies from mock and RML scrapie prion infected mice during disease time course. | 101 |
| Figure 19. Microarray analysis of gene expression from total RNA derived from <i>CA1</i> neuronal cell bodies from 70 dpi to endpoint (end) in RML scrapie prion infected mice. | 103 |
| Figure 20. Screen capture of TargetScan settings used for analysis. | 106 |
| Figure 21. Comparison of miR-128-3p TargetScan predicted mouse and human 3' UTR targets. | 108 |
| Figure 22. Comparison of miR-128-3p TargetScan predicted mouse and human 3' UTR targets to forebrain CAMK2 α neuron derived 3' UTR targets. | 110 |
| Figure 23. Fold change in <i>GRIN2B</i> and <i>PRNP</i> genes in total RNA derived from <i>CA1</i> neuronal cell bodies during RML scrapie prion infection in mice. | 114 |
| Figure 24. Flow chart for Luciferase reporter assay data analysis. | 120 |
| Figure 25. Luciferase Reporter Assay results for the binding of miR-128-3p to the human <i>GRIN2B</i> , <i>GRIN2D</i> , and <i>GRM5</i> 3' UTRs. | 121 |
| Figure 26. Electron Microscope images of three distinct layers isolated from the discontinuous Ficoll gradient including the synaptoneurosome layer. | 125 |
| Figure 27. Western blot of different stages of the forebrain synaptoneurosome isolation. | 129 |
| Figure 28. Overview of the RML scrapie prion infected CD1 mouse experiments from which synaptoneurosomes were isolated. | 130 |
| Figure 29. Western blot of synaptoneurosomes generated from mock and RML scrapie prion infected mice. | 133 |
| Figure 30. A representative RIN determination of total RNA extracted from synaptoneurosomes using the Pico 6000 chip on the 2100 Bioanalyzer. | 134 |

| | |
|---|-----|
| Figure 31. miRs detected in total RNA derived from hippocampal mock infected synaptoneuroosomes at 105 dpi with a threshold of Ct < 25 using miR PCR Arrays... | 136 |
| Figure 32. Changes in abundance of mature miR-128-3p in total RNA derived from hippocampal synaptoneuroosomes at 105 dpi in mock infected and RML scrapie prion infected mice..... | 137 |
| Figure 33. Examination of miR-128-3p in total RNA derived from forebrain synaptoneuroosomes during early (105 dpi) and late (165 dpi) RML scrapie prion infection in mice..... | 141 |
| Figure 34. Synaptoneuroosomes derived from prion infected forebrain exhibited temporal alterations in miR levels..... | 142 |
| Figure 35. Synaptic proteins identified in total protein isolated from forebrain synaptoneuroosomes of wild-type CD1 mice by mass spectrometry..... | 147 |
| Figure 36. Synaptic forebrain proteins compared to TargetScan predicted miR-128-3p 3' UTR mouse targets..... | 150 |
| Figure 37. mRNA transcripts present in the total RNA derived from hippocampal synaptoneuroosomes during early stages of RML scrapie prion infection in mice..... | 154 |
| Figure 38. Immunostaining of primary hippocampal neurons from E18-20 mice at 5, 8, 10, and 12 days <i>in vitro</i> (DIV)..... | 158 |
| Figure 39. Relative expression of <i>GAPDH</i> , <i>GRIN2B</i> , <i>GRIN2D</i> , <i>GRM5</i> , and <i>GFAP</i> mRNA captured using RT-qPCR on total RNA isolated from cultured primary hippocampal neurons from 1 to 12 days <i>in vitro</i> (DIV)..... | 160 |
| Figure 40. Relative expression of small RNAs detected in total RNA from cultured primary hippocampal neurons from 1-12 days <i>in vitro</i> (DIV) using RT-qPCR..... | 162 |

| | |
|--|-----|
| Figure 41. The action potential bursting paradigm using 4-aminopyridine (4-AP) and (+)-bicuculline (+-B) in primary hippocampal neurons..... | 164 |
| Figure 42. Assessment of mRNA induction of <i>ARC</i> and <i>HOMER1</i> after action potential bursting in primary hippocampal neurons..... | 166 |
| Figure 43. Detection of mature miR-128-3p in total RNA by RT-qPCR after action potential bursting in primary hippocampal neurons..... | 168 |
| Figure 44. Fold change in <i>GRIN2B</i> , <i>GRIN2D</i> , and <i>GRM5</i> mRNA in total RNA using RT-qPCR after action potential bursting in primary hippocampal neurons..... | 170 |
| Figure 45. Relative expression of <i>GAPDH</i> , <i>ARC</i> , <i>GRIN2A</i> , <i>GRIN2B</i> , and <i>GRIN2D</i> mRNA in total RNA from primary hippocampal neurons after excitotoxic levels of 100 μ M glutamate were bath applied, determined by RT-qPCR..... | 172 |
| Figure 46. Change in miR-128-3p levels in total RNA derived from primary hippocampal neurons exposed to excitotoxic levels of glutamate..... | 173 |
| Figure 47. Determination of miR-128-3p and gene target levels using RT-qPCR on total RNA derived from primary hippocampal neurons in the miR-128-3p gain of function experiment. | 178 |
| Figure 48. Levels of miR-128-3p and gene targets in total RNA derived from primary hippocampal neurons using RT-qPCR after knockdown with anti-miR-128-3p..... | 180 |
| Figure 49. Overview of methods used to obtain global proteome profiles of miR-128-3p gain of function experiments in primary hippocampal neurons using mass spectrometry with TMT labels..... | 182 |
| Figure 50. Protein profile of primary hippocampal neurons from miR-128-3p gain of function experiments..... | 185 |

| | |
|---|-----|
| Figure 51. Pathways identified in the proteins derived from primary hippocampal neurons from the miR-128-3p gain of function experiments..... | 186 |
| Figure 52. Identification of proteins that were significantly different in primary hippocampal neurons in miR-128-3p gain of function experiments..... | 193 |
| Figure 53. Protein levels of NMDAR2B and mGluR5 were unaltered in primary hippocampal neurons in miR-128-3p gain of function experiments..... | 194 |
| Figure 54. Diagram depicting change in the levels of miR-128-3p in CA1 neurons over the time course of RML scrapie prion infection in mice..... | 199 |
| Figure 55. The proposed relationship between miR-128-3p, NMDARs, mGluR5, and PrP ^C at early stages of prion infection..... | 209 |
| Figure 56. The relationship between miR-128-3p and glutamate/NMDAR signaling as discovered through the experimentation performed in cultured hippocampal neurons..... | 222 |
| Figure 57. The string interaction network of post NMDAR activation events..... | 229 |

List of Copyrighted Material for which Permission was Obtained

All copyright permissions can be found in Appendix 3.

The following figures were obtained or adapted from the doctoral thesis of Dr. Anna Majer, “Temporal Deregulation of Genes and MicroRNAs in Neurons during Prion-Induced Neurodegeneration”. 2015.

Figure 9. Detection of PrP^{Sc} in the hypothalamus of RML scrapie prion infected mice.

Figure 10. PrP^{Sc} detection in the Thalamus of RML scrapie prion infected mice. PrP^{Sc}

Figure 11. PrP^{Sc} detection in the forebrain of RML scrapie prion infected mice.

Figure 12. PrP^{Sc} detection in the hippocampus of RML scrapie prion infected mice.

Figure 13. Fluoro-Jade C staining of coronal hippocampal sections from mock infected and RML scrapie prion infected mice to detect neurodegeneration.

Figure 14. The detection of astrocytes within the CA1 region of the hippocampus in coronal brain sections from RML scrapie prion infected mice.

Figure 15. The detection of microglia using immunohistochemistry in the CA1 region during RML scrapie prion infection in mice.

Figure 16. The capture of the CA1 neuronal cell bodies using LCM technology.

Figure 17. RNA integrity determination of LCM captured CA1 neuronal cell body total RNA.

The following figures were obtained or adapted from Boese, A.S., Saba, R., Campbell, K., Majer, A., Medina, S., Burton, L., Booth, T.F., Chong, P., Westmacott, G., Dutta, S.M., Saba, J.A. & Booth, S.A. 2015, "MicroRNA abundance is altered in synaptoneuroosomes during prion disease", *Molecular and cellular neurosciences*, vol. 71, pp. 13-24.

Figure 8. A flow chart for synaptoneurosome preparation.

Figure 27. Western blot of synaptoneurosome preparation from mouse forebrain at different stages of the isolation procedure.

Figure 29. Western blot of synaptoneurosome prepared from mock and RML scrapie prion infected mice

Figure 34. Synaptoneurosome derived from prion infected forebrain exhibited temporal alterations in miR levels.

Abbreviations

(+)-B = (+)-bicuculline

4-AP = 4-Aminopyridine

Ago = Argonaut protein

Ago2 = Argonaut 2 protein

AMPA = α -amino-3-hydroxy-5-methyl-4-isoxazolepropionic acid

ANOVA = Analysis of variance

ARC = Activity Regulated Cytoskeleton Associated Protein

ARPP21 = cyclic adenosine monophosphate-regulated phosphoprotein

ATP = adenosine triphosphate

AUD = Animal Use Document

BCA = Bicinchoninic acid assay

BLASTN = Basic Local Alignment Search Tool Nucleotide

BSA = Bovine Serum Albumin

BSE = Bovine Spongiform Encephalopathy

CA1 = *Cornu Ammonis 1*

CA3 = *Cornu Ammonis 3*

CAG = cytosine-adenine-guanine

CAMK = Calcium/Calmodulin Dependent Protein Kinase

CAMK2 α = Calcium/Calmodulin Dependent Protein Kinase 2 α

CASPR = contactin-associated protein

cDNA = complementary DNA

CDS = coding DNA sequence

Cf = final concentration

CJD = Creutzfeldt-Jakob disease

CNS = Central Nervous System

CO₂ = carbon dioxide

CREB = cAMP response element-binding protein

CSF = Cerebrospinal Fluid

CTRL = Control

CWD = Chronic Wasting Disease

DAPI = 4',6-diamidino-2-phenylindole

DAVID = Database for Annotation, Visualization and Integrated Discovery

DCX = doublecortin

DIV = day *in vitro*

DM = Dissection Media

DMSO = Dimethyl sulfoxide

DNA = deoxyribonucleic acid

DPBS = Dulbecco's phosphate buffered saline

DPI = day post infection
DTT = dithiothreitol
EDTA = Ethylenediaminetetraacetic acid
ELISA = Enzyme linked immunosorbent assay
EP = Endpoint
FDR = False Discovery Rate
fCJD= Familial Creutzfeldt-Jakob disease
FFI = Fatal familial Insomnia
FI = Fatal Insomnia
GAPDH = Glyceraldehyde 3-phosphate dehydrogenase
GFAP = Glial fibrillary acidic protein
GFP = Green fluorescent protein
GO = Gene Ontology
GPI = glycosylphosphatidylinositol
GSS = Gertsman-Straussler-Scheinker disease
GWAS = Genome-wide association study
HBSS = Hank's Balanced Salt Solution
HEPES = 4-(2-hydroxyethyl)-1-piperazineethanesulfonic acid
HITS-CLIP = High-throughput sequencing of RNA isolated by crosslinking immunoprecipitation
HOMER1 = Homer protein homolog 1
HRP = horseradish peroxidase
HTT = Huntingtin
IAA = 3-Indoleacetic acid
IBA-1 = ionized calcium-binding adapter molecule 1
iCJD = iatrogenic Creutzfeldt-Jakob disease
IDP = intrinsically disordered protein component
IP = Intraperitoneal
IRES = internal ribosome entry site
KCC2A = Calcium/Calmodulin Dependent Protein Kinase II α
LB = Lysogeny broth
LC = Liquid Chromatography
LCM = Laser Capture Microdissection
LNA = Locked Nucleic Acid
LTD = Long-term depression
LTP = Long-term potentiation
MAP2 = Microtubule-associated protein 2
MgCl₂ = Magnesium Chloride
mGluR = metabotropic glutamate receptor
mGluR5 = metabotropic glutamate receptor 5
miR = microRNA

MK-801 = (+)-5-methyl-10,11-dihydro-5H-dibenzo[a,d] cyclohepten-5,10-imine maleate

MRI = Magnetic Resonance Imaging

mRNA = messenger RNA

MS water = Mass spectrometry grade water

NCBI = National Center for Biotechnology Information

Nefl = Neurofilament light peptide

Nefm = Neurofilament medium peptide

NMDA = N-Methyl-D-aspartate

NMDAR = N-Methyl-D-aspartate Receptor

NML = National Microbiology Laboratory

N-PER = Neuronal Protein Extraction Reagent

O₂ = Oxygen

OCT = Optimal cutting temperature

PANTHER = Protein ANalysis THrough Evolutionary Relationships

PBS = Phosphate buffered saline

PCR = Polymerase chain reaction

pCREB = phosphorylated cAMP response element-binding protein

PPDA = (2S*,3R*)-1-(Phenanthren-2-carbonyl)piperazine-2,3-dicarboxylic acid

PPi = pyrophosphate P₂O₇⁴⁻

PRNP = Prion Protein gene

PrP^C = host cellular prion protein

PrP^{Sc} = scrapie prion protein

PSD = post-synaptic density

PVDF = polyvinylidene difluoride

qPCR = quantitative Polymerase Chain Reaction

R3HDMI = R3H domain containing 1

RFP = Red Fluorescent Protein

RIN = RNA Integrity Number

RISC = RNA-induced silencing complex

RML = Rocky Mountain Laboratory

RNA = Ribonucleic Acid

RNAse = Ribonuclease

RNO = Rat miR sequence

RT-qPCR = Reverse Transcription quantitative polymerase chain reaction

sCJD = sporadic Creutzfeldt-Jakob disease

SDS = Sodium dodecyl sulfate

SEM = Standard error of the mean

SF3A3 = Splicing Factor 3a Subunit 3

SILAC = Stable Isotope Labeling by/with Amino acids in Cell culture

siRNA = short interfering RNA

SLIT3 = Slit Homolog 3 protein

SNAP25 = Synaptosome Associated Protein 25

snoRNA135 = small nuclear RNA 135

SOC = Super Optimal Broth

SV40 = Simian vacuolating virus 40

TBS = Tris buffered saline

TBS-T = Tris buffered saline with Tween-20

TE = Tris Ethylenediaminetetraacetic acid buffer

TMT = Tandem Mass Tags

UCSC = University of Santa Cruz

UK = United Kingdom

UPR = Unfolded Protein Response

UTR = Untranslated region

vCJD = variant Creutzfeldt-Jakob disease

1. Introduction

1.1 Neurodegenerative diseases

Central Nervous System (CNS) neurodegenerative proteinopathies are a group of diseases in which the abnormal aggregation of misfolded proteins is a common link. In humans, these diseases include transmissible spongiform encephalopathies or prion diseases, Alzheimer's disease, Huntington's disease, and Parkinson's disease. The normal host protein and its misfolded disease-associated form, are outlined in Table 1. All of these diseases are characterized by the appearance of these misfolded protein aggregates, varying degrees of inflammation, and neuronal damage and death, that invariably results in fatality. The process by which the neurons die is unclear, however aggregates of the misfolded protein are often found in close association, and sometimes within, degenerating neurons. The connections between neurons through which the cells communicate with each other are called synapses, and their loss is one of the earliest pathologies seen in disease (reviewed in (Mallucci 2009, Koffie, Hyman & Spires-Jones 2011)). Synapses are integral to neuronal functioning and form the basis for fundamental CNS processes including cognition, memory, movement, organ function, brain function, and hormonal regulation alongside others. For this reason, neurodegeneration affects a range of essential functions in the affected patient and the slow and gradual degeneration has a huge impact on quality of life.

Table 1. The proteins involved in a select subset of CNS neurodegenerative diseases.
The host proteins and their respective misfolded proteins implicated in disease are highlighted.

| Disease | Host Protein | Misfolded protein |
|----------------------|---|---|
| Prion disease | PrP ^C | PrP ^{Sc} |
| Alzheimer's disease | Amyloid Precursor Protein; Tau protein | Amyloid β ; Hyperphosphorylated Tau tangles |
| Huntington's disease | Huntingtin | Polyglutamine expanded Huntingtin |
| Parkinson's disease | α -synuclein | α -synuclein in Lewy bodies |

1.2 Prion diseases

1.2.1 Prion strains

The concept of prion strains was first noted when sheep scrapie was transmitted into goats and two distinct symptomatic diseases arose in the goats from the same inoculum. One disease course rendered the goats drowsy and the other, similar to the scrapie symptoms in sheep, caused the goats to scratch themselves on posts (reviewed in (Thakur, Vincent & Chaturvedi 2002)). Since this seminal observation, experimentation with prion strains have demonstrated different regional CNS presentation, pathological differences, and incubation periods. Many prion strain features have been elucidated in rodent models which have further demonstrated differences in PrP^{Sc} deposition and in tertiary and quaternary protein structure (Telling et al. 1996). For example, the Rocky Mountain Laboratory (RML) scrapie strain possesses a different glycosylation pattern than does the ME7 scrapie strain (Thackray et al. 2007) and it may be due to differences in the protein residue at amino acid positions 27-30.

An interesting example of strain similarity arose from the variant Creutzfeldt-Jakob disease (vCJD) outbreak, a result of ingesting contaminated Bovine Spongiform Encephalopathy (BSE) infected beef tissues in the United Kingdom (UK). The transmission of vCJD from humans into mice displayed the same strain characteristics as BSE transmitted into mice, confirming the species barrier had been breached (Hill et al. 1997). This provided the connection that humans were getting disease by exposure to the BSE contaminated beef tissues after the BSE outbreak was contained in the farming industry.

1.2.2 Prion diseases in animals

A number of prion diseases occur in animals, most notable of which is BSE that was responsible for the outbreak in the UK in 1989, which resulted in the cull of 4.4 million cows (reviewed in (Imran, Mahmood 2011)). This strain was able to jump the species barrier and infect humans in addition to a number of other animals from the ingestion of BSE contaminated feed, these prion diseases are thought to include transmissible mink encephalopathy in farmed mink and feline spongiform encephalopathy in domesticated cats, although sporadic forms of these two prion diseases are also documented. In addition, 18 exotic animals in UK zoos developed disease during the BSE outbreak called Exotic Ungulate Spongiform Encephalopathy. Since the abolishment of CNS tissues forming part of livestock feed, the rates of these rare prion diseases have declined sharply.

It is interesting to note that scrapie prion infection in sheep has been around for hundreds of years but there are no recognized instances of infection in humans despite the widespread consumption of meat from these animals. The species barrier may prevent PrP^{Sc} from scrapie in converting host PrP^C in humans. The species barrier is partially explained by the fact that different prion diseases have strains, which have specific characteristics that may prevent them from infecting a different species than the host species.

Chronic wasting disease (CWD) is a predominantly North American disease in cervids (deer, elk) but has been detected in Korea, and was recently identified in European reindeer (Benestad et al. 2016). This disease is found in captive as well as wild animals. CWD is unique because cervids shed infectious prions in their urine, feces, saliva, and blood (Mathiason et al. 2006), and horizontal transmission from these fomites has been demonstrated. In addition, reservoirs of infectivity in the environment can be created

through the persistence of these infectious prions, with some remaining in the environment for years. The spread of disease can occur by scavenging animals such as crows feeding on infected carcasses or remains left behind from hunting activities (reviewed in (Haley, Hoover 2015)). The current status of CWD to cross the species barrier into humans is unknown.

1.2.3 Human Prion diseases

The prion concept arose from the term ‘proteinaceous infectious particle’ or prion pronounced *pree-on* as coined by Nobel laureate Stanley Prusiner (Prusiner 1982). Prions are devoid of a nucleic acid genome and are comprised entirely of a normal cellular protein, PrP^C, that has an altered conformation that is highly resistant to chemical and physical treatments, commonly termed PrP^{Sc}. Prions can enter the brain through infection, or they can arise from mutations in the *PRNP* gene that encodes the protein. However, the most common human prion diseases are sporadic, whereby the misfolding appears to occur spontaneously without a known seed, perhaps via somatic mutation in aging neurons. Once present in the brain PrP^{Sc} is able to recruit the host PrP^C proteins and induce them to refold into the abnormal shape by a mechanism that is not completely understood. Host PrP^C is expressed endogenously, however its levels are extremely high in the brain, particularly in neurons, which explains the CNS as the predominant disease target. In fact, PrP^C is absolutely necessary in order for disease to occur; without this there would be no substrate for propagation, as evidenced by the complete lack of disease in animals in which the prion gene *PRNP* has been ablated (Bueler et al. 1993). The CNS pathology consists of vacuolation, astrocytosis, and spongiform appearance.

Epidemiological data from the U.S. indicates that for Creutzfeldt-Jakob disease (CJD), which is the most prevalent human prion disease, the rate of occurrence is approximately 1 in a million in the general population (Holman et al. 1996). This rate is higher, 5 per million, in the patient cohort of 60-74 years of age (Holman et al. 1996). Typically, after clinical presentation survival time is within months to a maximum of 3 years. The presentation of disease varies considerably and is strongly associated with a number of distinct clinical subtypes (Table 2). Sporadic disease accounts for 80-90% of cases while infectious and genetic types comprise the remaining 10-20% (Prusiner 2013).

The sporadic forms are sporadic CJD (sCJD), fatal insomnia (FI), and variably proteinase-sensitive prionopathy. Although sporadic disease is by far the most prevalent in humans, the cause is unknown. A few hypotheses include a mistake in the open reading frame of *PRNP* when being transcribed into PrP^C or the spontaneous post-translational conversion of PrP^C to PrP^{Sc} (reviewed in (Prusiner 2013)). The familial or genetic forms are a result of mutations in the human *PRNP* gene and represent up to 10% of all human prion diseases, these include familial CJD (fCJD), Fatal Familial Insomnia (FFI) and Gertsmann-Straussler-Scheinker disease (GSS). These are all autosomal dominant at the gene level and there are currently 40+ documented mutations in *PRNP* linked to disease (Capellari et al. 2011). There are two types of mutations that result in genetic disease, octapeptide repeat expansions in *PRNP* and/or point mutations resulting in a different amino acid in the PrP^C protein sequence. The octapeptide region is where PrP^C binds copper ions (Cu²⁺), which can be important in disease (Hornshaw, McDermott & Candy 1995).

The infectious prion diseases represent about 1% of human cases and include kuru, iatrogenic CJD (iCJD), and variant CJD (vCJD). The infectious prion diseases arise from the consumption of prion contaminated tissues or exposure to surgical instruments infected

Table 2. Human Prion disease types and nomenclature. There are genetic, sporadic, and infectious prion diseases that themselves have subtypes, adapted from (Puoti et al. 2012)

| Type | Disease Name or subtype |
|-------------|---|
| Genetic | Creutzfeldt Jakob Disease (CJD) |
| | Fatal Familial Insomnia |
| | Gertsmann-Straussler-Scheinker syndrome |
| | Heterogeneous or mixed subtype |
| Sporadic | CJD 129MM1 and CJD 129MV1 |
| | CJD 129VV1 |
| | CJD 129MM2 |
| | CJD 129MV2 |
| | CJD 129VV2 |
| | Fatal Insomnia |
| | Variably protein-sensitive prionopathy |
| Infectious | Kuru |
| | Iatrogenic CJD |
| | Variant CJD |

with prions. Kuru is limited to a tribe living in a remote part of Papua New Guinea that routinely practiced cannibalism and consumed brain material from deceased infected individuals (Mathews, Glasse & Lindenbaum 1968). After the cause was determined, this cannibalistic activity was outlawed and kuru has since disappeared. The iCJDs are caused by the accidental transmission of prion infection from a patient with CJD to other individuals, via contaminated materials during medical procedures. These have occurred through neurosurgery, hormone therapy (gonadotrophin and growth hormone), corneal transplants, stereotactic electroencephalograms, and dura mater grafts (reviewed in (Thakur, Vincent & Chaturvedi 2002)). The harvesting of hormones from cadavers has since been terminated in favor of recombinant proteins, thereby eliminating new cases. Current practice is that if a person is suspected of having a prion disease, they are not operated on with expensive neurological equipment to reduce the chance of iCJD transmission. However, given the lengthy asymptomatic period of disease the presence of sCJD in patients is not known prior to the onset of disease and so transmission still occurs occasionally. A new form of infectious human prion disease, vCJD arose from the consumption of beef that was contaminated with BSE. After the 1989 outbreak in cattle in the UK, new cases of CJD that were distinct from typical sCJD started occurring in the UK population. Experimentation in mice led to the discovery of the link between vCJD and BSE (Hill et al. 1997).

Mutations in *PRNP* can cause a rapid progression in disease incubation. One of the most studied mutations, which is present in both genetic and sporadic forms of disease, is at codon 129 of the *PRNP* gene, which codes for either methionine or valine in PrP^C. Homozygosity for methionine at codon 129 has been noted in a high percentage of sporadic cases (Palmer et al. 1991) and with an increased susceptibility for iCJD as well (Collinge,

Palmer & Dryden 1991). Interestingly, when vCJD appeared in the human population, patients that possessed a homozygous codon 129 developed the disease at a much earlier age but with a longer survival period than was typical for sCJD (reviewed in (Thakur, Vincent & Chaturvedi 2002)). In 2017, the first vCJD case with heterozygosity at codon 129 was documented, indicating a much longer incubation period compared to homozygous (Mok et al. 2017), whether other heterozygous cases will emerge remains to be seen but it may indicate that the heterozygous state lengthens incubation period of vCJD considerably.

Another interesting *PRNP* substitution that was identified as occurring at a higher rate in the survivors of the Papua New Guinea population was a valine substitution for glycine at codon 127. Experiments in mice revealed that a homozygous or heterozygous valine substitution into humanized mice rendered these animals resistant to multiple strains of human CJD including both sporadic and variant types (Asante et al. 2015). This demonstrated that presence of kuru in this isolated population had put accelerated evolutionary pressure through what is termed ‘bottleneck natural selection’. This has led to an increase in the incidence of the 127 valine polymorphism within this population in comparison with the general population worldwide. It is particularly interesting that not only does this mutation protect from kuru but also appears to confer resistance to all human prion diseases tested.

1.2.3.1 Prion disease symptoms

Clinical presentation of prion disease depends on the prion subtype infecting the patient. At early stages, there are three phenotypic subtypes of disease apparent which are classified as ataxic, cognitive, and non-phenotypical CJD (reviewed in (Puoti et al. 2012)).

The ataxic subtype account for 30% of cases and ataxia is the prominent feature at early stages of disease alongside cognitive impairment. In early disease, dizziness, mood alterations, unsteady gait, and the mind going vacant are reported which is followed at later stages by myoclonus. In the cognitive subtype, the age of onset is between 50-70 years of age and presents with impaired cognitive features including confusion, hypersensitivity to stimuli, anxiety, and difficulty concentrating. In this subtype, ataxia occurs as disease progresses. The non-phenotypical subtypes include sporadic FI and atypical CJD, which demonstrate a combination of cognitive and movement features that are not weighted in either the ataxic or cognitive direction. At advanced stages of disease, the symptoms are similar between the subtypes and involve ataxia, behavioral changes, sleep disturbances, and sensory disturbances.

1.2.3.2 Prion disease diagnosis

As per Centers for Disease Control and Prevention, prion disease can only be ascribed as a probable or possible diagnosis antemortem in humans as post-mortem brain autopsy remains the only definitive criteria for positive diagnosis. Alongside progressive dementia physical characteristics of disease must include at least two of the following symptoms, cerebellar/visual signs, myoclonus, akinetic mutism, and pyramidal or extrapyramidal signs. In addition, a positive result must be met on one of the following diagnostic tests, cerebrospinal fluid positive for 14-3-3 protein by Western blot (Zerr et al. 1998), abnormal signal using diffusion-weighted magnetic resonance imaging of the brain (Fujita et al. 2012), and/or periodic sharp wave complexes in Electroencephalogram recording (Steinhoff et al. 2004). PrP^{Sc} detection in post-mortem brain tissue is the only definitive diagnosis for prion disease in humans.

1.2.3.3 Prion disease treatment and strategies

The current therapies available for prion diseases merely treat the symptoms of disease and like other progressive neurodegenerative conditions, no therapeutic currently exists that can halt or even delay the progression of disease. The drug flupirtine is used to improve cognitive symptoms of disease in humans (Otto et al. 2004). Various other drugs have been examined in clinical trials to resolve neurodegeneration and/or the loss of brain mass such as quinacrine (Collinge et al. 2009, Geschwind et al. 2013), pentosan polysulfate (Bone et al. 2008, Tsuboi, Doh-Ura & Yamada 2009), and doxycycline (Haik et al. 2014) but none were considered successful. Memantine was found to increase survival when tested in prion infected mice (Riemer et al. 2008), but has not been tested clinically for human prion disease. It may be promising as it is already approved for use in Alzheimer's disease patients for similar symptoms.

A number of strategies for the treatment of prion disease have been explored through the use of animal models that may yet be translated to human trials. A proposed target of prion disease treatment is PrP^C itself since PrP^C knockout mice do not acquire the disease when infected with prions. To this end, a number of PrP^C gene silencing strategies have been used in animal models resulting in successful ablation of disease (reviewed in (Boese et al. 2013)). Synaptic dysfunction occurs in prion diseases well before irreversible neuronal loss is evident which can be reversed by targeting PrP^C at early stages of disease (reviewed in (Mallucci 2009)). This results in rescue of early cognitive changes and synapse function. One main problem for this in humans is that *PRNP* knockdown could lead to potentially damaging effects since the function of PrP^C in humans remains poorly defined. Indeed, PrP^C could have cognitive implications in humans that are not evident or testable in animal models. However, an interesting Genome-Wide Association Study

(GWAS) determined that truncated *PRNP* genes existed in the human population that rendered PrP^C inert with no detrimental effects (Minikel et al. 2016), suggesting humans may tolerate PrP^C knockdown as a therapy. Indeed, a human antibody PRN100, which targets PrP^C in mice and prevents not only prion disease but also synaptotoxicity in Alzheimer's mouse models, may enter clinical trials for CJD in the near future (Klyubin et al. 2014). Although the feasibility of knocking out PrP^C in humans is controversial, the targeting of synaptic function using other means may provide an avenue to rescue the neurodegeneration seen in prion disease and perhaps in Alzheimer's or Huntington's diseases as well. Another difficulty that needs to be resolved for sporadic or infectious cases is that disease onset is rapid after clinical symptoms, and treatment at the later stages of disease may be fruitless. That combined with often unclear antemortem diagnosis makes clinical testing difficult.

One other strategy is to target the accumulation of PrP^{Sc} aggregates. A group used compounds called luminescent conjugated polythiophenes that targeted PrP^{Sc} aggregates in mice and lengthened survival by ~12% after prion infection (Herrmann et al. 2015). These compounds may provide another avenue to explore in preventing disease or lengthening survival in humans.

In animal models of prion disease, the unfolded protein response (UPR) pathway was targeted using drugs, as this is activated not only during prion disease but also other neurodegenerative diseases (reviewed in (Freeman, Mallucci 2016)). The use of GSK2606414 which inhibits the UPR in prion infected mice led to the reduction of neurodegeneration and improvement in cognitive behavior even though PrP^{Sc} accumulated at the same rate as untreated animals and there was no change in survival time (Moreno et al. 2013). Unfortunately, recent evidence from CJD patients demonstrated that the UPR

activation may not be a factor in human disease (Wiersma et al. 2016). These studies highlight the need for further research into Prion disease treatments.

1.3 Related proteinopathies

Both Alzheimer's disease and Huntington's diseases are CNS neurodegenerative diseases that are similar to prion disease but more prevalent. These diseases have the same issues in that no cure currently exists and they share pathology resulting from misfolded host proteins. The prevalence of Alzheimer's disease is highest of all CNS neurodegenerative disease (reviewed in (Alzheimer's Association 2016)). The total number of Alzheimer's disease cases in the United States of America is about 5.4 million people with 5.1 million of those that are 65 or older. The economic cost of Alzheimer's disease is considerable and is approximately \$259,000,000 per year in the U.S. Alzheimer's disease is mainly sporadic with a low incidence of genetic disease that account for 1-10% of all cases. In genetic disease, three main genes have been identified, Amyloid Precursor protein (*APP*), Presenilin-1 (*PSEN1*), and Presenilin-1 (*PSEN2*). It is a disease with no cure and as with prion diseases, drug therapies target symptoms of disease while the disease itself is incurable and always fatal, often due to secondary infections such as pneumonia. The early symptoms of Alzheimer's disease are behavioural changes, memory loss, and mild cognitive impairment. As disease progresses patients have trouble communicating, swallowing, and walking.

The causative agents of Alzheimer's disease are believed to be the misfolded versions of host proteins, amyloid precursor protein and tau. Aggregates of these misfolded proteins have been identified in the brains of patients suffering with Alzheimer's disease, presenting as tangles of hyperphosphorylated tau and amyloid β plaques. There is a

progressive loss of neurons in the brain until death occurs, which is approximately 10 after onset of symptoms.

Although Alzheimer's disease is not considered infectious or contagious, amyloid β seeds from Alzheimer's diseased human brains were transmitted into animal models. The first transmissibility study involved early onset brain extracts which demonstrated amyloid β pathology but the neurofibrillary tau tangles were not detectable by time of sacrifice (Baker et al. 1994). This remains the case with all transmissibility studies. Since that initial study, amyloid β pathology has been transmitted from humans into transgenic mouse models (Meyer-Luehmann et al. 2006, Eisele et al. 2009). One study demonstrated that amyloid β was present in the brains of patients that previously received prion contaminated growth hormone treatments derived from the brains of cadavers (Jaunmuktane et al. 2015). The topic of Alzheimer's disease being infectious remains highly controversial among the scientific community (Collinge et al. 2016, Feeney et al. 2016).

The rodent models of Alzheimer's disease are currently insufficient because they do not recapitulate all aspects of disease (reviewed by (Elder, Gama Sosa & De Gasperi 2010)), whereas prion disease models, once adapted to the host animal, present the same way as in human disease. For example, most of the Alzheimer's disease models are genetic despite the rare occurrence of human genetic disease. Most Alzheimer's models that are well characterized are based upon amyloid β pathology and most do not demonstrate the neuronal loss reminiscent and critical in the development of human disease, nor do they demonstrate the hallmark neurofibrillary tau tangles that are also present alongside amyloid β plaques. For this reason, it is difficult to sufficiently model Alzheimer's disease in

animals and this is where animal models of prion disease can aid in modeling neurodegeneration to study and prevent neurodegeneration in other diseases.

Huntington's disease is an autosomal dominant genetic disease, caused by the misfolded Huntingtin protein (HTT) which possesses multiple glutamine repeats in the protein's primary sequence, resulting from cytosine-adenine-guanine (CAG) repeats in the deoxyribonucleic (DNA) sequence (The Huntington's Disease Collaborative Research Group 1993). The aggregates of mutated HTT appear to sequester into neurons specifically, particularly in the cortex and the corpus striatum even though it is expressed in the majority of the cells of the body (Rosas et al. 2002). Although healthy individuals can have up to 35 CAG repeats, those with 40-50 repeats have adult onset disease and beyond 50 repeats results in juvenile disease (reviewed by (Imarisio et al. 2008)). Huntington's affects the motor abilities of patients, resulting in involuntary, jerky movements (chorea) although a subset of patients display abnormal fine motor control of digits and balance instead of chorea. Cognitive function and behavioral symptoms can also be expected, especially with disease progression.

There is a great degree of variability in symptom onset as well as age at death due to the heterogeneous nature of the number of glutamine repeats present in the population (reviewed in (Baig, Strong & Quarrell 2016)). Typically, death occurs between 51-57 years of age and after symptom onset it can take 10-25 years before death. The epidemiology of disease globally is 5-10 per 100,000 affected, with a higher incidence in Europe, North America, and Australia.

The *in vivo* models of Huntington's disease include non-human primates produced through genetic modification by increasing the number of CAG repeats in the *HTT* gene. This allows developmental observation of disease at embryonic stages (Kocerha et al.

2014). There are a number of transgenic mouse models that express human HTT protein with polyglutamine expansions, most of them die within 6 months and the range of features include aggregated protein to apoptotic neuronal death. The features of disease are dependent on the number of CAG repeats introduced into the *HTT* gene, which results in varying degrees of human disease like symptoms. This makes the modeling Huntington's into animal models difficult because of the variability in human disease.

1.4 Characteristics and Functions of PrP^C

PrP^C is found in vertebrates including mammals, birds, reptiles, amphibians and fish (Premzl et al. 2004), and also in yeast (Goldschmidt et al. 2010). In humans, the *PRNP* gene is located on chromosome 20 and contains highly conserved regions with other vertebrates (Ahn, Son 2007). The wild-type form of the animal PrP^C is a 32 kiloDalton protein with 253 amino acids, that is post-translationally cleaved to yield a protein that is 209 amino acids long (Zahn et al. 2000) (Figure 1A). The unprocessed protein consists of a signal peptide, octapeptide region which is important in Cu²⁺ binding affinity, and a signal sequence for the glycosylphosphatidylinositol (GPI) anchor. The protein structure has two major domains spanning the N-terminus and C-terminus regions (Figure 1B). The N-terminus (amino acids 23-121) comprises an intrinsically disordered protein component (IDP), without a defined tertiary structure and as a result is flexible at this end. The C-terminal, amino acids 127-231, contains a highly organized tertiary component consisting of 2 β -sheet strands and 3 α -helices (Zahn et al. 2000). Notably, proteins containing IDPs have a higher potential to spontaneously misfold and require a number of chaperones in order to fold correctly (De Simone et al. 2012, Qiao, Bowman & Huang 2013).



Figure 1. The domain organization and tertiary protein structure of PrP^C. A) the domain organization of mouse PrP^C adapted from (Deriziotis, Tabrizi 2008) B) tertiary structure adapted from (Liebert, Bicknell & Adams 2014) and visualized using PYMOL (Riek et al. 1996). Note the abundance of α helices and a small amount of β sheets.

PrP^C can exist in two states in the host cell, a membrane situated insoluble glycosylated form and a non-glycosylated soluble cytosolic form (reviewed in (Taylor, Hooper 2006)). The membrane bound protein is found ubiquitously, with a minority of cells expressing the cytosolic form. The glycoprotein type contains a GPI anchor and can be found in lipid rafts at the membrane surface (Colby, Prusiner 2011). The GPI-anchored PrP^C functions presumably with other molecules at the cell surface through a process called macromolecular crowding. Once at the cell surface, PrP^C has a fairly high turnover rate and is internalized back into the cell by either clathrin coated pits (Shyng, Heuser & Harris 1994) or through caveolae (Peters et al. 2003).

Movement of PrP^C between different cells occurs by two main pathways, which can be important for how PrP^{Sc} propagates in the disease state. The cytosolic PrP^C can move freely in extracellular space due to its soluble nature via exosomes (Robertson et al. 2006, Vella et al. 2007, Guo, Bellingham & Hill 2016). The GPI-anchored PrP^C can potentially detach from the membrane by cleavage of its GPI anchor and be taken up into other cells as other GPI proteins are known to shuttle in this way (Liu et al. 2002). However, this requires direct contact between adjacent cells and likely occurs when cell surface crowding becomes high. This crowding is also believed to be how PrP^C, with its IDP region, engages in promiscuous binding with up to 45 different ligands being reported in the literature including laminin (Beraldo et al. 2011) and reelin (Devanathan et al. 2010).

Although PrP^C knockout mice develop normally and display no distinct behavioural phenotype, a number of functions have been described for PrP^C particularly in neurons. A caveat to some of these discoveries is that the genetic basis for the knockout mice was different between studies (reviewed in (Steele, Lindquist & Aguzzi 2007)). Some of the

key findings for PrP^C in neuronal health and function from knockouts and experimental PrP^C manipulation are highlighted in Table 3.

1.4.1 Metal Ion Homeostasis

Experiments have indicated that PrP^C has a role in CNS metal ion homeostasis and regulates Cu²⁺ (Brown et al. 1997), Fe²⁺ and Zn²⁺ (Walter et al. 2007). It has been proposed that PrP^C serves as an antioxidant through metal ion binding in neurons (Kralovicova et al. 2009), however this remains controversial as PrP^C did not appear to behave as such in one study in cultured primary hippocampal neurons (Cingaram et al. 2015). In genetic forms of human prion disease, there are often expansion mutations in the octapeptide repeat region of the *PRNP* gene which result in lowered Cu²⁺ binding affinity (Stevens et al. 2009), and this affinity has an inverse correlation with the number of expansions. Also indicative of a PrP^C role in metal ion homeostasis is that PrP^C knockout mice possess a differing pattern of metal distribution within their brains compared to wild-type (Pushie et al. 2011). Interestingly, differential Cu²⁺, Zn²⁺, and Fe²⁺ is also found in the CNS of Alzheimer's disease patients (Lovell et al. 1998, Dong et al. 2003, Miller et al. 2006) and Cu²⁺, and Fe²⁺ in Parkinson's disease patients (Pall et al. 1987, Castellani et al. 2000). Zn²⁺ binding by PrP^C has been demonstrated to affect α -amino-3-hydroxy-5-methyl-4-isoxazolepropionic acid receptor (AMPA) signaling, where mutant PrP^C derived from genetic disease alters Zn²⁺ binding (Watt et al. 2012). In addition, Zn²⁺ is involved with Shank3 protein, which is a downstream effector of glutamate receptors (Tao-Cheng et al. 2016) while Cu²⁺ binding affects PrP^C interaction with N-Methyl-D-Aspartate receptors (NMDAR) (You et al. 2012).

Table 3. A select list of functions attributed to PrP^C in neurons.

| Function | Reference |
|--|--|
| Metal ion binding Cu ²⁺ , Zn ²⁺ , and Fe ²⁺ | (Brown et al. 1997, Walter et al. 2007, Pushie et al. 2011) |
| Glutamate Receptor interaction | (You et al. 2012, Rangel et al. 2009, Lauren et al. 2009, Khosravani et al. 2008a) |
| Circadian rhythm | (Tobler et al. 1996, Tobler, Deboer & Fischer 1997) |
| Neural stem cell maintenance | (Steele et al. 2006, Santos et al. 2011, Lee, Baskakov 2014) |
| Synapse formation | (Collinge et al. 1994) |
| Synaptic vesicle release | (Robinson et al. 2014, Carleton et al. 2001) |
| Olfactory signal processing | (Le Pichon et al. 2009) |
| Myelination | (Bremer et al. 2010, Kuffer et al. 2016) |
| Neuritogenesis | (Beraldo et al. 2011, Chen et al. 2003, Santucciono et al. 2005) |

1.4.2 Glutamate Receptors

PrP^C has been recognized as interacting as a coreceptor with various glutamate receptors at the cell surface of neurons (You et al. 2012, Rangel et al. 2009, Lauren et al. 2009, Khosravani et al. 2008a). The involvement of PrP^C with glutamate receptors is important because they are the main excitatory neurotransmitter signaling receptors in the CNS and there are a number of glutamate receptors which are responsible for long-term potentiation (LTP), long-term depression (LTD), neuroprotection, learning, memory, fear extinction, synaptic plasticity, and cell death (reviewed in (Traynelis et al. 2010)). There are two main types of glutamate receptors in the brain, ionotropic, which are fast acting ligand-gated channels and permit cations into the cell, and metabotropic (mGluR), which are slow acting G protein coupled receptors which affect intracellular signaling cascades. Various studies have determined links between PrP^C and both glutamate receptor classes in neuronal cells.

The group I mGluRs, specifically mGluR5 and mGluR1, have been shown to interact with PrP^C (Beraldo et al. 2011, Haas, Kostylev & Strittmatter 2014). Studies have shown that PrP^C acts as a coreceptor with mGluR5 and mGluR1 in binding laminin to promote neuronal differentiation and outgrowth (neuritogenesis) (Beraldo et al. 2011). The gene responsible for encoding mGluR5, *GRM5*, interacts with the *PRNP* gene in an Alzheimer's disease mouse model (Haas et al. 2016). PrP^C also interacts with mGluR5 as a coreceptor in binding soluble amyloid β oligomers derived from Alzheimer's patients to mediate synaptic toxicity in rodents (Um et al. 2013) by impairing LTP. This amyloid β synaptotoxicity is ablated when PrP^C access is restricted by blocking it with antibodies (Barry et al. 2011). Additionally, the activation of PrP^C with mGluR5 results in

downstream regulation of the ionotropic NMDAR (Hu et al. 2014), which PrP^C may interact with.

The involvement of NMDAR with PrP^C was first recognized in experiments in PrP^C knockout mice in which it was noted that the NMDAR2D receptor was increased in the absence of PrP^C (Khosravani et al. 2008b). Neurons cultured from the hippocampus of knockout mice were more prone to excitotoxicity when exposed to NMDA as evidenced through electrophysiological recordings, and this resulted in increased cell death. The conclusion drawn was that PrP^C regulated the NMDAR in a way that attenuated excitotoxicity in neurons. The homeostatic function of the NMDAR2D receptors is unclear, however recent evidence suggests that mutations in the *GRIN2D* gene, which codes for this receptor, results in severe epilepsy in children due to the toxic buildup of glutamate in the brain (Li et al. 2016). Other abnormal NMDAR related functions obtained from PrP^C knockout mice is that they display depressive behaviours (Gadotti, Bonfield & Zamponi 2012) that are regulated by NMDAR in the hippocampus through LTP. Evidence has long existed that synapses of neurons from PrP^C knockout mice are impaired in LTP function (Collinge et al. 1994). The PrP^C null mice also have an increased reaction to pain, which is restored to control levels by using the NMDAR inhibitor (+)-5-methyl-10,11-dihydro-5H-dibenzo[a,d] cyclohepten-5,10-imine maleate (MK-801) (Gadotti, Zamponi 2011). An experimentally demonstrated mechanism of NMDAR inhibition by PrP^C is through the binding of Cu²⁺ ions which caused S-nitrosylation of molecules within cells, the end result being NMDAR deactivation (Gasperini et al. 2015). In that study, amyloid β also blocked PrP^C from deactivating the NMDAR, resulting in increased neurotoxic events.

1.4.3 Other PrP^C functions

PrP^C affects neurite outgrowth through a mechanism which involves contactin-associated protein (CASPR). CASPR is typically shed at the neuronal cell surface to stop neurite outgrowth and PrP^C inhibits CASPR by binding CASPR through a laminin-like domain. Due to this binding, CASPR cannot be shed, a growth cone is maintained, and neurite outgrowth is promoted. PrP^C achieves this by inhibiting the proteolytic activity of an extracellular matrix glycoprotein, reelin, whose target is CASPR (Devanathan et al. 2010). In addition to affecting neurite outgrowth, there have been vital roles identified for PrP^C at the synapses of neurons for proper signaling as well.

Prion protein participates in the formation of synapses (Spielhaupter, Schatzl 2001) and recent work has demonstrated that it facilitates vesicle release at presynaptic terminals. PrP^C does this by participating in the creation of a larger pool of synaptic vesicles in both the mouse hippocampus (Carleton et al. 2001) and at the neuromuscular junction in *Drosophila* (Robinson et al. 2014). A number of other homeostatic functions have been attributed to PrP^C, including Neural stem cell formation (Steele et al. 2006, Santos et al. 2011, Lee, Baskakov 2014), Circadian rhythm (Tobler et al. 1996, Tobler, Deboer & Fischer 1997), Olfactory sense (Le Pichon et al. 2009) and myelination of peripheral neurons (Bremer et al. 2010, Kuffer et al. 2016).

1.5 PrP^{Sc}

The properties and potential functions of the misfolded PrP^{Sc} have not been elucidated to the degree of depth of PrP^C, particularly due to difficulty in PrP^{Sc} isolation. However, key differences are outlined in Table 4. Due to the insoluble nature of PrP^{Sc}, it

Table 4. Characteristics of PrP^C and PrP^{Sc}. Adapted from (Thakur, Vincent & Chaturvedi 2002)

| PrP ^C | PrP ^{Sc} |
|--|---|
| <ul style="list-style-type: none"> • Host form • Proteinase K sensitive • No aggregation • Secondary structure mainly α-helical (43%) with low β-sheet content (3%) • Soluble in detergent • Cell surface form mainly with a cytoplasmic form | <ul style="list-style-type: none"> • Disease state • Proteinase K resistant • Can aggregate to form plaques and/or amyloid • Secondary structure has high β-sheet (54%) and lower α-helices (21%) • Amyloid fibrils and rods are formed in detergent • Located in cytoplasmic vesicles and extracellular space |

cannot be studied by high resolution X-ray crystallography or nuclear magnetic resonance techniques for visualization, therefore its higher ordered structure remains elusive. Most of what is known is based on lower resolution techniques (reviewed in (Poggiolini, Saverioni & Parchi 2013)). However, it is known that the primary amino acid sequence is identical between PrP^C and PrP^{Sc} (Stahl et al. 1993) as are their molecular weights and both products arise from the same gene, *PRNP* (Basler et al. 1986). The changes in PrP^{Sc} are post-translational and arise at the tertiary structure. There is a notable increase in β -sheet structure and a reduction in α -helices. Specifically, PrP^{Sc} contains 43-54% β -sheet structure compared to 3% in PrP^C and for α -helices, it contains 21% compared to 43% (Caughey et al. 1991, Pan et al. 1993). Much of the information garnered about PrP^{Sc} is from computer models but these do not often match findings from immunochemical experiments (reviewed by (Poggiolini, Saverioni & Parchi 2013)) therefore the true, full structure of PrP^{Sc} remains unknown. It can be hypothesized that the increase in β -sheet structure likely results in a higher hydrophobicity of the PrP^{Sc} isoform and this hydrophobicity leads to a hydrophobic core in multimeric structures including amyloids or fibrils. This can be seen as PrP^{Sc} forms aggregates while PrP^C does not, and in detergent, PrP^{Sc} forms rods and fibrils while PrP^C remains soluble.

Another known feature of PrP^{Sc} is that it has a residue at amino acid 27-30 that is resistant to proteinase K digestion and this feature is exploited to identify prion disease in infected tissues. The tissue samples are treated with Proteinase K to destroy PrP^C and other native proteins, which are sensitive to digestion prior to immunochemical staining with PrP^C antibody. As the amino acid sequence between PrP^C and PrP^{Sc} is similar, the Proteinase K resistant PrP^{Sc} isomer remains behind and is detected. A structural study used electron cryoscopy to determine a high resolution model of the anchorless PrP^C 27-30

fragment and determined that the higher order was a four rung structure which is β -solenoid like (Vazquez-Fernandez et al. 2016), fitting previous X-ray fiber diffraction data (Wille et al. 2009).

1.6 PrP^C to PrP^{Sc} conversion, propagation, and accumulation

Current data supports the seeded (nucleation) polymerization model for the conversion and propagation of PrP^C into PrP^{Sc} (Figure 2). The seeded model has gained support due the ability to induce PrP^{Sc} conversion *in vitro* using recombinant PrP^C as substrate and chemicals such as Sodium Dodecyl Sulfate (SDS) to cause the spontaneous formation of PrP^{Sc} and ultimately fibrils (Stohr et al. 2008). This hypothesis suggests that PrP^C is the more thermodynamically stable isoform compared to PrP^{Sc} (reviewed in (Soto 2004)). It implies that spontaneous production of PrP^{Sc} must reach a point where an unknown, critical number of unstable monomers combine to form a stable and persistent oligomer. As conversion continues, the PrP^{Sc} oligomers behaves as seeds, recruiting monomeric PrP^{Sc} molecules and resulting in an exponential increase in PrP^{Sc} over time. These larger oligomers then break off and serve as seeds in further converting host PrP^C into PrP^{Sc} leading to the eventual conversion of most of the PrP^C within the host cell.

The conversion process occurs post-translationally, likely in the lipid rafts where PrP^C localizes after being processed. Also, PrP^{Sc} can be spread from cell to cell and results in PrP^{Sc} being found within the cell as well as in the extracellular matrix, an area where PrP^C is typically not found. There are also prion conversion co-factors reported that speed up PrP^{Sc} accumulation including pentosan polysulfate, heparin, sulfated dextran compounds, synthetic poly(A) ribonucleic acid (RNA), phosphatidylethanolamine, and

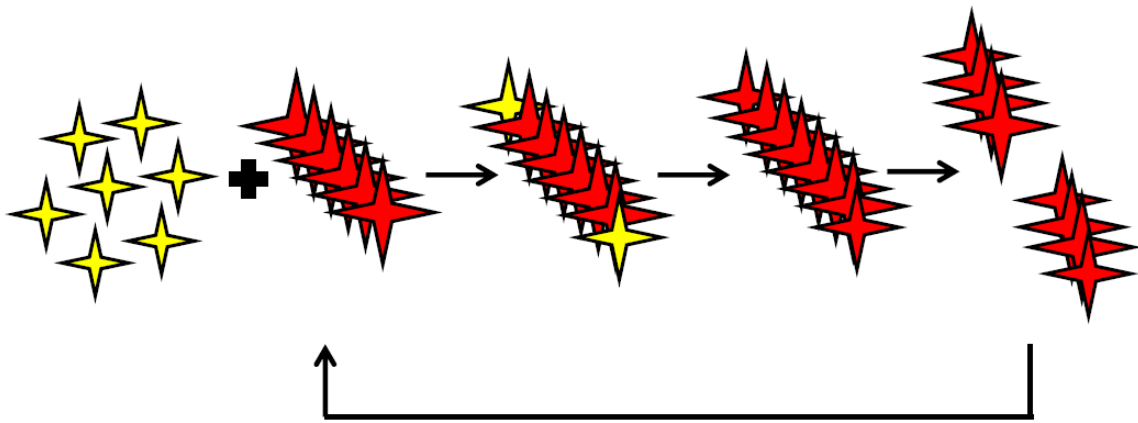


Figure 2. The recruitment and propagation of PrP^{Sc} from the normal host cellular PrP^C. The seeding hypothesis suggests that there is an equilibrium between the PrP^C and PrP^{Sc} isoforms in the host with the PrP^C being the more stable form of the two. However, PrP^{Sc} events increase with time, as PrP^C misfolds spontaneously, yielding more PrP^{Sc}. This increase in PrP^{Sc} allows oligomers of PrP^{Sc} to form which are more thermodynamically stable than PrP^C or PrP^{Sc} on their own, and these oligomers result in a more rapid PrP^C conversion into PrP^{Sc}. The oligomeric form of PrP^{Sc} breaks off creating seeds that more easily convert PrP^C, resulting in the accumulation and propagation of PrP^{Sc} in its new oligomeric form. Although the exact size of the more stable infectious PrP^{Sc} oligomer is not known. Adapted from (Soto 2004)

RNA from normal mouse liver (reviewed in (Poggiolini, Saverioni & Parchi 2013)). However, the roles of these chemicals *in vivo* in the propagation of PrP^{Sc} and prion infection are unknown.

1.7 Mouse model of RML scrapie prion disease

There are a number of prion disease models available and all of them involve the injection of prion infected brain homogenate from critically ill animals into the next set of animals to propagate the disease. The scrapie prion models have been adapted into mice from sheep and required serial passaging to produce a stable mouse model. In this thesis, the mouse-adapted scrapie termed RML scrapie, a prototypic and widely used strain with a well described clinical and pathological phenotype, was chosen as an experimental model of prion disease.

The RML strain of scrapie originates from an ovine source, where it was passaged from scrapie-infected sheep (SSBP/1) to goats then passaged and adapted into CD1 mice (Chandler 1961) and has since become mouse-adapted. The RML strain has distinct biochemical properties and localization in the brain compared to other scrapie strains such as ME7. For example, the RML PrP^{Sc} is more sensitive to proteinase K digestion (Thackray et al. 2007) and is less conformationally stable than ME7. Data has suggested that RML associates with astrocytes and glial cells in the thalamus, and neurons in the substantia nigra (Carroll et al. 2016).

The RML scrapie prion mouse model is propagated by injecting infected brain homogenate into the peritoneal cavity of adult mice from which the prion infection spreads from the spinal cord into the CNS in a caudal to rostral fashion (Kimberlin, Walker 1982). The pathology of disease includes vacuolation (lesions) in the grey matter of the brain,

progression of astrocytosis and gliosis, and eventual neuronal death (Cole, Kimberlin 1985). These pathological features of the RML scrapie model are similar to human forms of prion disease including kuru (Hadlow 1995). As the prion agent itself has not been isolated therefore limiting the development of an *in vitro* disease model, the *in vivo* model is required to study the effects of prion infection in neurons.

1.8 The involvement of glutamate receptors in neurodegenerative disease

The GluRs have been implicated in various neurodegenerative diseases. The interactions between glutamate receptors, notably the ionotropic NMDAR and the metabotropic mGluR5, and PrP^C have been documented as mentioned earlier (reviewed by (Hamilton, Zamponi & Ferguson 2015)). Dysfunction of glutamate receptors, both the NMDARs and the mGluRs has been reported in Alzheimer's disease. Other studies have demonstrated that PrP^C binds to mGluR5 and together these co-receptors bind amyloid β oligomers to signal the release of intracellular Ca²⁺ stores which lead to dendritic spine loss (Um et al. 2013). A comprehensive study into the mediators of the PrP^C-mGluR5 pathway has revealed that there is a genetic interaction of these two components. The removal of *PRNP* and *GRM5* genes decreased amyloid β oligomer signaling by reducing the activation of intracellular mediators calcium/calmodulin dependent protein kinase 2 (CAMK2), Homer1b/c, and tyrosine kinase 2 β (Haas et al. 2016).

Studies into the role of the mGluR5 in neurodegeneration have found that it may serve as a potential drug target. Experimental manipulation of the mGluR5 gene by *GRM5* deletion in mouse models of Alzheimer's disease have demonstrated a reduction in cognitive impairment and pathology (Hamilton et al. 2014). When mGluR5 was targeted by drugs in two Alzheimer's disease mouse models, behavioural deficits as well as amyloid

β plaque burden was improved (Hamilton et al. 2016). In prion diseases, a *GRM5* knockout mouse infected with RML scrapie displayed a delay in symptom onset, but died at the same time as the RML scrapie infected wild-type mice (Beraldo et al. 2016).

The strict regulation of glutamate levels is required to maintain the health of neurons as excessive levels can cause excitotoxicity mediated cell death. This excitotoxic cell death is initiated through extrasynaptic NMDAR signaling, however, at lower glutamate levels synaptic NMDAR signaling results in a neuroprotective transcriptional response (reviewed in (Hardingham 2006)), (Figure 3). The neuroprotective role is executed through calcium (Ca^{2+}) influx which causes the phosphorylation of cAMP element response binding protein (CREB) protein. The phosphorylated CREB (pCREB) in turn enters the nucleus and results in the transcription of numerous neuroprotective genes, including a number that have been shown to have a pivotal role as inhibitors of cell death. However, if excessive glutamate levels are present in the extracellular space surrounding neurons, extrasynaptic NMDAR signaling results in excessive Ca^{2+} influx which results in CREB shut off and the induction of genes that have been related to excitotoxicity cell death.

Previous work in our laboratory demonstrated that many potentially neuroprotective genes associated with synaptic NMDAR signaling are increased in expression during early stages of mouse prion infection in CA1 neurons (Majer et al. 2012). The gene response in the CA1 resulted in the upregulation of 6 of 9 genes that have been reported to function as core activity-regulated genes in the inhibition of cell death. In addition, the NMDAR2B gene *GRIN2B* was downregulated in the CA1 during early disease, and this gene is known to form part of the excitotoxic pathway (Tackenberg et al. 2013). In addition to the CA1 study, Shott *et al* (Shott et al. 2014) also found that a neuroprotective response was activated in the brains of RML scrapie infected mice during

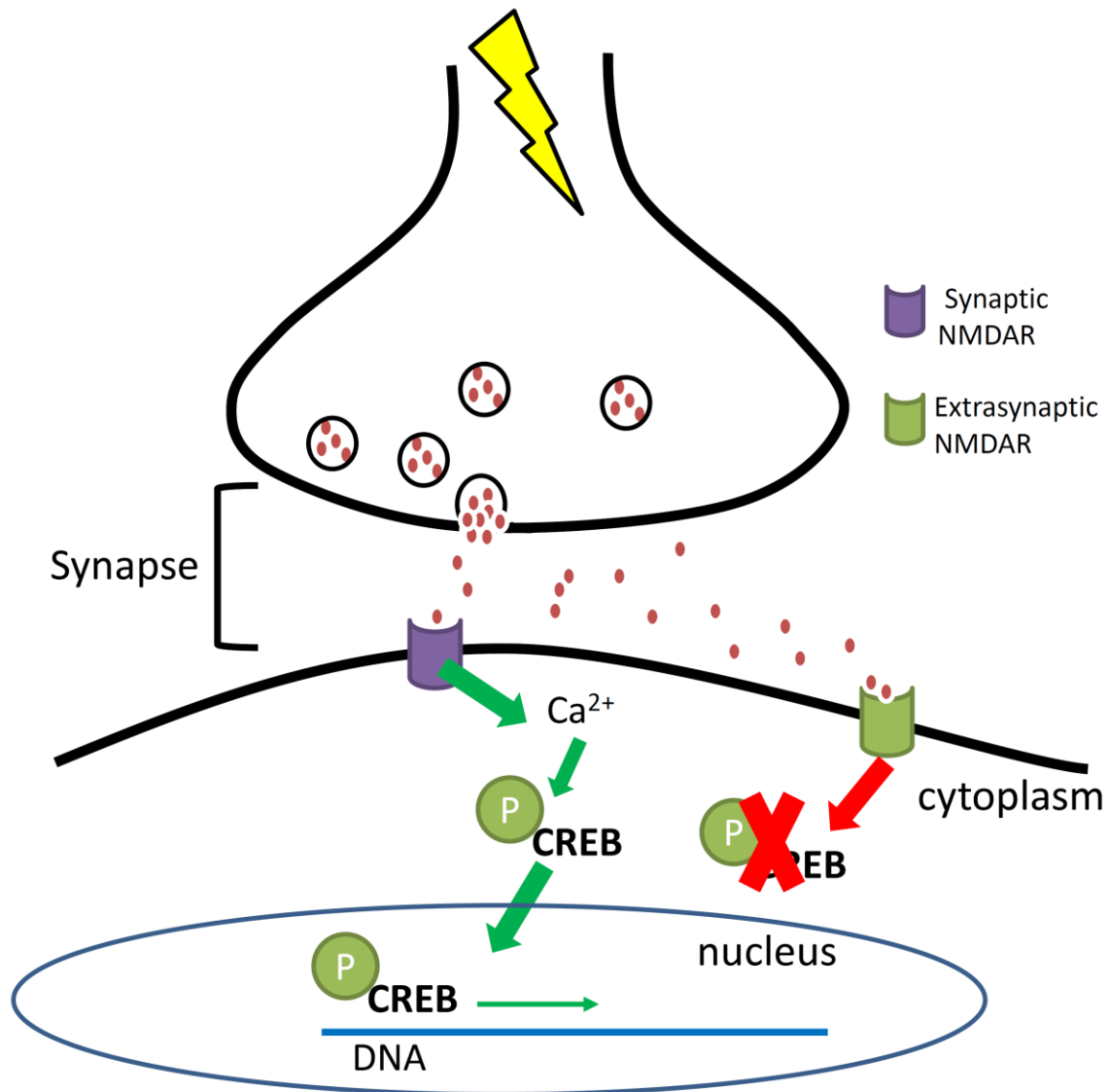


Figure 3. The synaptic response to glutamate in neurons. The levels of glutamate (red dots) present outside the neuron affect the activation of synaptic (low levels) or extrasynaptic (high levels) NMDARs at the cell surface of neurons. At low levels, the activation of synaptic NMDARs results in the phosphorylation of CREB protein through Ca^{2+} entry, pCREB then enters the nucleus and results in the transcription of 185 neuroprotective genes after binding DNA. When excess levels of glutamate are present, extrasynaptic NMDARs outside the synapse become activated, resulting in the shutting off of CREB protein, the deactivation of neuroprotective gene transcription and ultimately cell death.

early stages of disease. In that study, the protein kinase expression in three different brain regions was examined for changes and indeed, kinases involved in a CaMK4 β /CREB pro-survival pathway were increased in the cortical, subcortical, and cerebellar regions. By late stages of disease, this response had diminished and a pro-death signaling pathway was induced.

In Alzheimer's disease, there are experimental models demonstrating that both amyloid β and tau proteins are involved in glutamate signaling events (reviewed in (Rudy et al. 2015)). Not only does oligomeric amyloid β enhance presynaptic glutamate release in hippocampal neurons (Arias, Arrieta & Tapia 1995, Brito-Moreira et al. 2011), it also causes astrocytes in hippocampal slices to release glutamate, which in turn activates excitotoxic signaling in nearby neurons (Pirttimaki et al. 2013, Talantova et al. 2013). The activation of NMDARs also appears linked to tau degradation and death (Amadoro et al. 2006), which can be prevented by blocking the NMDAR2B containing NMDARs (Tackenberg et al. 2013). Studies into the effects of amyloid β peptides on cultured hippocampal neurons also reveal that a neuroprotective response against the peptide can be initiated by increasing synaptic NMDAR activity using EphB2 to phosphorylate CREB (Geng et al. 2013). Additionally, in a GWAS of Alzheimer's disease patients, glutamate signaling was identified as a potential risk factor at the genetic level (Perez-Palma et al. 2014) and could serve as a therapeutic target strategy. A GWAS assessment of CJD patients also revealed aberrant glutamate genes as a risk factor for disease (Sanchez-Juan et al. 2015).

1.9 microRNAs and their role in neurodegenerative disease

When trying to understand the mechanism that leads to neuronal dysfunction and cell death that is triggered by prion replication in the brain, resolving transcriptional alterations, biochemical pathways and the key regulatory molecules involved, is important. A class of post-transcriptional regulators termed microRNA (miR) were identified with far reaching roles in the development of disease. These are a group of noncoding RNAs that are small in size, 18-22 nucleotides, that regulate genes at the post-transcriptional level through RNA silencing machinery and are found in animals, plants, and viruses (reviewed in (Ha, Kim 2014b)). The production, modification, and mode of action of miRs can be found in Figure 4. MiRs are frequently encoded within introns and are therefore often transcribed at the same time as genes, usually on the same strand as the gene (Meunier et al. 2013), although they can be transcribed independently. They are transcribed as a multiple stem loop sequence which is processed by the enzyme DROSHA/DGCR8 to produce 70 bp pre-miRs that are exported from the nucleus by Exportin-5. DICER then chops up the pre-miRs in the cytoplasm to produce a miR duplex, one strand of which is preferentially loaded by Argonaut protein (Ago) into the RNA-induced silencing complex (RISC).

MiRs bind to the 3' or 5' untranslated regions (UTR) or within the coding region of messenger RNA (mRNA) transcripts in the cytoplasm guided by the RISC. Target binding of mRNA is achieved through the seed sequence of miR which is a conserved 6-8 nucleotide sequence located near the 5' end, which is complementary to the target sequence on the mRNA, which is brought into contact by RISC. Once the miR binds target mRNA, protein translation is stopped either through mRNA degradation or steric hindrance. Interestingly, in the CNS of mammals the 3' UTRs of mRNA targets tend to be longer which allows regulation by more than 1 miR, due to increased potential binding sites

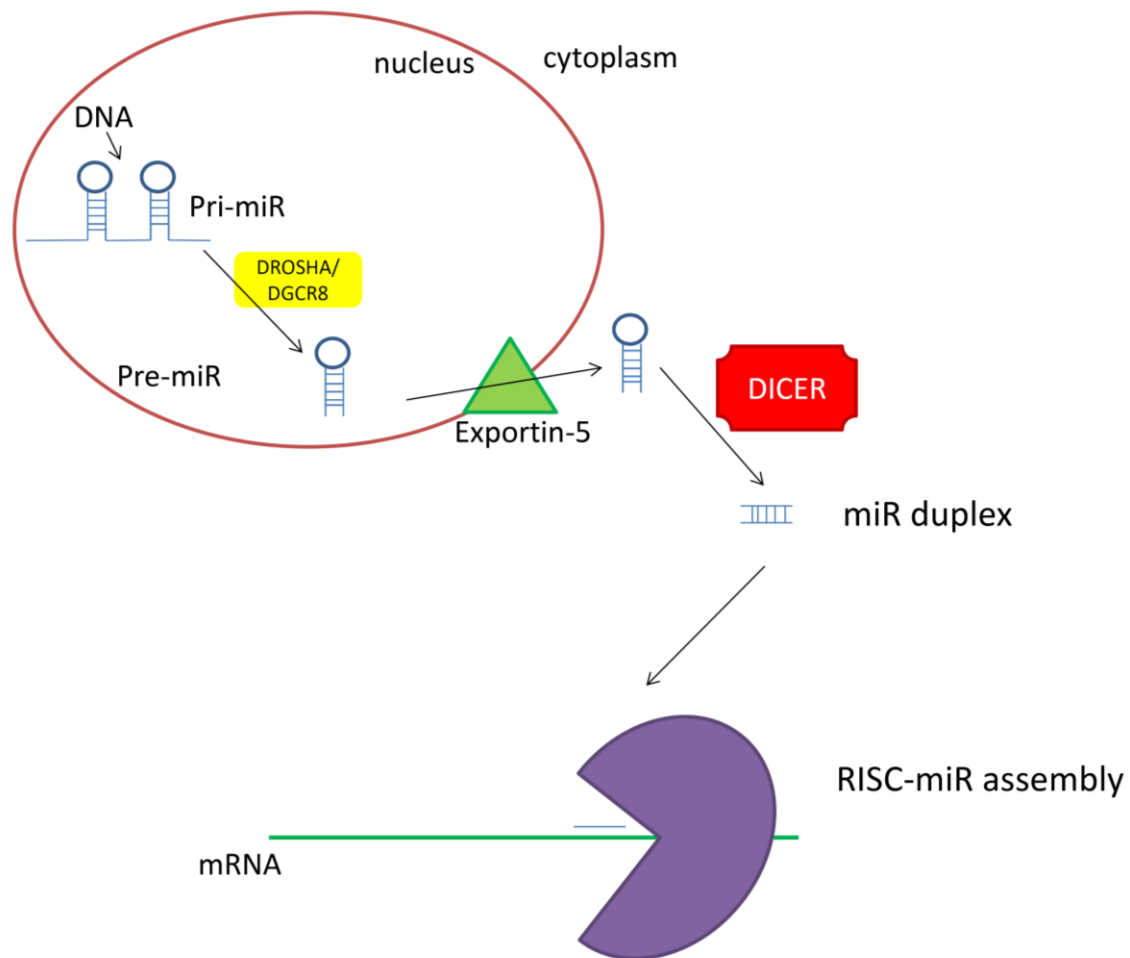


Figure 4. The production of miR from transcription to processing and mode of action. Primary transcripts of miR are transcribed in the nucleus, often at the same time as genes, these are processed by DROSHA/DGCR8 in the nucleus into pri-miR and exported into the cytoplasm by nuclear membrane protein Exportin-5. In the cytoplasm the DICER enzyme processes the stemloop pri-miRs to yield miR duplexes. One strand of the miR is incorporated into the RISC complex which then guides the miR to the mRNA target site, where it binds mRNA at the 3', 5' or CDS to prevent mRNA translation into protein or alternatively the mRNA is degraded.

(Meunier et al. 2013). In addition, different tissue and cell types express varying amounts of miR causing miRs to have different regulatory capacities within different tissues. Furthermore, the mammalian CNS, over other tissues, contains a particularly rich selection of miRs; over 70% of all identified miRs are expressed in the brain (Adlakha, Saini 2014).

1.9.1 miR-128-3p

One important miR in neurodegenerative disease is miR-128-3p. Human and mouse miR-128-3p, designated hsa-miR-128-3p and mmu-miR-128-3p respectively, have two isoforms that arise from two independent chromosomal locations and genes (Cunningham et al. 2015) (Figure 5). These miR isoforms were previously designated mir-128-1 and mir-128-2 (Hsu et al. 2006) but they both result in the same mature sequence and were renamed miR-128-3p (Landgraf et al. 2007). It is important to note that the isoforms have differing tissue expression patterns. While mir-128-1 is found in the respiratory system and nervous system, mir-128-2 is found predominantly in the nervous system (Smith et al. 2014). Also, miR-128-1 is located in the R3H domain containing 1 (*R3HDM1*) gene while mir-128-2 is located in the intron of cyclic adenosine monophosphate-regulated phosphoprotein (*ARPP21*), also called the regulator of calmodulin signaling (Lin et al. 2011).

1.9.2 miR-128-3p role in Central Nervous System

The CNS cell type specificity of miR-128-3p indicates that it is more highly expressed in neurons than astrocytes (Smirnova et al. 2005) and that it is present in the neuronal synapses of rodents (Pichardo-Casas et al. 2012). Tan and colleagues (2013b) performed a miR-128-3p knockdown study in mice and found that 100% knockdown is developmentally fatal. They also discovered that miR-128-2 is responsible for 80% CNS

A)

```

hsa-miR-128-3p      UCACAGUGAACCGGUCUCUUU
mmu-miR-128-3p    UCACAGUGAACCGGUCUCUUU
                    *****

```

B)

```

hsa-mir-128-1      UGAGCUGUUGGAUUCGGGGCCGUAGCACUGUCUGAGAGGUUUACAUUUCUCACAGUGAAC
mmu-mir-128-1    -----GUUGGAUUCGGGGCCGUAGCACUGUCUGAGAGGUUUACAUUUCUCACAGUGAAC
                    *****

hsa-mir-128-1      CGGUCUCUUUUUCAGCUGCUUC
mmu-mir-128-1    CGGUCUCUUUUUCAGC-----
                    *****

```

C)

```

hsa-mir-128-2      UGUGCAGUGGGAAGGGGGCCGAUACACUGUACGAGAGUGAGUAGCAGGUCUCACAGUGA
mmu-mir-128-2    ----CAGUGGGAAGGGGGCCGAUGCACUGUAAGAGAGUGAGUAGCAGGUCUCACAGUGA
                    *****

hsa-mir-128-2      ACCGGUCUCUUUCCCUACUGUGUC
mmu-mir-128-2    ACCGGUCUCUUUCCCUACUG-----
                    *****

```

Figure 5. Mature and Primary microRNA-128-3p sequences. A) mature human, hsa-miR-128-3p, and mouse (red), mmu-miR-128-3p, sequence B) miR-128-1 primary transcript for humans and mice (red) C) miR-128-2 primary transcript sequence for humans and mice (red). Differences between sequences are underlined. Adapted from miRBase (Kozomara, Griffiths-Jones 2014) and sequences were aligned in Clustal Omega (Copyright © EMBL-EBI 2017).

expression while miR-128-1 is responsible for the remaining 20%. The authors found that miR-128-1 knockdown had no discernible effect on mice while miR-128-2 knockdown resulted in fatal seizures with death occurring at 2-3 months post-natally. This was true for miR-128-2 whole body knockdown or selective forebrain CAMK2 α neuron knockdown, where CAMK2 α is found in glutamate receptor containing neurons.

The specific knockdown of miR-128-2 in forebrain D1 dopamine neurons increased survival from 2-3 months to 5 months. Interestingly, lethality due to miR-128-2 knockdown was abolished by the administration of the anticonvulsant drug, Valproate, or by the re-introduction of miR-128-3p. The neurons that were cultured from the forebrains of these knockdown mice displayed an increase in excitability (McSweeney et al. 2016).

In other studies, the overexpression of miR-128-3p has been established as important in the proliferation of neural progenitor cells into neurons in the cortex with no indication of apoptosis (Zhang et al. 2016). It has also been demonstrated as important in the migration of cortical neurons during brain development (Franzoni et al. 2015). In addition, when miR-128-3p is increased in pluripotent stem cells or immortalized neurons, it results in their differentiation into mature neurons (Guidi et al. 2010, Zare et al. 2015).

Another CNS role for miR-128-2 was found in fear extinction memory formation in rodents. The levels of miR-128-2 were increased in the infralimbic prefrontal cortices of mice when fear extinction memory was formed (Lin et al. 2011). When certain aspects of the fear extinction pathway were blocked, there was no increase in miR-128-2 expression and fear extinction memories did not form when miR-128-2 was blocked using lentiviral expression vectors. These authors also discovered that miR-128-2 was higher during adulthood in mice and through the use of Luciferase reporter assays found genes associated with fear extinction plasticity were targeted by miR-128-2.

There are a few reported gene targets for miR-128-3p in neuronal cells. These include Reelin which has been demonstrated as regulated by PrP^C (Devanathan et al. 2010) and doublecortin (*DCX*) (Evangelisti et al. 2009). Other neuron specific targets remain to be identified.

1.9.3 miR-128-3p involvement in CNS neurodegenerative disease

A number of studies have indicated that miR-128-3p has an association with neurodegenerative diseases due to its deregulation in the CNS during disease. The evidence includes prion disease (Saba et al. 2008, Montag et al. 2009), Alzheimer's disease (Lukiw 2007, Alexandrov et al. 2012, Muller et al. 2014, Chen et al. 2016a), and Huntington's disease (Kocerha et al. 2014, Marti et al. 2010, Lee et al. 2011) (Table 5).

In prion disease, miR-128-3p is upregulated in whole brain homogenate at end stages of prion disease in 22A scrapie infected mice (Saba et al. 2008) and at end stages in the basis pontis region in BSE infected cynomolgus macaques (Montag et al. 2009). In Alzheimer's disease, miR-128-3p upregulation is seen in hippocampal homogenate (Lukiw 2007) in addition to neocortical extracellular fluid and cerebrospinal fluid of patients close to the end stages of disease (Alexandrov et al. 2012). A distinction between subtypes of Alzheimer's disease revealed differences in miR-128-3p levels in the hippocampus between Braak III/IV patients and Braak VI patients (Muller et al. 2014). The Braak staging refers to the regions where neurofibrillary tau tangles have spread. In Braak III/IV patients where the tangles are limited to the hippocampal area, the upregulation of miR-128-3p in the hippocampus was detected. Whereas Braak VI patients have hippocampal and cortical spread of tau tangles, and miR-128-3p was downregulated in the hippocampus.

Table 5. Specifics for miR-128-3p deregulation in the CNS neurodegenerative conditions. The disease, species and strain, tissue sampled, temporal characteristics and references are indicated, EP= endpoint, CSF= Cerebrospinal fluid. Unless otherwise specified the homogenates of tissues were sampled for miR-128-3p.

| Disease | Species and model | Tissue sampled | Temporal characteristics | References |
|------------------|------------------------------|------------------------|---------------------------------|----------------------------------|
| Prion | Mouse 22A | Whole brain | ↑ EP | (Saba et al. 2008) |
| | scrapie Macaque, BSE | Basal pons | ↑ EP | (Montag et al. 2009) |
| Alzheimer's | Human | Hippocampus | ↑ EP | (Lukiw 2007, Muller et al. 2014) |
| | Human | Hippocampus | ↓ EP | (Muller et al. 2014) |
| | Human | CSF | ↑ EP | (Alexandrov et al. 2012) |
| | Human | Extracellular fluid | ↑ EP | (Alexandrov et al. 2012) |
| | Mouse, amyloid β | Hippocampus | ↑ adult | (Chen et al. 2016a) |
| Huntington's | Human | Forebrain and striatum | ↓ EP | (Marti et al. 2010) |
| | Primate | Forebrain | ↓ embryonic | (Kocerha et al. 2014) |
| | Mouse, YAC128 and R6/2 | Striatum | ↓ adult | (Lee et al. 2011) |
| Parkinson's-like | Mouse | Whole brain | ↓ EP | (Tan et al. 2013a) |

In Huntington's disease, miR-128-3p has been examined in human patients (Marti et al. 2010), mouse models (Lee et al. 2011) and a non-human primate model (Kocerha et al. 2014). In these, the miR-128-3p was decreased in the cortex or striatum or both. In the non-human primate model, pre-natal brain tissues yielded evidence that miR-128-3p was downregulated in the CNS early after the zygote was formed and this downregulation persisted postnatally. In humans, miR-128-3p was also decreased in the cortex and striatum of patients at post-mortem (Marti et al. 2010), while two different mouse models demonstrated a decrease at adulthood (Lee et al. 2011).

The brain contains many different cell types while neuronal cells have traditionally accounted for 10% of the brain, which varies widely dependent on subregions (Herculano-Houzel, Lent 2005), thus the cell specificity of miR-128-3p deregulation in the brain homogenates from the neurodegenerative diseases was not isolated to neurons specifically. Also, the samples for prion and Alzheimer's disease were obtained at end stages of disease, where potential therapeutic intervention is limited due to the advanced stage of disease. Therefore, insight into miR-128-3p beginning from early stages of disease in an animal model and in a neuronal specific manner may help determine if therapeutic potential exists. Indeed, if miR-128-3p is deregulated at early stages and in neurons specifically, its modulation could serve to reverse synapse loss at early stages of disease to alleviate symptoms of disease and potentially lengthen survival.

The miR-128-3p validated target, Reelin, is found at decreased levels in the cortex of Alzheimer's disease patients at early stages of disease and in the hippocampi of Alzheimer's disease mouse models (Herring et al. 2012). The mGluR5 gene, *GRM5*, was also reported as a target by luciferase reporter assay (Kocerha et al. 2014) whose association with neurodegenerative disease was described in previous sections and is also

a factor in Huntington's disease. In addition, *DCX* mediated behavioural impairment by miR-128-3p in the hippocampus of mice was demonstrated in a water maze learning paradigm (Chen et al. 2016b). These authors also showed that this behavior was impaired in mice that were infused with amyloid β . The amyloid β infusion resulted in the increase of miR-128-3p and concurrent decrease in *DCX*, suggesting a link to Alzheimer's disease. These data together imply a potential role for miR-128-3p during the development of neurodegenerative disease, given the well-documented deregulation of miR-128-3p and a number of its neuronally enriched targets.

1.10 Use of Laser Capture Microdissection as a means of isolating neuron specific miR-128-3p deregulation *in vivo*

In order to capture a neuronal population from the hippocampus to profile miR-128-3p during RML scrapie prion infection *in vivo*, CA1 neuronal cell bodies can be isolated using laser capture microdissection (LCM). In this method, the tissue is first sectioned and subsequently stained in order to visually detect the distinct CA1 neuronal cell bodies, which are then captured using laser and infrared coupled to a computer. From these source cells, total RNA is extracted and analyzed before using Reverse transcription quantitative Polymerase Chain Reaction (RT-qPCR) to determine levels of miR abundance. Indeed, the same RNA that was used for the previously published work was available to be probed for miR-128-3p levels (Majer et al. 2012). The use of LCM provides distinct advantages over other methods in that it preserves the physical location of the neuronal cell bodies and it enables selection of specific sub regions compared to a cell sorting method, in which microdissection and fluorescent labeling of neurons must take place (reviewed in (Poulin et al. 2016)). The use of LCM on brain sections obtained from the early to late stages of

RML scrapie prion infected and mock infected mice can facilitate miR-128-3p characterization of the CA1 neuronal cell bodies during a neurodegenerative disease.

1.11 miR Target prediction and validation

In mammals, miRs have a vast number of potential targets due to partial complementarity in 5' seed sequence binding to the 3' UTR target binding site through the RISC (Bartel 2009). This allows miRs to have predicted binding sites in the hundreds which results in a high number of targets to examine on a case by case basis. On top of the sheer abundance of potential mRNA targets, different tissue types express different levels and families of miRs, which adds to the complexity of determining relevant mRNA targets to test experimentally. One approach in tackling the number of mRNA targets to validate is to study predicted binding sites using algorithms which examine the binding of the 5' miR seed sequence to the 3' UTR of mRNA target transcripts and relate them to the cell type of interest and disease state. Three popular algorithms, TargetScan, miRanda, and RNA22, use sequences compiled in the University of Santa Cruz (UCSC) and National Center for Biotechnology Information (NCBI) Ensembl databases to determine 3' UTRs to match against the miR seed sequence. These three algorithms have strengths and limitations in that they have varying amounts of overlap in predicted mRNA targets (Ritchie, Flamant & Rasko 2009). TargetScan is the most stringent when compared to miRanda and RNA22.

TargetScan (Lewis, Burge & Bartel 2005) is a filtering algorithm that examines the miR seed sequence commencing at nucleotide 2 against 3' UTRs of target genes using 6, 7, and 8mer base matching. The target sequences for version 7 are obtained from the NCBI Ensembl database. The predicted 3' UTRs are given a context score which is based on 14

parameters some of which include site type, supplementary pairing, minimum distance, 3' UTR length, target site abundance, seed-pairing stability, and probability of conserved targeting, the full list can be found in (Agarwal et al. 2015). The output of targets is canonical, 100% seed sequence matching is required for a target hit from the 6, 7, and 8mer, and TargetScan is conservative in that it does not permit mismatches between the 5' miR seed sequence and the target 3' UTR. The algorithm does take thermodynamic stability of miR-mRNA interaction into account as well as conservation between species. The free energy (ΔG) is calculated using the RNAfold algorithm (Lorenz et al. 2011). TargetScan possesses the limitation that it does not examine the expression levels of the mRNA in a tissue specific manner, nor does it take mRNA secondary structure into account when determining putative targets. Tissue specificity must be examined using other programs such as Database for Annotation, Visualization and Integrated Discovery (DAVID) (Huang da, Sherman & Lempicki 2009b, Huang da, Sherman & Lempicki 2009a). In addition, the targets can be compared to previously generated information from neuronal tissue. For neurons, this includes a dataset that was generated by targeting and isolating Calcium/Calmodulin Dependent Protein Kinase 2 α (CAMK2 α) expressing neurons, where CAMK2 α is specifically present in forebrain glutamate receptor containing neurons (Jones, Huntley & Benson 1994). This dataset was generated by the pull down of total RNA by using High-throughput sequencing of RNA isolated by crosslinking immunoprecipitation (HITS-CLIP) with Ago2 protein which loads miR and mRNA onto the RISC. The RNA was explored with next generation sequencing to generate a gene list, which was matched to the seed sequence of miR-128-3p for active targets. In this way, the predicted targets from TargetScan, which is currently the most updated algorithm publicly

available when compared to miRanda and RNA22, can be examined for neuronal cell specificity.

The miRanda algorithm (Enright et al. 2003) differs from TargetScan in that it permits mismatches when comparing seed sequence to mRNA target which ultimately increases the number of targets that are predicted. However, there is a lower stringency within the miRanda algorithm that can be modified by the end user to change cutoff for the alignment scores and the free energy. The miRanda algorithm has similar limitations to TargetScan in that it does not permit inclusion of tissue specific expression nor does it take RNA secondary structure into account.

The RNA22 algorithm (Miranda et al. 2006, Loher, Rigoutsos 2012) is unique in that it allows G bulges which is an extra G base at positions 5 and 6 of the miR seed sequence (Chi, Hannon & Darnell 2012), and G:U wobbles within the seed region when matching miR with the target sequence. Another distinction is that RNA22 predicts targets outside the 3' UTR including 5' UTR and coding DNA sequence (CDS) which have been discovered to contain miR binding sites (Lytle, Yario & Steitz 2007, Duursma et al. 2008, Lal et al. 2008, Tay et al. 2008, Krishnan et al. 2013). The RNA22 algorithm has a high signal-to-noise capacity (Ritchie, Flamant & Rasko 2009, Hammell et al. 2008) and uses the pattern based teiresias algorithm (Rigoutsos, Floratos 1998) to discover targets. Ultimately, these features produce a much larger list of predicted sites than do miRanda or TargetScan algorithms, which makes narrowing targets to validate challenging.

For this study, it was decided that the conservative TargetScan algorithm was ideal and sufficient in determining targets for miR-128-3p. The number of false positives would be lower using this algorithm due to the high stringency in binding site prediction restricted to the 3' UTR. Additionally, protein changes due to miR regulation are more likely to be

detected through experimentation when the binding sites are contained with the 3' UTR as opposed to the 5' or CDS binding sites (Baek et al. 2008). As protein targets were later to be explored, the 3' UTR targets were of interest to identify. After a list of predicted sites is established, those that are of relevance to the hypothesis at hand can be validated using a Luciferase reporter assay.

The Luciferase reporter assay is widely used to determine whether a miR binds to the 3' UTR of a gene (Kocerha et al. 2014, Saba et al. 2008, Taganov et al. 2006). The plasmid reporter contains a gene encoding luciferase (reporter) and the 3' UTR of the gene of interest is cloned in after it. Luciferase is an oxidative enzyme that can cleave the substrate luciferin to produce the bioluminescent product of light, which can be quantified using a luminometer (Figure 6A). In the miR binding assay, the reporter construct is co-transfected with the miR of interest (Figure 6B) or a scrambled miR, which has been tested and does not bind mammalian mRNA targets. If the miR binds to the 3' UTR of the mRNA, then translation of the luciferase gene is inhibited reducing luciferase activity which is detected by diminished light production when luciferin substrate is added. In this way, binding of miR to the mRNA of interest can be determined and the luciferase reporter assay is a useful tool in screening potential targets.

1.12 Synaptic Loss and miR detection in Prion Disease

Synapses form the functional communication units between two neurons and comprise presynaptic and postsynaptic membranes separated by a synaptic cleft. Both regions contain specific molecules that facilitate synapse formation and the propagation of signals between neurons. In neurodegenerative disease, one of the earliest manifestations of disease is the loss of synapses both in prion disease (reviewed in (Mallucci 2009)) and

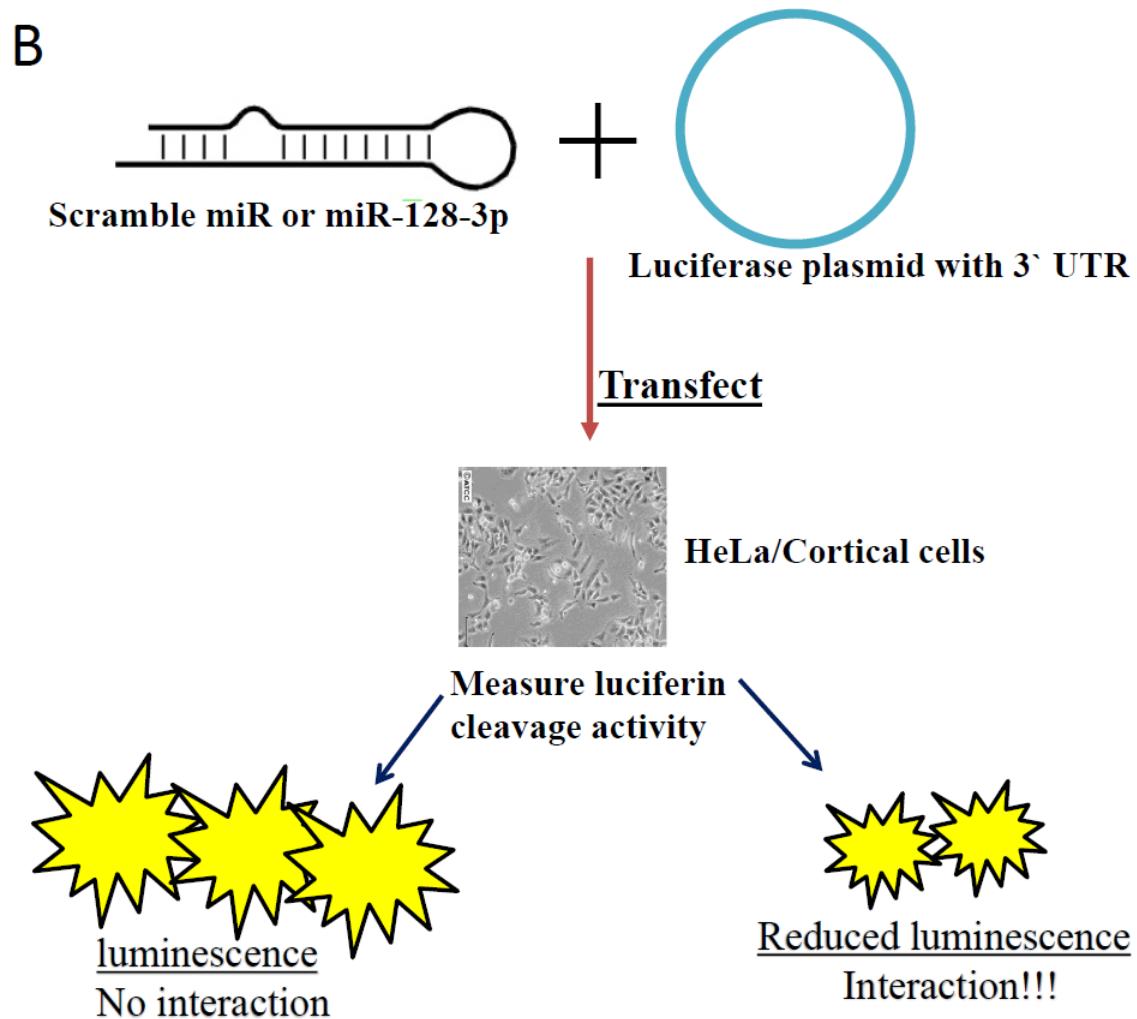


Figure 6. The Luciferase Reporter Assay for miR binding to 3' UTR. A) Luciferin cleavage by Luciferase enzyme in the presence of oxygen (O₂) and Adenosine triphosphate (ATP) to yield oxyluciferin, adenosine monophosphate (AMP), carbon dioxide (CO₂) diphosphate, (PP_i) and light which is measured by a luminometer. B) Luciferase reporter assay to determine miR binding to 3' UTR target, where a luciferase reporter plasmid and scramble miR or miR-128-3p are co-transfected into HeLa or Cortical cells and luciferase activity is measured by detecting light output after luciferin substrate is added. If an interaction between the 3' UTR and miR exists, there will be decreased light production due to the block in luciferase protein translation.

Alzheimer's disease (Naslund et al. 2000), which results in behavioural symptoms. The loss of presynaptic terminals of CA1 neurons during ME7 scrapie infection was determined using immuno-staining to reveal decreasing amounts of synaptophysin, a protein used as a marker for presynaptic terminals (Cunningham et al. 2003). Notably, turning off the expression of neuronal PrP^C during the preclinical stage of RML scrapie in a mouse model was shown to delay the onset of neurological signs and to reverse synapse loss (Mallucci et al. 2007). This suggests that targeting prion replication and neurotoxicity specifically at synapses is a potential strategy to treat prion disease.

However, since the effects of PrP^C knockdown in humans is unknown, strategies for synapse rescue may represent a supportive strategy for treatment. This is an area where the application of miRs, or their inhibitors, could be beneficial as studies suggest they play a significant role in synapse remodeling.

Many miRs are enriched at the neuronal synapse, both at the presynaptic and post-synaptic terminals (Kye et al. 2007, Lugli et al. 2008, Siegert et al. 2015, Nesler et al. 2016, Kos et al. 2016) (Figure 7). Specific functions for some of these have been defined with some of the most well characterized being the involvement of miR-132, miR-134, and miR-138 in the regulation of dendrite formation (reviewed in (Bicker et al. 2014)). Additionally, examinations into the synaptic compartment of various brain regions of the rat have revealed a set of 31 miRs that are specific to neuronal synapses regardless of brain area (Pichardo-Casas et al. 2012). Indeed, some of these miRs are exclusive to the hippocampal synapse such as miR-324-5p. Supporting evidence that miRs are directly involved in the regulation of protein translation at the synapse is the presence of the miR regulation machinery (Lugli et al. 2008, Lugli et al. 2005).

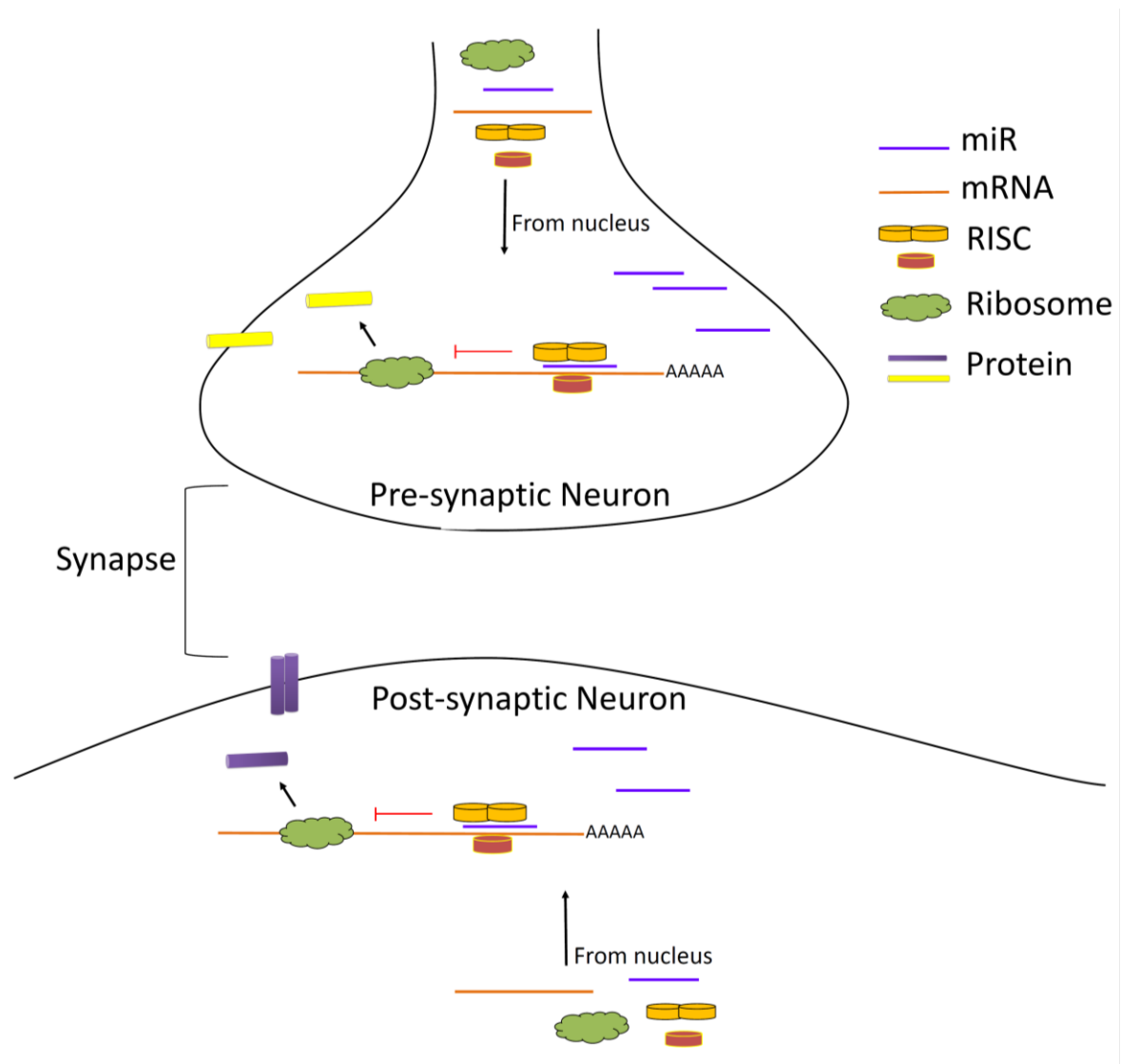


Figure 7. The neuronal synapse contains miRs, mRNA, RISC complex proteins, ribosomes, and protein. The presence of the protein translation machinery at the pre- and post-synapse indicates local activity dependent rapid protein translation which is governed at least in part by miRs. The changes in miRs due to neurodegenerative disease and its alteration of protein translation is currently unknown.

Although many insights have been gained into the regulation of miRs in the synapses of wild-type animals, not many studies have directly examined changes to the miR complement during a neurodegenerative disease state. The established protocol devised by Verity (Verity 1972) allows the preparation of purified synaptoneurosomes by exploiting features which allow synapses to be isolated using high centrifugation speeds in a Ficoll gradient. Previous studies have isolated total RNA from this layer and determined both miR and transcript levels in wild-type rodents (Pichardo-Casas et al. 2012, Saba et al. 2012).

Although the procedure is relatively straight forward, its application in understanding the role of synaptic miRs in neurodegenerative disease have been virtually non-existent. Some data has been reported previously describing the transcripts (Williams et al. 2009) and proteins (Reddy et al. 2005) altered in synaptoneurosomes prepared from post mortem brain tissue of Alzheimer's patients, however no miR studies have been published. One issue with the interpretation of these results is that after death, the profiles of molecules active at the neuron are likely compromised and neuronal death is rampant. In addition, the study of early disease processes and physiological changes that protect or repair synapses, are likely not at play at such late stages of disease. Therefore, examining altered miRs in the RML scrapie prion mouse model could provide information for miR therapeutic potential at early stages of disease.

1.13 Protein target determination strategies

To truly understand the regulatory capacity of miRs, proving downstream protein regulation by miRs is important to demonstrate functional effects in the biological setting. There are a few strategies to elucidate the potential impact of miRs on protein translation.

The manipulation of miR by gain of function or loss of function in cultured primary neurons is the most frequently used method to determine downstream effects, which can be detected by global proteome analysis (reviewed in (Steinkraus, Toegel & Fulga 2016)).

The main methods to experimentally increase or decrease miR levels in neurons, is via expression plasmids or miR oligonucleotides. The plasmid based expression system can be introduced by direct transfection, or by using viral particles such as lentiviruses which integrate the miR sequence into the host DNA (Jovicic et al. 2013). Visualization of delivery efficiency can be performed by co-expression of a fluorescent marker gene such as green fluorescent protein (GFP). However, the miR copy number cannot be controlled and it can take time before the miR reaches sufficient levels for the experiment. Another issue is that both miR strands will be expressed at equivalent levels, i.e. miR-128-3p (target) and miR-128-5p, therefore the functional effects attributable to miR-128-3p alone cannot be isolated.

A different strategy is to use miR oligonucleotides (pre-miRs), which are double-stranded and similar to short interfering RNA (siRNA) but employ chemical modifications such that the antisense strand is targeted for degradation. These represent the mature miR sequence, which is desired when multiple primary miR isoforms exist, as is the case for miR-128-3p. Furthermore, the transfection efficiency of small RNAs is high in primary neurons (Tonges et al. 2006) and the miR concentration delivered to cells can be controlled. In addition, there are number of mimics available that contain modifications such as LNA to render the molecules more stable.

For loss of function experiments, the inhibition of miR can be achieved using plasmids that express inhibitors of miR including miR sponges (Ebert, Neilson & Sharp

2007) or tough decoys TuDs (Haraguchi, Ozaki & Iba 2009). The miR sponges are plasmids that express sequences with multiple target sites for the miR of interest and once bound, removes miR activity. The TuDs are plasmids that are designed such that they possess stem loops in their RNA secondary structure which improves miR binding efficiency over sponges (reviewed in (Steinkraus, Toegel & Fulga 2016)). Although the elimination of miRs is high using these plasmid-based methods, the caveats are the same as for the gain of function experiments in that levels cannot be controlled, transfection/transduction efficiency can be low, and the neurons may not withstand the cellular disruption over a prolonged period. In addition, the genetic design of binding sites in sponges or TuDs can be problematic because the sites are based on prediction which contains false positives and negatives (Rajewsky 2006).

For this reason, the use of antisense oligonucleotides (or anti-miRs) can be advantageous. Similar to the pre-miRs, they are double-stranded inhibitors but they are 100% complementary to the mature miR sequence of interest, negating the need for complex seed sequence design (Boutla, Delidakis & Tabler 2003). The anti-miRs have been used successfully in primary hippocampal neurons to downregulate mRNA targets (Saba et al. 2012) and can be used *in vivo* to target the CNS (Krutzfeldt et al. 2007). Ultimately, the benefits of oligonucleotide based pre-miRs and anti-miRs outweigh their plasmid counterparts for miR manipulation in primary neurons for determining functional protein effects.

The study of protein regulation by miR is currently an emerging field, especially for neurons. There are reports of miRs directly targeting specific proteins as detected using Western blots (Chen et al. 2016a, Mao et al. 2017), however this method requires the existence of specific antibodies for the protein of interest. Mass spectrometry for global

proteome profiling is a useful approach in multiplex experiments where there are a number of controls and treatments, and can detect thousands of proteins in one run. The stable isotope labeling with amino acids in cell culture (SILAC) mass spectrometry labeling method has detected small but significant protein shifts in miR gain of function studies in immortalized cell lines such as HeLa (Baek et al. 2008) and glioblastoma (Yang et al. 2015). SILAC incorporates heavy isotope amino acids into the cell from surrounding specialized media, which are then added to synthesized proteins after experimental manipulation (Ong et al. 2002). However, the SILAC method does not allow for multiplexing beyond 3 samples. Instead, post experimental isobaric labeling using tandem mass tags (TMT) allows multiplexing of many samples to determine differential protein levels across replicates and experimental conditions (Thompson et al. 2003). The TMT methodology consists of reporter ions within each label which are released during mass spectrometry, quantitating peptide and hence protein levels across labeled treatments.

The increasing or knockdown of a miR within the cell of interest and the direct examination of mRNA targets can help improve the likelihood that the miR will have an effect on protein translation. To this end, those mRNA targets that have 3' UTR binding sites for miR tend to demonstrate quantitative protein changes detectable by mass spectrometry compared to those in the CDS (Baek et al. 2008). Therefore, it is useful to first identify changes at the mRNA level by miR manipulation before continuing with costly mass spectrometry based protein detection. The use of mass spectrometry allows the detection of a wide range of proteins that could form pathways of target mRNA if the target itself is not directly captured in the sampling timeframe. The down-side of using mass spectrometry is that the technology is not as advanced for this purpose and there are a number of aspects of the technology that still require optimization. One of these is that the

sensitivity of the method is relatively low, therefore low copy number proteins that are often the targets of miRs are often below detectable levels. In addition, reference methodology to assign protein IDs to the detected proteins is relatively unsophisticated meaning that a peptide may be wrongly assigned as a different protein product.

However, this approach in knocking down or increasing miR-128-3p in primary hippocampal neurons coupled with mRNA detection of target genes is useful as a first step in identifying proteome changes. After establishing that mRNA changes result from the modulation of miR-128-3p levels in the cultured neurons, the global proteome can be examined using TMT labelled peptides in a quantitative mass spectrometry experiment.

2. Hypothesis and Objectives

2.1 Overall Hypothesis

MiR-128-3p regulates gene targets that are vital for proper synaptic function and is deregulated at early stages of prion induced neurodegeneration, when synaptic dysfunction and dendrite remodeling are apparent in RML scrapie prion infected mice.

2.2 Objectives

- 1) Characterize miR-128-3p levels in the CA1 neuronal cell bodies during RML scrapie prion infection in CD1 mice.
- 2) Determine miR-128-3p gene targets through computational prediction and target validation.
- 3) Characterize miR-128-3p in the synapses of the hippocampus and forebrain during early stages of RML scrapie prion infection in mice.
- 4) Examine miR-128-3p in glutamate signaling pathways in cultured hippocampal neurons.
- 5) Obtain functional protein targets using gain of function/loss of function of miR-128-3p in cultured hippocampal neurons using mass spectrometry.

3. Methods

3.1 Ethics statement

All animals used in this study were approved internally at the Canadian Science Center for Human and Animal Health through the Animal Care Committee, which follows guidelines set forth by the Canadian Council on Animal Care whose mandate it is to minimize the number of and the discomfort experienced by laboratory animals used in experimental procedures. The animal use documents (AUD) approved for use include H-08-009, H-08-012, and H11-020 for the RML scrapie prion mouse models, and for primary hippocampal culture, AUDs H11-020, H12-016, and H15-032.

3.2 RML scrapie Mouse Model

The RML scrapie mouse model used in these experiments was produced by an intraperitoneal injection of 1% brain homogenate into mice. Specifically, 200 μ L of either 1) mock infected brain homogenate from mice injected with phosphate buffered saline (PBS) control or 2) RML infected brain homogenate was injected into the peritoneal cavity of 4-6 week old female CD1 mice. For LCM experiments, mice were sacrificed and brains were then collected at the following timepoints post-infection during asymptomatic disease consisting of 70 days post infection (dpi), 90 dpi, and 110 dpi, and at the onset of subtle clinical signs at 130 dpi in addition to disease endpoint (EP), which was 177 +/- 11 dpi. For synaptoneurosome isolations, the brains were collected at two timepoints, a preclinical stage of 105 dpi and a clinical stage of 165 dpi.

3.3 LCM mediated isolation of neuronal cell bodies from the CA1 region of the hippocampus and total RNA extraction

At the time of collection, the brains destined for LCM were flash frozen in optimal cutting temperature media (OCT, Sakura Finetech) and maintained at -80°C before processing. Coronal sections of 8 micron thickness were cut using the cryostat and placed onto polyethylene-naphthalate membrane slides (Fisher Scientific) and kept at -80°C for a maximum of 4 weeks before staining with the LCM staining kit (Fisher Scientific). The slides were fixed in 95% ethanol for 30 seconds, followed by 70% ethanol for 30 seconds, and 50% ethanol for 30 seconds and then excess alcohol was removed. The coronal section was outlined with the Barrier pen from the kit before incubating with Cresyl Violet for 40 seconds and excess dye removed by tapping the slide on a Kimwipe. Slides were placed in 50% ethanol for 30 seconds, followed by 70% ethanol for 30 seconds, and 95% ethanol for 30 seconds. The slides were then placed in 100% ethanol for 30 seconds, which was repeated a second time. The final step of the staining was a quick xylene dip before being placed in fresh xylene for 5 minutes, after which the slide was dried at room temperature for 5 minutes.

The LCM was performed with the Arcturus LCM instrument with a laser power of 50-100mW and a maximum of 2 laser pulses to capture neuronal CA1 cell bodies. Total RNA extractions were performed on these cells using the RNAqueous Micro Kit (Fisher Scientific). The films from the LCM caps was removed and submerged in 100 μL lysis buffer for 30 minutes at 42°C . Then, 3 μL of LCM additive was added to the solution, the tube was vortexed and 129 μL of 100% ethanol was added. This mixture was then passed by spinning at 10,000 x g for 1 minute through a micro filter column assembly that was

pre-equilibrated with lysis buffer. One wash with 180 μ L of wash buffer 1 followed by 2 washes with 180 μ L of Wash buffer 2/3 were performed at 10,000 x g for 1 minute with the flow through being discarded. The filter was then dried for 1 minute at 10,000 x g before eluting RNA with 2 rounds of 10 μ L preheated elution solution.

The resulting RNA was stored at -80°C before assessing quantity and quality with the 2100 Bioanalyzer (Agilent) to determine RNA Integrity Number (RIN) with the Pico 6000 kit, as per manufacturer's recommendations. The Bioanalyzer performs an on chip electrophoresis of the RNA using capillary action and compares it to a standard ladder (0.2 kb, 0.5 kb, 1.0kb, 2.0kb, 4.0 kb, and 6.0 kb) using a polymer matrix and fluorescent dyes. For RNA, it puts the ratio of the 2 ribosomal RNA markers (18S and 28S) into an algorithm in order to determine RIN values. Only RNA having RINs of > 5.8 were used for PCR analysis.

3.4 Immunohistochemistry of brain sections for PrP^{Sc} and anti-Ionized calcium binding adaptor molecule 1

For immunohistochemistry, 5 micron coronal sections were obtained from brains fixed in 10% buffered formalin which were paraffin embedded. These were heated overnight at 37°C, followed by deparaffinization and rehydration. The sections were blocked with 2.5% hydrogen peroxide (Fisher Scientific) and treated with 5% ethanol at 35°C for 10 minutes. The antigen retrieval step was performed by adding 10 mM sodium citrate buffer (pH 6) to the slides for 10 minutes at 121°C. The slides were brought to room temperature and for anti-Ionized calcium binding adaptor molecule 1 (IBA-1) detection, a rabbit raised antibody (Wako 019-19741) was used with a final volume of 100 μ L per slide at 1:1,500 in EnVision FLEX antibody diluent (Dako) and incubated at 4°C overnight. The

primary antibody was detected by Klear Mouse Horse Radish Peroxidase (HRP)-Polymer DAB (Golden Bridge International Inc.) as per the manufacturer's instructions. The slides were then counterstained for nuclei using hematoxylin (Surgipath), dehydrated, clarified using xylene (Surgipath) and coverslips were added using Faramount mounting media (Dako).

For the PrP^{Sc} staining, the slides were processed as above, however, after the antigen retrieval step, the sections were treated with 80% formic acid at room temperature for 10 minutes, rinsed with Tris Buffered saline (TBS) with 0.1% Tween-20 (TBS-T), and treated with 4 M guanidine thiocyanate at 4°C for 2 hours to destroy native proteins leaving PrP^{Sc} intact (Doi-Yi, Kitamoto & Tateishi 1991). After rinsing with TBS-T, the sections were incubated overnight at 4°C with rabbit anti-PrP^C antibody (Abcam EP1802Y). They were processed as the IBA-1 sections above. Images for both IBA-1 and PrP^{Sc} were obtained with the MIRAX scanner.

3.5 Immunofluorescence of brain sections with Fluoro-Jade C and for Glial

Fibrillary Acidic Protein

The slides were processed as for IBA-1 mentioned previously and then diverged after the antigen retrieval step. The sections were blocked in 5% normal goat serum (Dako) at room temperature for 1 hour. For Glial Fibrillary Acidic Protein (GFAP) detection, a rabbit antibody was used (Abcam 7260), at 1:500 with an overnight incubation at 4°C. The slides were rinsed in TBS-T and then incubated with secondary antibody, AlexaFluor 594 anti-rabbit (Fisher Scientific) at 1:1,000 for 1 hour at room temperature. For counterstaining of nuclei, 4', 6-diamidino-2-phenylindole (DAPI) was used at 1:1,000 and incubated at room temperature for 20 minutes. The slides were then rinsed with water,

dehydrated, clarified, and then mounted with coverslips using DPX Mountant (Sigma-Aldrich) which is composed of distyrene, plasticizer, and xylene.

For the detection of degenerating neurons, Fluoro-Jade C (Millipore) was used after the antigen retrieval step by incubating the sections in the solution at room temperature for 30 minutes. After rinsing with water, the sections were mounted with the DPX mountant. Images for both the GFAP and Fluoro-Jade C slides were obtained with the MIRAX scanner.

3.6 RT-qPCR with miR TaqMan probe assays

RNA from cell bodies micro-dissected from the CA1 regions of 3-4 mice were pooled and 1 ng of RNA in 7 μ L nuclease free water plus 4 μ L of ¼ diluted 5X miR RT primer was used for each multiplex RT reaction. For the RT step, 0.15 μ L of 100 mM dNTPs, 1 μ L of MultiScribe Reverse Transcriptase, 1.5 μ L of 10X RT buffer, 0.19 μ L of RNase inhibitor, plus 3.16 μ L nuclease free water was prepared per sample in a master mix. The copy DNA (cDNA) was produced in a thermal cycler, the run was 30 minutes at 16°C, 30 minutes at 42°C, 5 minutes at 85°C followed by a hold at 4°C before proceeding to the qPCR stage.

The qPCR was performed by mixing 1.33 μ L of cDNA produced from the RT step with 1 μ L miR TaqMan probe, 10 μ L TaqMan Universal PCR Master Mix II with no AmpErase UNG, and 7.67 μ L nuclease free water. These were done in triplicate wells per sample and made as a 4X master mix. The samples were loaded into a 96 well optical plate (Fisher Scientific) with a final volume of 20 μ L per well, sealed with optical film (Fisher Scientific), and spun in a centrifuge at 1200 rpm for 2 minutes before loading into the ABI 7900HT with the following run conditions: 95°C for 10 minutes followed by 40 cycles of

95°C for 15 seconds and 60°C for 1 minute. The resulting data was subject to automatic threshold and baseline settings to obtain Cts in RQ Manager, which were then analyzed in Microsoft Excel to obtain fold changes using the delta delta Ct method.

3.7 Fold change determination using the delta delta Ct method

The fold change for miRs and later, genes was calculated using the delta delta Ct Method (Livak, Schmittgen 2001). The endogenous reference used to normalize the Cts of the miR or gene of interest was determined by examining the stable expression of different reference genes or small RNAs. The average Ct for each sample was calculated for the gene/miR of interest and the endogenous reference gene/miR. Then, the average of the endogenous reference gene/miR was subtracted from the average of the gene of interest for each sample to obtain delta Ct. This was followed by averaging the delta Cts of the control treatment before subtracting each delta Ct from this average to obtain delta delta Ct. In order to linearize this data and obtain fold changes, each delta delta Ct was transformed by 2 to the power of negative delta delta Ct [$2^{(-\text{delta delta Ct})}$].

3.8 *In silico* prediction of miR-128-3p targets

The TargetScan Human 7.1 algorithm was used to determine both human and mouse 3' UTR targets of miR-128-3p. These lists were then compared using the Gene Venn program (Pirooznia, Nagarajan & Deng 2007) to identify target genes that overlapped in both species. The targets were put through DAVID analysis to examine tissue expression of the targets that were predicted. The overlapping targets were probed for neuronal specificity by comparing to previously published data.

3.9 Experimental Validation of 3' UTR targets using Luciferase Reporter Assay

3.9.1 Luciferase reporter plasmid constructs

The pMirTarget luciferase reporter plasmids containing the human 3' UTR for genes *GRIN2B* (NM_000834) and *GRIN2D* (NM_000836) were purchased from OriGene (Rockville, Madison). The lyophilized plasmids were reconstituted in 100 μ L nuclease free water and kept at -20°C until they were transformed into *Escherichia coli* to produce stock plasmid DNA. The human *GRM5* 3' UTR (NM_000842) was cloned in house into the pmirGLO luciferase reporter plasmid (Promega) using the restriction enzyme sites for SacI and Xho I which were incorporated into the 3' UTR.

3.9.2 3' UTR plasmid stock preparation

Plasmid DNA was mixed with Top 10 chemically competent *E. coli* (Takara Clontech) and incubated on ice for 30 minutes before being chemically transformed at 42°C for 30 seconds, followed by 1 minute on ice before adding 500 μ L prewarmed to 37°C Super Optimal broth with Catabolite repression (SOC). This mixture was then shaken at 300 rpm for 1 hour at 37°C before plating 50 μ L on prewarmed LB agar plates containing 50 μ g/mL carbenicillin and incubating overnight at 37°C. A single colony was then placed into 4 mL of LB broth containing 50 μ g/mL carbenicillin in a 12 mL tube to incubate at 37°C with shaking at 300 rpm. After 8 hours, 100 μ L of the resulting bacterial culture was used to inoculate 100 mL LB broth plus 50 μ g/mL carbenicillin in a 500 mL Erlenmeyer flask. After an overnight incubation at 37°C with 300 rpm shaking, plasmid DNA extraction was performed according to manufacturer's recommendations for the EndoFree Plasmid Maxi Prep kit (Qiagen). The cells were pelleted by centrifuging at 6,000 x g for

15 minutes at 4°C. The supernatant was decanted and the bacterial pellet lysed in 10 mL buffer P1 with vortexing to ensure sufficient lysis. Following this, 10 mL of buffer P2 was added and the tube inverted 6 times to mix, and the mixture was incubated at room temperature for 5 minutes. Then 10 mL of prechilled buffer P3 was added to the tube, inverted 6 times, and immediately placed into the barrel of a capped QIAfilter assembly and incubated for 10 minutes at room temperature. The cap of the QIAfilter was removed and the solution was plunged into a 50 mL conical tube and 2.5 mL of Buffer ER was added followed by inversion 10 times, and a 30 minute incubation on ice. During this time a QIAGEN-tip 500 was assembled and equilibrated with 10 mL Buffer QBT. The filtered lysate was added to the QIAGEN-tip and the flow through discarded. The QIAGEN-tip was then washed twice using a total of 60 mL Buffer QC and DNA eluted in 15 mL Buffer QN. Then 10.5 mL of room temperature isopropanol was added to the eluate to precipitate DNA. After vortexing briefly and centrifuging at 5,000 x g for 1 hour at 4°C, the supernatant was carefully decanted and the DNA pellet was then washed with 5 mL of endotoxin-free 70% ethanol and centrifuged at 5,000 x g for 1 hour at 4°C. The ethanol was decanted and the DNA pellet air dried for 10 minutes before dissolving in 1 mL of endotoxin-free Tris-Ethylenediaminetetraacetic acid (TE) buffer. Plasmids were analyzed using the ND-100 Nanodrop spectrophotometer for quality and quantity before sequence confirmation.

3.9.3 3' UTR Sequence confirmation

Reporter plasmids containing the 3' UTRs of *GRIN2B* and *GRIN2D* were sequenced using forward pMirTarget_F 5' AGAAGCTGCGCGGTGGTGTGTTGTG 3' and reverse pMirTarget_R 5' CTGGAGGATCATCCAGCCGGCGT 3' primers by National

Microbiology Laboratory (NML) DNA Core services. The *GRM5* 3' UTR reporter plasmid was sequenced using forward primer 5' CACAATGGCAAGCATAGTC 3'. The resulting sequences were submitted to Basic Local Alignment Search Tool Nucleotide (BLASTN) searches (Altschul et al. 1990) to confirm the sequence was correct. The *GRIN2B* and *GRIN2D* 3' UTRs were aligned using Lasergene MegAlign to analyze sequence homology (Version 12.0 DNASTAR Madison, WI).

3.9.4 Luciferase Reporter Assay

HeLa cells (CCL-2 ATCC) were maintained in Eagle's Minimum Essential Medium (ATCC) supplemented with 10% heat inactivated Fetal Bovine Serum (Fisher Scientific) in a humidified 37°C incubator with 5% CO₂. The day before transfections took place, cells were plated 10,000 cells/well in a 96 well white walled plate (Costar). Transfections were performed the next day using Effectene (Qiagen) transfection reagent as per manufacturer's recommendations to add 100 ng of 3' UTR Luciferase Reporter plasmid to each well plus either 1) pre-miR-scramble or 2) pre-miR-128-2 and the controls of 3) plasmid only, and 3) cells only. The pre-miR miR precursor molecules were purchased (Fisher Scientific) and consisted of pre-miR-128-2 and pre-miR-negative control 2, a scrambled control sequence. Four concentrations were tested 5 nM, 10 nM, 25 nM, and 50 nM.

After a 24 hour transfection, the Red fluorescent protein (RFP) was read on the plate using the Cy3 filter on the GloMax Multi (Promega). Then half of the media was removed with 75 µL remaining and 75 µL Dual-Glo luciferase reagent (Promega) was added to each well, the plate was mixed for 10 minutes at 100 rpm, and luminescence measurements were obtained.

For the *GRM5* 3' UTR, the luciferase reporter assay was performed in 4 days *in vitro*

(DIV) cortical neurons derived from embryonic 18-20 CD1 mice plated at 50,000 per well. The cells were maintained in NbActiv1 media in a humidified 37°C incubator with 5% CO₂. The transfection protocol was identical to that performed in HeLa cells. After a 48 hour transfection, chemiluminescence was measured for both *Renilla* and Luciferase.

3.9.5 Luciferase Data analysis

The measurements for RFP, *Renilla*, and Luciferase were exported into Microsoft Excel and a series of calculations was performed therein. The cells only background was subtracted, and data was normalized using RFP or *Renilla* values. The normalized luciferase values were then divided by plasmid only. To obtain relative expression, the data was then divided by the scrambled miR values. The resulting relative luciferase expression was graphed as mean and standard error of the mean (SEM). One-tailed t-tests were performed to assess significance at each concentration using a p-value below 0.05 being deemed significant, graphs and t-test calculations were performed in GraphPad Prism 6.0.

3.10 Synaptoneurosome experiments

3.10.1 Synaptoneurosome isolation

Two wild-type CD1 adult mice were used for initial studies to determine the robustness of the procedure. The mice were anaesthetized by isoflurane and underwent cervical dislocation before their brains were dissected using scissors and forceps. The brains were placed into homogenization buffer (0.1 mM Ethylenediaminetetraacetic acid (EDTA), 0.25 mM Dithiothreitol (DTT), 2 mM 2-[4-(2-hydroxyethyl)piperazin-1-yl] ethanesulfonic acid (HEPES), 0.32 M sucrose, pH 7.4) before being directly processed for synaptoneurosome isolation as described in the next section.

For the RML scrapie infected mice, brain tissue was obtained at two timepoints, 105 dpi and at end-point 165 dpi. For early stage hippocampal isolations, 16 mice were used, 8 mock infected and 8 RML scrapie infected. For the early stage forebrain, a total of 16 mice were used, 8 mock infected and 8 RML infected. For the late stage forebrain, a total of 12 mice were used, 4 mock infected and 8 RML scrapie infected.

The synaptoneurosome isolation procedure was based on a published protocol by Verity (Verity 1972), see Figure 8. The forebrain, consisting of the two cerebral cortices, was isolated from the brain by removing the midbrain, hindbrain, and olfactory bulbs using sterilized fine surgical dissection instruments and razor blades. The forebrain was minced into smaller fragments with the razorblade and transferred into a 7 mL Teflon-coated Dounce-Potter homogenizer (Wheaton) which contained 5 mL of homogenization buffer and subjected to 8 strokes. For the hippocampal samples, the hippocampi from 8 mice were pooled before being homogenized with the Dounce-Potter homogenizer in the same manner as the forebrain. The resulting homogenates were placed into 2 mL microcentrifuge tubes and underwent a series of centrifuge steps using a tabletop microcentrifuge (Eppendorf). The 5 mL were divided into smaller aliquots to accommodate the 2 mL tubes and then combined after each step.

To pellet cell debris and nuclei, cells were spun for 2 minutes at 2,000 x g. The supernatant was transferred to a new tube and spun for 10 minutes at 14,000 x g, with the resulting pellet containing the synaptoneurosomes. The pellet was resuspended in 1 mL homogenization buffer and transferred to a 4°C chilled discontinuous Ficoll gradient of 5-13% which contained 10 µg/mL DNase and centrifuged at 26,000 x g for 45 minutes in an ultracentrifuge (Beckman Coulter). The resulting fractionation had a middle layer that

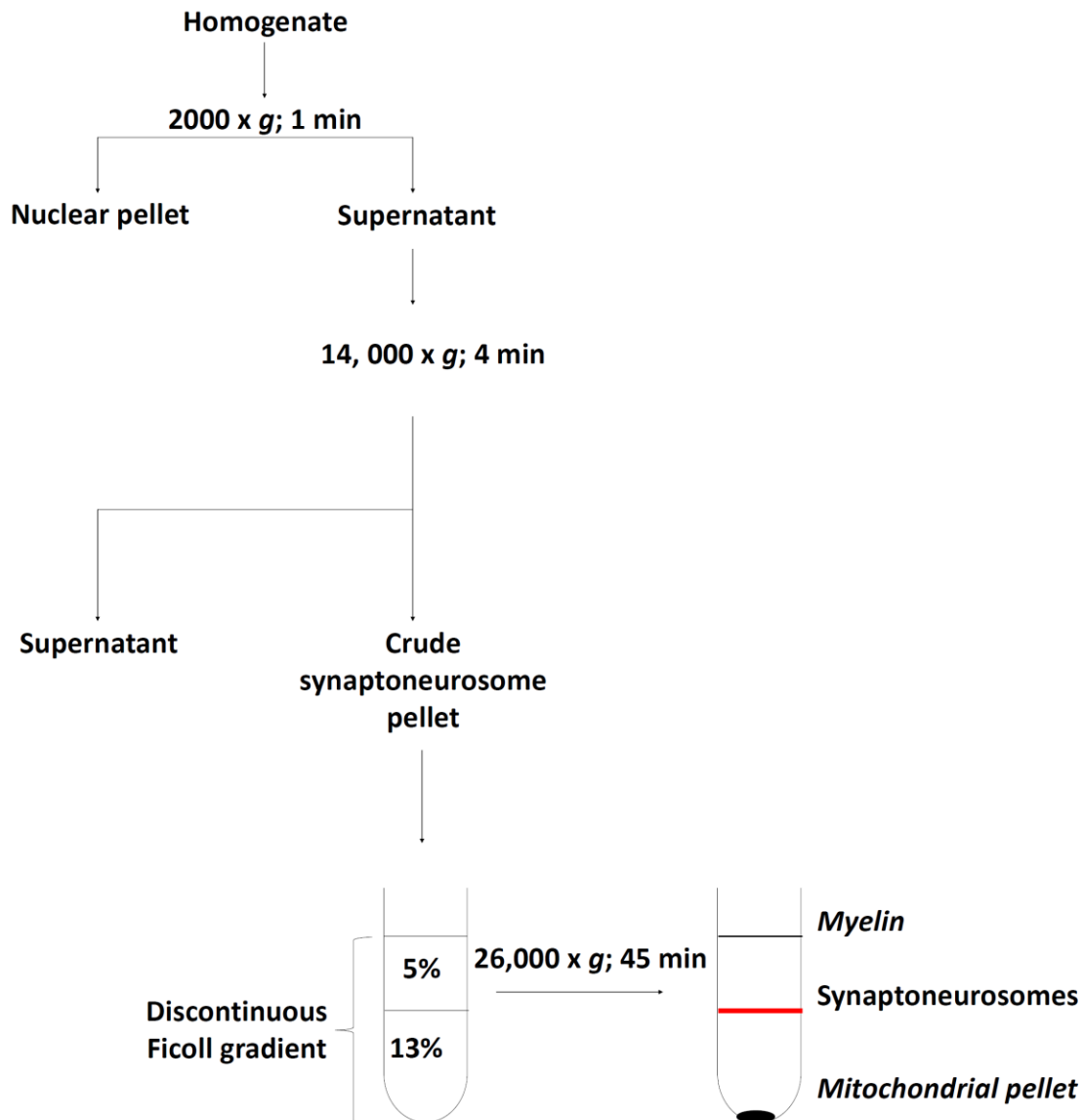


Figure 8. Flow chart for synaptoneurosome preparation. After the forebrain or hippocampi were dissected out and homogenized, the homogenate was centrifuged for 1 minute at 2,000 x *g* and the supernatant transferred to a new tube. This was centrifuged for 4 minutes at 14,000 x *g* after which the supernatant was removed and the crude synaptoneurosome pellet was resuspended in homogenization buffer before being placed into a prechilled 5/13% Ficoll gradient before being ultracentrifuged at 26,000 x *g* for 45 minutes. The three layers, with synaptoneurosome depicted by the red bar, were pipetted carefully into tubes for analysis and storage. Adapted from (Boese et al. 2015)

contained the synaptoneurosomes, while the top layer contained lipid myelin sheaths and the pellet contained mitochondria. The three layers were collected into 1.5 mL tubes using a P1000 pipette.

3.10.2 Total RNA and protein extraction from Synaptoneurosomes

The synaptoneurosome layer (~1.2 mL) was carefully pipetted into 2 fractions, one for protein analysis. These were then mixed one to one with homogenization buffer and the synaptoneurosomes were pelleted by spinning at 14,000 x *g*. Then the pellets were either mixed into cell disruption buffer for protein or for RNA analysis in cell lysis/binding buffer from the mirVana PARIS Kit (Fisher Scientific). Total protein lysates were placed on ice for 10 minutes before storing at -80°C. Protein quantification was performed using the Bicinchoninic acid assay (BCA) kit from Pierce. Protein lysates were thawed on ice while Bovine Serum Albumin (BSA) from the kit was prepared with PBS to yield the following standards: neat (2 mg/mL), 1 mg/mL, 0.5 mg/mL, 0.25 mg/mL, 0.125 mg/mL, 0.0625 mg/mL, 0.03125 mg/mL, and 0.015625 mg/mL. The BSA standards were run in triplicate in a 96 well plate and the protein samples (unknowns) were run in duplicate with 25 µL volume per well. The BCA solution was prepared by placing 500 µL of solution B to 25 mL of solution A (1:50 dilution) and 200 µL was added to each well of the plate. The plate was sealed and then briefly vortexed before incubating at 37°C for 30 minutes. After 30 minutes, the plate was cooled to room temperature before obtaining absorbance measurements in the GloMax Multi under the BCA setting (absorbance 560 nm). The BSA sample concentrations were plotted against their average absorbance to yield a standard

curve upon which a linear equation helped to determine the protein concentrations of the synaptoneurosome protein fractions.

For RNA extraction, 60 μL of miR homogenate additive was added per tube, vortexed briefly, and incubated on ice for 10 minutes. After this, a phenol-chloroform extraction was performed by adding 600 μL of Acid-Phenol:Chloroform (Fisher Scientific) and vortexed for 60 seconds. The subsequent step was a 5 minute centrifuge spin at 10,000 $\times g$ followed by a careful recovery of the aqueous phase which was pipetted into a new 1.5 mL tube. To this aqueous phase of $\sim 600 \mu\text{L}$, a 1.25 volume of 100% ethanol was added (750 μL) and mixed by pipetting up and down. The lysate/ethanol mixture (700 μL at a time) was then transferred to a filter cartridge assembly and spun down at 10,000 $\times g$ for 15 seconds. The flow through was discarded and 700 μL of miR Wash solution 1 was added to the filter column and spun through for 10 seconds at 10,000 $\times g$, with the flow through being discarded before washing twice with 500 μL Wash Solution 2/3. After discarding the flow through, the filter column was dried for 1 minute at 10,000 $\times g$. To elute RNA, nuclease-free water was heated to 95°C and 100 μL was added to each column, incubated for 2 minutes, and then the RNA was recovered by spinning for 30 seconds at 10,000 $\times g$. The RIN for each sample was obtained as per the LCM section 3.3, with all RNA having RIN of 5.5 or more, which was used in further analysis.

3.10.3 Electron Microscopy of Synaptoneurosomes

Samples from the 2 wild-type CD1 mice from each gradient layer synaptoneurosomes, myelin, and mitochondrial pellet, were fixed using fixative solution consisting of 5% glutaraldehyde, 4% paraformaldehyde in 100 mM sodium cacodylate and 3.4 mM calcium chloride (pH 7.2). The resulting blocks were cut into 80 nanomicon

sections and imaged using a charge-coupled device camera attached to a transmission electron microscope.

3.10.4 Western Blot analysis

Each protein lysate was run at 10 µg per lane in 20 µL final volume of SDS buffer (Fisher Scientific) of a 10% bis-Tris gel (Fisher Scientific) and separated by SDS-Polyacrylamide gel electrophoresis alongside the protein standards, Novex Sharp Pre-stained Protein ladder and MagicMark XP Western Protein Standard (both from Life Technologies) for 55 minutes at 200 volts in MOPS buffer using the Novex apparatus (Fisher Scientific). The gel was then blotted onto a polyvinylidene difluoride (PVDF) membrane using the iBLOT transfer apparatus (Fisher Scientific) with a 7 minute transfer time. The blot was blocked with 5% skim milk in PBS containing 0.2% Tween-20 (PBS-T) for 1 hour before adding the primary antibody diluted in 0.5% skim milk-PBS overnight at 4°C. The next morning, the blots were washed 3 times in PBS-T before incubating with secondary antibody for 1 hour at room temperature before washing 3 times in PBS-T. The secondary antibodies were detected using the West Pico Chemiluminescent Substrate (Fisher Scientific) and imaged using the VersaDoc Imaging System (Bio-Rad). The antibodies used for detection were anti-post-synaptic density (PSD)-95 (Abcam ab18258), anti-synapsin (Abcam ab64581), anti-GFAP (Abcam ab7260), and anti- α -tubulin (Sigma T9026). All primary antibodies were raised in rabbit except for α -tubulin which was mouse. The secondary antibodies were goat-anti-rabbit HRP (Dako P0448) and goat-anti-mouse HRP (Dako P0447).

3.10.5 miR Microarray Analysis of Synaptoneurosome derived RNA

100 ng of total RNA was dephosphorylated with calf intestinal alkaline phosphatase, then denatured using dimethyl sulfoxide, and labeled with pCp-Cy3 at the 3' end. These were dried down using a Speedvac and hybridized using the Microarray System labeling kit (Agilent) onto the rodent microarrays (Agilent) at 55°C for 20 hours. Following hybridization, the arrays were washed and scanned using a microarray scanner (Agilent) to obtain signal intensities. Those miR probes with intensities >100 were considered present in the sample. The miRs present in the samples were compared using the Gene Venn program (Pirooznia, Nagarajan & Deng 2007).

3.10.6 RT-qPCR using miR PCR Array Rodent Panel I

Total RNA was reverse transcribed into a universal cDNA pool using the Universal cDNA II synthesis kit (Exiqon), 20 ng of RNA was added to a final volume of 13 µL of nuclease free water, to which 4 µL of 5X reaction buffer, 1.0 µL RNA Spike-in UniSp6, and 2 µL enzyme mix were added from a master mix. The tubes were placed in a thermal cycler (MJ Research) with a heated lid and the following program was run: 42°C for 1 hour followed by 95°C for 5 minutes and cooled to 4°C.

To perform the real-time PCR Rodent Panel I (Exiqon), 1980 µL nuclease free water was added to 20 µL of cDNA, and 2 mL of 2x SYBR Green PCR Master Mix (Exiqon) was mixed in. 10 µL of the cDNA-Master Mix solution was added to the PCR Panel using a Repeater Pipette (Eppendorf). The plate was otherwise treated the same as the individual LNA primer assays. The plate was sealed with optical adhesive film, and spun down for 2 minutes at 1600 *x g*. The plate was then run on the ABI 7900HT or ViiA7 thermal cycler with the following conditions under the standard setting ramp rate of

1.6°C/second: 10 minute 95°C step followed by 40 cycles of 95°C for 10 seconds and 60°C for 60 seconds, at which point fluorescence data was measured. After the 40 cycles were complete, a melt curve analysis was performed to determine whether there was more than one PCR amplicon in the well. The Cts were then obtained by using the automatic baseline and threshold settings in the RQ Manager or ViiA7 software before analyzing further.

The Cts were input into GenEx version 5 software (MultiD Analyses) and processed. Cts that were >35 or missing (not determined) were removed from the dataset, then the interplate calibrator option was used. The data was normalized against the global mean of all expressed miRs before calculating fold changes using the delta delta Ct method. For the forebrain samples, two-tailed t-tests were performed between mock and RML scrapie prion infected using a p-value of < 0.05 to determine significance.

3.10.7 Protein Preparation for Mass spectrometry

100 µg of protein lysate was acetone precipitated by adding 5X volume of cold acetone (chilled to -20°C), vortexing, and placing in a -20°C freezer overnight. The next day the solution was centrifuged at 20,000 x g for 10 minutes at room temperature, the supernatant was decanted, and the protein pellet air dried for 20 minutes. Each protein pellet was then resuspended in 70 µL Optima LC/MS grade water (MS water) (Fisher), 10 µL 0.5 M HEPES buffer, and 20 µL 20% SDS (Sigma). This mixture was then heated to 95°C for 5 minutes in a thermomixer (Eppendorf), cooled to room temperature, and then 10 µL of 1 M DTT (100 mM final concentration) was added to each tube to reduce the protein. This mixture was then incubated at 95°C for 5 minutes before cooling to room temperature. The samples were then placed in a -20°C freezer overnight before proceeding to the trypsin digestion step.

The next day, the samples were brought to room temperature while the urea exchange buffer (UEB) was made. The UEB consisted of 4.8 g PlusOne Urea (GE) added to 1 mL of 0.5 M HEPES and 6.5 mL MS water. The samples had 490 μ L UEB added, vortexed, and incubated at room temperature for 10 minutes. During this step a Nanosep 10K omega cartridge (Pall Life Sciences) was labeled and equilibrated by spinning down for 2 minutes at 10,000 x *g* with 200 μ L MS water followed by 200 μ L UEB. The flow through was discarded and 300 μ L of protein sample was loaded onto the cartridge and spun for 10 minutes at 10,000 x *g* until all sample had passed through but ensuring the column did not dry out.

The cartridge was then washed a total of 3 times with UEB by adding 250 μ L, spinning at 10,000 x *g*, and discarding flow through at the end of each wash. After the washes, the cartridge was subject to Iodoacetamide (IAA) (Sigma) treatment, which was prepared by adding 9.26 mg IAA to 1 mL UEB. Each sample had 100 μ L IAA added to it and was placed in the thermomixer to shake at 600 rpm for 1 minute. The samples were then incubated at room temperature in the dark for 20 minutes after which the cartridges were spun down at 10,000 x *g* for 10 minutes and the flow through discarded. This was followed by a total of 3 washes where each wash consisted of 100 μ L UEB placed on the cartridge, spun at 10,000 x *g* for 10 minutes, and the flow through discarded.

The cartridge was then subject to 2 washes with 50 mM HEPES with 150 μ L per wash and a 10 minute spin at 10,000 x *g*. Afterwards, 50 μ L of Benzonase solution [4 μ L of 25 mM MgCl₂ (Roche), 1000 units of Benzonase (Roche) and 42 μ L of 50 mM HEPES] was added to each cartridge and mixed at 600 rpm for 2 minutes. After mixing, the solution was incubated for 30 minutes. Then, the cartridge was subject to 3 washes total with 100

μL of 50 mM HEPES per wash, centrifuging at 10,000 $\times g$ for 10 minutes, and discarding flow through. The sample cartridges were then transferred to a new 1.5 mL tube.

The final step of the digestion was to incubate with 50 μL of trypsin solution with 1.5 μg trypsin per sample overnight. The trypsin was added to each cartridge and then mixed in the thermomixer at 600 rpm for 1 minute. Then the cartridge assembly was placed into a moisture chamber which consisted of a 50 mL Falcon tube with 1 mL of MS water and incubated at 37°C overnight.

The peptide elution step was performed the next morning, which started by cutting off the top rim of the Nanosep cartridge with a razor blade. The cartridge was then inverted into a new collection tube, spun at 10,000 $\times g$ for 3 minutes, and the flow through containing the peptides was kept. The cartridge was then turned right side up, 50 μL of 50 mM HEPES buffer was added, and the assembly was shaken at 600 rpm for 2 minutes. The cartridge was then inverted and spun at 10,000 $\times g$ for 3 minutes. The HEPES elution was performed a total of 3 times and the resulting peptides were dried down with the Speed Vacuum (Fisher Scientific) All spectra were processed using Proteome Discoverer v1.3 (Fisher Scientific) and search was conducted with the Mascot v2.3 database (Matrix Science). The searches were performed against a mouse subset within the SwissProt database which was comprised of 10,090 sequences. The decoy database option was selected along with the following search parameters: Carbamidomethyl was selected as a fixed modification, Oxidation as a variable modification, 0.5 Dalton fragment ion mass tolerance, 10 ppm parent ion tolerance, and trypsin with up to 1 missed cleavage. The Mascot search results were imported into Scaffold 4 (version 4.6.2, Proteome Software)

(Searle 2010) and filtered using at least 1 peptide per protein with a 0.1% False Discovery Rate (FDR) for peptides, and a 1.0% FDR for proteins.

This list was then exported into Microsoft Excel and processed to remove decoy proteins and any proteins not ubiquitously detected. To determine the GO features of the protein detected, the Protein ANalysis THrough Evolutionary Relationships Version 11.1 (PANTHER) program was used to ascertain protein class (Mi et al. 2017) and DAVID was used to determine synapse related proteins. The list of synaptic proteins was compared to the mouse TargetScan predicted targets using the Gene Venn program.

3.10.8 RT-qPCR with the TaqMan Gene Expression Assay for mRNA detection

For the RT portion of the TaqMan assay, the High Capacity cDNA reverse transcriptase kit with RNase inhibitor (Fisher Scientific) was used following manufacturer's recommendations. To produce cDNA, 2 ng of RNA in a final volume of 10 μ L nuclease free water was used as template to which the following was added: 2 μ L of 10X RT Buffer, 0.8 μ L of 25X dNTPs (100 mM), 2.0 μ L of 10X RT Random Primers, 1 μ L of RNase inhibitor, 1 μ L of MultiScribe Reverse Transcriptase, and 3.2 μ L nuclease-free water per reaction in a 0.2 mL PCR tube. For RT, the thermal cycling conditions consisted of 25°C for 10 minutes, 37°C for 2 hours, 85°C for 5 minutes, and cooled to 4°C before proceeding to cDNA clean up with ChargeSwitch PCR clean-up (Fisher Scientific).

For clean-up, in a new RNase free 1.5 mL tube, 20 μ L of purification buffer N5 was added to 20 μ L of cDNA from the previous step along with 10 μ L of ChargeSwitch Magnetic Beads. This mixture was pipetted up and down then incubated for 1 minute at room temperature before placing on the MagnaRack (Invitrogen) for 1 minute, where the magnet drew the beads away from the solution. The beads were then subject to two washes

consisting of mixing the beads in 150 μ L of Wash Buffer (W15) followed by 1 minute on the MagnaRack and the solution at the bottom discarded. After the final wash step, the cDNA was eluted by adding 20 μ L of elution buffer (E5, 10 mM Tris-HCl, pH 8.5) and mixing the beads by pipetting. The solution was then incubated for 1 minute at room temperature, followed by 1 minute on the MagnaRack, at which time the cDNA was recovered by pipetting into a new RNase free 1.5 mL tube while avoiding magnetic bead contamination. The cDNA was then assessed for quantity using the ND-1000 Nanodrop.

For the qPCR step, 50 ng of cDNA was diluted to final volume of 10 μ L with nuclease-free water and combined with 10 μ L of the TaqMan Fast Universal PCR master mix (2X) with no AmpErase UNG (Fisher Scientific) along with 1 μ L of TaqMan gene expression probe for a final volume of 20 μ L per reaction. Each cDNA reaction was run in at least duplicate in a 96 well optical plate, which was sealed, and spun down at 1600 x *g* for 2 minutes before loading onto the thermal cycler, either the ABI 7900 HT or the ViiA7. The cycling conditions were an initial step of 95°C for 20 seconds followed by 40 cycles of 95°C for 1 second and 60°C for 20 seconds. The Ct for each reaction was obtained on either the RQ Manager software or the ViiA7 software by using the automatic baseline and threshold settings with the curves being examined before accepting the Ct value and graphed using GraphPad Prism 6.

3.11 Primary Hippocampal Experiments

3.11.1 Cultured mouse primary hippocampal neurons: dissection, culture, and maintenance

The day prior to primary hippocampal neuron preparation, plates were coated with poly-D-lysine (Corning) at a concentration of 20 $\mu\text{g}/\text{mL}$ per well by diluting a stock solution of 1 mg/mL with borate buffer, made by adding 4.76 g boric acid plus 2.54 g Borax in 1000 mL double distilled water and using 5 M NaOH to pH 8.4, and placed into a humidified 37°C incubator with 5% CO₂ overnight. The next day the wells were washed twice with autoclaved double distilled water, 60% of the final volume of NbActiv1 (Brainbits LLC) media was added, and the plates were placed into a humidified 37°C incubator with 5% CO₂ until the primary neurons were ready to be plated. The dissection media (DM) composed of Hank's Balanced Salt Solution (HBSS) plus 100 mM MgCl₂, 10 mM Kynurenic acid (Sigma) and 100 mM HEPES was prepared by diluting a 10X stock to 1X in HBSS. Both papain and trypsin inhibitor were prepared prior to obtaining the mouse tissue. The papain (Worthington) was prepared by adding 100 units (100 μL) of the stock solution to 5 mL of DM, incubated briefly at 37°C until the papain went into solution, 25 μL Deoxyribonuclease I (DNAse) from bovine pancreas (Sigma) 50 $\mu\text{g}/\text{mL}$ final concentration (Cf) was added, and the entire solution filter sterilized using a 10 mL syringe and a 0.2 micron filter (Fisher Scientific). The trypsin inhibitor was prepared by measuring and adding 0.15 g of trypsin inhibitor (Sigma) into 15 mL of DM resulting in a final concentration of 10 mg/mL and incubated at 37°C until in solution. Then, to achieve a pH of 8.5, 15 μL of 0.1 M NaOH was added and pH checked by litmus paper (Sigma). After this, 75 μL of DNAse (50 $\mu\text{g}/\text{mL}$ Cf) was added before filter sterilizing using a 30 mL

syringe and 0.2 micron filter. Both the papain and trypsin inhibitor enzymes were placed in a 37°C water bath until required for enzymatic dissociation.

For the primary neuronal preparation, a timed pregnant mouse (day 18-20) was deeply anesthetized by isoflurane and decapitated before the abdomen was cut open using sterile scissors and the uterus with attached embryos were removed. The heads of the embryos were cut with scissors and placed in 15 mL DM, these steps were performed by NML Veterinary Technical Services. The heads were then transferred using sterile forceps to a petri dish containing fresh DM where a minimum of 6 brains were dissected out of the skull using fine dissecting scissors and forceps and the brains were placed into a new chilled petri dish containing fresh DM. In the new dish, the meninges were removed, the cortices isolated from the rest of the brain, and the hippocampi dissected. These hippocampi were placed by P1000 pipette into a 15 mL conical tube containing 1 mL of DM. When all the hippocampi required were collected, the excess DM was removed by aspiration and replaced with 5 mL of DM containing 100 units of papain and incubated at 37°C for 4 minutes, with gentle tapping at 2 minutes to resuspend the tissues. The papain was then removed by aspiration and replaced by 5 mL of trypsin inhibitor (10 mg/mL) to deactivate the papain. The trypsin inhibitor step was performed 3 times, at each time the hippocampi were incubated for 3 minutes in a 37°C water bath and then trypsin inhibitor removed by aspiration. After the third and final step, 5 mL of prewarmed NbActiv1 was added to the hippocampi, which was promptly removed once the hippocampi settled at the bottom of the tube. The final step involved adding 1 mL of prewarmed NbActiv1 and triuration of 8-10 times using a P1000 pipette set to 1 mL. The cells were then counted by adding 10 µL to 90 µL trypan blue (Gibco) (dilution factor of 10), vortexed briefly and 10

μL added to one side of a hemocytometer and the 4 outer squares counted. The cell count was determined by the following equation, where **X** is the number of cells:

$$\# \text{ of cells counted} \div 4 \times 10 \text{ (dilution factor)} = \mathbf{X} \times 10^6 \text{ cells/mL}$$

The cell density was dependent on experiment but generally 70,000 cells for a 24 well plates, 140,000 for a 12 well, and 250,000 for a 6 well were used. For plating, the cells went into wells containing prewarmed NbActiv1, for example, 300 μL of media was already in the recipient well of a 24 well plate to which 200 μL of cells were added. The plates were maintained in a humidified 37°C incubator with 5% CO_2 . Media was replenished every four days by removing 40% media (i.e. 200 μL of a 24 well) and adding 50% (250 μL) prewarmed NbActiv1. Experiments were conducted from 7-12 days *in vitro* (DIV) as stated in appropriate sections. To ensure neurons were growing well and formed the majority of the culture, they were immunostained and imaged using fluorescent microscopy.

3.11.2 Immunostaining of primary neuronal cells

Neurons were grown in chamber slides and fixed with 4% paraformaldehyde-sucrose solution for 12 minutes followed by 3 Dulbecco's PBS (DPBS) washes and permeabilized with 0.5% Triton-X-100 (Sigma) in DPBS. The slides were blocked with 5% donkey serum (Dako) made in DPBS for 30 minutes at room temperature. Two primary antibodies were used to detect both neurons and astrocytes in the same chamber, Microtubule associated protein 2 (MAP2) raised in chicken (Abcam, ab5392) at 1:1,000 to detect neurons, and GFAP raised in rabbit (Dako z0334) at 1:500 to detect astrocytes, both were diluted in 5% donkey serum in DPBS. For secondary antibodies, Alexafluor conjugated 488 and 555 (Fisher Scientific) were used, 488 for GFAP and 555 for MAP2 at

a concentration of 1:500 diluted in 5% donkey serum in DPBS. After 3 washes with DPBS, the chambers were removed, ProLong Gold antifade mountant with DAPI (Invitrogen) was added and a coverslip placed on top. The slides were cured for 24 hours at room temperature before being imaged on the Laser Scanning Microscope 700 (Zeiss) using the 405 (DAPI), 488 (GFAP), and 555 (MAP2) filters. The images were then processed in the Zen Lite Software from Zeiss Microscopy.

3.11.3 Total RNA extraction from primary cell cultures

To isolate total RNA from the hippocampal neurons, either the mirVana kit (Fisher Scientific) or the Total RNA extraction kit (Norgen) was used. The Norgen kit was used in later experiments due to its versatility in terms of time and safety as a fume hood is not required to do these extractions. In either case, media was aspirated from the cells, lysis buffer was added, cells were scraped and pipetted into a 1.5 mL RNase free tube. The tube was then vortexed briefly and frozen at -80°C until the RNA extraction procedure.

For the mirVana kit, cells were disrupted in 600 μL of Lysis/Binding solution, scraped and vortexed before freezing at -80°C before processing as per the previous section 2.10.2. For the Norgen Total RNA extraction kit, 350 μL of Buffer RL was added to the cells to produce lysates in the same manner as the mirVana kit. After lysates were thawed, 200 μL of 100% ethanol was added to the 350 μL RNA lysates and vortexed for 10 seconds. This mixture was then passed through a spin filter column at 3,500 x g for 1 minute. The flow through was discarded and the spin column was subject to 3 washes that involved adding 400 μL of wash buffer each time and spinning down out at 3,500 x g. The flow through from the washes was discarded between washes and after the third and final wash, the column was dried by spinning for 2 minutes at 3,500 x g. The spin column was then

placed into a new collection tube and to elute RNA, 50 μ L of nuclease free water was added to the column. The column was then spun at 200 x *g* for 2 minutes followed by a 14,000 x *g* spin for 1 minute to elute RNA. The resulting RNA was quantified on the Nanodrop ND-1000 spectrophotometer, where concentration was determined by measuring light absorbance at wavelengths of 260nm and 280nm to assess RNA concentration and purity. For initial experiments, RNA was analyzed for quality using the Bioanalyzer 2100 to assess RIN similar to section 3.3, but using the RNA Nano 6000 kit as per manufacturer's instructions instead of the Pico, and samples with RIN > 8 were used for PCR.

3.11.4 RT-qPCR with Locked Nucleic Acid primers for miR detection

The RT kit used to produce cDNA was the Universal cDNA synthesis kit II (Exiqon). The RT step consisted of adding 10 ng of RNA to nuclease free water to a final volume of 6.5 μ L per reaction. The remaining components of each RT reaction included 2 μ L of 5X reaction buffer, 0.5 μ L of the UniSp6 spike-in RNA, and 1 μ L of enzyme mix which were made as master mixes. The master mix tube was flicked a few times and spun down in a microcentrifuge before pipetting 3.5 μ L into 0.2 mL PCR tubes. Then the 6.5 μ L of RNA template was added to each corresponding tube before running on a thermal cycler with the following conditions under a heated lid: 42°C for 1 hour followed by 95°C for 5 minutes and maintained at 4°C before being stored at -20°C.

For the qPCR portion, the cDNA was thawed, then diluted 1:79 by adding 1 μ L cDNA to 79 μ L nuclease free water. For each qPCR reaction, 4 μ L of diluted cDNA template was added to 5 μ L of ExiLent SYBR green master mix (Exiqon) and 1 μ L of miR primer. The cDNA for each treatment was run in at least triplicate in a 96 well optical plate, the plate was sealed with optical adhesive film, and spun down for 2 minutes at 1600 x *g*.

The plate was then run on the ABI 7900HT or ViiA7 thermal cycler with the following conditions under the standard setting ramp rate of 1.6°C/second: 10 minute 95°C step followed by 40 cycles of 95°C for 10 seconds and 60°C for 60 seconds, at which point fluorescence data was measured. After the 40 cycles were complete, a melt curve analysis was performed to determine whether there was more than one PCR amplicon in the well. The Cts were then obtained by using the automatic baseline and threshold settings in the RQ Manager or ViiA7 software before analyzing further in Microsoft Excel. Fold change was obtained as per section 3.7 with graphs and statistical testing performed in GraphPad Prism 6.

3.11.5 RT-qPCR for TaqMan gene expression assays

These were done as per section 3.10.8 with significance testing using one-tailed t-tests between fold changes, with Welch's correction for unequal variance applied as necessary. The graphs and statistical testing were done in GraphPad Prism 6.

3.11.6 Action potential bursting experiment using 4-aminopyridine and (+)-bicuculline

For the action potential bursting experiments, primary hippocampal neurons (9-12 DIV) were used to induce action potential bursts with 250 μ M 4-aminopyridine (Tocris) diluted in water and 50 μ M (+)-bicuculline (Tocris) diluted in DMSO. Both were diluted in prewarmed Neurobasal media before being added to the cells with the control being Neurobasal only. The treatments were bath applied by removing the media in the wells and adding respective treatments. Total RNA was then collected at two timepoints, 4 hours and 16 hours.

3.11.7 Induction of glutamate excitotoxicity

To induce glutamate excitotoxicity, mouse primary hippocampal neurons that were 8 DIV were used. Glutamate treatments were prepared by adding L-glutamic acid (Sigma) to nuclease free water to produce a working stock of 10 mM which was then diluted in prewarmed Neurobasal media (Fisher Scientific) to make the final concentration. For the excitotoxic glutamate conditions, 100 μ M glutamate was used as well as NMDAR inhibitors 10 μ M MK-801 (Tocris), and 10 μ M PPDA (Tocris). The treatments were bath applied to each well after removing media, with each condition being performed in triplicate wells.

3.12 Gain of function and Loss of function experiments

3.12.1 Lipofectamine 2000 transfection of pre-miRs or anti-miRs

The transfection was modified from manufacturer's instructions to minimize the amount of Lipofectamine 2000 (Fisher Scientific) added to cultured hippocampal neurons. There were three treatments: pre-miR/anti-miR-scramble, pre-miR/anti-miR-128-3p, and Lipofectamine 2000 (vehicle only). The first step was a 5 minute incubation of 1 μ L of Lipofectamine with 25 μ L of NbActiv1 media at room temperature, while the appropriate amount of pre-miR or anti-miR was incubated with 25 μ L of NbActiv1 as well. After the 5 minutes, the RNA/NbActiv1 mixture was added to the Lipofectamine/NbActiv1 mixture and gently pipetted up and down 5 times. This complex was then incubated for 20 minutes before adding 50 μ L to each well and the plates were rotated gently back and forth to mix. The treatments were performed in triplicate with master mixes made for the transfection.

The transfection proceeded for 24 hours then the total RNA was collected by aspirating media and adding lysis buffer and RNA extracted and quantitated as per section 3.11.3.

3.12.2 Global proteome detection of miR-128-3p gain of function in primary hippocampal neurons

For these experiments, primary hippocampal neurons were plated at a density of 250,000 per well in a 6 well plate and maintained in NbActiv 1 media in a humidified 37°C incubator with 5% CO₂. When the neurons were 11 DIV, they were transfected with 1) 10 nM pre-miR-scramble (negative miR control), 2) 10 nM pre-miR-128, or 3) vehicle only control in triplicate wells. Each well received 50 µL of the treatment to ensure a final concentration of 10 nM for the pre-miR-scramble or pre-miR-128-3p. The experiments were performed in 4 independent neuronal preparations resulting in 12 samples total.

The protein was collected and processed as per section 3.10.2 but with some modifications. Protein collection was done by adding 400 µL Neuronal Protein Extraction Reagent (N-PER) (Fisher Scientific), and incubating the plate on ice for 5 minutes for lysis to occur. After the 5 minutes, each well was scraped using a cell scraper and 4 wells were combined per treatment into a low protein retention 1.5 mL tube (Fisher Scientific). The low protein retention tubes were used for the remainder of the protein work. The tubes were spun down at 10,000 x g for 10 minutes at room temperature to remove the cell pellet while the supernatant containing the final protein lysate was carefully placed into a new 1.5 mL tube and stored at -80°C until protein was quantified using the BCA described in section 3.10.2.

The protein concentration (x) for the 12 samples was extrapolated from the BSA standard curve formula $x = (y - 0.2227) / 1.0879$ where y = average sample absorbance. The

next step was acetone precipitation of 100 μg of protein lysate and digestion of protein to peptides which was performed in the same manner as section 3.10.7 before labeling with TMTsixplex labels (Fisher Scientific).

3.12.3 TMT Labeling of proteins for Mass spectrometry

The TMT labels from the TMTsixplex Label Reagent Set (Fisher Scientific), 2 of each type (-126, -127, -128, -129, -130, -131) for a total of 12, were thawed to room temperature for 5 minutes before the tubes were spun down at 20,000 $\times g$ for 1 minute. The lyophilized TMT labels were then resuspended in 45 μL 100% acetonitrile (Fisher Scientific), vortexed for 5 seconds, spun down for 5 seconds at 20,000 $\times g$, and then incubated at room temperature for 5 minutes. During this time, the digested protein samples were resuspended in 59 μL 100 mM HEPES buffer and shaken in the thermomixer for 10 minutes at 600 rpm. Finally, the total volume (\sim 45 μL) of each TMT label was added to a specific sample such that treatment condition or replicate did not overlap in label type. The labeled proteins were incubated overnight at room temperature.

To quench the labeling reaction, 8 μL of 5% hydroxylamine was added to each sample, incubated for 30 minutes, and then dried down using the speed vacuum. These were then made up to 35 μL with MS water and 1 μL of each sample was added to 48 μL with nano-LC buffer A (0.1% formic acid and 2% acetonitrile). This was then run on a nano-liquid chromatograph for a 2 hour gradient. The peak list in Proteome Discoverer 2.0 (Fisher Scientific) with an in-house Perl script was used to produce histograms of count against ratio for each TMT report ion pair. The histogram centroid was used to make corrections to the final 6-plex volumes (2 batches) for a final volume of 40 μL for each run.

3.12.4 Peptide Fractionation

Each 6plex batch was spiked with 4 μL of 200 mM ammonium formate pH 10 (Fisher Scientific) and this mixture was added to a Waters XBridge C18 Guard column on a micro-flow 1200 Series HPLC pump (Agilent). The peptides were separated by utilizing a 80 minute gradient of 3 to 75% LC Buffer B (20 mM ammonium formate and 90% acetonitrile) at a flow rate of 150 $\mu\text{L}/\text{minute}$ with a total of 12 peptides collected. These were then dried down using a vacuum centrifuge and resuspended in 80 μL of nano-LC Buffer A.

3.12.5 Mass spectrometry

Each LC fraction was analyzed using a nano-flow Easy 1000 in-line to a Q-Exactive Plus mass spectrometer possessing a nano-electrospray ion source at 2.0 kV (Fisher Scientific). First, 2 μL of fractionated peptides were loaded and washed on a C18 reversed phase Easy-Spray column (Fisher Scientific) with 100% nano-LC buffer A. Then, the peptides were eluted using a 105-minute 5-22% gradient of nano-LC buffer B (0.1% formic acid and 98% acetonitrile) followed by a 15 minute gradient of 22-32% nano-LC buffer B at constant flow rates of 200 nL per minute. The complete run time was 175 minutes including loading, linear gradient, 15 minute column wash with 90% nano-LC buffer B, and column re-equilibration with 5 μL nano-LC buffer A. The full mass spectrometer scan was obtained in the Orbitrap over m/z 375-1500 with automatic gain control target of $3e6$, target resolution of 70,000 at m/z 2000, and 80 milliseconds maximum injection time.

Data-dependent acquisition was used by dynamically choosing the top 15 abundant precursor ions from each survey scan with an isolation width of 1.4 m/z for fragmentation by Higher energy collisional dissociation (34% normalized collision energy). The intensity

threshold for selecting a precursor ion for fragmentation was $1e5$ ions, with charge state recognition of 2-5, and a dynamic exclusion for 20 seconds. The fragment ion MS2 scans were also acquired in the Orbitrap over a dynamic m/z range with a target resolution of 17,500 at m/z 200, AGC target of $1e5$, and maximum injection time of 80 ms. Lock Mass was used with polysiloxane.

3.12.6 Global proteome data processing and analysis

All spectra were processed using Proteome Discoverer v2.0 (Fisher Scientific) and the search was conducted with the Mascot v2.5 database (Matrix Science). The searches were performed against a mouse subset within the SwissProt database which comprised of 17,170 sequences. The decoy database option was selected along with the following search parameters: Carbamidomethyl was selected as a fixed modification, Oxidation as a variable modification, 0.5 Dalton fragment ion mass tolerance, 10 ppm parent ion tolerance, and trypsin with up to 1 missed cleavage. The quantitation method was selected as TMT 6plex. The Mascot search results were imported into Scaffold 4 and filtered using at least 2 peptides per protein with a 0.1% FDR for peptides, and a 1.0% FDR for proteins.

This list was then exported into Microsoft Excel and processed to remove any proteins not ubiquitously detected and decoy proteins that were added for the MASCOT search. To determine the overall features of the protein detected using GO, the PANTHER program was used. For differential analysis, the Q+ function of Scaffold 4 was used, Mann Whitney tests were applied between the three datasets, vehicle versus Scramble, vehicle versus miR-128-3p, and Scramble versus miR-128-3p. To adjust for multiple hypothesis testing, the Benjamini-Hochberg correction was applied to the p-value of < 0.05 in each test. Those proteins that were significantly different in each test were then examined

through the Venn diagram program to determine the final list of proteins that were significantly altered. Graphs were produced in GraphPad Prism 6.

4. Results

4.1 miR-128-3p is temporally dysregulated in neurons of prion infected mice

4.1.1 Rationale

Previous work by Majer *et al* (2012) in the RML scrapie prion mouse model indicated a neuroprotective transcriptional response was occurring in the CA1 region of the hippocampus during early stages of disease. During this time, elevated levels of pCREB were also noted, and pCREB was the transcriptional activator of many of the genes found. The CA1 region undergoes significant synaptic degeneration during prion infection in mouse models and its damage is important in the development of the clinical signs that develop during disease. In addition, to study transcriptional alterations specifically in a neuronal context requires selective isolation of these cells from other cell types that may be more abundant such as inflammatory glia that accumulate significantly. The CA1 region is enriched in neuronal cell bodies that can be captured by laser microdissection, enabling specific determination of the levels of neuronally-enriched transcripts such as miR-128-3p.

Brains of 3-4 mice from mock and RML infected mice were used for immunohistochemical detection of PrP^{Sc}, as a marker of prion disease, and GFAP and IBA-1 as markers of astrocytosis and microglia respectively. Two temporal profiles were considered, the early stages of disease from 70, 90 and 110 dpi when no obvious signs of disease were observed in the mice, and the clinical stage of disease, 130 dpi and EP, when altered behaviour and neurological signs were evident. The behavioural alteration consistently observed was a deficiency in nest building. Mice were provided with nest building material as a 2” square of pulped cotton fiber that the mice shred and build into nests as a natural behaviour. After 130 dpi, mice were observed to take progressively

longer times to shred and build nests. In addition, these nests were increasingly disordered. Mice were sacrificed when severe clinical signs of disease developed, which included dull ruffled fur, >20% weight loss, ataxia, forward rounding of the back (kyphosis), and clasping.

Coronal sections immunostained with antibodies to detect prion protein demonstrated the presence of PrP^{Sc} at 70 dpi in the hypothalamus, thalamus, and forebrain (Figures 9, 10, and 11). The hippocampus displayed the presence of PrP^{Sc} at 90 dpi (Figure 12), mostly in the *stratum locunosum-moleculare* which projects to the *stratum pyramidale* layer (where CA1 neurons are located). The *stratum pyramidale* layer first had detectable PrP^{Sc} at the 110 dpi timepoint, towards the end of the asymptomatic stage. The PrP^{Sc} staining is consistent with the literature which indicates that a granular layer of immunoreactivity is evident alongside the telltale PrP^{Sc} aggregate deposits (Chiti et al. 2006).

The CA1 region, being the neuronal rich region of interest for miR-128-3p levels, was next examined for neurodegeneration, astrocytosis, and microglial invasion to ascertain these potential contaminants to the total RNA extracted. To assess neurodegeneration, the hippocampal area was stained with Fluoro-Jade C (Schmued et al. 2005). This fluorescent stain has been used to detect the same patterns of neurodegeneration as seen using lower resolution methods such as Nissl but with higher sensitivity due to the fluorescent signal. There was no neurodegeneration detected in the hippocampus until EP, at which time degenerating neurons were present in the *stratum pyramidale*, *stratum radiatum*, and *stratum locum-moleculare* (Figure 13).

Astrocytosis, a hallmark of prion disease, was visualized by immunohistochemical staining with an antibody specific to GFAP and a fluorescent secondary antibody. Despite astrocytosis being evident throughout the brain from 70 dpi onwards, significant numbers of astrocyte cell

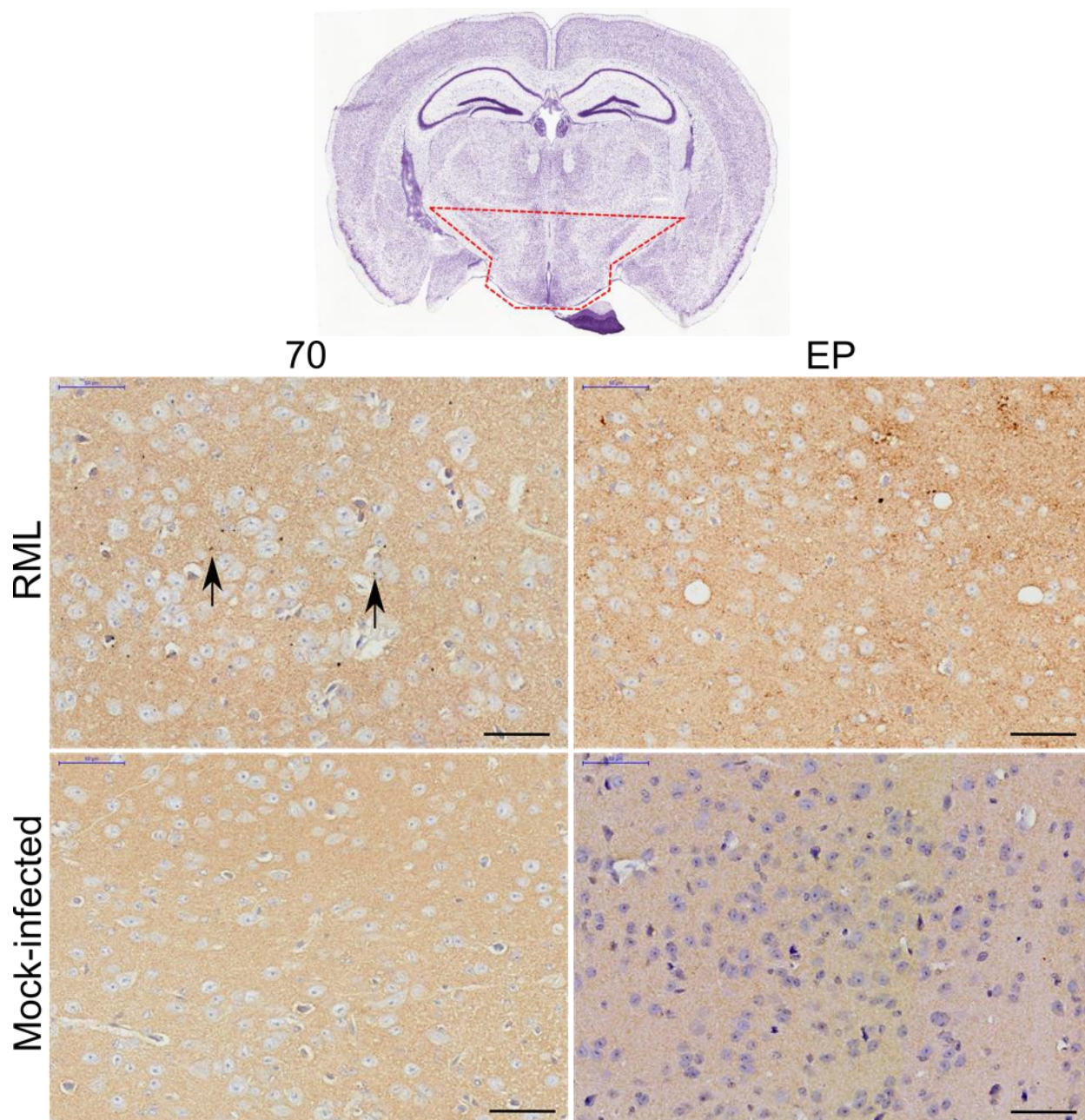


Figure 9. Detection of PrP^{Sc} in the hypothalamus of RML scrapie prion infected mice. PrP^{Sc} deposits are detected in the hypothalamic region in the RML scrapie prion model of IP injected CD1 mice first at 70 days post infection (70) and to compare, at EP of disease. PrP^{Sc} deposits are brown stained with DAB substrate, and blue denotes nuclei stained with hematoxylin. The coronal brain section to depict the magnified hypothalamic area is from Allen Brain Atlas. The scale bar represents 100 microns. (© Anna Majer, used with permission)

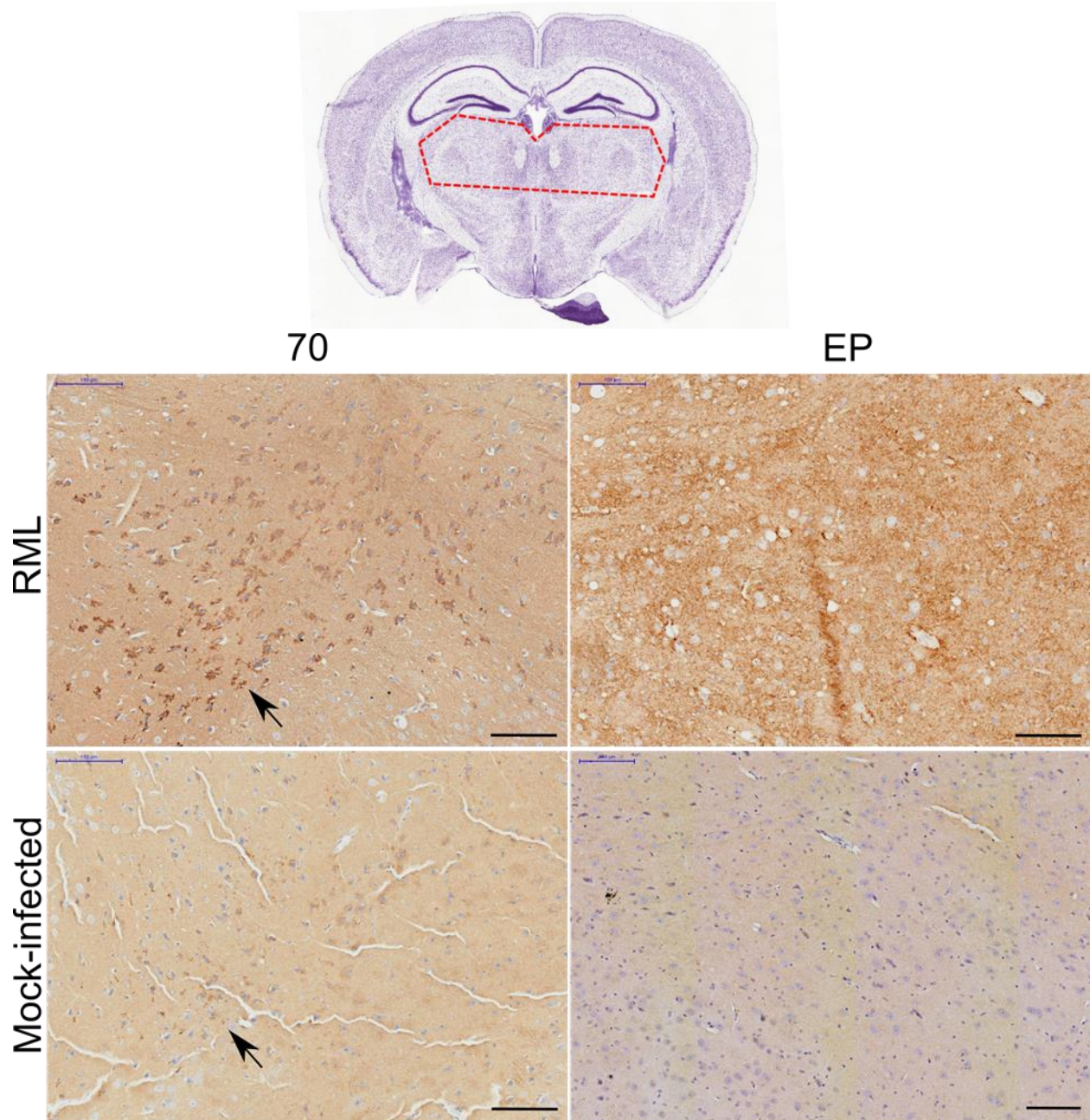


Figure 10. Detection of PrP^{Sc} in the thalamus of RML scrapie prion infected mice. PrP^{Sc} deposits are detected in the thalamic region in the RML scrapie prion model of IP injected CD1 mice at 70 dpi (70) and is increased by EP. The coronal brain section to depict the magnified thalamic area is from Allen Brain Atlas. The scale bar represents 100 microns (© Anna Majer, used with permission)

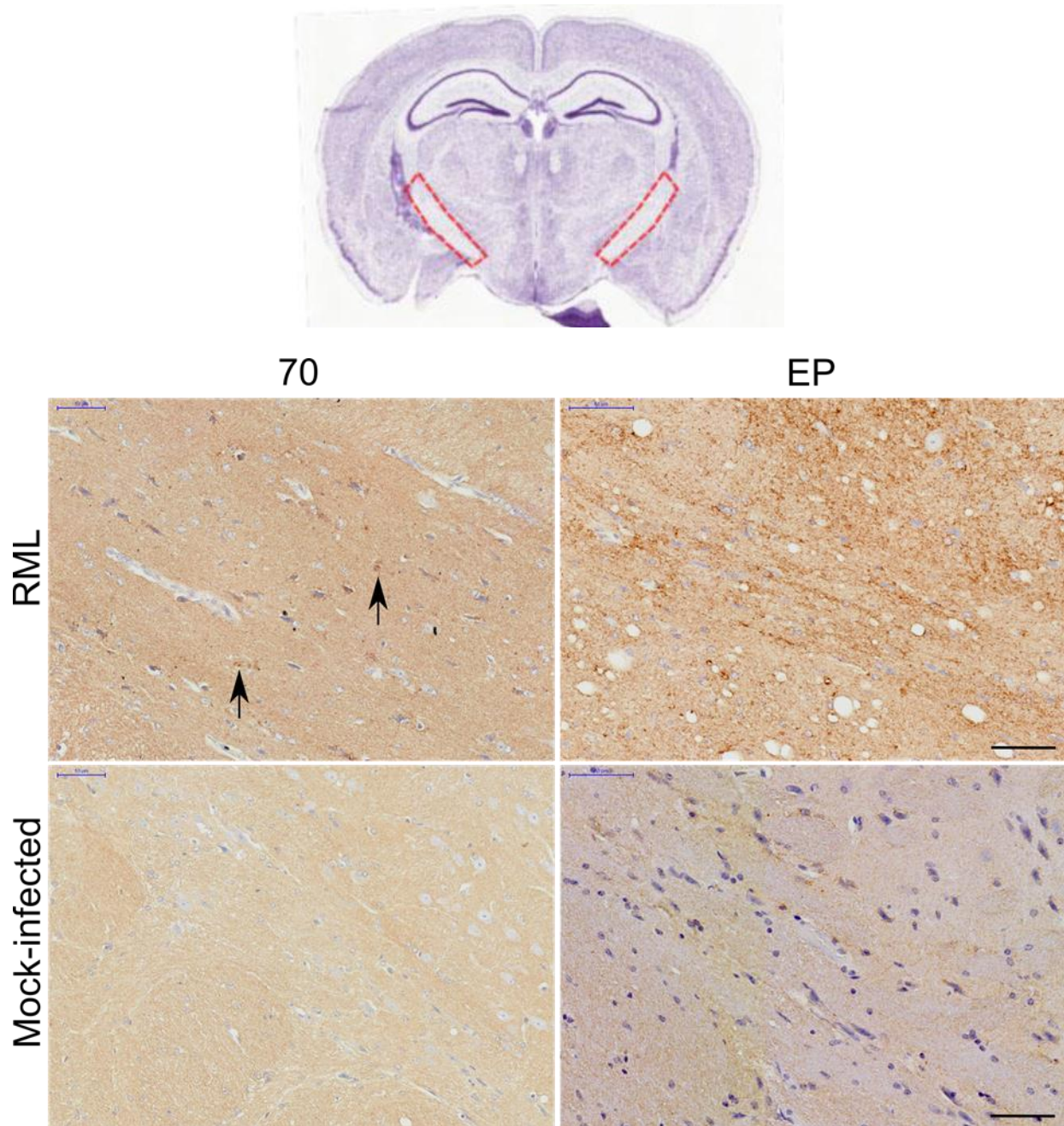


Figure 11. Detection of PrP^{Sc} in the forebrain of RML scrapie prion infected mice. PrP^{Sc} deposits are detected in the forebrain region in the RML scrapie prion model of IP injected CD1 mice at 70 dpi (70) and is increased by EP. The coronal brain section to depict the magnified forebrain bundle area is from Allen Brain Atlas. The scale bar represents 100 microns (© Anna Majer, used with permission)

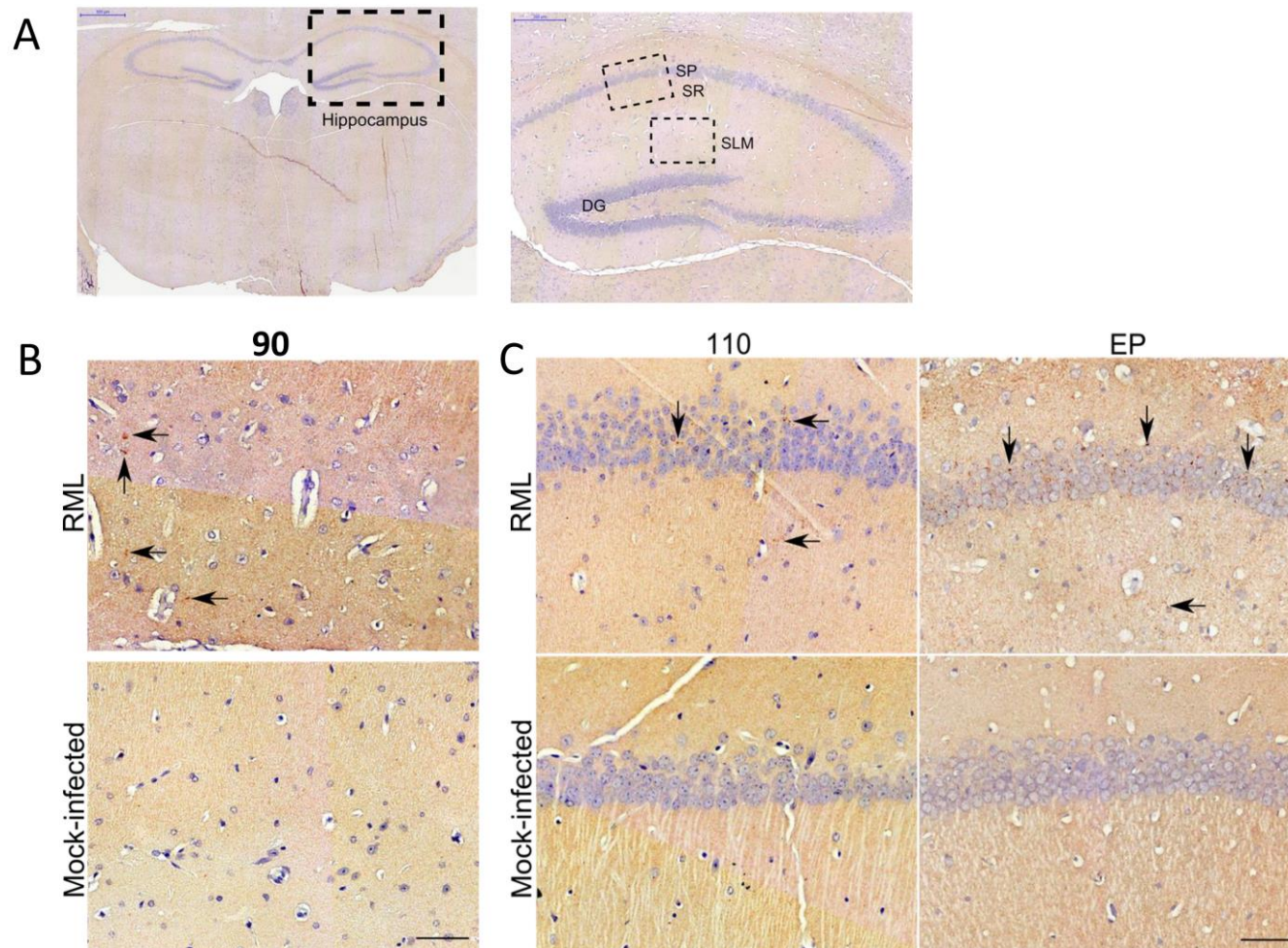


Figure 12. Detection of PrP^{Sc} in the hippocampus of RML scrapie prion infected mice. Hippocampal PrP^{Sc} detected in the RML scrapie prion infection model of IP injected CD1 mice. Panel A indicates the hippocampus area, with the *Stratum Pyramidale* (SP), *Stratum radiatum* (SR), *stratum lacunosum-moleculare* (SLM), plus *dentate gyrus* (DG) depicted, B) at 90 dpi (90) PrP^{Sc} is detected only in the SLM, and B) at 110 dpi (110), PrP^{Sc} is detected in the SP and SR, which persists at endpoint. The scale bar in panels B and C represent 50 microns. (© Anna Majer, used with permission)

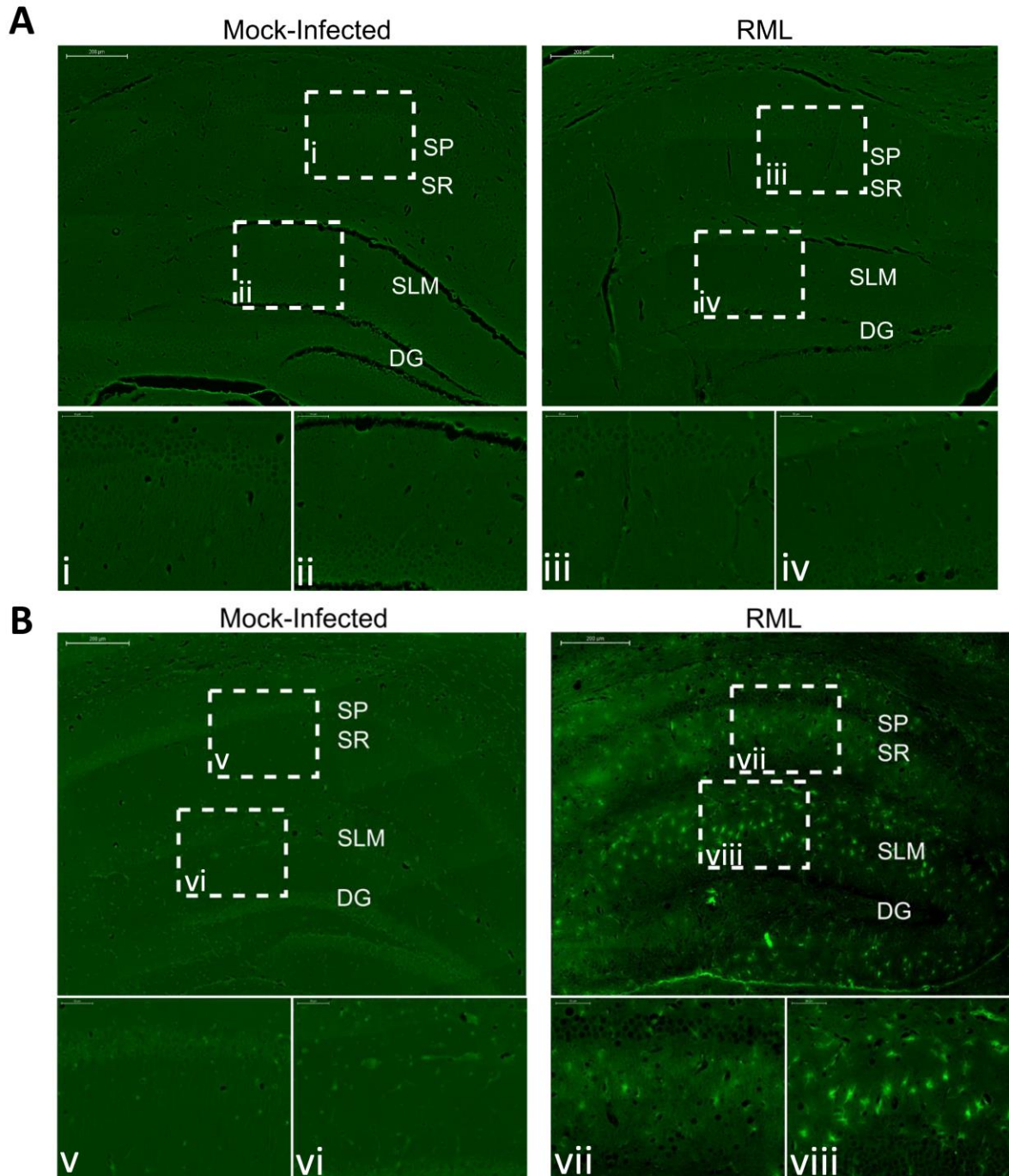


Figure 13. Fluoro-Jade C staining of coronal hippocampal sections from mock infected and RML scrapie prion infected mice to detect neurodegeneration. A) at 70 dpi no staining is evident, i-iv insets represent higher magnification of SP/SR and SLM areas, and B) at endpoint, neurodegeneration detected in the RML scrapie infected mice with increased magnification of SP/SR (vii) and (viii) SLM areas but none is detected in the age-matched mock infected mice (v & vi). Scale bar for larger images is 200 microns and 50 microns for insets. (modified from © Anna Majer, used with permission).

bodies were only observed within the *CA1* region at EP of disease (Figure 14). It was concluded that astrocyte expressed transcript contribution to the total RNA captured from the *CA1* region was limited at time points prior to EP. Therefore, the levels of miR-128-3p analyzed during preclinical disease likely reflected neuronal expression. In addition to astrocytes, the microglial cells in this region were examined using classical immunohistochemistry with a specific microglial antibody to the IBA-1 protein (Imai et al. 1996), commonly used to detect activated microglia in prion disease (v Eitzen et al. 1998). Some microglia were evident within the *CA1* region but activation, as evidenced by increased numbers of ramified microglial cells, were only evident within the *CA1* region in prion infected mice at EP (Figure 15). The RNA extracted from this *CA1* region during RML scrapie prion infection in mice was thus sampled for the expression of miR-128-3p in a neuronal population for this thesis.

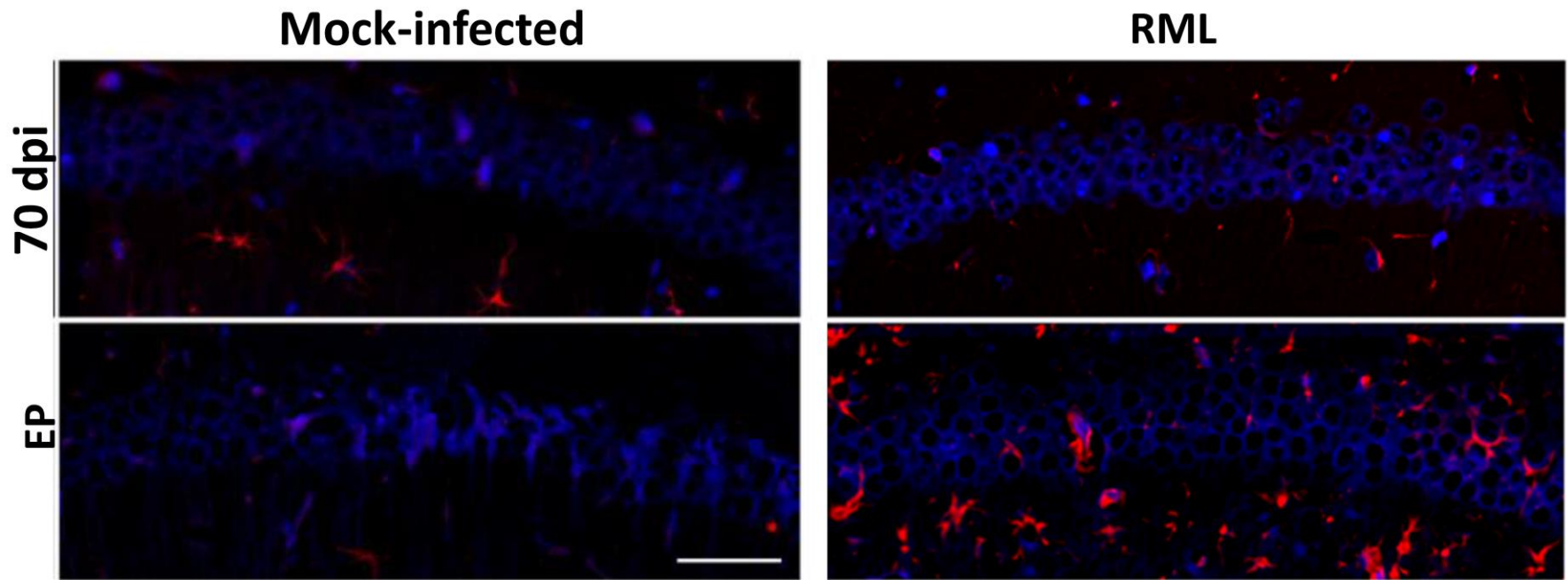


Figure 14. Detection of astrocytes within the CA1 region of the hippocampus in coronal brain sections from RML scrapie prion infected mice. A GFAP antibody was used with immunofluorescence to detect the infiltration of astrocytes in the CA1 during RML scrapie prion infection in mice at endpoint but not mock infected mice, denoted by the red fluorescent signal. Scale bar is 50 microns. (modified from Majer et al. 2012, reproduced under creative commons license).

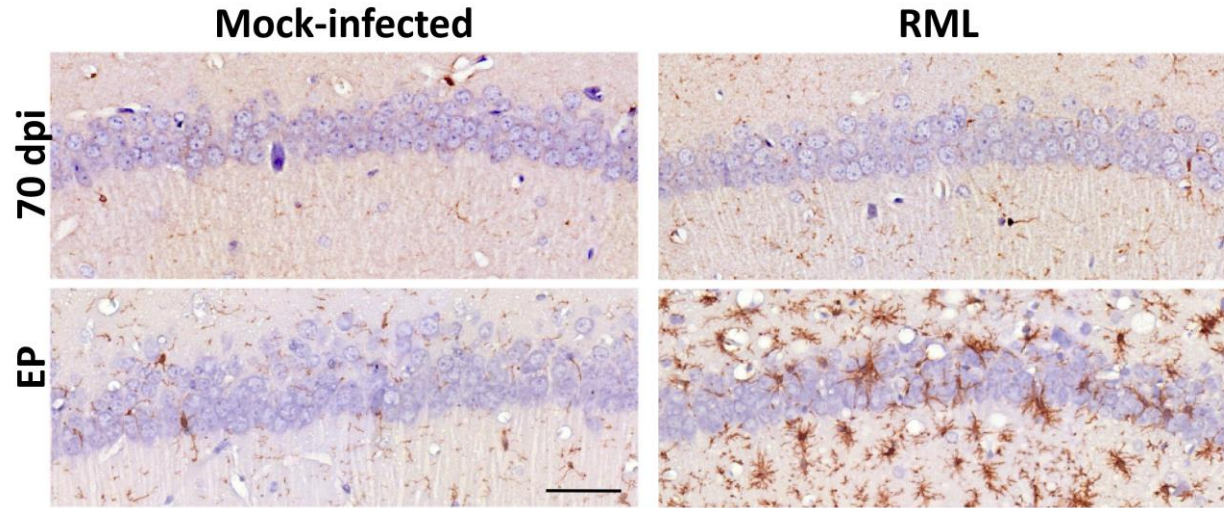


Figure 15. Detection of microglia in the CA1 region using immunohistochemistry during RML scrapie prion infection in mice. Microglia invade the CA1 cell bodies at EP of prion disease while there are minimal microglia detected at 70 dpi. The purple layer indicates the CA1 neuronal cell bodies while the brown staining is immunohistochemical detection of microglia using IBA-1 antibody (scale bar = 50 microns; modified from Majer et al. 2012, reproduced under creative commons license).

4.1.2 Hypothesis

The abundance of miR-128-3p undergoes temporal changes in the cell bodies of neurons localized in the CA1 region of the hippocampus.

4.1.3 miR-128-3p is increased during preclinical disease in micro-dissected neuronal cell bodies from the CA1 region of the hippocampus

LCM was used to select the CA1 neuronal cell bodies to extract RNA from in order to delineate the levels of miR-128-3p during RML scrapie infection in mice. LCM provided a reliable method which could isolate a relatively homogeneous CA1 neuronal cell body population. The LCM capture of CA1 neuronal cell bodies was performed at 5 timepoints during disease including early asymptomatic of 70 dpi, 90 dpi and 110 dpi, and symptomatic including 130 dpi and EP. Microdissection was performed on 8 micron coronal brain sections that were preserved in OCT media. After cutting and placing onto slides, the sections were processed with dyes to enable the selection of the CA1 cell bodies using laser pulses. Approximately 700-1500 cell bodies were captured onto a cap, and caps from multiple sections from one animal were combined (Figure 16). After total RNA isolation, which yielded both small and large RNA species, the RIN values were obtained and only those with RIN >5.8 were used for RT-qPCR (Figure 17). For the detection of miRs, the RNA from 3-4 animals per treatment per timepoint were combined as the RNA yield was too low to obtain the miR-128-3p signature for each animal individually.

The small nuclear RNA 135 (snoRNA135) was used to normalize the data as it had previously been validated for these CA1 samples (Majer et al. 2012), and displayed little variation (Figure 18A). The fold change in miR-128-3p in the CA1 was calculated using mock infected as a baseline at each timepoint. Indeed, miR-128-3p did display a temporal induction during RML scrapie prion infection in mice (Figure 18B). At the earliest timepoint examined, 70 dpi, before

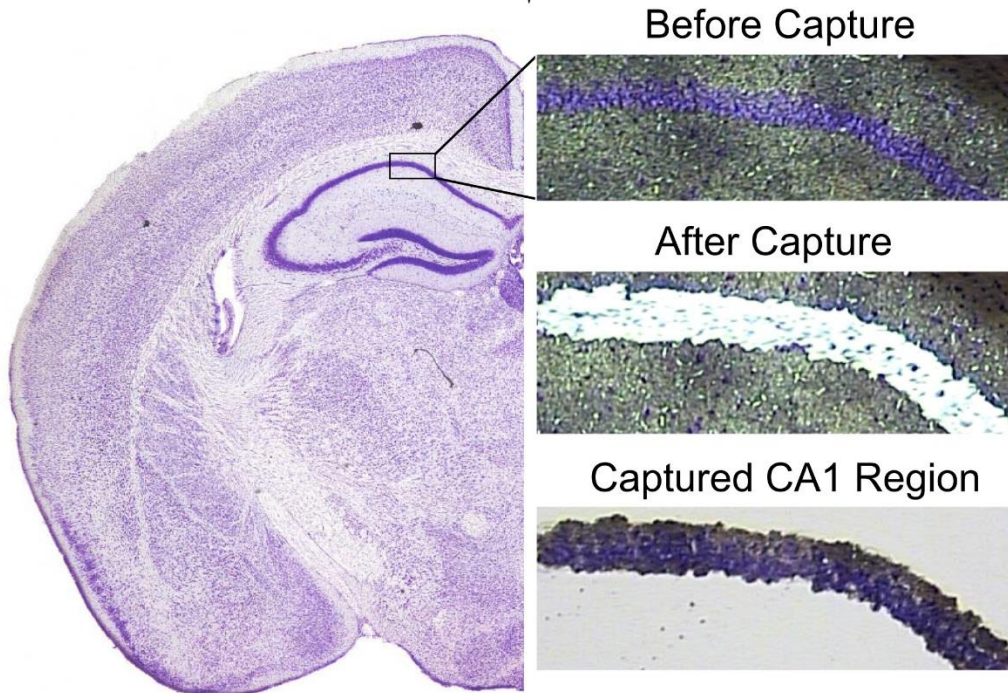


Figure 16. Capture of the CA1 neuronal cell bodies using LCM technology. The coronal brain section is stained with cresyl violet and the CA1 nuclei are then captured by laser onto plastic caps before extracting total RNA. Each animal has numerous sections cut to yield between 700-1500 neuronal cell bodies from this distinct region. (© Anna Majer, used with permission)

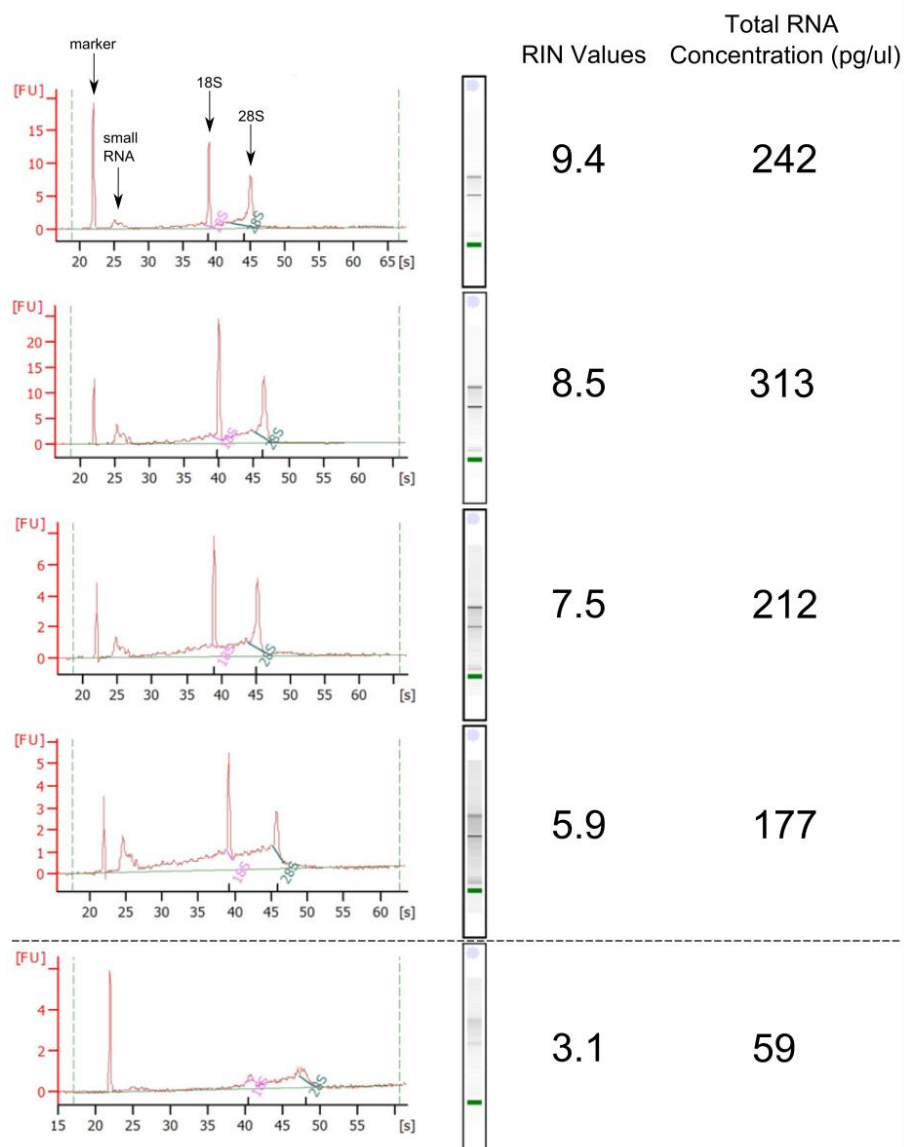


Figure 17. RNA integrity determination of total RNA from LCM captured CA1 neuronal cell bodies. The Bioanalyzer 2100 with the Pico 6000 chip was used to determine RIN values by the ratio of 18S and 28S with an algorithm applied, only RNA with RIN >5.8 were used for PCR analysis (above the dashed horizontal line). Adapted from Majer et al 2012 and reproduced under creative commons license.

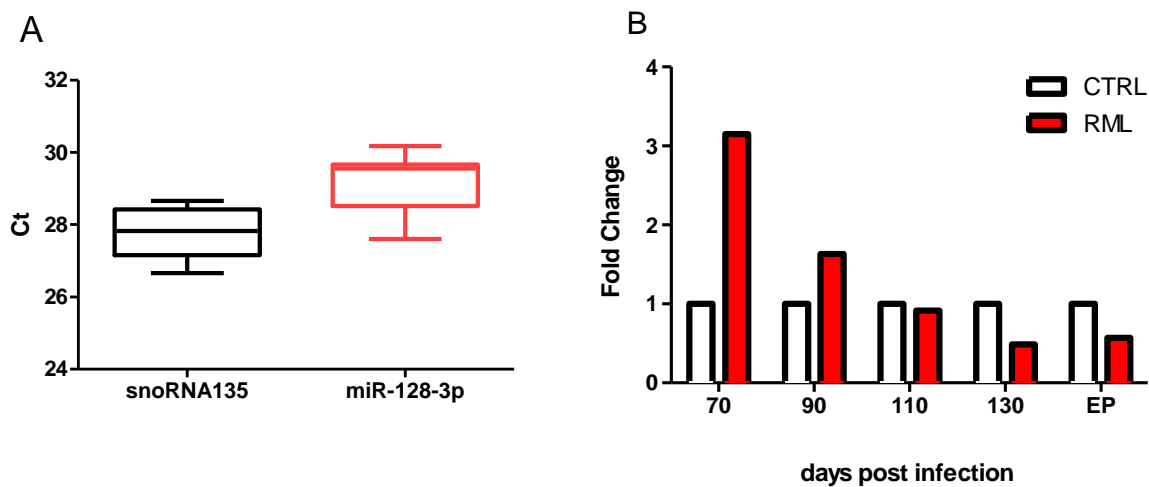
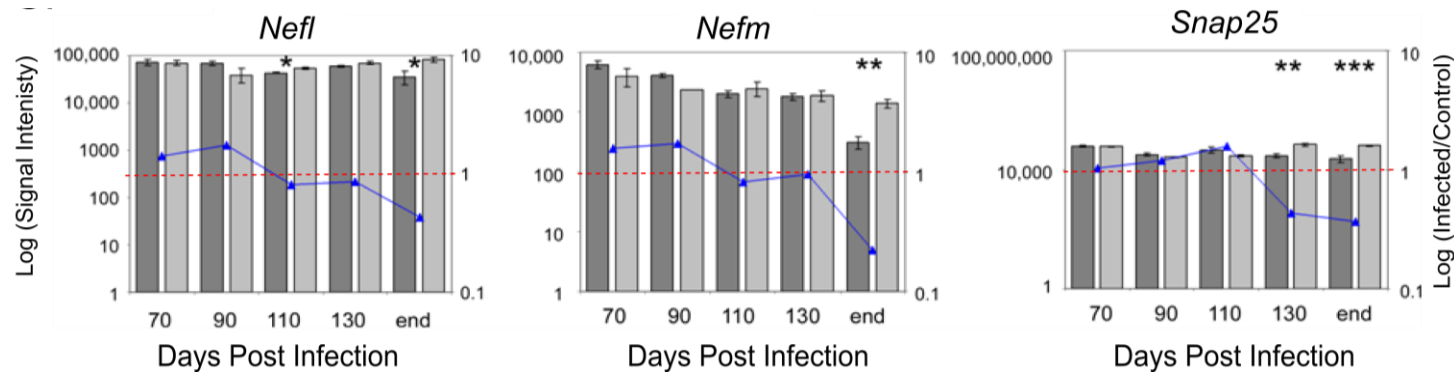


Figure 18. Fold change in mature miR-128-3p from total RNA derived from CA1 neuronal cell bodies from mock and RML scrapie prion infected mice during disease time course. A) Box and whisker plots depicting the variation in the small nuclear RNA135, which was used to normalize the Cts of miR-128-3p, and B) Fold change in miR-128-3p in mock infected (CTRL) and RML scrapie infected (RML) from 70dpi to EP of disease. The total RNA from 3-4 mice was pooled per timepoint per treatment to obtain cDNA before performing TaqMan miR assays and fold change was calculated using the delta delta Ct method, with mock infected serving as baseline.

PrP^{Sc} is detectable by immunohistochemistry, miR-128-3p levels are increased by 3.1fold, an increase which persisted at 90 dpi by 1.6fold, and then levels returned to mock infected baseline by 110 dpi. During the clinical stages of disease, at 130 dpi and EP, the levels of miR-128-3p drop to -2fold and -1.8fold respectively in the RML scrapie prion infected animals. From the pathology conducted on this region, these later stages of disease are when the neuronal profile have shifted to include microglia and astrocytes, as these are detected in this region during late stages of disease. This change in cell composition likely accounts for some of the decreased levels of miR-128-3p at symptomatic stages of disease.

To verify the neuronal features of the LCM derived RNA, previously published work from gene microarray analysis on these same RNA samples over the time course of disease demonstrated the neuronal specificity at earlier stages of disease (Figure 19). The neuronal genes examined were neurofilament light (*Nefl*) and medium (*Nefm*) plus the synaptosomal 25 (*SNAP25*). These three genes displayed stable expression during the early stages of infection, then were decreased at late stages (Figure 19A). The microglial gene *Ibal* drastically increased at 130 dpi and EP while the astrocyte gene *Gfap* was only detected at EP (Figure 19B). The gene expression data mimicked the pathology seen in CA1 immunohistochemistry, where microglia and astrocytes invaded the CA1 at the late stages of disease. This indicated that the early stages had a mostly neuronal composition of RNA while the later stages of 130 dpi and EP contained a glial component alongside neuronal.

A.



B.

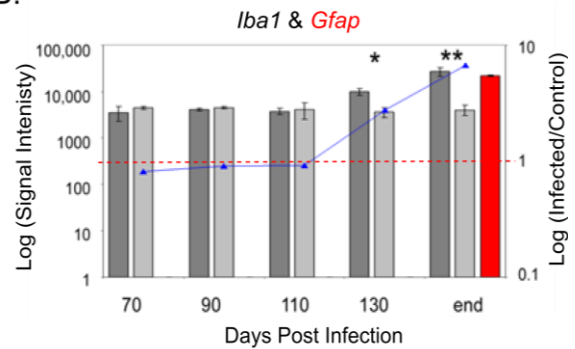


Figure 19. Microarray analysis of gene expression from total RNA derived from CA1 neuronal cell bodies from 70 dpi to endpoint (end) in RML scrapie prion infected mice. A) neuronal markers, *Nefl*, *Nefm*, and *Snap25*. B) microglial *Iba1* and astrocytic *Gfap*. Dark grey bars represent RML scrapie infected and light grey bars are mock infected, the bars indicate log signal intensity detected by microarray, while the red dashed bars indicate log fold change of infected/control set at a baseline of 1 (no change), and the blue triangles and line represents the log fold change of RML scrapie infected over mock infected. Adapted from Majer et al 2012.

4.2 Bioinformatic prediction of miR-128-3p targets

4.2.1 Rationale

Given that the hippocampus is affected during early stages of prion disease, exhibiting PrP^{Sc} build-up, altered dendritic complexity, and transcriptional changes as well as miR-128-3p over-expression it was of interest to determine those genes that miR-128-3p targets. In this section, the targets of miR-128-3p pertaining to neurons and prion disease were predicted bioinformatically and some of these were validated experimentally. The first strategy in narrowing down potential targets of a given miR is to use computer generated algorithms to find potential binding sites between the miR 5' seed sequence, which is 6-8 base pairs, against all 3' UTRs that are annotated in databases containing human sequences, which are then aligned to mouse. These lists were then filtered for targets that are important in neurons and also for those that have context in the realm of prion disease pathogenesis. Finally, the target list was further filtered to choose a small number of potentially important targets for experimental validation. Given that there may be hundreds of predicted targets, even when using a stringent prediction algorithm, it is not a feasible venture to validate all of them.

4.2.2 Hypothesis

miR-128-3p is a post-transcriptional regulator of target genes that have important roles in neurons that may prove vital in the pathogenesis of prion disease.


4.2.3 TargetScan predicted 3' UTR sites for miR-128-3p seed sequence binding

The TargetScan Human 7.1 algorithm was used to predict miR-128-3p binding sites within the 3' UTR of mRNA. This algorithm is conservative because it uses 100% binding

of 6, 7, and 8 nucleotides on the seed sequence of 3' UTR target without any G:U wobble or bulges permitted while taking free energy and thermodynamic stability into account (Lewis, Burge & Bartel 2005). For *Homo sapiens*, the sequences are obtained from NCBI Ensembl, which are then aligned with *Mus musculus* sequences from UCSC Genome Bioinformatics to determine binding site conservation. The human sequences are longer and better described compared to mouse, thus the alignment of mouse with human annotations provides better coverage when seeking targets.

The total number of sequences contained in the TargetScan Human 7.1 (henceforth TargetScan) database is 19,475 with a total of 28,353 transcripts. Predicted target analysis was performed by selecting Human or Mouse in the species tab and inputting miR-128-3p into the broadly conserved families tab in TargetScan (Figure 20). This prediction analysis for human yielded a total of 1,217 3' UTR target transcripts containing a total of 1,382 conserved binding sites and 672 poorly conserved binding sites for the miR-128-3p seed sequence (Table 6). The predicted targets for mouse revealed 978 transcripts containing a total of 1,101 conserved sites and 563 poorly conserved sites. The total number of conserved and poorly conserved sites were combined and used for further analysis. The total binding sites in common between mouse and human was 901 (Figure 21A). These overlapping targets were put through DAVID analysis for tissue expression and 55% of these were annotated as expressed in the brain (Figure 21B). The remaining tissues that were represented were not major organs, some of the cell types found are indicative of lung tissue, for example mesangial, epithelium, and vascular smooth muscle, which is significant as miR-128-3p is also expressed in the lungs.

A comparison was performed between the list of human and mouse gene targets



TargetScanHuman

Prediction of microRNA targets

Release 7.1: June 2016

Agarwal et al., 2015

Search for predicted microRNA targets in mammals

1. Select a species

AND

2. Enter a human gene symbol (e.g. "Hmga2")
or an Ensembl gene (ENSG00000149948) or transcript (ENST00000403681) ID

AND/OR

3. Do one of the following:

- Select a broadly conserved* microRNA family
- Select a conserved* microRNA family
- Select a poorly conserved but confidently annotated microRNA family
- Select another miRBase annotation

Note that most of these families are star miRNAs or RNA fragments misannotated as miRNAs.

- Enter a microRNA name (e.g. "miR-9-5p")

[\[Go to TargetScanMouse\]](#)

[\[Go to TargetScanWorm\]](#)

[\[Go to TargetScanFly\]](#)

[\[Go to TargetScanFish\]](#)

Figure 20. Screen capture of TargetScan settings used for analysis. To obtain human targets, the settings that were adjusted were 1. Select a species = Human and 3. Select a broadly conserved* microRNA family to miR-128-3p. For mouse, the 1. Select a species was changed to Mouse while all other settings remained the same.

Table 6. The TargetScan predicted targets for miR-128-3p in Human and Mouse. The species, number of predicted 3' UTR targets with conserved and poorly conserved sites are indicated.

| Species | # of predicted 3' UTRs | Conserved sites | Poorly conserved sites |
|----------------|-------------------------------|------------------------|-------------------------------|
| Human | 1,216 | 1,382 | 672 |
| Mouse | 977 | 1,101 | 563 |

A



B

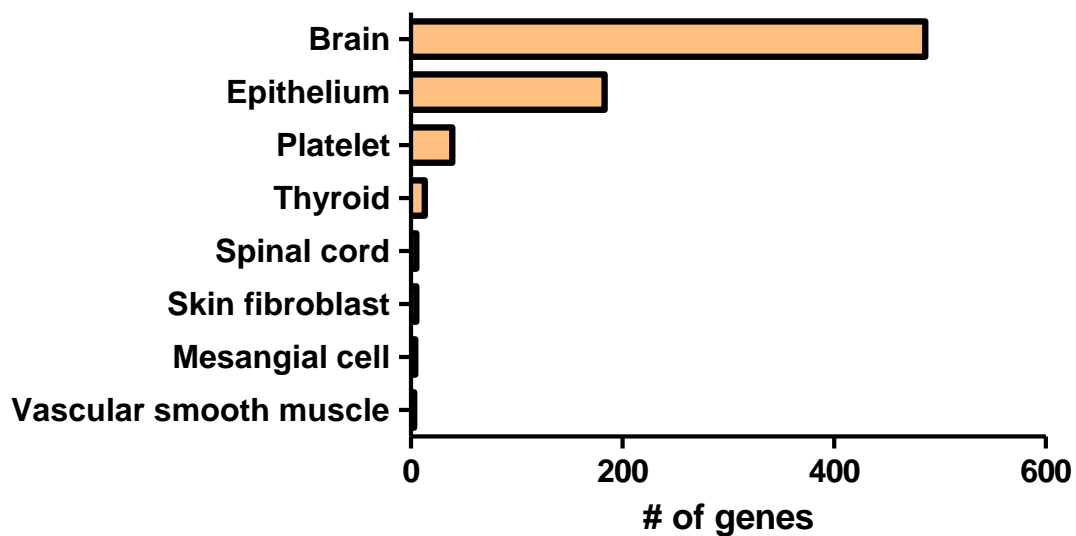
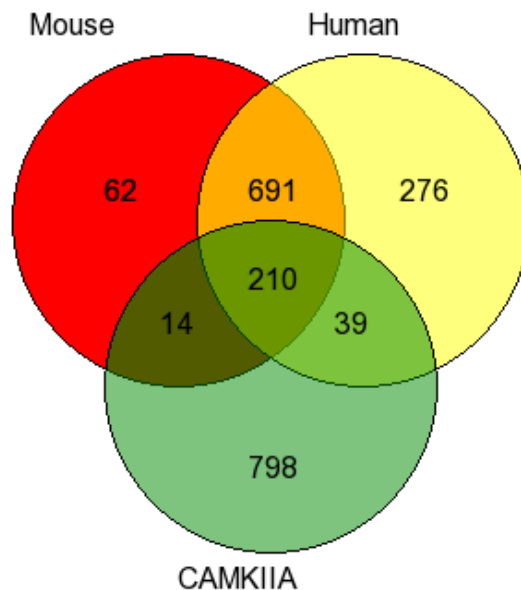


Figure 21. Comparison of miR-128-3p TargetScan predicted mouse and human 3' UTR targets. A) Venn diagram depicting 901 targets are in common between mouse and human and B) the tissue expression analysis of the 901 overlapping genes using DAVID with a large representation in the brain.

predicted by TargetScan, and a previously published list of miR-128-3p targets derived experimentally by HITS-CLIP from CAMK2 α forebrain neurons (Tan et al. 2013a). CAMK2 α is a protein kinase that is expressed in glutamatergic neurons that can be used to pulldown neuronal specific targets. The HITS-CLIP mRNA was derived from Ago2 precipitated RNA, which forms part of the RISC complex in which miRs and mRNA are bound. This data was previously mined for miR-128-3p binding sites, resulting in a list of 1,061 genes. In comparing the TargetScan predicted targets to the 1,061 CAMK2 α gene dataset, there were 210 targets represented in all 3 groups, and 263 in at least 2 (Figure 22A). It was interesting to note that half of the 691 genes that were not found in the CAMK2 α dataset demonstrated gene expression in the brain (Figure 22B).

Indeed, a number of experimentally published targets for miR-128-3p that are important in neuronal function are absent in the CAMK2 α dataset (Ching, Ahmad-Annur 2015), thus the TargetScan predictions were examined separately as well. To narrow down the 901 human/mouse consensus targets, they were filtered by total number of binding sites within each 3' UTR and the top 100 of both was compared. This resulted in 32 overlapping targets, with more than 50% which had neuronal significance that were absent in the CAMK2 α dataset (Table 7).

A



B

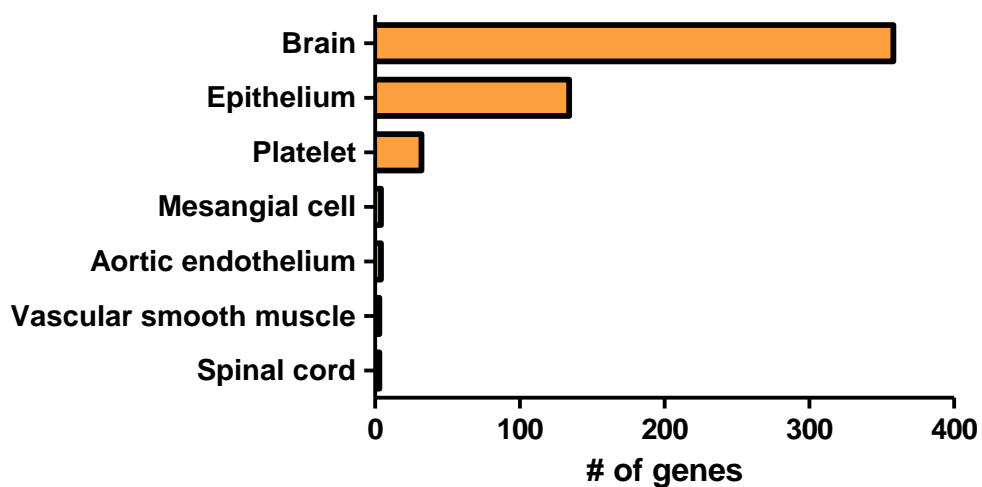


Figure 22. Comparison of miR-128-3p TargetScan predicted mouse and human 3' UTR targets to forebrain CAMK2 α (CAMKIIA) neuron derived 3' UTR targets. A) Venn diagram depicting the overlap between CAMK2 α (CAMKIIA) neuron, and predicted mouse and human targets, and B) tissue expression of 691 genes that were not found in the CAMK2 α neurons using DAVID analysis with brain being highly represented.

Table 7. Top 32 miR-128-3p TargetScan predicted 3' UTR targets in common between human and mouse. When most number of bindings sites within the UTR were considered. The 3' UTR, total number of bindings sites in human and mouse, those that were not present in forebrain CAMK2 α neurons and references for neuronal function in those not detected in the CAMK2 α neurons, are shown.

| 3' UTR Target | Total number of binding sites <i>Homo sapiens</i> | Total number of binding sites <i>Mus musculus</i> | Not in CAMK2 α dataset | Reported in neuronal function |
|---------------|---|---|-------------------------------|--------------------------------|
| AFF4 | 7 | 6 | X | (Komori et al. 2012) |
| AGO2 | 11 | 8 | | |
| ARHGAP19- | 10 | 7 | X | |
| SLIT1 | | | | |
| ARL8B | 5 | 5 | | |
| BEND4 | 6 | 5 | | |
| CNNM2 | 7 | 7 | X | (Arjona et al. 2014) |
| DCAF7 | 6 | 8 | | |
| DCP2 | 6 | 8 | X | (Ren et al. 2012) |
| DYNLL2 | 10 | 6 | X | (Suyama et al. 2016) |
| GPAM | 5 | 8 | X | (Urban et al. 2012) |
| GRIN2B | 8 | 7 | X | |
| GRIN2D | 8 | 6 | | |
| IFFO2 | 5 | 8 | | |
| JHDM1D | 7 | 5 | X | (Smith, Kimyon & Watters 2014) |
| KCNJ6 | 7 | 10 | X | (Cooper et al. 2012) |
| KCNN3 | 7 | 6 | | |
| MAP3K2 | 5 | 7 | X | (Wang, Su & Xia 2006) |
| MAPK1 | 9 | 5 | | |
| NFAT5 | 7 | 6 | | |
| NFIA | 5 | 6 | X | (Wang et al. 2010) |
| NFIB | 9 | 8 | | |
| NOVA1 | 6 | 6 | | |
| NT5C1A | 5 | 7 | X | |
| ONECUT2 | 9 | 14 | | |

| | | | | |
|---------|----|----|---|------------------------------|
| PGAP1 | 5 | 8 | | |
| QKI | 7 | 8 | X | (Hardy 1998) |
| RORB | 5 | 6 | X | (Jabaudon et al. 2012) |
| SLC24A4 | 7 | 6 | X | (Li, Lytton 2014) |
| SLC8A1 | 6 | 9 | X | (Mohammadi, Bigdeli 2014) |
| SMAD2 | 6 | 5 | X | (Stegmuller et al. 2008) |
| ZBTB20 | 9 | 12 | | |
| ZBTB37 | 14 | 13 | X | |

4.2.4 Selection of genes for glutamate receptors NMDAR and mGluR5 as targets for further validation

The presence of the NMDA genes *GRIN2B* and *GRIN2D* in Table 2.2 was of interest because of the synaptic NMDAR gene transcription response launched at early stages of disease in *CA1* neurons during RML scrapie prion infection (Majer et al. 2012). Specifically, the gene encoding *GRIN2B* was downregulated in the *CA1* region during early RML scrapie infection in mice as detected by microarray and RT-qPCR (Figure 23A). Therefore, it was possible that miR-128-3p which was increased at the early stages could be targeting *GRIN2B* and with 8 binding sites in human and 7 in mouse in the 3' UTR (Table 8), it was a desirable target to validate. The *GRIN2D* gene was notable as it was found in the *CAMK2 α* neuronal derived targets as well as TargetScan predicted with 8 binding sites in human (Table 8). With relevance to prion disease, *GRIN2D* codes for the subunit of the NMDAR2D receptor which is up regulated in PrP^C null mice (Khosravani et al. 2008b). This leads to increased excitotoxicity in the neurons cultured from the hippocampus of these mice. As PrP^C transcripts were decreased in the *CA1* during the earliest stage of disease (Figure 23B), this suggested that *GRIN2D* could be affected at this time as well.

Another target of interest within the predicted dataset was *GRM5*, which is a gene for mGluR5, another vital glutamate receptor in proper neuronal function. In fact, this mGluR5 interacts with NMDARs in the *CA1* region to drive the changes between NMDAR2B and NMDAR2A (Matta et al. 2011). This receptor also has a role in prion disease because the mGluR5 is known to interact with PrP^C at the cell surface (Beraldo et al. 2011, Hu et al. 2014, Beraldo et al. 2016). Thus the 3' UTRs of the three targets of

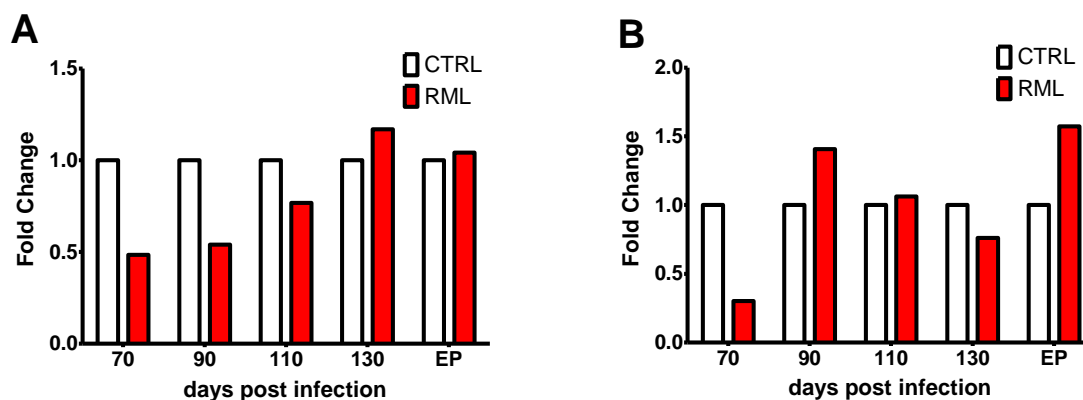


Figure 23. Fold change in *GRIN2B* and *PRNP* genes in total RNA derived from CA1 neuronal cell bodies during RML scrapie prion infection in mice. A) fold change of *GRIN2B* mRNA over 5 timepoints of infection in mock infected (CTRL, white bars), and RML scrapie prion infected (RML, red bars) mice B) fold change of *PRNP* mRNA. Fold change was calculated on data obtained from RT-qPCR with TaqMan Gene Expression assays using *GAPDH* as an endogenous control reference. Total RNA was pooled from 3-4 mice per timepoint per treatment. Adapted from Majer et al. 2012 and Majer 2015.

Table 8. Glutamate receptor subunit 3' UTR target sites assessed by TargetScan. The 3' UTR subunit name, species, total number of binding sites, types of binding sites and whether they were identified in previous versions of TargetScan.

| 3' UTR Target | Species | Total # of binding sites | Type of binding sites | Identified in previous versions of TargetScan |
|----------------------|---------------------|---------------------------------|------------------------------|--|
| <i>GRIN2B</i> | <i>Homo sapiens</i> | 8 | 7- 7mer; 1- 6mer | No |
| | <i>Mus musculus</i> | 7 | 6-7mer; 1-6mer | No |
| <i>GRIN2D</i> | <i>Homo sapiens</i> | 8 | 7- 7mer; 1 -6mer | 2009, 2011 |
| | <i>Mus musculus</i> | 6 | 5- 7mer; 1- 6mer | 2009, 2011 |
| <i>GRM5</i> | <i>Homo sapiens</i> | 2 | 1-7mer; 1-6mer | 2011 |
| | <i>Mus musculus</i> | 3 | 1-7mer; 2-6mer | 2011 |

GRIN2B, *GRIN2D*, and *GRM5* were examined at depth from the TargetScan analysis. The types, number of binding sites and whether they were predicted in previous versions are described in Table 8. Since the total number of binding sites were highest for *GRIN2B* and *GRIN2D*, their 3' UTR sequence homology was examined to determine if there were consensus sites between the UTRs. A pairwise sequence alignment in LaserGene MegAlign resulted in 0 % consensus.

4.2.5 Luciferase Reporter Assays confirms miR-128-3p binding to 3' UTR of *GRIN2B*, *GRIN2D*, and *GRM5*

In vitro validation of the binding of miR-128-3p to the predicted target sites within the 3' UTR of the *GRIN2B*, *GRIN2D*, and *GRM5* genes, using Luciferase Reporter plasmids (Table 9). The human and mouse binding regions are highly conserved and so pMirTarget luciferase reporter plasmids containing the human *GRIN2B* and *GRIN2D* 3' UTR constructs were obtained commercially (Origene). These contained an internal ribosomal entry site (IRES) promoter for the expression of the firefly luciferase gene after which the 3' UTR was located (Appendix 1). The normalizer for this plasmid was the RFP which was under the cytomegalovirus (CMV) promoter. For the *GRM5* 3' UTR, the human sequence was cloned into the pmirGLO plasmid under a phosphoglycerate kinase (PGK) promoter and a *Renilla* luciferase under a SV40 promoter (Appendix 2).

The Luciferase Reporter Assay was performed in either HeLa cells (*GRIN2B/GRIN2D*) or mouse cortical cells cultured from embryonic mice (*GRM5*), these transfections were performed in triplicate wells in three independent cell preparations. For

Table 9. The 3' UTR sequences inserted in the Luciferase reporter plasmid. Gene name, 3' UTR length, NCBI Accession ID, and updated sequence ID are given.

| 3' UTR | Length of UTR | NCBI Accession ID | Updated sequence ID |
|---------------|----------------------|--------------------------|----------------------------|
| <i>GRIN2B</i> | 1,306 | NM_000834 | NM_000834.3 |
| <i>GRIN2D</i> | 994 | NM_000836 | NM_000836.2 |
| <i>GRM5</i> | 781 | NM_000842 | NM_000842.4 |

miR-128-3p binding in the luciferase reporter assay, it was decided to use pre-miRs. These molecules are comparable to siRNAs but are chemically modified to ensure the opposing strand, in this case miR-128-5p, is not incorporated into the RISC. The experimental effects are thus limited to the mature miR-128-3p molecule. The miR concentration can also be controlled with the use of pre-miRs and dose dependent effects can be determined. Additionally, other studies have successfully used these pre-miRs in luciferase reporter assays (Basu et al. 2011, Kocerha et al. 2014, Saba et al. 2008).

A number of controls were used alongside the experimental conditions (outlined in Table 10). Cells alone were used to determine background signal so this could be removed from the raw data. Other controls were transfection of the plasmid alone and a negative control miR that consisted of a scrambled sequence that is not known to bind to human mRNA. Both the control and miR-128-3p pre-miRs were tested at various concentrations for 24 hour transfections. Raw data was obtained and processed as per the flow chart in Figure 24. The 'cells only' value was subtracted from all data and the resulting values were normalized by dividing luciferase values by RFP or *Renilla* values. These were then divided by plasmid only to yield relative expression. The ratios were divided by the miR scramble control for each independent concentration to obtain final relative expression.

The luciferase assays for miR-128-3p binding to the 3' UTRs for *GRIN2B*, *GRIN2D*, and *GRM5* demonstrated a significant reduction in luciferase activity (Figure 25). The *GRIN2B* 3' UTR luciferase assay resulted in 25-30% reduction of luciferase activity (p-values ≤ 0.008) (Figure 25A). The *GRIN2D* binding by miR-128-3p was strongest (Figure 25B) with 61-77% reduction in luciferase activity (p-values < 0.0001), while the *GRM5* subunit, which had only 2 predicted binding sites, had significant

Table 10. Summary of treatments for each Luciferase Reporter Assay performed. The treatment type, miR added or not, objective of the treatment plus number of wells treatment was applied to in a 96 well are mentioned.

| Treatment | miR added | Objective | # of wells |
|-----------------------------|------------------|--|--------------------------------|
| Plasmid and miR of interest | miR-128-3p | Test miR-128-3p binding to target | 3 per miR concentration tested |
| Plasmid and control miR | miR-scramble | Obtain biological control readings for increased miR in cell | 3 per miR concentration tested |
| Plasmid only | No | Obtain baseline luminescence readings | 3 |
| Cells only | No | Obtain background fluorescent and luminescence readings | 3 |

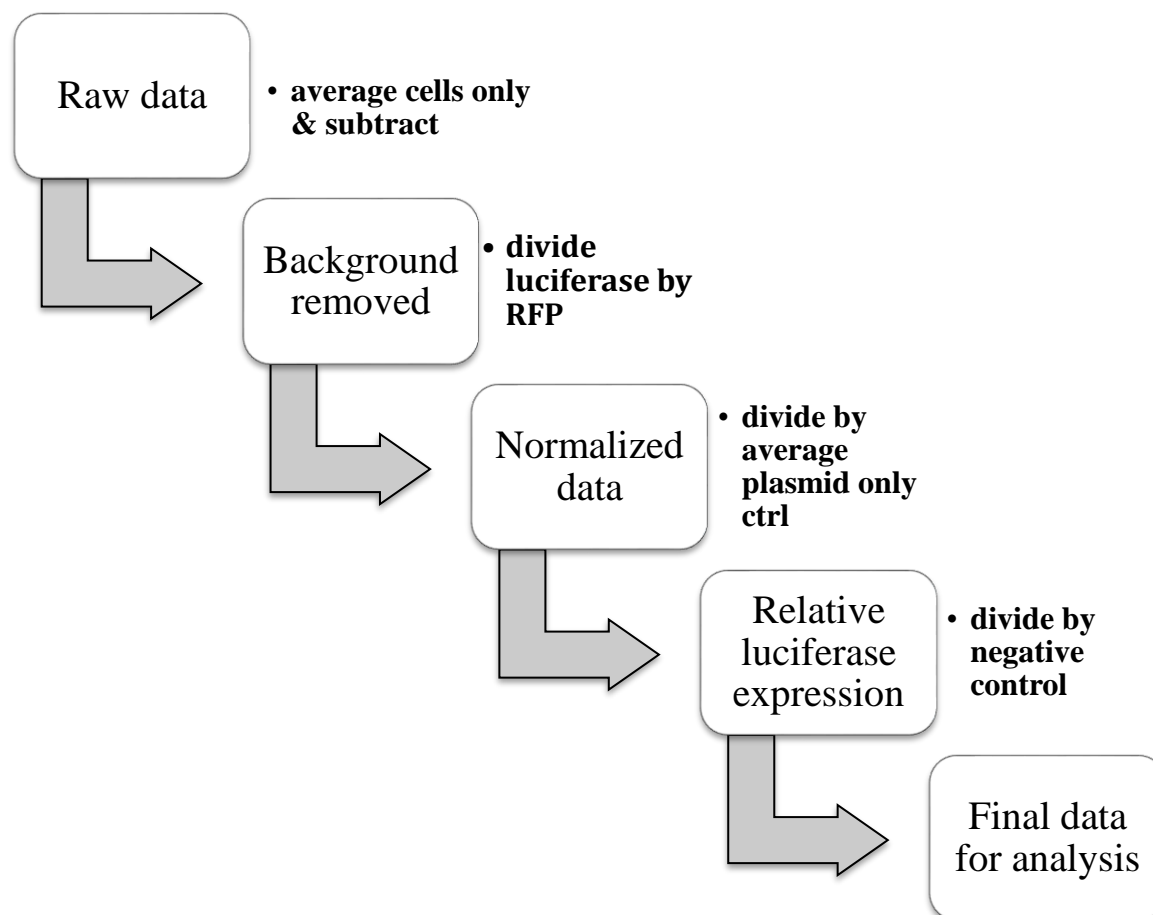


Figure 24. Flow chart for Luciferase reporter assay data analysis. First the raw data from both the normalizer (RFP/*Renilla*) and the luciferase has cells only background removed by subtraction. Then the luciferase values are divided by the normalizer (RFP or *Renilla*) to yield normalized data. This data is then divided by the average of the plasmid only control to give the relative expression of luciferase activity compared to background plasmid activity. Finally, the data is expressed as a ratio over the negative control miR scrambled data to give the final data which is a percentage of miR-128-3p over the scrambled miR negative. This final data is then analyzed by statistical t-tests and plotted as mean and standard error mean to visualize results.

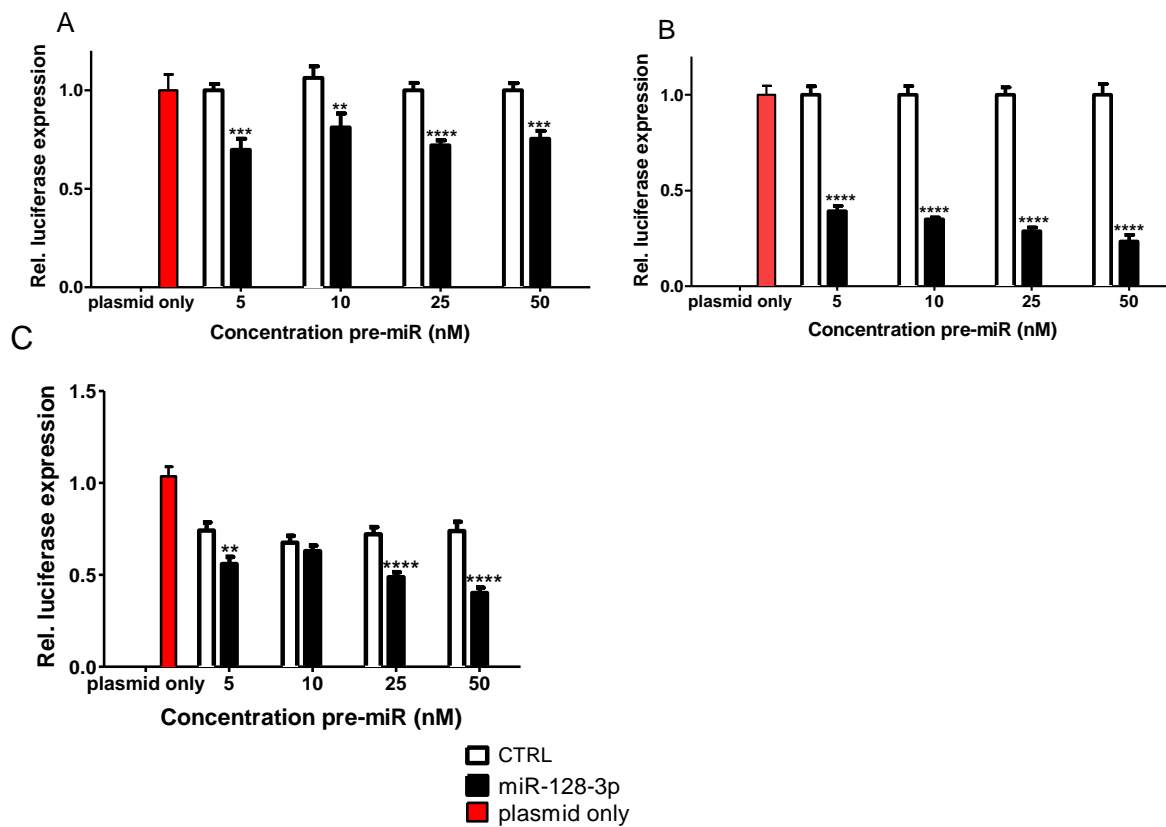


Figure 25. Luciferase Reporter Assay results for the binding of miR-128-3p to the human *GRIN2B*, *GRIN2D*, and *GRM5* 3' UTRs. The relative luciferase expression is depicted against four concentrations 5, 10, 25, and 50 nM of miR-scramble (CTRL, white bar) or miR-128-3p (black bar) were co-transfected with the luciferase reporter plasmid for 24 hours with plasmid only control (red), results for A) *GRIN2B* 3' UTR, B) *GRIN2D* 3' UTR, and C) *GRM5* 3' UTR. The mean and SEM indicated by the error bars is plotted, significance was assessed with one-tailed t-tests between control and miR-128-3p treated at each concentration. ****= p-value < 0.0001, ***= p-value < 0.001, **= p-value < 0.01.

reductions in luciferase activity at all but one concentration of 10 nM (Figure 25C). The concentrations of 5, 25, and 50 nM displayed a 23-34% decrease in luciferase activity (p-values ≤ 0.002).

4.3 Enrichment of miR-128-3p within the synaptoneurosomes prepared from forebrain and hippocampus

4.3.1 Rationale

It is well documented that synapse regions possess the ribosomal translational machinery to enable localized protein synthesis (Steward, Levy 1982) as well as components of the RISC suggesting that miR regulation of translation is also occurring (Lugli et al. 2005, Ashraf et al. 2006, Lugli et al. 2012). Furthermore, a number of synaptic miRs have previously been shown to provide a rapid regulatory response triggered by synaptic activity (Pichardo-Casas et al. 2012, Saba et al. 2012, Schrott et al. 2006). However, very little is known regarding whether the miRs that are localized at the synapse play roles during neurodegenerative disease. As the functions of miRs localized in such distal cellular locations as dendritic spines and synapses may be completely independent of their expression within the cell body it is important to determine miR abundance specifically within the synapse. Therefore, the goal of this chapter was to determine the synaptic miRNome, including miR-128-3p specifically, and identify any changes in abundance that are associated with prion infection and the stage of the disease.

4.3.2 Hypothesis

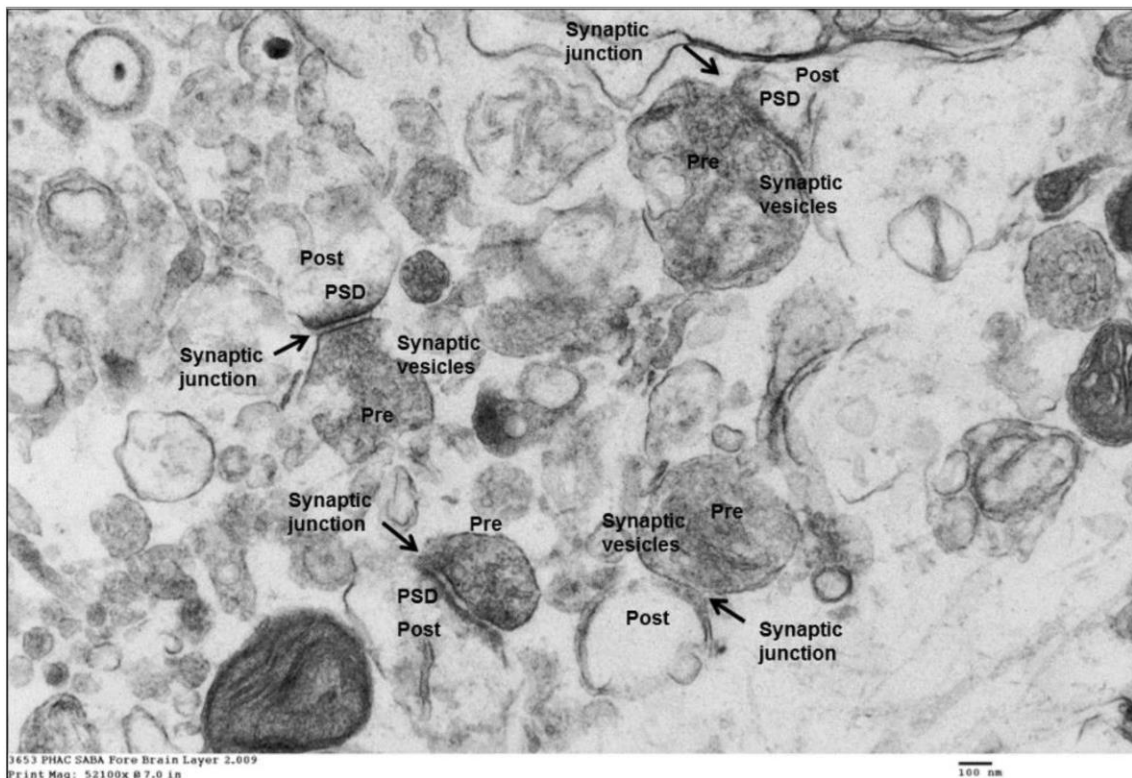
The abundance of miR-128-3p, and potentially other disease associated miRs, is altered in the forebrain and hippocampal synaptic compartments during the progression of RML scrapie prion disease in mice.

4.3.3 Validation of isolated synaptoneuroosomes reveals synaptoneuroosome defining features

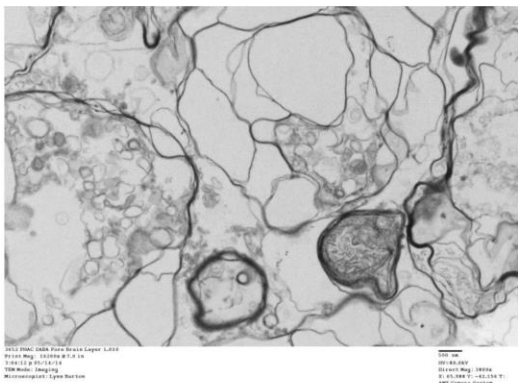
Images generated from Electron Microscopy of the synaptoneuroosomes established postsynaptic densities, presynaptic vesicles and intact mitochondria, hallmarks of synaptoneuroosomes (Rao, Steward 1991, Palay 1956) (Figure 26A). Images also showed that the myelin sheath layer contained empty lamellae and the pellet consisted of mitochondria (Figure 26B and C).

The miR complement of the forebrain synaptoneuroosome fraction was examined to ensure that it contained previously identified miRs enriched at synaptic compartments (Pichardo-Casas et al. 2012). This was performed by microarray of total RNA isolated from the synaptoneuroosomes of 2 adult wild-type CD1 mice. Using a signal intensity of > 100 units as the criterion by which a miR was deemed to be present, a total of 134 miRs were identified in synaptoneuroosomes from the first mouse and 119 miRs from the second. Of these, 110 miRs were found in common confirming that the methodology was reasonably consistent. Furthermore, 29 of these 110 miRs belonged to a 31 miR set that has previously been reported to be ubiquitous to synaptoneuroosomes prepared from all regions of the brain (Garza-Manero et al. 2014) (Table 11). In addition to this, 7 miRs that are reportedly enriched in the forebrain synaptoneuroosomes compared to whole forebrain tissue were also detected in the sample, including miR-132-3p, miR-204-5p, miR-212, miR-361, miR-139-5p, miR-146a, and miR-30a (Pichardo-Casas et al. 2012). Western blots were performed on proteins collected at different stages of the synaptoneuroosome preparation procedure to confirm enrichment of synapses. These demonstrated the presence of markers of the post and pre-synapse, synapse specific PSD95 and synapsin (pre- synaptic marker).

A



B



C

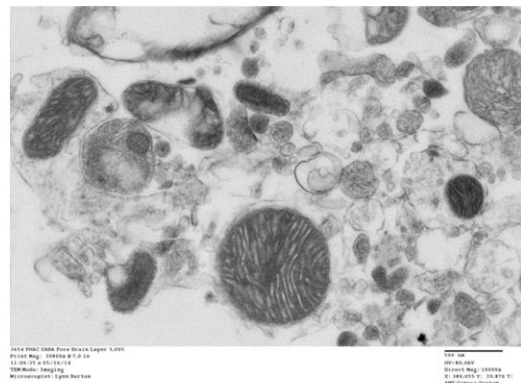


Figure 26. Electron Microscope images of three distinct layers isolated from the discontinuous Ficoll gradient including the synaptoneurosome layer. A) representative image of the synaptoneurosome fraction demonstrating features such as presynapses, post-synaptic densities (PSD), synaptic junctions, synaptic vesicles, and mitochondria, B) Myelin layer, containing empty lamellae and rings of lipid sheaths, and C) mitochondrial pellet containing many mitochondria compared to the synaptoneurosome

Table 11. 29 miRs that were detected through microarray analysis at the synaptoneurosome compartment of adult wild-type CD1 mice in common with rats.

The data from the miR microarray was compared to that found by Garza-Manero *et al* (2014). The miR, Agilent probe ID, and the mean signal intensity of three microarrays per mouse are indicated.

| miR | Agilent probe ID | Mouse 1, mean intensity | Mouse 2, mean intensity |
|----------------------|-------------------------|--|--|
| mmu-let-7a-5p | MIMAT0000521 | 10665 | 9804 |
| mmu-let-7b-5p | MIMAT0000522 | 4528 | 5276 |
| mmu-let-7c-5p | MIMAT0000523 | 8973 | 10016 |
| mmu-let-7d-5p | MIMAT0000383 | 4806 | 3287 |
| mmu-let-7e-5p | MIMAT0000524 | 3274 | 2362 |
| mmu-miR-100-5p | MIMAT0000655 | 770 | 897 |
| mmu-miR-124-3p | MIMAT0000134 | 25568 | 27084 |
| mmu-miR-125a-5p | MIMAT0000135 | 3055 | 2317 |
| mmu-mir-125b-2 | MI0000152 | 16242 | 22906 |
| mmu-miR-128-3p (a,b) | MIMAT0000140 | 3667 | 4761 |
| mmu-miR-129-5p | MIMAT0000209 | 252 | 420 |
| mmu-miR-132-3p | MIMAT0000144 | 2606 | 718 |
| mmu-miR-138-5p | MIMAT0000150 | 1279 | 1136 |
| mmu-miR-16-5p | MIMAT0000527 | 2024 | 1875 |
| mmu-miR-181a-5p | MIMAT0000210 | 930 | 1031 |
| mmu-miR-181b-5p | MIMAT0000673 | 404 | 608 |
| mmu-miR-181c-5p | MIMAT0000674 | 312 | 528 |
| mmu-miR-204-5p | MIMAT0000237 | 1413 | 1313 |
| mmu-miR-221-3p | MIMAT0000669 | 706 | 517 |
| mmu-miR-29a-3p | MIMAT0000535 | 16191 | 1745 |
| mmu-miR-29b-3p | MIMAT0000127 | 8281 | 1171 |
| mmu-miR-29c-3p | MIMAT0000536 | 4717 | 1102 |

| | | | |
|----------------|--------------|-------|-------|
| mmu-miR-324-3p | MIMAT0000556 | 289 | 462 |
| mmu-miR-34a-5p | MIMAT0000542 | 1467 | 323 |
| mmu-miR-9-3p | MIMAT0000143 | 10361 | 21876 |
| mmu-miR-9-5p | MIMAT0000142 | 6814 | 12060 |
| mmu-miR-99a-5p | MIMAT0000131 | 1140 | 2017 |

The relative amount of astrocyte specific marker protein GFAP, was also shown to be diminished in the synaptoneurosome preparations (Figure 27), and although astrocytes form part of the tripartite synapse, this method of preparation provides a purification step (Ficoll gradient) to select for sub cellular synaptoneurosomes with a largely neuronal population.

4.3.4 Synaptoneurosomes in RML scrapie prion infected forebrain and hippocampus are not contaminated with astrocytes

Next, miR profiles from synaptoneurosomes were analyzed to determine those that were altered in abundance in prion infected mice during asymptomatic and terminal disease. Synaptoneurosomes from both the forebrain and hippocampus were examined at the early stage, while those from forebrain alone were analyzed during terminal disease (Figure 28). For the early forebrain, 6 synaptoneurosome samples were obtained including 3 preparations each of mock infected and RML scrapie infected, using 8 animals per treatment (Table 12). After the brains were micro dissected, 2-3 forebrains were pooled and homogenized per sample due to space constraints in the ultracentrifuge. For the hippocampal preparations the pooling of 8 hippocampi was required in order to visually detect the purified synaptoneurosome layer during the gradient step, resulting in one pooled sample from each treatment. For the late forebrain synaptoneurosome collections, each forebrain was independently processed, for the mock infected there were 4 animals and for RML scrapie infected, 8.

As astrogliosis is a hallmark of prion disease (Bell, Ironside 1993), the synaptoneurosome derived protein was probed for GFAP by Western blot to detect astrocyte invasion in the samples. Overall, GFAP presence was similar across samples

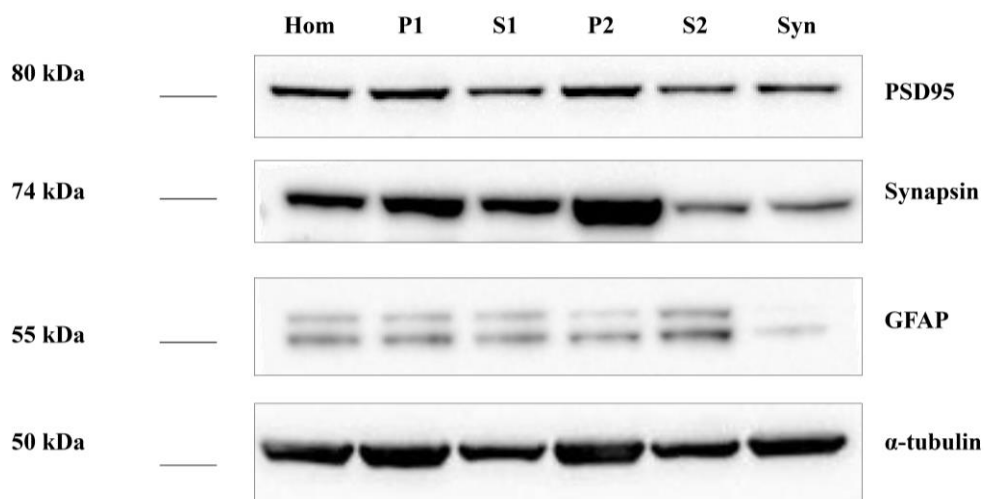


Figure 27. Western blot of different stages of the forebrain synaptoneurosome isolation. The presence of PSD95 (post-synapse), synapsin (pre-synapse) is identified in the purified synaptoneurosome (Syn) while astrocyte specific GFAP is decreased. The loading control used was α -tubulin. Hom= homogenate, P1=nuclear pellet, S1=supernatant from 2,000 x g spin, P2=crude synaptoneurosome pellet, S2=supernatant from 14,000 x g spin. Adapted from (Boese et al. 2015)

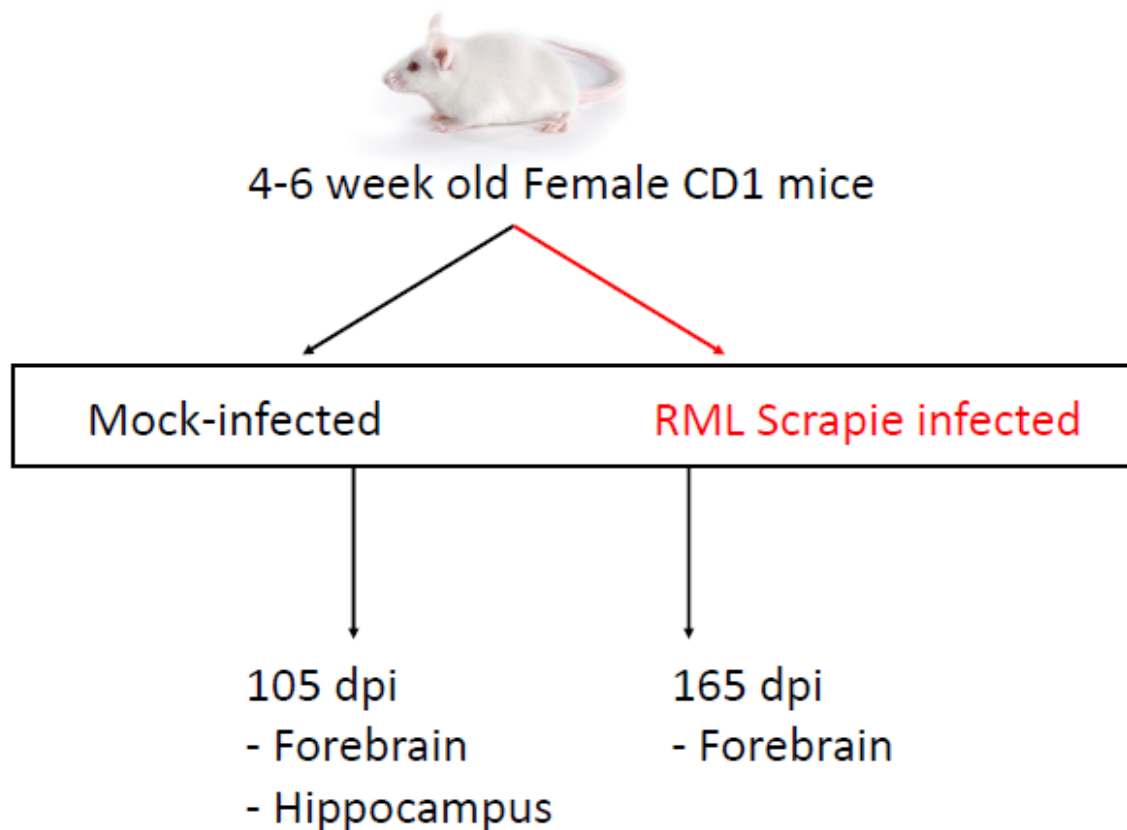


Figure 28. Overview of the RML scrapie prion infected CD1 mouse experiments from which synaptoneuroosomes were isolated. In mock infected (PBS brain homogenate) and RML scrapie prion infected mice, two timepoints of disease were examined, a preclinical stage of infection (105 dpi) and a late, clinical stage of infection (165 dpi). At the early stage, forebrain and hippocampal synaptoneuroosomes were collected while at the clinical stage of infection forebrain was collected. CD1 Mouse image ©Charles River Laboratories.

Table 12. Total number of mice used to isolate synaptoneurosomes at asymptomatic (105 dpi) and late, symptomatic (165 dpi) stages of infection. A breakdown of treatment, brain region, total number of mice used, pooled mouse brains, and final total number of samples per treatment are indicated.

| Treatment | Brain region | # of mice | # of pooled mice | Total # of samples |
|----------------------------|---------------------|------------------|-------------------------|---------------------------|
| Early mock infected | Forebrain | 8 | 3, 3, & 2 | 3 |
| | Hippocampus | 8 | 8 | 1 |
| Early RML scrapie infected | Forebrain | 8 | 3, 3, & 2 | 3 |
| | Hippocampus | 8 | 8 | 1 |
| Late mock infected | Forebrain | 4 | 0 | 4 |
| Late RML scrapie infected | Forebrain | 8 | 0 | 8 |

suggesting that there was no increase in astrocytes due to RML scrapie prion infection (Figure 29). An antibody against PSD95 demonstrated an overall decrease of this protein at later stages of prion infection, indicating a potential loss of dendrites at terminal stages of disease.

4.3.5 miRs were detected in synaptoneurosomes from RML scrapie prion infected samples by PCR Arrays

The synaptoneurosome layer was combined with an equal amount of binding/lysis buffer and total RNA was extracted and examined on the Bioanalyzer 2100 for RIN (Figure 30). All samples had a minimum RIN of 5.5 with a mean RNA yield of 150 ng. The cDNA for all samples within a timepoint was produced simultaneously using a universal miR primer RT kit. The cDNA was then prepared and loaded to the PCR Array Rodent Panel I, which contained LNA based primers for the detection of 372 different miRs and 12 controls including empty wells, interplate calibrator, and a spike-in RNA control. These arrays were subject to PCR and the resulting Cts were processed with GenEx software. This analysis was performed by calibrating all data within a timepoint and brain region (i.e. Early forebrain) with the interplate calibrator to account for plate to plate variability. The data was then processed to remove miRs that were not reliably detected, set as Ct > 35 or missing values due to non-detection. In normalizing data, the global mean of remaining miRs was used as a nonbiased approach. Further analysis per brain region is outlined in the proceeding sections.

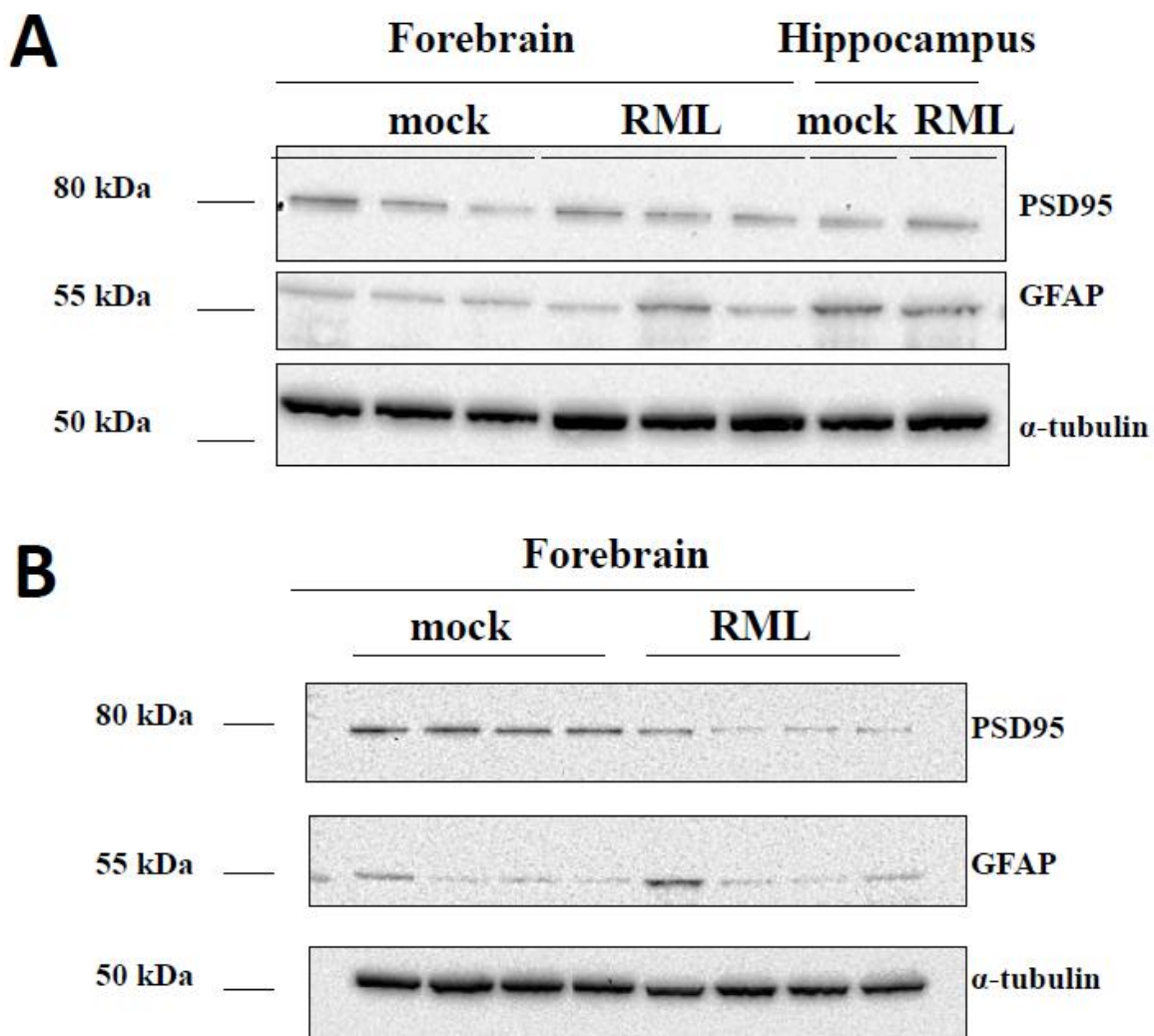
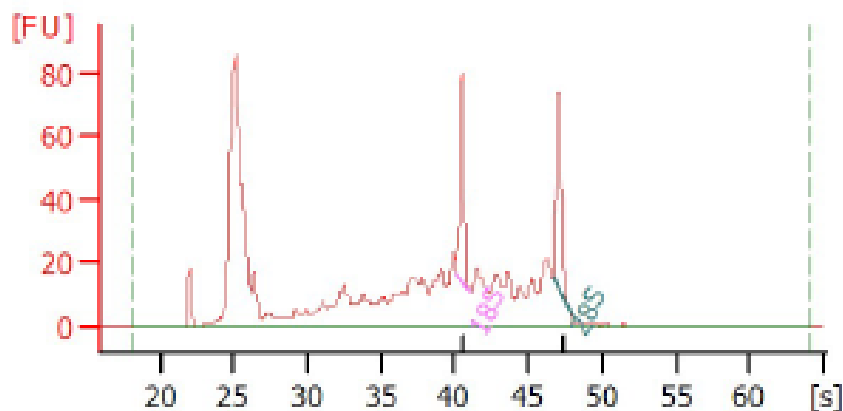


Figure 29. Western blot of synaptoneurosomes generated from mock and RML scrapie prion infected mice. A) early stages of prion disease in forebrain and hippocampus, B) late stages from the forebrain. PSD95, a dendritic marker, and GFAP, and astrocyte marker are detected alongside the α -tubulin loading control. Each lane represents an independent synaptoneurosomes sample. Adapted from (Boese et al. 2015)



Overall Results for sample 1 : syn_ctrl_h_1

RNA Area: 989.2
 RNA Concentration: 3,412 pg/ μ l
 rRNA Ratio [28s / 18s]: 1.2
 RNA Integrity Number (RIN): 5.5 (B.02.08)
 Result Flagging Color:
 Result Flagging Label: RIN: 5.50

Fragment table for sample 1 : syn_ctrl_h_1

| Name | Start Time [s] | End Time [s] | Area | % of total Area |
|------|----------------|--------------|------|-----------------|
| 18S | 40.14 | 41.02 | 51.7 | 5.2 |
| 28S | 46.65 | 47.95 | 61.4 | 6.2 |

Figure 30. A representative RIN determination of total RNA extracted from synaptoneurosomes using the Pico 6000 chip on the 2100 Bioanalyzer. A representative RIN chromatogram from the control (mock infected) synaptoneurosomes obtained from the early timepoint. The 18S and 28S ribosomal subunits upon which the RIN is based is clearly depicted with a RIN value of 5.5 indicated.

4.3.6 Hippocampal synaptoneurosome miR levels are changed during early stages of RML scrapie prion infection

In total 284 miRs (Ct < 35) were detected in synaptoneurosome prepared from both mock and RML infected mice using the miR PCR Arrays. The hippocampal synapse specific miR-324-5p was detected, as were all 31 of the synaptoneurosome enriched miRs identified by Pichardo-Casas *et al* (Pichardo-Casas *et al.* 2012). The miR-28-3p was amplified within the first 10% of miRs and was 27th in rank (Figure 31). The global mean used to calculate miR levels can be found in Figure 32A. Although miR-128-3p did not meet the fold change threshold of ≥ 2 fold, it was increased by 1.8fold (Figure 32B), which coincided with the increase of miR-128-3p in the CA1 cell bodies at early stages of RML scrapie prion infection. The synapse-enriched miR-132-5p did not display any significant changes, although the hippocampal synapse specific miR-324-5p was increased in abundance by 7.4fold. There were many miRs that showed at least 2fold differences in abundance including 19 that were increased and 21 that were decreased (Table 13). Significantly, many of these miRs have previously been identified in brain tissues from animal models of prion disease. Several members of the miR-200 family were detected by both mouse and rat primers, which are the same sequence in this case, indicating consistent detection as fold changes calculated with both were similar. Using TaqMan miR probes, six of these miRs were validated and miR-15a, a miR that was stable in all replicates, was used to normalize the Cts. This miR is expressed at the synapse (Gao *et al.* 2015) and as it had a low standard error between samples, it was used as the endogenous reference.

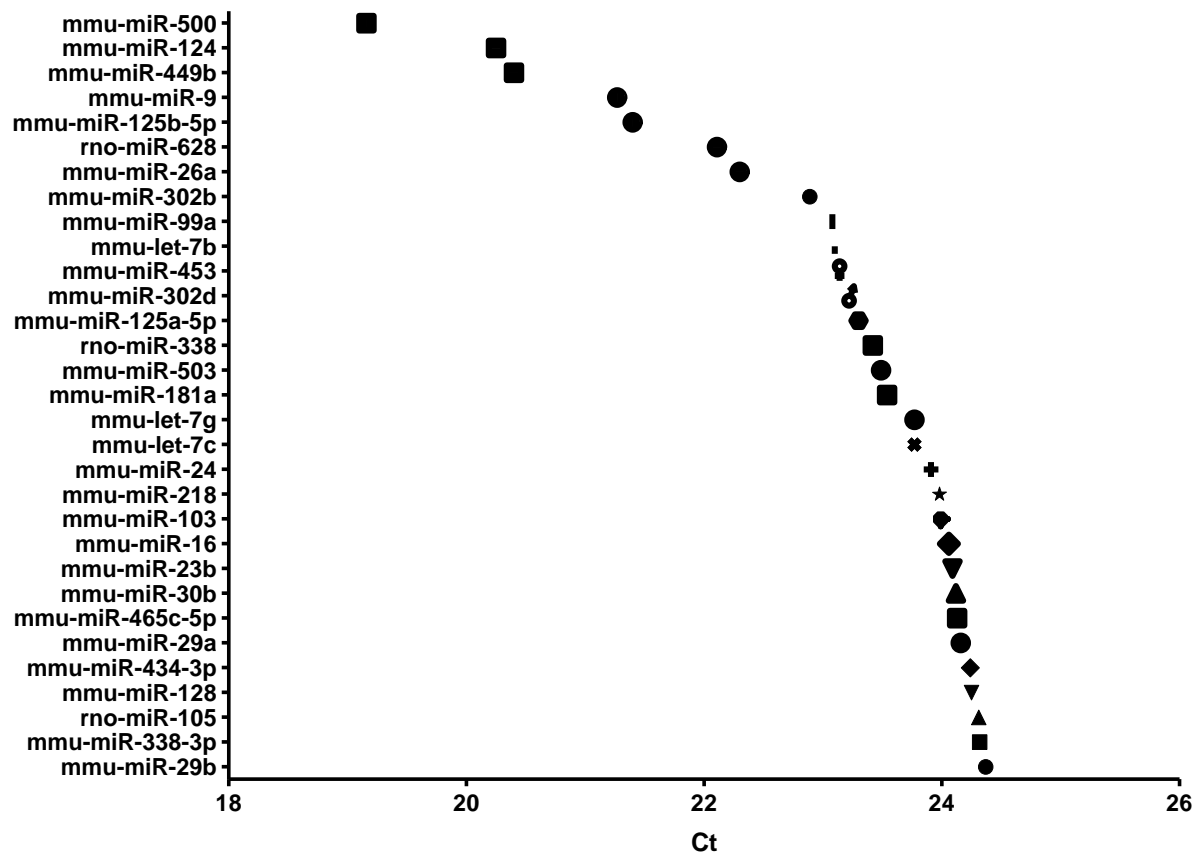


Figure 31. miRNAs detected in total RNA derived from hippocampal mock infected synaptoneurosomes at 105 dpi with a threshold of Ct < 25 using miR PCR Arrays. These PCR reactions were run on a thermal cycler, the raw data was obtained using automatic threshold and plotted as Ct values obtained.

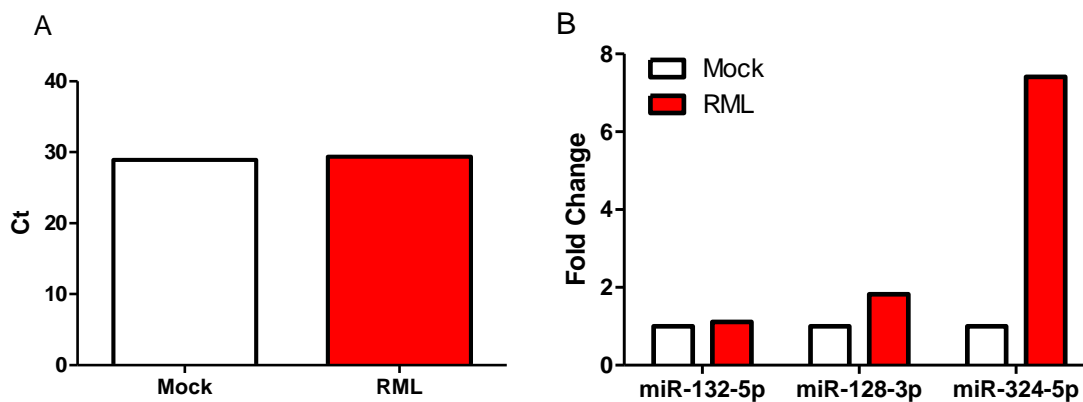


Figure 32. Changes in abundance of mature miR-128-3p in total RNA derived from hippocampal synaptoneurosomes at 105 dpi in mock infected and RML scrapie prion infected mice. A) global mean Ct of all miRs (detected Ct <35), used to normalize all Cts before calculating changes, and B) miR-132-5p, miR-128-3p, and miR-324-5p levels in hippocampal derived synaptoneurosomes with the mock used as a baseline.

Table 13. The miRs detected in hippocampal synaptoneurosomes at the early timepoint of RML scrapie prion infection in mice that were increased or decreased by ≥ 2 fold. The miRs, fold change, the fold change that was obtained through TaqMan miR probe validation and references for previous detection in prion disease are indicated. RNO = Rat miR primers.

| miR | Fold change | TaqMan validated FC | Found in prion disease |
|------------------|-------------|---------------------|------------------------|
| miR-466d-3p | 9.1 | | |
| miR-324-5p | 7.4 | | |
| miR-136-5p | 3.9 | 3.4 | (Majer et al. 2012) |
| miR-148b-5p | 3.9 | | |
| miR-33-5p | 3.8 | | |
| miR-670-5p | 3.7 | | |
| miR-466a-3p | 2.9 | | |
| miR-376a-3p | 2.7 | 2.0 | |
| miR-326-3p | 2.7 | | |
| miR-339-3p | 2.7 | | |
| miR-130a-3p | 2.6 | | |
| miR-30c-5p | 2.6 | | |
| miR-300-3p | 2.4 | | |
| miR-32-5p | 2.2 | 2.1 | |
| miR-340-5p | 2.1 | | |
| miR-381-5p | 2.1 | | (Gao et al. 2016) |
| miR-466c-5p | 2.0 | | |
| miR-22-3p | 2 | | |
| miR-193a-3p | -2.3 | | |
| miR-146b-5p | -2.3 | | |
| miR-106a-5p | -2.4 | | |
| miR-133a-3p | -2.4 | | |
| miR-17-5p | -2.5 | | |
| miR-451a | -2.7 | | (Majer et al. 2012) |
| miR-342-5p | -2.9 | | |
| miR-214-3p (RNO) | -3.3 | | |
| miR-96-5p | -4.0 | | (Gao et al. 2016) |
| miR-455-5p | -4.8 | | |
| miR-200c-3p | -5.5 | -8.9 | (Gao et al. 2016) |

| | | | |
|------------------|-------|------|----------------------|
| miR-183-5p | -6.1 | -5.7 | (Gao et al. 2016) |
| miR-182-5p | -7.4 | | (Gao et al. 2016) |
| miR-429-3p | -7.8 | | (Gao et al. 2016) |
| miR-200b-3p | -8.3 | | (Gao et al. 2016) |
| miR-493-3p (RNO) | -9.0 | | |
| miR-711 (RNO) | -9.7 | | |
| miR-141-3p | -9.9 | -8.9 | (Gao et al. 2016) |
| miR-200a-3p | -18.1 | | (Gao et al. 2016) |

4.3.7 Forebrain synaptoneuroosomes demonstrate a temporal profile during RML scrapie prion infection

In total 263 miRs were detected ($Ct < 35$) across all 6 forebrain samples as compared to 208 miRs at the late stage of disease. In terms of abundance, miR-128-3p was 10th in rank in the early forebrain preparation and 4th in rank in the late forebrain sample, detected at a mean Ct of 23.77 and 24.24 respectively. In order to determine the changes in abundance, the Cts were normalized against the global mean, log₂ fold change was calculated, and two tailed t-tests were applied using a p-value of 0.05 for significance cut-off. The data was analyzed separately for early and late timepoints.

The examination of miR-128-3p by box and whisker plot of Cts from both the early and late infection timepoints revealed it was similar in amount (Figure 33A). Indeed, there were no significant differences in miR-128-3p levels between mock infected and RML scrapie infected synaptoneuroosomes at early or late stages of infection (p-value of 0.45 and 0.55) (Figure 33B and C). The synaptic miR-132-5p did not differ significantly either. However, other miRs displayed temporal alterations in the forebrain during RML scrapie prion infection (Figure 34).

During the early stages of infection in the forebrain, 6 miRs met the threshold of a 2fold increase in abundance (p-value < 0.05) and no miRs showed any significant decrease. Those increased were miR-136-5p, miR-361-5p, miR-212-3p, miR-129-2-3p, miR-345-5p, and miR-376a-5p (Table 14). Several had been identified previously in prion disease including miR-136-5p, miR-361-5p, and miR-129-5p. Interestingly, none of these changes persisted into the terminal stages of infection. During clinical infection, there were 15 miRs that were altered in abundance by 2fold or more (p-value < 0.05); 8 that were increased and 7 that were decreased (Table 15). Five of these were validated using TaqMan probe

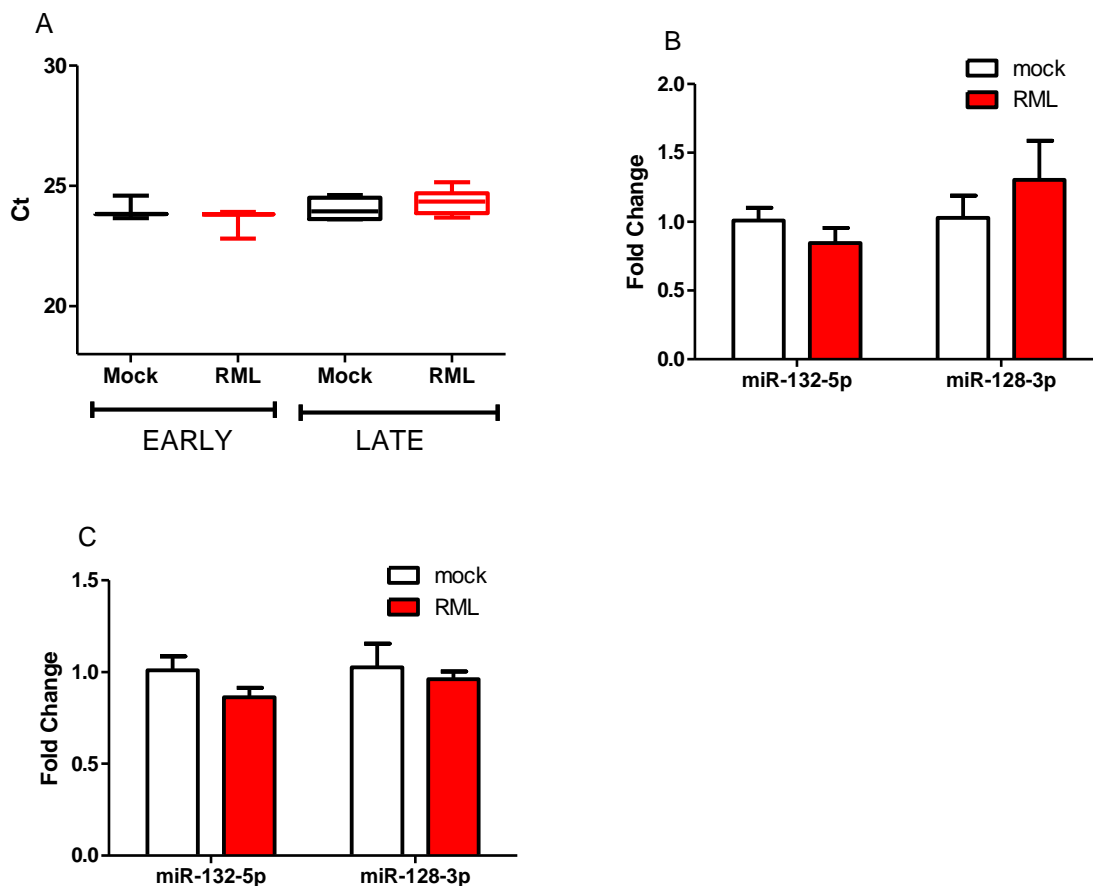


Figure 33. Examination of miR-128-3p in total RNA derived from forebrain synaptoneurosomes during early (105 dpi) and late (165 dpi) RML scrapie prion infection in mice. A) Box and whisker plots of miR-128-3p Cts detected by RT-qPCR at early and late timepoints, B) miR-132-5p (a synaptic miR) and miR-128-3p fold change at early timepoint of infection, and C) miR-132-5p and miR-128-3p fold change at late timepoint of infection. Neither was significantly different when subject to a two-tailed t-test using p-value <0.05 for significance.

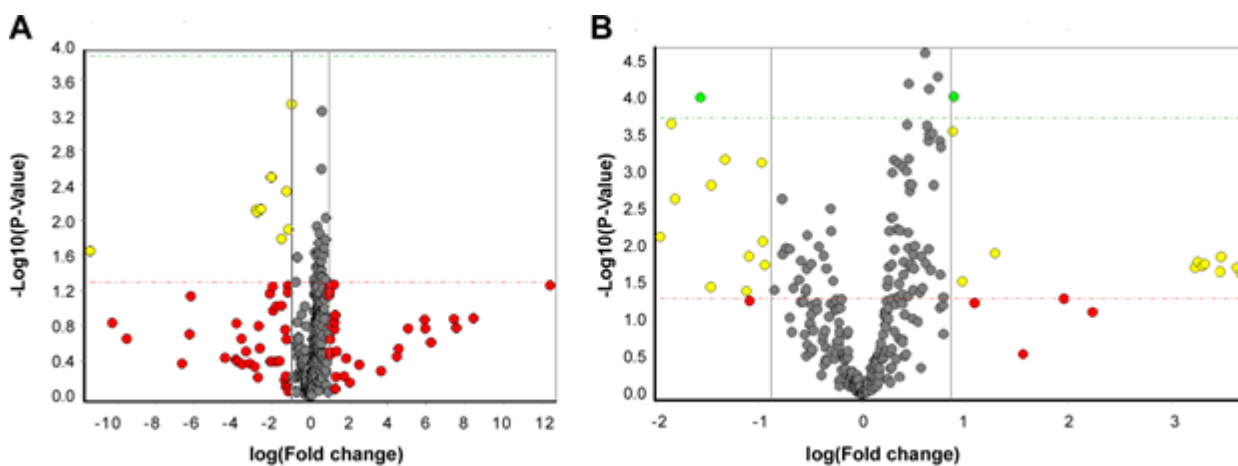


Figure 34. Synaptoneurosome derived from prion infected forebrain exhibited temporal alterations in miR levels. Volcano plots depicting changes in miR abundance between mock infected and prion infected forebrains at (A) early stages of disease, 105 dpi, and (B) late stages of disease, 167 dpi. The negative log₁₀ transformed p-values of the two-tailed student's t-test are plotted against the log fold change. The horizontal dashed lines represents the 95% confidence interval of the data while the vertical bars denote ≤ 1.75 -fold decrease or ≥ 1.75 -fold increase. Yellow and green circles are significantly altered miRs, red are altered miRs that did not meet the significance threshold while grey circles are those that displayed no changes in levels.

Table 14. The miRs at early stages of RML scrapie prion infection that were increased ≥ 2 fold in forebrain synaptoneuroosomes. Breakdown of the miR, fold change, associated p-values from two-tailed t-tests, TaqMan miR probe validation fold change, and whether they were detected in early hippocampal synaptoneuroosomes. Also, whether these miRs were found previously in prion disease is indicated.

| miR | Fold change | p-value | Detected in early hippocampal | Found in prion disease |
|--------------|--------------------|----------------|--------------------------------------|-------------------------------|
| miR-136-5p | 266.6 | 0.023 | X | (Majer et al. 2012) |
| miR-361-5p | 6.9 | 0.0077 | | (Montag et al. 2009) |
| miR-376a-5p | 5.7 | 0.0075 | X | |
| miR-212-3p | 4.0 | 0.0033 | | |
| miR-129-2-3p | 2.8 | 0.0164 | | (Majer et al. 2012) |
| miR-345-5p | 2.1 | 0.0129 | | |

Table 15. The miRs that were increased or decreased ≥ 2 fold at late stages of RML scrapie prion infection in forebrain synaptoneuroosomes. Breakdown of the miR, fold change, associated p-values from two-tailed t-tests, TaqMan miR probe validation fold change, and whether they were detected in early hippocampal synaptoneuroosomes. Also, whether these miRs were found previously in prion disease is indicated.

| miR | Fold Change | p-value | TaqMan fold change | Detected in hippocampal | Found in prion disease |
|-------------|--------------------|----------------|---------------------------|--------------------------------|--|
| miR-146a-5p | 3.9 | 0.0075 | 7.0 | | (Majer et al. 2012, Saba et al. 2008, Gao et al. 2016) |
| miR-211-5p | 3.6 | 0.0002 | | | |
| miR-142-3p | 3.5 | 0.0023 | 5.2 | | (Majer et al. 2012, Saba et al. 2008) |
| miR-150-5p | 3.00 | 0.0001 | 10.2 | | (Majer et al. 2012) |
| miR-144-3p | 2.8 | 0.0356 | | | |
| miR-143-3p | 2.8 | 0.0015 | | | (Montag et al. 2009) |
| miR-142-5p | 2.2 | 0.0402 | | | (Gao et al. 2016) |
| miR-451a | 2.1 | 0.0135 | | X | (Majer et al. 2012) |
| miR-682 | -2.4 | 0.0124 | | | |
| miR-141-3p | -9.4 | 0.02 | -3.6 | X | (Gao et al. 2016) |
| miR-200b-3p | -9.6 | 0.0162 | | X | (Gao et al. 2016) |
| miR-182-5p | -10.0 | 0.0173 | | X | (Gao et al. 2016) |
| miR-200c-3p | -11.2 | 0.0139 | -7.8 | X | (Gao et al. 2016) |
| miR-200a-3p | -12.5 | 0.0194 | | X | (Gao et al. 2016) |
| miR-429-3p | -12.8 | 0.0235 | | | (Gao et al. 2016) |

assays and several of these miRs have previously been identified to have altered profiles in the CNS during prion infection in multiple animal models, including mice and macaques (Saba et al. 2008, Montag et al. 2009), as well as specifically in the CA1 region during RML scrapie prion infection (Majer et al. 2012). These included miR-146a-5p, miR-142-3p, miR-150-5p, miR-143-3p, and miR-451a. The majority of these are immune-related including miR-146a-5p, which was increased 3.8fold (p-value 0.0075).

4.3.8 The synaptoneurosome proteome contains predicted miR-128-3p targets

As the level of miR-128-3p was increased in the synaptoneurosome of the hippocampus at early stages of infection, and some validated regulatory targets of this miR are known to reside at the synapse, I decided to further determine the full extent of proteins within the synaptoneurosome complement that contain predicted miR-128-3p target sites. It was decided to use mass spectrometry to determine the global protein profile within synaptoneurosome. Unfortunately for biosafety reasons it is not possible to introduce protein from prion infected material to the mass spectrometer. Therefore, the forebrain synaptoneurosome proteome from uninfected CD1 mice was resolved and this was used as a 'master list'. Protein lysate was cold acetone precipitated to remove detergents that interfere with mass spectrometry, then treated with SDS and reduced with DTT. Afterwards, the protein was alkylated with IAA, benzonase treated, and digested with trypsin overnight to yield peptides. These peptides were then separated using LC and analyzed with a Orbitrap Elite hybrid mass spectrometer. The resulting raw data files were searched using Proteome Discoverer version 1.3 with Mascot and SEQUEST search engines, using *Mus musculus* as the NCBI database selected and mouse Uniprot database

containing 10,090 proteins. The data was imported into Scaffold 4 software and peptides were matched to proteins using analysis settings described in methods section 3.10.7.

The first replicate contained 3,519 proteins and the second 879. In total 500 proteins were identified as present in both samples (Figure 35A). These proteins were input into PANTHER to garner GO information about protein class (Figure 35B). The PANTHER database queries input protein IDs against a curated database which is part of the GO Reference Genome Project. It contains 13,096 protein families with 78,442 subfamilies that are distinct in function and examines the gene component of the given proteins as well.

The PANTHER analysis indicated the presence of macromolecular complexes, membrane, extracellular region, synapse, cell junction, and extracellular matrix proteins, typical for proteins localized to the synaptic compartment. Using GO analysis from curated databases and the tool DAVID, synapse related (GO:0045202~synapse) proteins that were apparent in the two samples were SNAP25, SHANK, CAMK2 α , HOMER1, and others (Table 16). Glutamate receptors were not ubiquitously identified and GRIA2 was the only one detected in both samples, however all major receptors including NMDAR2A, NMDAR2D, mGluR5, and AMPA and kainate receptors were detected in one of the two samples.

The proteins detected in the wild-type forebrain synaptoneuroosomes were compared to the TargetScan list of predicted miR-128-3p targets for mouse, resulting in 48 proteins in common (Figure 36A). The GO of cellular activity of these proteins indicated 5 processes binding, catalytic, structural molecule, transporter, and receptor (Figure 36B). It was fascinating that many of the genes encoding the 48 synaptoneurosomal proteins

A



B

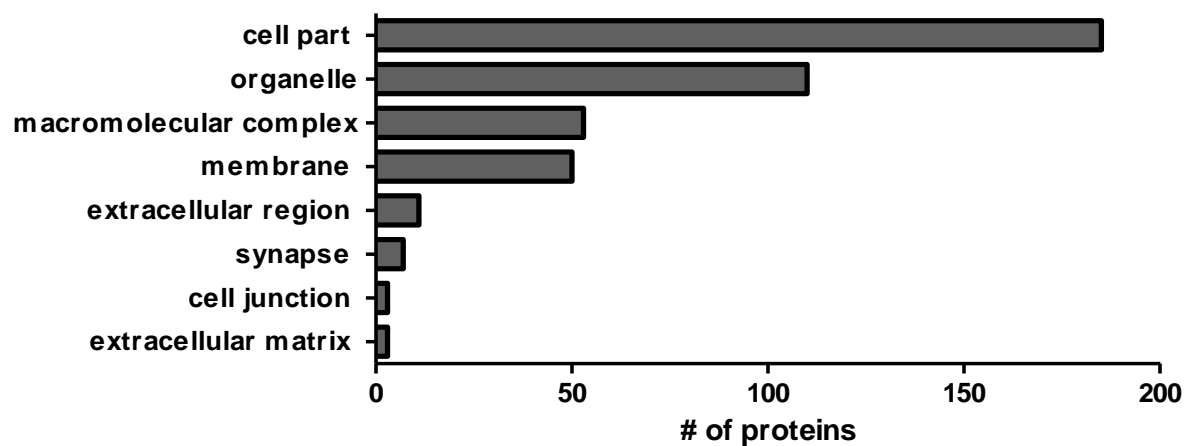


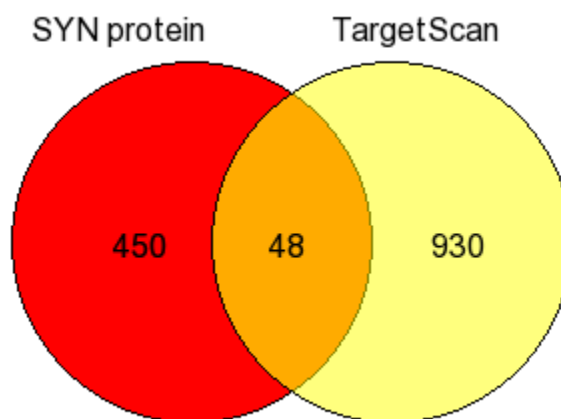
Figure 35. Synaptic proteins identified in total protein isolated from forebrain synaptoneurosomes of wild-type CD1 mice by mass spectrometry. A) the overlap of the 2 adult CD1 wild-type synaptoneurosomes proteins detected, and B) protein class of the 500 overlapping proteins determined through PANTHER.

Table 16. Synaptic neuronal proteins detected by mass spectrometry in the wild-type CD1 derived forebrain synaptoneurosomes. The gene symbol and protein name are identified.

| Gene symbol | Protein Name |
|--------------------|---|
| AMPH | Amphiphysin |
| ANK2 | Ankyrin 2 |
| ATP2B1 | ATPase plasma membrane Ca ²⁺ transporting 1 |
| BSN | Bassoon Presynaptic Cytomatrix protein |
| CAMK2A | Calcium/calmodulin-dependent protein kinase II α |
| DLG1 | Discs large MAGUK scaffold protein 1 |
| DLG4 | Discs large MAGUK scaffold protein 4 |
| DMXL2 | Dmx like 2 |
| DNM1L | Dynamin 1-like |
| ERC2 | ELKS/RAB6-interacting/CAST family member 2 |
| GAP43 | Growth associated protein 43 |
| GRIA2 | Glutamate receptor, ionotropic, AMPA2 |
| HOMER1 | Homer scaffolding protein 1 |
| KCTD12 | Potassium channel tetramerization domain containing 12 |
| MAP1B | Microtubule-associated protein 1B |
| MINK1 | Misshapen like kinase 1 |
| MPDZ | Multiple PDZ domain protein |
| NCS1 | Neuronal calcium sensor 1 |
| PACSIN1 | Protein kinase C and casein kinase substrate in neurons 1 |
| PCLO | Piccolo presynaptic cytomatrix protein |
| PRKCG | Protein kinase C gamma |
| PRRT2 | Proline rich transmembrane protein 2 |
| PSD3 | Pleckstrin and Sec7 domain containing 3 |
| RPH3A | Rabphilin 3A |

| | |
|--------|---|
| SHANK1 | SH3 and multiple ankyrin repeat domains 1 |
| SNAP25 | Synaptosome associated protein 25 |
| SRCIN1 | SRC kinase signaling inhibitor 1 |
| STX1A | Syntaxin 1A |
| SV2A | Synaptic vesicle glycoprotein 2 a |
| SV2B | Synaptic vesicle glycoprotein 2B |
| SYN1 | Synapsin I |
| SYN2 | Synapsin II |
| SYP | Synaptophysin |
| SYT1 | Synaptotagmin 1 |
| TANC1 | Tetratricopeptide repeat, ankyrin repeat and coiled-coil containing 1 |
| TLN2 | Talin 2 |
| VAMP2 | Vesicle-associated membrane protein 2 |

A



B

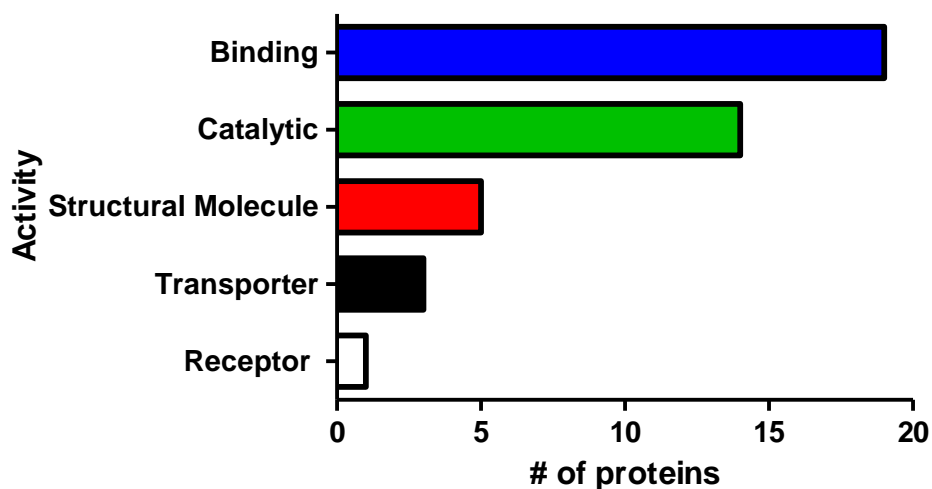


Figure 36. Synaptic forebrain proteins compared to TargetScan predicted miR-128-3p 3' UTR mouse targets. A) adult forebrain synaptoneurosome proteins identified by mass spectrometry (red circle) compared against miR-128-3p TargetScan predicted mouse 3' UTR targets (yellow circle) yield 48 identical proteins, and B) Molecular Activity attributed to the overlapping 48 synaptic proteins as assessed by PANTHER.

contained multiple 3' UTR binding sites for miR-128-3p, with over 80% having ≥ 2 predicted sites (Table 17).

4.3.9 NMDAR and mGluR5 mRNA transcripts are present at the synapse

The non-ubiquitous detection of NMDAR2D or mGluR5 protein in both forebrain synaptoneurosome samples by mass spectrometry was most likely due to a low detection threshold. To determine whether the mRNA transcripts for these could be detected by RT-qPCR in the RNA derived from hippocampal synaptoneurosome samples at the early timepoint. To this end, TaqMan gene expression assays were used to detect GAPDH, *GRIN2B*, *GRIN2D*, *GRM5*, and *PRNP* which codes for PrP^C. These transcripts were detected in the hippocampal synaptoneurosome samples of the early stages (105 dpi) with Cts < 35 (Figure 37). The presence of these transcripts locally at the synapse suggests that these mRNA are transported from the cell body to the synapses, and are potentially translated locally in response to specific stimuli. This could also mean that their translation is under the regulation of synapse enriched miRs such as miR-128-3p.

Table 17. Synaptic proteins derived from wild-type mouse forebrain whose genes contain TargetScan predicted 3' UTR binding sites for miR-128-3p. The gene symbol, gene name, and number of miR-128-3p binding sites within the 3' UTR as determined by TargetScan Human is given.

| Gene symbol | Gene name | # of binding sites |
|--------------------|--|---------------------------|
| ERC2 | ELKS/RAB6-interacting/CAST family member 2 | 11 |
| SLC8A1 | solute carrier family 8 (sodium/calcium exchanger), member 1 | 9 |
| DYNLL2 | dynein light chain LC8-type 2 | 6 |
| PPAP2B | phosphatidic acid phosphatase type 2B | 5 |
| PPP1R9A | protein phosphatase 1, regulatory (inhibitor) subunit 9A | 5 |
| SLC6A1 | solute carrier family 6 (neurotransmitter transporter, GABA), member 1 | 5 |
| CCDC88C | coiled coil domain containing 88c | 4 |
| KIAA1549L | KIAA1549 like | 4 |
| MARCKS | myristoylated alanine rich protein kinase C substrate | 4 |
| PFKM | phosphofructokinase, muscle | 4 |
| PGM2L1 | phosphoglucomutase 2-like 1 | 4 |
| ZFXH3 | zinc finger homeobox 3 | 4 |
| ZNF516 | zinc finger protein 516 | 4 |
| ANK2 | Ankyrin-2 | 3 |
| ARID2 | AT-rich interaction domain 2 | 3 |
| CORO1C | coronin, actin binding protein 1C | 3 |
| DAB2IP | disabled 2 interacting protein | 3 |
| DST | dystonin | 3 |
| EHD3 | EH-domain containing 3 | 3 |
| GPD2 | glycerol-3-phosphate dehydrogenase 2 | 3 |
| LSAMP | limbic system-associated membrane protein | 3 |
| OPA1 | OPA1, mitochondrial dynamin like GTPase | 3 |
| PURA | purine rich element binding protein A | 3 |
| SNAP25 | synaptosomal-associated protein 25 | 3 |
| TPPP | tubulin polymerization promoting protein | 3 |
| ATP2B1 | ATP2B1 ATPase plasma membrane Ca ²⁺ transporting 1 | 2 |

| | | |
|----------|--|---|
| DDAH1 | dimethylarginine dimethylaminohydrolase | 2 |
| FAM49B | family with sequence similarity 49, member B | 2 |
| GCC2 | GRIP and coiled-coil domain containing 2 | 2 |
| HIVEP3 | human immunodeficiency virus type I enhancer binding protein 3 | 2 |
| KIF5C | kinesin family member 5C | 2 |
| NAV2 | neuron navigator 2 | 2 |
| NCAM1 | neural cell adhesion molecule 1 | 2 |
| PCP4L1 | Purkinje cell protein 4-like 1 | 2 |
| RAB14 | RAB14, member RAS oncogene family | 2 |
| SV2A | synaptic vesicle glycoprotein 2A | 2 |
| SYT1 | synaptotagmin I | 2 |
| TPD52L2 | tumor protein D52-like 2 | 2 |
| YWHAB | tyrosine 3-monooxygenase/tryptophan 5- monooxygenase activation protein, β polypeptide | 2 |
| CCDC88A | coiled coil domain containing 88A | 1 |
| EPB41L1 | erythrocyte membrane protein band 4.1 like 1 | 1 |
| HSP90AA1 | heat shock protein 90, α (cytosolic), class A member 1 | 1 |
| HSPD1 | heat shock protein 1 (chaperonin) | 1 |
| MLLT10 | myeloid/lymphoid or mixed-lineage leukemia; translocated to, 10 | 1 |
| NDUFS4 | NADH dehydrogenase (ubiquinone) Fe-S protein 4 | 1 |
| NPTX1 | neuronal pentraxin 1 | 1 |
| PDHX | pyruvate dehydrogenase complex, component X | 1 |
| UBE2V1 | ubiquitin-conjugating enzyme E2 variant 1 | 1 |

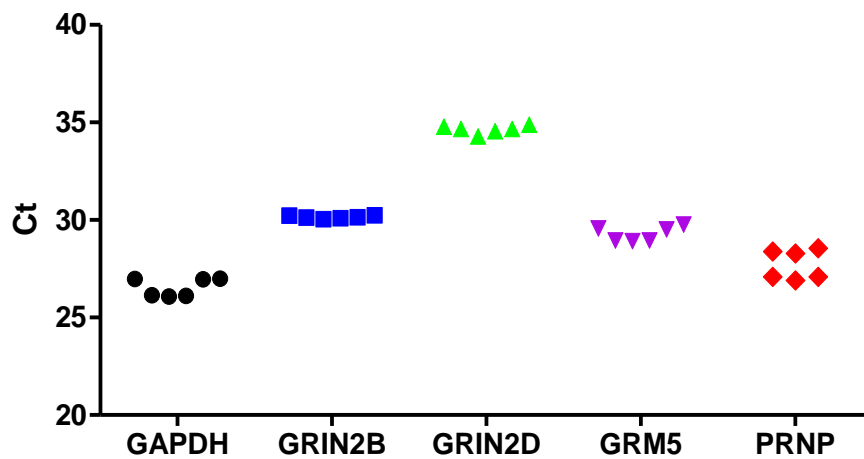


Figure 37. mRNA transcripts present in the total RNA derived from hippocampal synaptoneurosomes during early stages of RML scrapie prion infection in mice. The individual dots represent the Ct's from both the mock infected and RML scrapie prion infected samples after TaqMan gene expression assay from one pooled sample of RNA from each treatment from 8 individual animals per treatment.

4.4 miR-128-3p is involved in excitotoxic glutamate signaling in hippocampal neurons

4.4.1 Rationale

As previously determined, there was an abundance of miR-128-3p within the synaptoneurosome compartment along with glutamate receptors found at pre- and post-synaptic locales within neurons. Furthermore, miR-128-3p levels are decreased in the CA1 neurons during late stages of RML scrapie infection in mice and increased at early stages in both the synaptoneurosomes of the hippocampus as well as within CA1 neuronal cell bodies. Coincidentally, in the same CA1 neurons, transcriptional profiling is suggestive of the activation of a glutamate-mediated NMDAR neuroprotective program of gene expression during early RML scrapie prion infection (Majer et al. 2012). There are also multiple similar lines of evidence demonstrating that glutamate signaling is involved in Alzheimer's disease progression (reviewed in (Rudy et al. 2015)). Further evidence for the involvement of glutamate signaling in prion disease comes from a GWAS study of CJD patients in which the glutamate signaling pathway was identified as a risk factor for the development of disease (Sanchez-Juan et al. 2015). Striking experimental data has also shown that PrP^C is directly involved in glutamate signaling regulation alongside mGluR5 and NMDARs (Hamilton, Zamponi & Ferguson 2015). In addition, amyloid β oligomers are known to accumulate in the hippocampus and the co-receptor complex of PrP^C-mGluR5 binds amyloid β oligomer at the cell surface, leading to aberrant signaling in Alzheimer's disease (Lauren et al. 2009, Hu et al. 2014).

Given that miR-128-3p was shown to bind to the 3' UTR of a number of glutamate receptors described in previous chapters of this thesis and is upregulated in the CA1 during

early stages of RML scrapie prion infection in mice, this suggests that glutamate signaling may directly affect miR-128-3p levels in hippocampal neurons. Therefore, miR-128-3p may well play a role in the regulation of the aberrant activation of glutamate signaling that appears to be a factor during neurodegenerative diseases caused by prions and in Alzheimer's disease.

4.4.2 Hypothesis

Synaptic activation of glutamate receptors mediates calcium influx and the induction of a transcriptional program including miR-128-3p and neuroprotective gene expression, in cultured murine hippocampal neurons, mirroring early stages of prion pathogenesis.

4.4.3 Establishment of Primary Hippocampal Neuron Culture

Primary hippocampal neurons, rather than immortalized cell lines, were used to study the effects of glutamate signaling on miR-128-3p levels in neurons for a number of reasons. First, primary neurons are well differentiated with functional synaptic connections, which is the site of synaptic NMDAR signaling that is of interest in relation to miR-128-3p regulation. These types of mature neuronal connections are lacking in commonly used cancer derived cell lines. In addition, the levels of miR-128-3p are altered in cancer, which could result in anomalous effects in immortalized cell lines (reviewed in (Adlakha, Saini 2014)). The hippocampus is significantly affected in the RML scrapie mouse model and hippocampal degeneration is related to early, as well as late, clinical signs in this model. Indeed, this is the region in which miR-128-3p deregulation has been shown to occur during preclinical stages of RML infection. The hippocampal pyramidal neurons are therefore ideal to study the effects of synaptic and extrasynaptic glutamate

receptor activation on miR-128-3p expression as well as to determine the neuronal specificity of miR-128-3p targets that may be of importance in prion disease. The CD1 mouse strain was chosen as the source for primary culture to provide continuity of host strain between the *in vivo* infection model which was the source of the gene and miR data that formed the basis of the study.

Hippocampal neurons from embryonic day 18-20 CD1 mice were cultured by pooling the dissected hippocampi from at least 6 mice which were subject to enzymatic digestion and mechanical disruption similar to other published protocols (Seibenhener, Wooten 2012). Neurons were maintained in NbActiv1 media which is comprised of the serum-free Neurobasal plus B-27 supplement that promotes neuronal versus glial cell growth (Brewer et al. 1993). Antibiotic was not added to the media as antibiotics are known to affect epileptiform activity in hippocampal neurons (Wong, Prince 1979), an activity that miR-128-3p is believed to regulate (Tan et al. 2013a).

Primary hippocampal neurons were plated at a density of 70,000 per well for a 24 well plate, a density that has been shown to be beneficial to the maintenance of appropriate extracellular signal-regulated kinase activation after synaptic NMDAR activation (Ivanov et al. 2006). In order to visualize neuronal morphology and health, cells were grown in chamber slides and collected at 5, 8, 10, and 12 DIV. They were fixed in 4% Paraformaldehyde and stored in 1X DPBS before immunostaining. To detect neurons, the slides were co-immunostained with a MAP2 antibody to detect dendrites of neurons and a GFAP antibody to detect astrocytes. The MAP2 antibody was produced in chicken and GFAP in rabbit, enabling two different fluorescent secondary antibodies to be used simultaneously. The slides were then mounted using ProLong Gold antifade mountant which contained DAPI, a nuclear stain. As can be seen in Figure 38, the cultures consisted

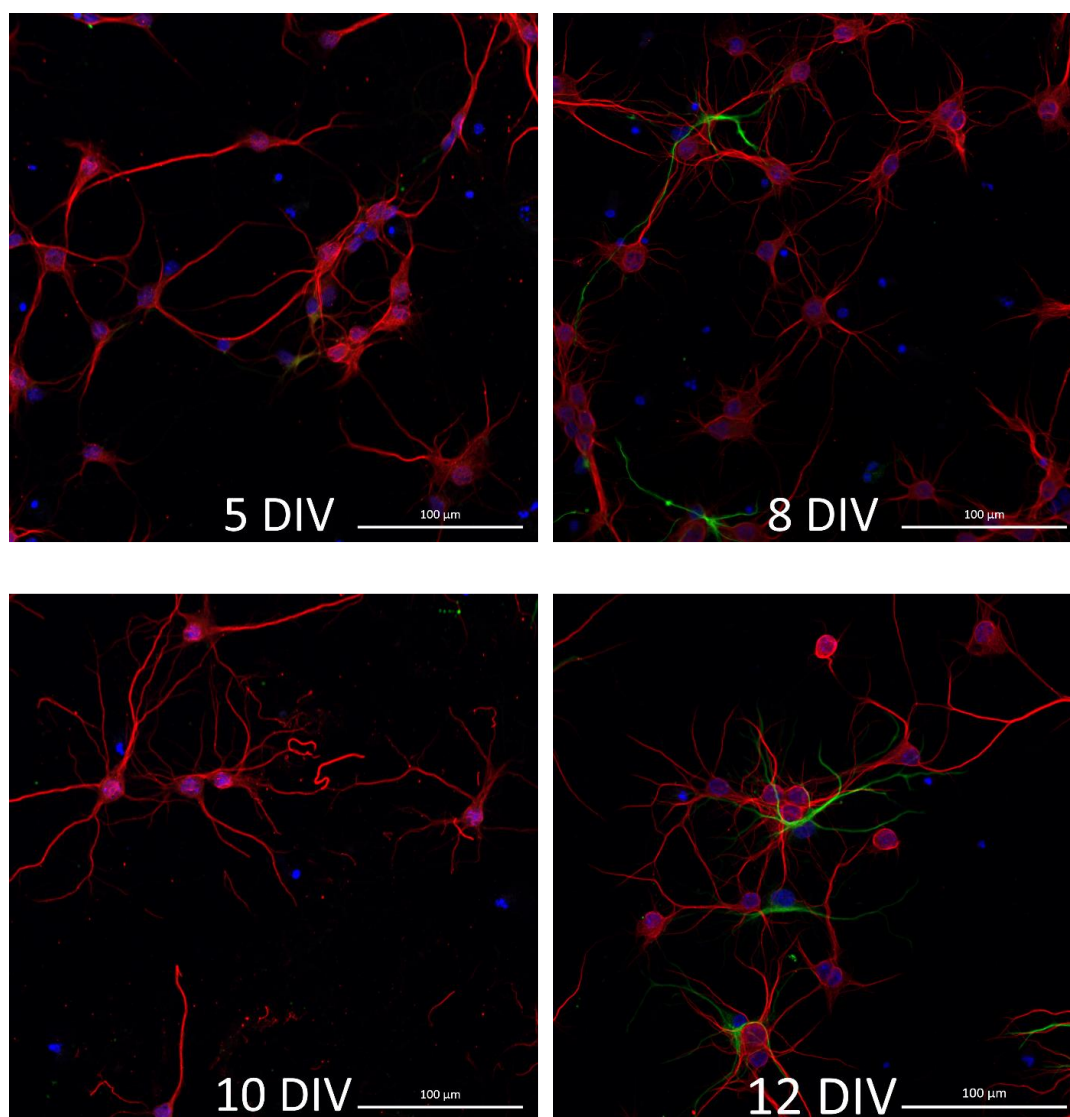


Figure 38. Immunostaining of primary hippocampal neurons from E18-20 mice at 5, 8, 10, and 12 days in vitro (DIV). MAP2, a neuronal specific dendrite marker is visualized with a Alexafluor 555 labeled secondary antibody (red), GFAP, an astrocyte specific marker is visualized with a Alexafluor 488 labeled secondary antibody (green). Nuclei are stained with DAPI (blue). The white scale bar represents 100 microns and the images were obtained using a Laser Scanning Microscope 7 (Zeiss) and exported into TIFF images using ZenLite software.

mostly of neurons that had synaptic connections by 5 DIV, with connections branching out further from 8 DIV to 12 DIV. Some astrocytes were also detected in culture but these were much fewer in number in comparison to neurons.

4.4.4 Expression of *GRIN2B*, *GRIN2D*, and *GRM5* genes increases during the maturation and growth of primary hippocampal neurons

Some genes and miRs are developmentally regulated and therefore the expression of transcripts of interest was determined in primary hippocampal neurons from time of plating until the cells reached maturity. Total RNA was collected each day from 1 DIV-12 DIV and the relative expression of *GRIN2B*, *GRIN2D*, *GRM5*, and *GFAP* genes over time in culture were determined from two independent neuronal preparations. After the total RNA was quantified and RIN value (> 8) obtained to ensure RNA was of good quality, RT-qPCR was performed. TaqMan gene expression assays were used with *GAPDH* serving as the endogenous control reference gene (Khudayberdiev et al. 2013). Firstly, *GAPDH* was evaluated for suitability as an endogenous reference by examining its expression across all samples and to ensure its expression was not altered during neuronal maturation as shown in the box and whisker plot in Figure 39A. Next, the Cts of the genes were plotted over the timeline of the culture.

All genes were expressed at detectable levels during the time cells were cultured (Figure 39B). After normalizing to *GAPDH*, fold change was calculated over time for each gene using the delta delta Ct method where the levels at 1 DIV served as the baseline for expression. The levels of the glutamate receptor genes *GRIN2B* and *GRM5* increased significantly over the first 5-6 days in culture before stabilising, while the level of *GRIN2D* continued to increase until 9 DIV (Figures 39C-E). This increase in expression coincided

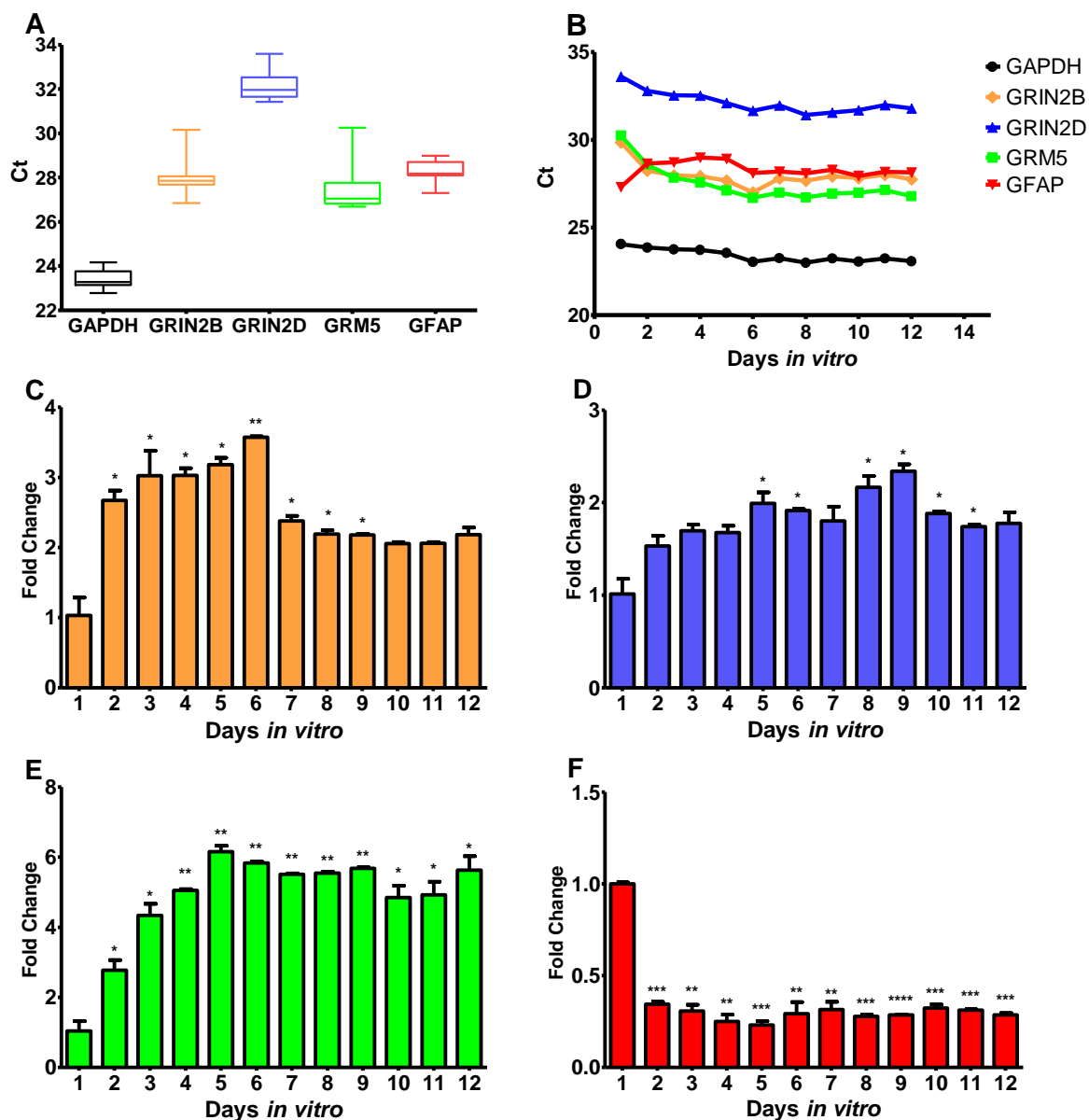


Figure 39. Relative expression of *GAPDH*, *GRIN2B*, *GRIN2D*, *GRM5*, and *GFAP* mRNA captured using RT-qPCR on total RNA isolated from cultured primary hippocampal neurons from 1 to 12 days *in vitro* (DIV). A) Box and whisker plots for all Ct values per gene, B) Ct over DIV for each gene C) *GRIN2B* fold change, D) *GRIN2D* fold change, E) *GRM5* fold change, and F) *GFAP* fold change. For graphs B-F, error bars represent SEM. For graphs C-F, *GAPDH* was used as the endogenous control reference gene and significance levels were determined by one-tailed t-test between 1 DIV fold change and each DIV, *= p-value <0.05, **= p-value <0.01, *= p-value < 0.001, ****= p-value <0.0001**

with the degree of maturation of the neurons as they steadily grew dendrites and formed synapses. The level of the GFAP gene was relatively stable over time indicating that although some astrocytes were present in the culture, they were not dividing and increasing significantly over the 12 day culture period.

4.4.5 The expression of miR-128-3p increases as murine hippocampal neurons mature in culture

Given that miR-128-3p is enriched in neurons and synapses, it was postulated that its expression would increase over time in culture in a similar way to the glutamate receptor subunits. RT-qPCR was performed using the total RNA collected from 1 DIV to 12 DIV in two independent cell preparations. To ensure that the reverse transcription step was at equivalent efficiency amongst samples, the spike-in RNA control UniSp6 was added before the production of cDNA. Before examining the other small RNAs, the UniSp6 spike-in was assessed and confirmed to have a low standard error (0.136) ensuring the transcription of cDNA rates between samples was equivalent (Figure 40A and B). In addition to miR-128-3p, the levels of other miRs were determined as controls. These were miR-132-3p, a miR previously shown to exhibit increased expression in hippocampal neurons as they arborize and produce dendrites (Magill et al. 2010), miR-342-3p, a miR that is expressed in primary hippocampal neurons (Butovsky et al. 2014), and U6, a commonly used small nuclear reference in miR work (Khudayberdiev et al. 2013, Zhang et al. 2011). From the box and whisker plot in Figure 40A, it was evident that the expression of U6 was quite variable and in this particular case miR-342-3p was detected within a much narrower range and was therefore chosen as the endogenous control reference for normalization. The expression of miR-132-3p increased significantly over

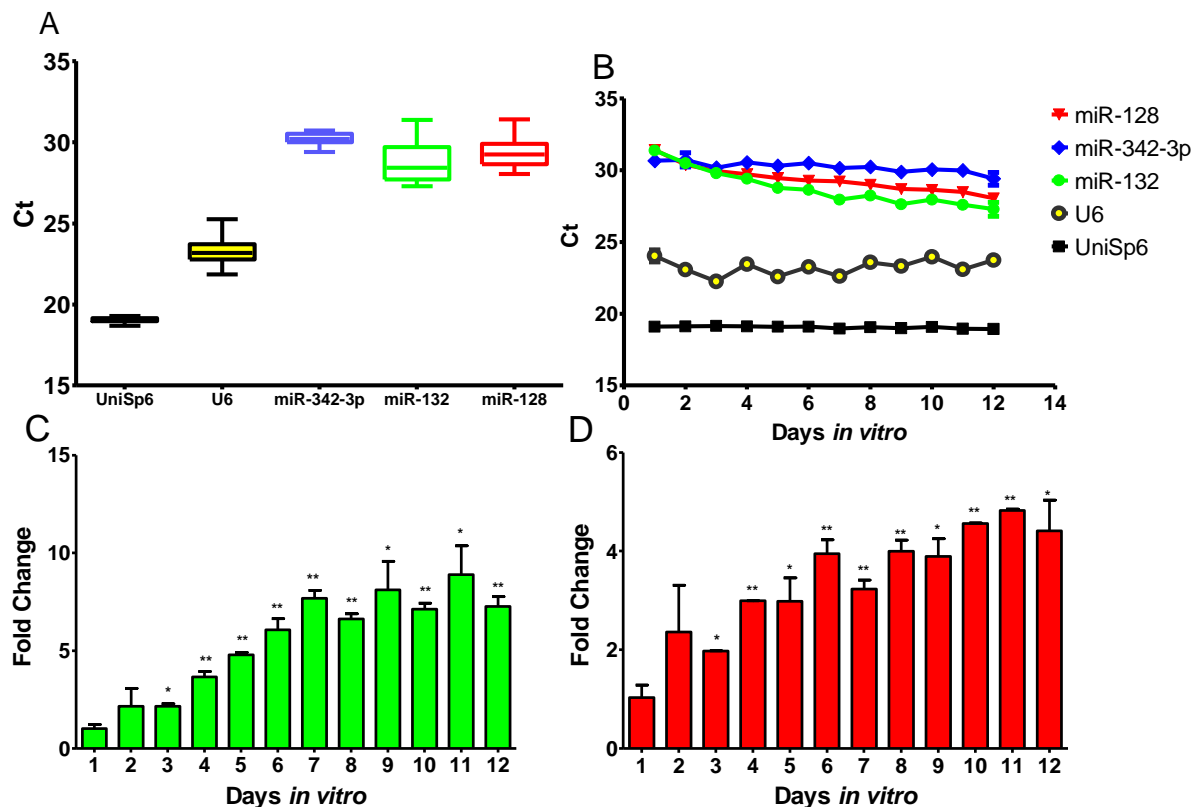


Figure 40. Relative expression of small RNAs detected in total RNA from cultured primary hippocampal neurons from 1-12 days *in vitro* (DIV) using RT-qPCR. A) Box and whisker plot of Cts across all samples over the 12 day collections, B) Cts over DIV for the UniSp6 (spike-in control), small nuclear U6, miR-132-3p, miR-342-3p, and miR-128-3p, and C) miR-132-3p Fold change over time and D) miR-128-3p fold change over time. For C and D, miR-342-3p was used as the endogenous reference control and 1 DIV as the baseline for fold change calculations while significance testing was conducted as one-tailed t-tests between 1 DIV fold change and remaining DIVs. For Graphs B, C and D, error bars denote SEM. *= p -value < 0.05, **= p -value < 0.01.

time in culture as expected (Magill et al. 2010, Vo et al. 2005). Levels increased significantly from 3 DIV onwards (Figure 40C), reaching 8fold by 7 DIV. The level of miR-128-3p also significantly increased from 3 DIV to 11 DIV (Figure 40D). The levels of miR-128-3p were at 4fold higher at 11 DIV compared to 1 DIV. Interestingly, miR-128-3p expression appeared to increase in the culture slightly longer than miR-132-3p following more closely the expression profile of *GRIN2D*, with the expression profile of miR-132-3p more closely following that of *GRIN2B* and *GRM5*. Since the expression of miR-128-3p and glutamate receptor genes had essentially plateaued by 8-9 days in culture, further functional studies were performed in neurons that had matured for at least 8 days in culture.

4.4.6 Action potential bursting model in cultured hippocampal neurons elicits the downregulation of miR-128-3p and related mRNA transcripts during chronic activation

It was of interest to determine whether the induction of action potential bursting in cultured hippocampal neurons would lead to the similar induction of miR-128-3p expression as the gene expression profile induced in this way has previously been shown as having extensive similarity to that seen in CA1 neurons during early stages of RML scrapie prion infection (Majer et al. 2012, Zhang et al. 2007). Experimental conditions to induce action potential bursting were performed according to the method described by Zhang and colleagues and involved the addition of 250 μ M 4-aminopyridine and 50 μ M (+)-bicuculline to the cultured neurons (Figure 41). The 4-aminopyridine selectively blocked K^+ shaker channels and (+)-bicuculline was an antagonist for GABA_A receptors as well as calcium gated K^+ channels (Khawaled et al. 1999). The blockage of K^+ channels

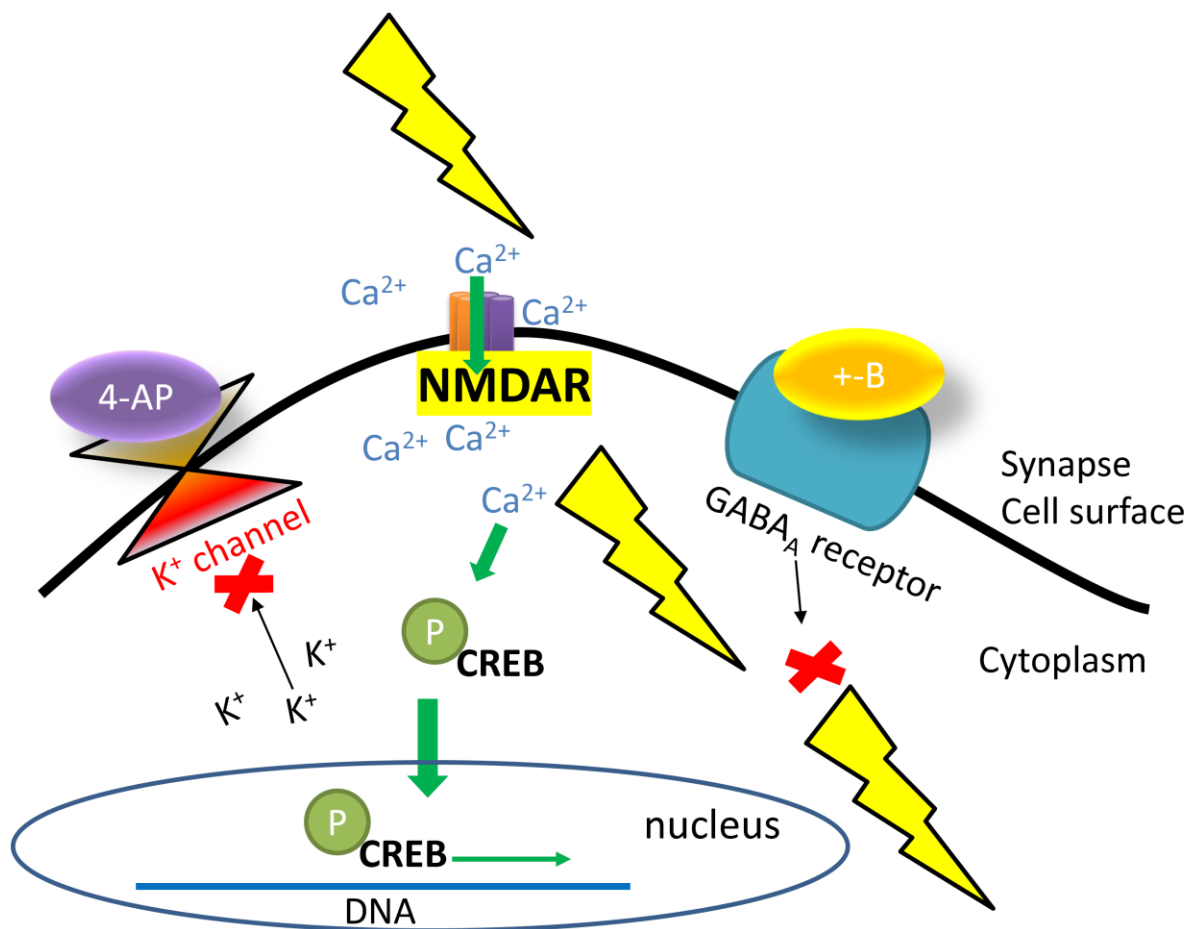


Figure 41. The action potential bursting paradigm using 4-aminopyridine (4-AP) and (+)-bicuculline (+-B) in primary hippocampal neurons. 4-AP and +-B blockage of potassium gated channels and GABA_A receptors respectively, leads to an increase in action potential bursts in the neuron. This occurs because the potassium ions (K⁺) cannot exit the cell as the potassium channels are blocked by 4-AP and at the same time the GABA_A receptor cannot inhibit the excitatory transmission (lightning bolt) occurring in the neuron and being propagated to neighboring neurons. Ultimately, the action potential bursts continue, leading to a net increase of calcium ions (Ca²⁺) in the cell through transient channels such as NMDAR. This increase in Ca²⁺ leads to the phosphorylation of CREB protein and its translocation to the nucleus to activate the transcription of neuroprotective genes.

by 4-aminopyridine results in Ca^{2+} influx into the neuron through transient Ca^{2+} channels such as NMDARs (Tibbs et al. 1989). The (+)-bicuculline action on GABA_A channels results in the disinhibition of the propagation of action potentials, which means unremitting action potentials occur in the neuron (Nowak, Young & Macdonald 1982). The ultimate result of action potential bursting within neurons is Ca^{2+} influx mediating the phosphorylation of CREB protein, and the translocation of pCREB to the nucleus where it activates the transcription of numerous genes, many of which have also been shown to confer neuroprotectivity (Hardingham, Arnold & Bading 2001). I determined the expression of two of these genes, *HOMER1* and *ARC* as positive controls for this treatment as they are a part of the suite of neuroprotective genes induced by this treatment. Gene and miR expression was determined at two time points, 4 hours and 16 hours post-treatment. For the action potential bursting experiments, 9-12 DIV cultured primary hippocampal neurons were used and 250 μM 4-aminopyridine and 50 μM (+)-bicuculline was bath applied to the cells after being diluted to the appropriate concentration in Neurobasal media which served as the media only control. The endogenous control reference gene used to normalize the genes was *GAPDH*, also used by Zhang et al (Zhang et al. 2009). These experiments were performed in triplicate wells from 3 independent neuronal preparations.

As can be seen in Figure 42A, the *GAPDH* Ct box and whisker plot demonstrated the stability of *GAPDH* gene expression within each experiment confirming it as a good choice for an endogenous control reference to normalize Cts. After the genes were normalized against *GAPDH*, the fold changes were calculated for *ARC* and *HOMER1* using the delta delta Ct method and mock treatment with media only as the negative control. Both *ARC* and *HOMER1* were induced significantly at 4 hours post treatment (Figure 42B), with increased gene expression of 3.2fold for *ARC* (p-value 0.0001) and 4.6fold for

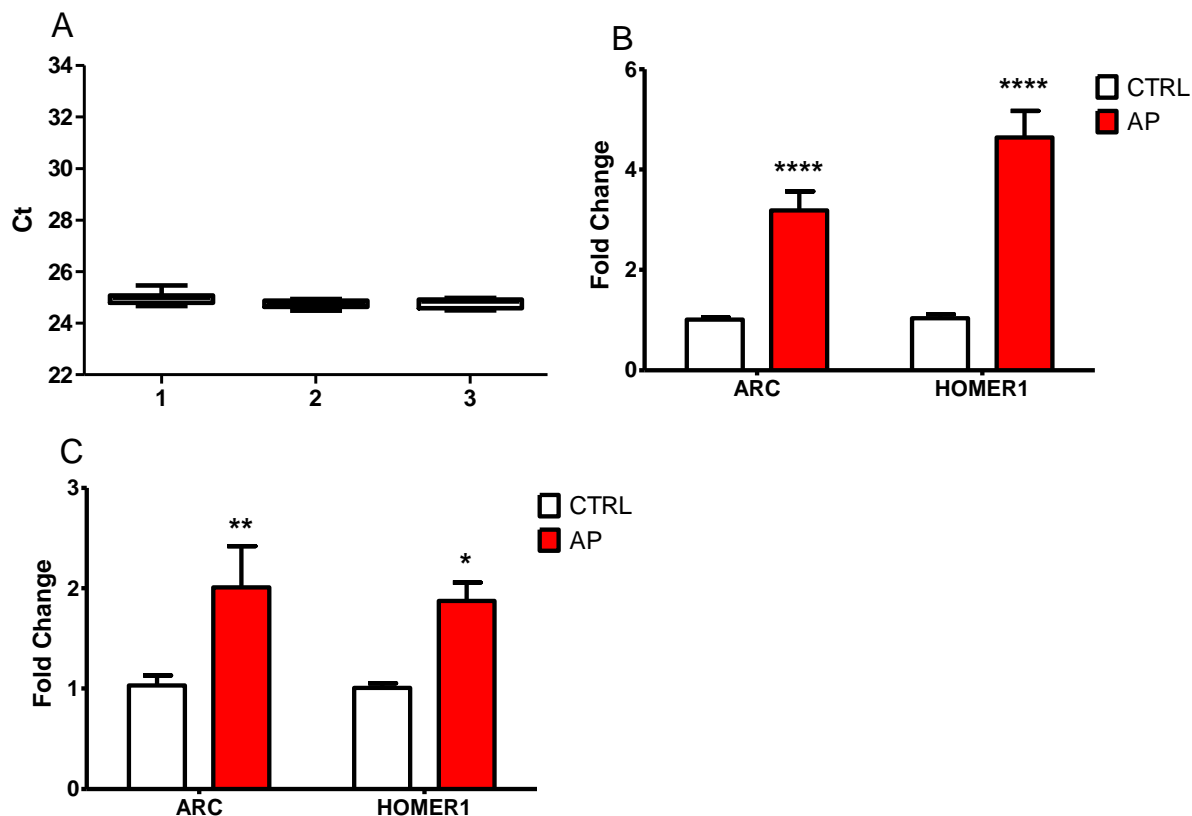


Figure 42. Assessment of mRNA induction of *ARC* and *HOMER1* after action potential bursting in primary hippocampal neurons. After the induction of action potential bursting in primary hippocampal neurons by 4-aminopyridine and (+)-bicuculline, RT-qPCR was used to determine the levels of the *ARC* and *HOMER1* genes that are known to be induced by this programming. A) box and whisker plots demonstrating that *GAPDH* had little variation in each experiment and was used as an endogenous control reference to normalize Cts. B) fold change in *ARC* and *HOMER1* genes at 4 hours, media only control (CTRL, white bars) and action potential burst treated (AP, red bars), and C) fold change in *ARC* and *HOMER1* at 16 hours. In Graphs B and C, error bars represent standard error of the mean and significance was assessed with a 2-way ANOVA. ****= p -value < 0.0001 , **= p -value < 0.01 , *= p -value < 0.05 .

HOMER1 (p-value < 0.0001). By 16 hours, both genes were still significantly induced compared to control, however, with lower fold changes; induction of *ARC* being 2fold (p-value 0.03) and *HOMER1* being 1.9fold (p-value 0.0019). The significance testing was conducted as a one-tailed t-test with Welch's correction as the variance was unequal between the sample sets.

In determining miR-128-3p levels, the spike-in control for UniSp6 was used to ensure equivalency of the RT across all the samples. As can be seen in Figure 43A with a representative graph from 4 hours post treatment, the cDNA was indeed transcribed at a similar rate across samples in each experiment. The stable expression of endogenous control reference small RNA U6 was assessed (Figure 43B). The U6 was then used to normalize miR-128-3p Ct values before calculating fold change at 4 hours and 16 hours post treatment. Although miR-128-3p was not significantly changed at the 4 hour timepoint, it demonstrated a trend towards downregulation by a mean fold change of -1.5 at the 16 hour timepoint (p-value 0.08) when subject to a 2-way ANOVA (Figure 43C). These data clearly showed that the treatment that resulted in action potential bursting and subsequent expression of the CREB regulated genes associated with neuroprotection, *ARC* and *HOMER1*, did not result in the induction of expression of miR-128-3p in cultured hippocampal neurons. In fact, miR-128-3p displayed a trend towards downregulation by 16 hours. Therefore, the induction of miR-128-3p detected previously in CA1 neurons during early stages of RML scrapie prion infection must be occurring through a pathway other than synaptic NMDAR Ca²⁺ influx and subsequent CREB regulated transcription.

The levels of the miR-128-3p target genes, *GRIN2B*, *GRIN2D* and *GRM5*, were also examined in the action potential experiment using TaqMan gene expression assays on the same cDNA that was used to analyse expression of *ARC* and *HOMER1*. None of these

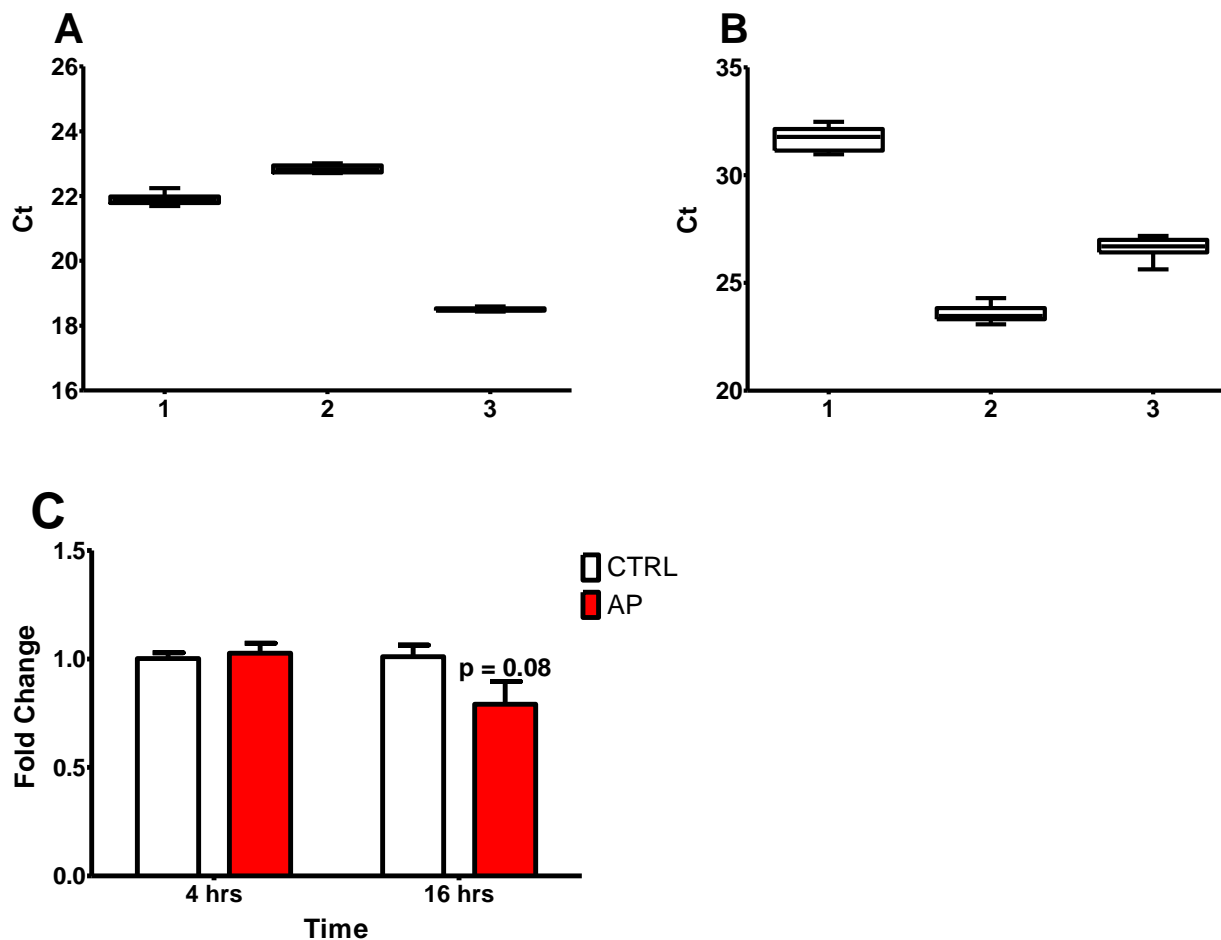


Figure 43. Detection of mature miR-128-3p in total RNA by RT-qPCR after action potential bursting in primary hippocampal neurons. A) Box and whisker plots for the spike-in control UniSp6 RNA for the 3 experiments B) Box and whisker plots for the endogenous control reference small RNA U6, C) Fold change in miR-128-3p at 4 hours and 16 hours post media only (CTRL) or action potential bursting treatment using 4-aminopyridine and (+)-bicuculline (AP), mean with error bars reporting SEM. Significance testing with a 2-way ANOVA.

genes were altered relative to the control at 4 hours post treatment (Figure 44A). However, by 16 hours post treatment all three genes, *GRIN2B*, *GRIN2D*, and *GRM5* were significantly downregulated (Figure 44B). In order to determine significance for the downregulation of the genes a one-tailed t-test was applied, although a Welch's correction was required for *GRIN2B* and *GRM5* as the variance was unequal. The *GRIN2D* gene demonstrated the greatest reduction with a -2.2fold downregulation (p-value 0.0064). The levels for *GRIN2B* and *GRM5* were similarly decreased, at -1.7fold (p-value 0.0079) and -1.6fold (p-value 0.0047) respectively. These data suggested that the regulation of miR-128-3p and three of its targets was potentially via a similar mechanism in hippocampal neurons during prolonged action potential bursting.

4.4.7 Chronic excitotoxic levels of glutamate lead to a reduction in miR-128-3p in primary hippocampal neurons

One function of the host PrP^C is the Cu²⁺ dependent regulation of NMDARs, and when PrP^C is knocked out in mouse models, excitotoxicity occurs in hippocampal neurons cultured from these mice (Khosravani et al. 2008b). Also, in Alzheimer's disease, excitotoxicity has been proposed as a hypothesis of disease particularly as the drug memantine, which preferentially blocks NMDAR2B (Xia et al. 2010), improves cognition in patients (reviewed in (Esposito et al. 2013)). It was therefore a possibility that activation of an excitotoxic glutamate mechanism in cultured primary neurons could result in altered miR-128-3p levels. I therefore tested a second hypothesis, whether miR-128-3p is deregulated by treatment of primary hippocampal cells with chronic excitotoxic levels of glutamate. Cultured primary hippocampal neurons at 8 DIV were treated with 100 μ M of L-glutamic acid in neurobasal media, while the media alone was used as a mock treatment

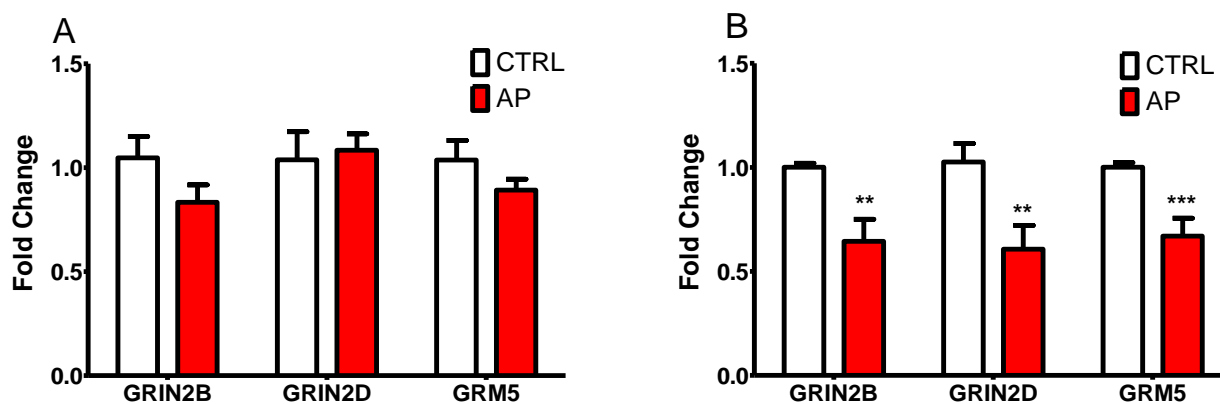


Figure 44. Fold change in *GRIN2B*, *GRIN2D*, and *GRM5* mRNA in total RNA using RT-qPCR after action potential bursting in primary hippocampal neurons. Media only (CTRL, white bar) or 4-aminopyridine and (+)-bicuculline (AP, red bars). At A) 4 hours and B) 16 hours post treatment. Mean fold change is reported with error bars representing SEM. Significance testing was performed as a one-tailed t-test between control and AP treated. ***= p-value < 0.001, **= p-value < 0.01

control. Total RNA was collected at 24 hours and the levels of genes were first assessed to confirm the experimental model. As can be seen in Figure 45A, GAPDH was expressed at stable levels in the samples and was the endogenous reference gene used to normalize Cts. In this case the expression of *ARC* was examined as a negative control as it has not been shown to be involved in excitotoxicity, in fact it has previously been shown to become deactivated in chronic excitotoxic conditions (Zhang et al. 2009). There was no significant difference in expression of *ARC* between the media only control and cells treated with 100 μ M glutamate (Figure 45B). Next, the levels of the NMDAR genes *GRIN2A*, *GRIN2B*, and *GRIN2D* were determined. Previous studies have shown that these genes are all downregulated during excitotoxic conditions *in vivo* in rat neurons (Goebel, Poosch 2001). Indeed, all three genes were significantly downregulated in the mouse hippocampal neurons 24 hours following treatment with 100 μ M glutamate (Figure 45B). The *GRIN2A*, *GRIN2B*, and *GRIN2D* transcripts were all decreased by similar levels with mean fold changes of -4.4fold (p-value 0.0172), -5.3fold (p-value 0.0013), and -5.9fold (p-value 0.0026) respectively. Next, the levels of miR-128-3p were examined using RT-qPCR with LNA primers. As performed previously, the first step was to evaluate the controls of RNAs UniSp6, U6, and miR-342-3p. The box and whisker plot in Figure 46A demonstrated that the spike-in control UniSp6 was transcribed equivalently across the samples confirming the consistency of the methodology. Therefore, the endogenous control references of U6 and miR-342-3p were examined for stable expression. While miR-342-3p was within a narrow range (Figure 46A), the expression of U6 was again highly variable (data not shown). Therefore, Cts of miR-128-3p were normalized to miR-342-3p before fold changes were calculated. The levels of miR-128-3p were significantly downregulated in the 100 μ M glutamate treated hippocampal neurons (Figure 46B), to a mean of -1.7fold

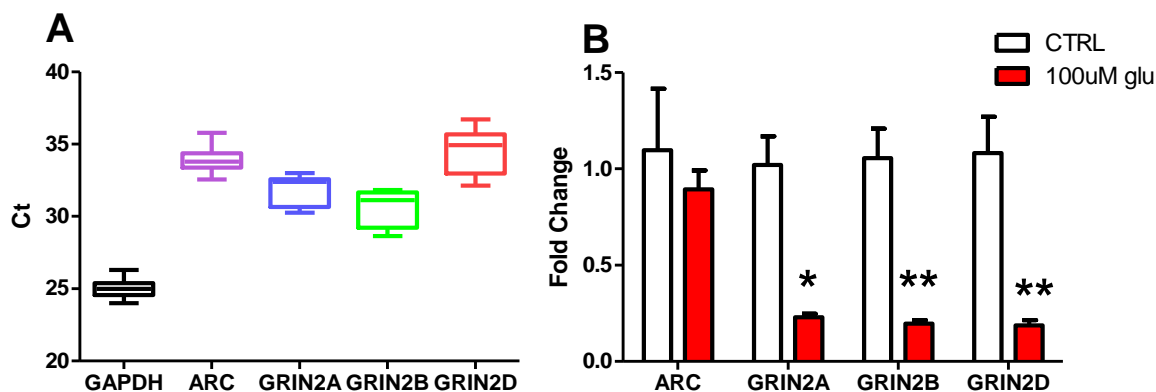


Figure 45. Relative expression of *GAPDH*, *ARC*, *GRIN2A*, *GRIN2B*, and *GRIN2D* mRNA in total RNA from primary hippocampal neurons after excitotoxic levels of 100 μ M glutamate were bath applied, determined by RT-qPCR. A) Box and whisker plot for *GAPDH*, *ARC*, *GRIN2A*, *GRIN2B*, and *GRIN2D* Cts, and B) fold change in *ARC* and the 3 NMDAR subunits *GRIN2A*, *GRIN2B*, *GRIN2D* mRNA from media only (CTRL, white bars) or 100 μ M glutamate treated (100 μ M glu, red bars). In B, the error bars denote SEM and one-tailed t-tests with Welch's correction for unequal variance were applied to determine significance. **=p-value < 0.01, *=p-value < 0.05.

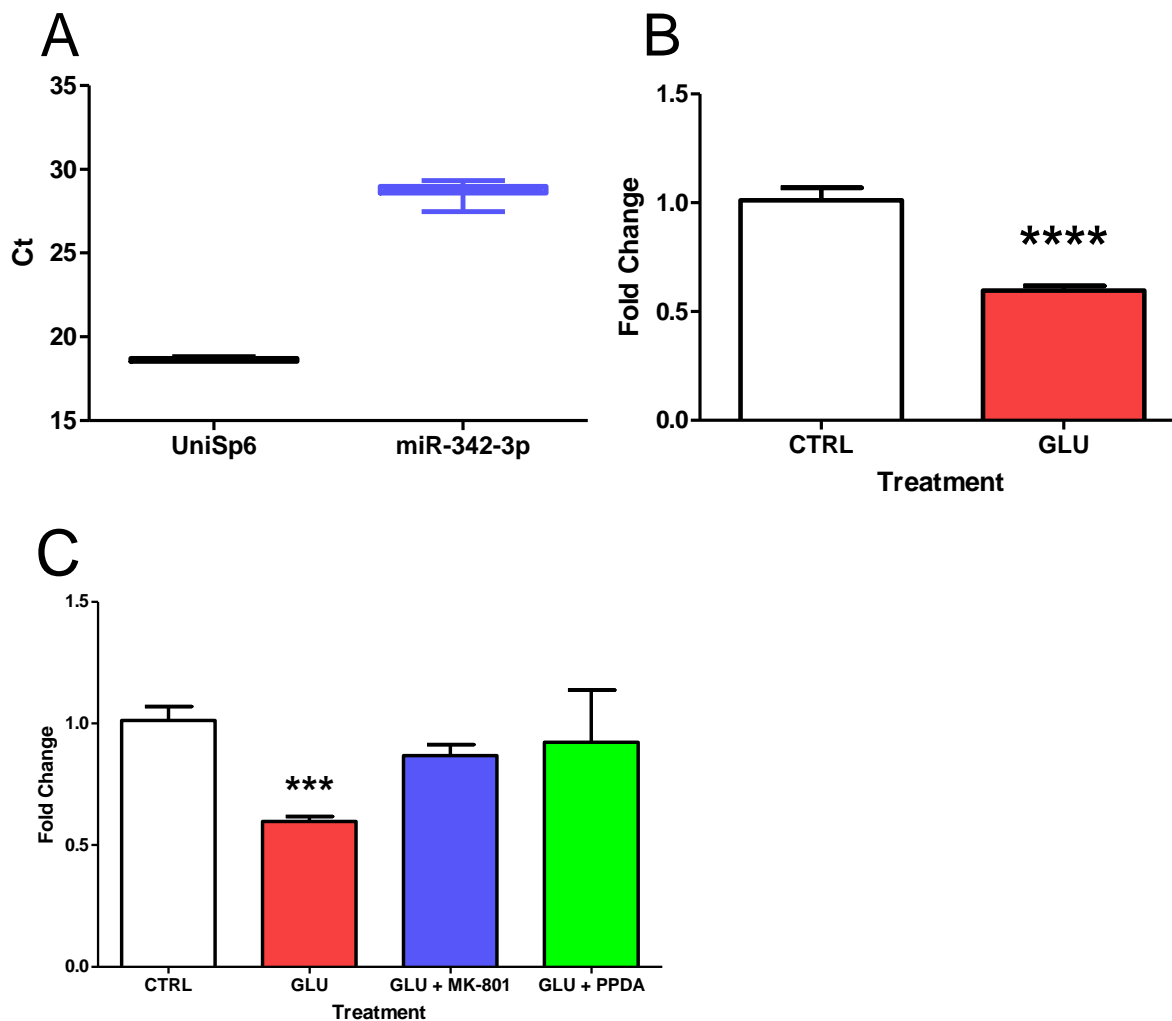


Figure 46. Change in miR-128-3p levels in total RNA derived from primary hippocampal neurons exposed to excitotoxic levels of glutamate. A) box and whisker plot for controls UniSp6 and miR-342-3p, B) levels of miR-128-3p after media only (CTRL) or 100 μ M L-glutamate treatment (GLU) and C) levels of miR-128-3p after 100 μ M glutamate treatment plus NMDAR inhibitors MK-801 and PPDA. Error bars represent SEM. Significance testing in B was performed using a one-tailed t-test with Welch's correction, while a 1-way ANOVA comparing all groups to the control was used for C to determine significance. ***=p-value <0.0001

(p -value < 0.0001) when subject to a one tailed t -test with Welch's correction for unequal variance.

To confirm whether glutamate stimulation of NMDARs was responsible for triggering miR-128-3p downregulation, NMDAR inhibitors were used to block signaling specifically through these receptors. To this end, two different types of NMDAR inhibitors were used. The first one, MK-801, is a general antagonist of the NMDAR (Wong et al. 1986) that possesses a high affinity for NMDA receptors and binds only when the channel is open. The second NMDAR inhibitor was (2S*, 3R*)-1-(phenanthrene-2-carbonyl) piperazine-2,3-dicarboxylic acid (PPDA), which has a demonstrated increased affinity by 5-6fold specifically for NMDAR2D as compared to NMDAR2A or NMDAR2B (Jespersen et al. 2014), although it does bind these with a lower affinity as well (Feng et al. 2004). Primary hippocampal neurons were treated with each of these inhibitors along with the application of excitotoxic 100 μ M L-glutamate. The concentrations used for the inhibitors were 10 μ M as per previous studies (Baron et al. 2010, McKay et al. 2013, Costa et al. 2009). The inhibitors and glutamate were bath applied to the hippocampal neurons at 8 DIV and total RNA was collected at 24 hours before examining for miR-128-3p expression.

In a preliminary experiment, following treatment with either of these inhibitors in the presence of 100 μ M L-glutamate, the levels of miR-128-3p were remained similar to those of mock treated control cells (Figure 46C) when tested statistically through a 1-way ANOVA. In the post Dunnett's Multiple Comparison Test comparing all treatments to the media only control, only the treatment of 100 μ M glutamate demonstrated a significant reduction of miR-128-3p levels by -1.7fold (p -value 0.0004). Thus it was concluded that miR-128-3p is downregulated specifically by excitotoxic stimulation of NMDARs. It

appeared that the specific inhibitor of NMDAR subunit 2D was as efficient as the broad-spectrum inhibitor MK-801 although the specificity of PPDA requires further validation.

4.5 A proteomics approach to determine novel miR-128-3p targets

4.5.1 Rationale

In prior experiments, I found that miR-128-3p was upregulated in early prion disease in the CA1 neurons, then downregulated at later stages of disease. In synaptoneurosomes, there was an increase of miR-128-3p presence during early stages of disease in the hippocampus with no observable changes in the forebrain. Additionally, miR-128-3p targeted the 3' UTR of *GRM5*, *GRIN2B*, and *GRIN2D*, and it was downregulated during chronic action potential and excitotoxic glutamate signaling in cultured hippocampal neurons, although the exact mechanism for this deregulation is as yet unknown. Numerous other predicted miR-128-3p targets were determined to be present within hippocampal neurons as well as synaptoneurosomes and identifying those proteins whose levels are responsive to miR-128-3p may shed light on the potential regulatory pathways that may be at play during neurodegeneration. Of particular interest, based on the putative functions ascribed to PrP^C and data reported in previous chapters, is the role of miR-128-3p downstream of glutamate receptor signaling. Insight into this function can be gleaned by identifying the specific targets of miR-128-3p in hippocampal neurons.

4.5.2 Hypothesis

The manipulation of miR-128-3p levels in primary hippocampal neurons leads to quantitative changes in the proteins levels of targets, particularly NMDAR2B and NMDAR2D that are involved in excitotoxic glutamate signaling.

4.5.3 Increasing miR-128-3p levels in primary hippocampal neurons decreases

GRM5 and *GRIN2D* levels

Functional genomics was used to study the effect of manipulating the level of miR-128-3p on the cellular levels of hippocampal neuron proteins. For gain of function, miR-128-3p levels were increased in cultured hippocampal neurons by transfecting in pre-miR-128-3p or the negative control, pre-miR-scramble, which is designed and validated to not bind any known mammalian mRNA sequence. Transfection into 7 DIV hippocampal neurons was performed using Lipofectamine 2000 which is a cationic based reagent with low cytotoxicity in primary hippocampal neurons (Ohki et al. 2001) and has been used by others to deliver RNA into primary neurons (Saba et al. 2012, Saba, Medina & Booth 2014, Dalby et al. 2004). Two concentrations, 10 nM and 50 nM, of pre-miR-128-3p were transfected into primary hippocampal neurons and the vehicle alone was used as a control. After 24 hours, total RNA was extracted and miR-128-3p levels were assessed using LNA based primers in RT-qPCR. After confirming that the RNA spike-in control UniSp6 was transcribed equally across all samples and that small RNA U6 was stably expressed in each sample, U6 was used as the endogenous reference (Figure 47A). The levels of miR-128-3p increased significantly (Figure 47B) at both 10 nM and 50 nM of pre-miR-128-3p concentration, by 100fold for 10 nM (p-value= 0.0003) and 475fold for 50 nM (p-value 0.0008) when tested using one-tailed t-tests. The vehicle only control had fold change similar to pre-miR-scramble control, indicating that lipofectamine introduction did not alter the endogenous levels of miR-128-3p. At the 50nM concentration of pre-miR-128-3p, the glutamate receptor *GRIN2D* and *GRM5* genes were significantly downregulated by -3.0fold (p-value < 0.0001) and -1.8fold (p-value 0.003) respectively (Figure 47C) while *GRIN2B* displayed no change.

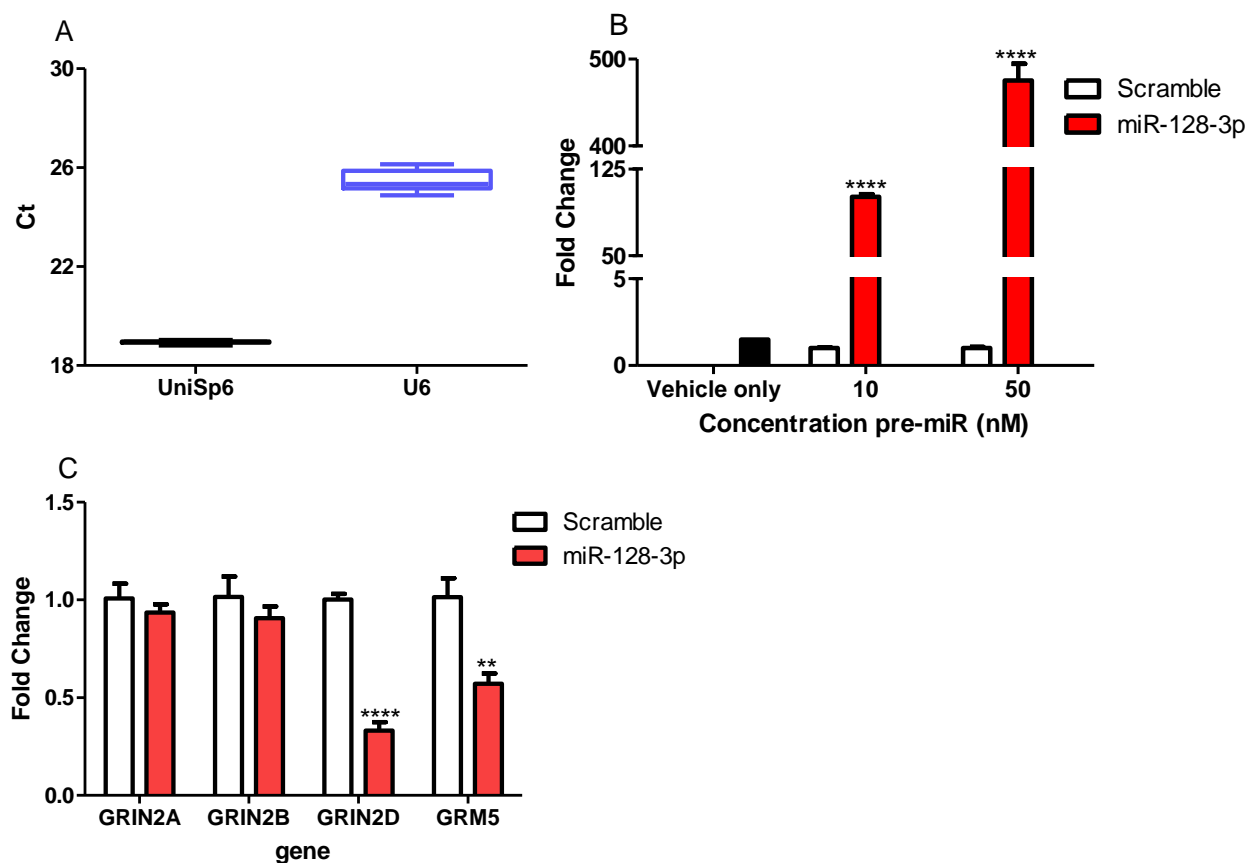


Figure 47. Determination of miR-128-3p and gene target levels using RT-qPCR on total RNA derived from primary hippocampal neurons in the miR-128-3p gain of function experiment. A) box and whisker plot of Cts for UniSp6 RNA spike-in control and U6, B) Representative miR-128-3p fold change in vehicle only, miR-scramble, and miR-128-3p at 10 and 50 nM of pre-miR, and C) Fold change in *GRIN2A*, *GRIN2B*, *GRIN2D*, and *GRM5* mRNA using *GAPDH* as an endogenous control reference gene in the RT-qPCR with TaqMan gene expression assays. Error bars in B and C represent SEM and statistical testing in B and C was performed using one-tailed t-tests between scramble and miR-128-3p treated. ****=p-value <0.0001, **=p-value <0.01.

4.5.4 The knockdown of miR-128-3p does not change *GRIN2B* or *GRIN2D* levels in primary hippocampal neurons

Anti-miR inhibitors were used to knock-down miR-128-3p, these have been reported to successfully change gene targets of miRs in primary hippocampal neurons (Saba et al. 2012). The negative control, anti-miR-scramble, consisted of a random sequence which does not bind to any known miRs in mammalian cell lines. In total, 50 nM of anti-miR-128-3p or anti-scramble was transfected into 7 DIV primary hippocampal neurons for 24 hours before total RNA was collected and subject to RT-qPCR for the detection of miR-128-3p and small RNA U6, the endogenous control reference. The spike-in RNA UniSp6 was added at the RT step to ensure equal cDNA transcription across samples (Figure 48A) and normalized against U6. The knockdown of miR-128-3p was successful and significant with a -57fold downregulation (p-value 0.004) when a one-tailed t-test was applied (Figure 48B). There were no significant changes in the levels of *GRIN2B* or *GRIN2D* transcripts after miR-128-3p knockdown (Figure 48C), while *GRM5* was not tested.

4.5.5 Mass spectrometry of cultured hippocampal neurons detects many proteins

TMT labeling was used in conjunction with mass spectrometry to facilitate the semiquantitative analysis of protein levels following miR-128-3p transfection. The TMTs are isobaric chemically modified labels which are applied to peptides that are digested from protein samples (Thompson et al. 2003, Dayon et al. 2008). These labels contain reporter ions that are lost during MS/MS fragmentation and are quantified to obtain protein profiles. The TMT sixplex format allows for multiplexing with up to 6 samples per mass spectrometer run, which enables replicates to be used within a single run for the

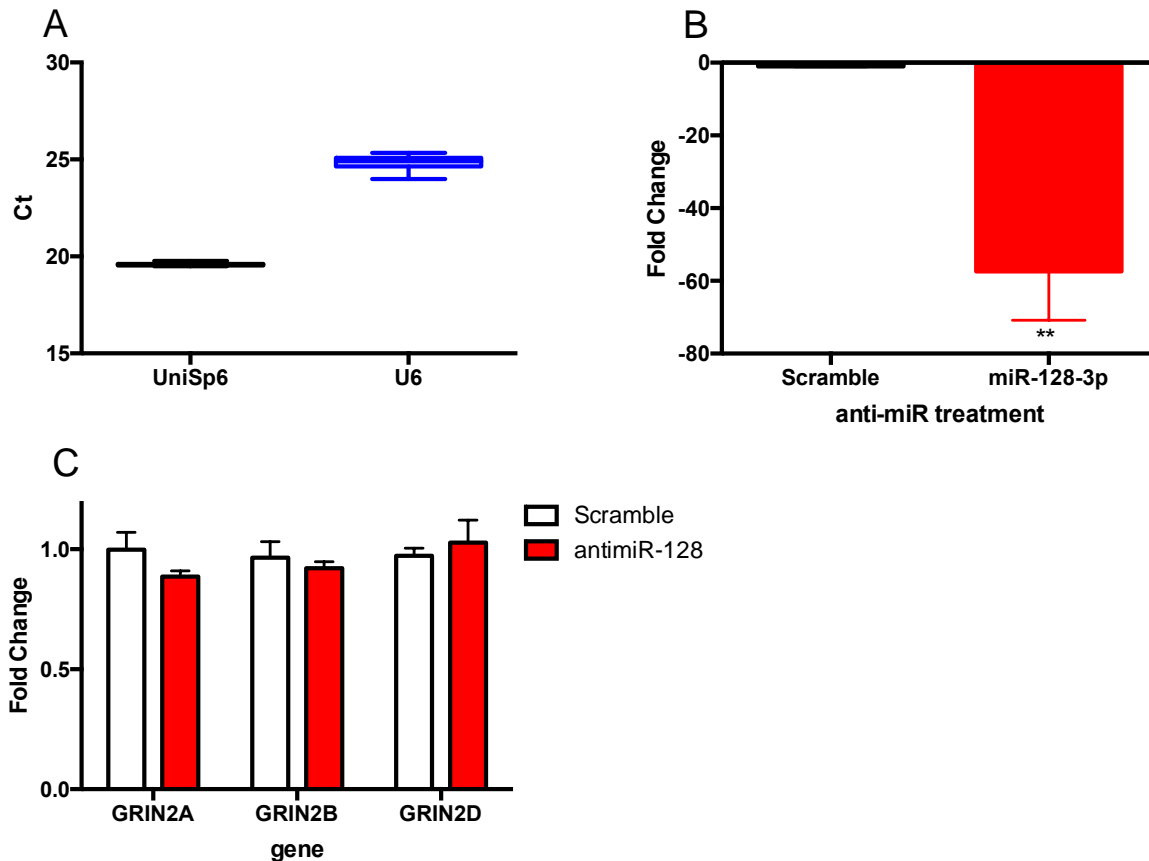


Figure 48. Levels of miR-128-3p and gene targets in total RNA derived from primary hippocampal neurons using RT-qPCR after knockdown with anti-miR-128-3p. A) Box and whisker plot of Cts from UniSp6 RNA spike-in control and endogenous reference U6, B) Representative miR-128-3p fold change, and C) Fold change in *GRIN2A*, *GRIN2B*, and *GRIN2D* mRNA using *GAPDH* as an endogenous control reference in TaqMan gene expression assays. Error bars in B and C represent S.E.M. and statistical testing in B and C was performed using one-tailed t-tests between scramble and anti-miR-128-3p treated.

generation of statistical comparisons to be made of protein abundances in biological replicates. Three treatments were performed on transfected primary hippocampal neurons, these were; Lipofectamine only (vehicle control), 10 nM of pre-miR-scramble, or 10 nM pre-miR-128-3p. This pre-miR concentration resulted in ~100fold increase in miR-128-3p in neurons (Figure 47B). These experiments were performed in 4 separate hippocampal neuron preparations at 11 DIV resulting in a total of 12 samples. Similar to the HeLa study, 24 hours after transfection total protein lysates were harvested in N-PER. A summary of the collection and processing of samples can be visualized in Figure 49.

The equivalent of 100 µg total protein from each sample was subject to acetone precipitation (Table 18) which removed detergents in N-PER that interfere with mass spectrometry. The protein pellet was then digested with trypsin and labeled with TMTsixplex labels, ensuring no overlap in label between the same treatment type. There was a total of 6 TMT isobaric labels which differed in heavy isotope content in the mass reporter ion (126, 127, 128, 129, 130, and 131). The reporter ion generates the relative intensity information upon which quantitative differences between the samples are generated (Rauniyar, Yates 2014). The labels were N-hydroxysuccinimide activated and labelled the primary amine groups within the digested peptides. The multiplexed samples were combined 6 at a time, thus for 12 samples two separate runs were performed. After the samples were labeled, they were mixed at a 1:1 ratio and separated into 12 fractions with a high-pH reverse phase C18 column (Waters) using the Agilent 1200 micro-flow liquid chromatograph. Each fraction was subsequently analyzed on an Easy nano-flow Liquid Chromatograph 1000 combined to the Q-Exactive Plus mass spectrometer. The generated sequences of peptides was probed using Mascot v2.5 using the SwissProt

Transfection of pre-miRs or vehicle control

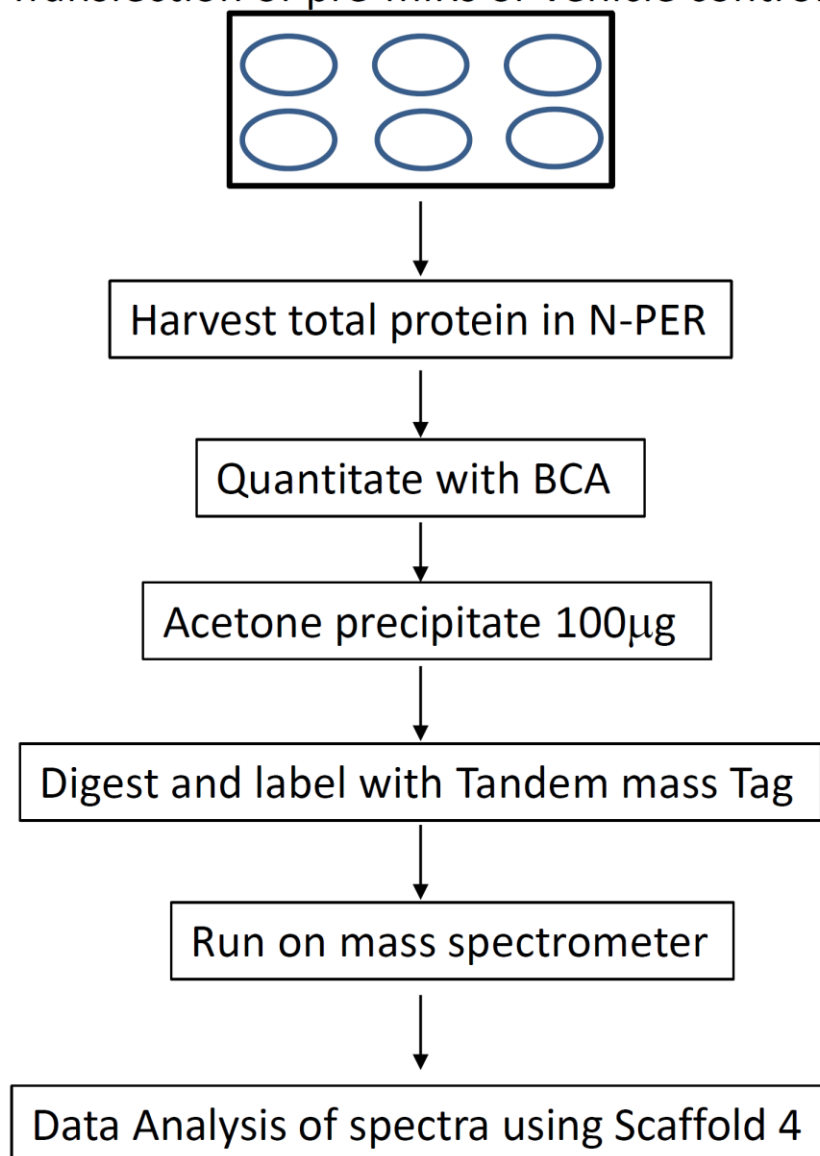


Figure 49. Overview of methods used to obtain global proteome profiles of miR-128-3p gain of function experiments in primary hippocampal neurons using mass spectrometry with TMT labels. After cells were transfected with either pre-miR-128-3p, pre-miR-Scramble, or vehicle only, the total protein was harvested in N-PER buffer and quantitated using the BCA. This was followed by acetone precipitation of 100 µg of protein which was then digested and labeled with tandem mass tags before running on the mass spectrometer. The resulting data generated on the mass spectrometer was imported into Scaffold 4 and analyzed.

Table 18. The concentrations and volumes used to TMT label each protein sample from the miR-128-3p proteomic experiment in primary hippocampal neurons. The samples names, concentration, volume for acetone precipitation, and TMT labels are indicated.

| Sample | Concentration ($\mu\text{g}/\mu\text{L}$) | Volume for 100ug (μL) | Acetone added (μL) | TMT label |
|---------------|---|--|---|------------------|
| vehicle 1 | 0.565 | 176.9 | 884.6 | 126 |
| scramble 1 | 0.529 | 189.1 | 945.3 | 127 |
| miR-128-3p 1 | 0.486 | 205.9 | 1029.3 | 128 |
| vehicle 2 | 0.461 | 216.6 | 1083.2 | 129 |
| scramble 2 | 0.445 | 224.4 | 1122.1 | 130 |
| miR-128-3p 2 | 0.446 | 224.0 | 1120.1 | 131 |
| vehicle 3 | 0.408 | 245.0 | 1224.9 | 127 |
| scramble 3 | 0.402 | 248.5 | 1242.3 | 128 |
| miR-128-3p 3 | 0.431 | 231.7 | 1158.3 | 129 |
| vehicle 4 | 0.502 | 199.0 | 994.7 | 130 |
| scramble 4 | 0.457 | 218.8 | 1093.9 | 131 |
| miR-128-3p 4 | 0.429 | 232.8 | 1163.9 | 126 |

Mouse Protein database for which the decoy database was selected. The resulting hits were imported as 2 MudPit files, one for each run, into Scaffold 4.

In Scaffold 4, the detected proteins were filtered by using a protein threshold of 1% FDR and a peptide threshold FDR of 0.1% with a minimum of 2 peptides. The resulting profile included 5,509 proteins containing 37 decoys from the MASCOT search. The 5,509 protein list was then processed to remove the decoys as well as those proteins that were not detected ubiquitously, which resulted in 4,063 proteins ranging in size from 6kDa to 540 kDa. This list was then subjected to pathway analysis using PANTHER, the list of 4,063 proteins was input manually into the Gene List Analysis under PANTHER Tools, *Mus musculus* was selected as species and the Functional classification viewed in gene list was selected. Of the proteins, 4,012 IDs matched to the database and were examined for molecular function, protein class, and pathways involved.

In molecular function, most proteins belonged to the catalytic activity and binding categories, while structural, transporter, and receptor activity were also represented (Figure 50A). Many protein classes were present including enzymes, cytoskeletal, signaling, trafficking, receptor, and membrane proteins (Figure 50B). In the pathway analysis, 151 pathways were identified, those containing 20 or more proteins are highlighted in Figure 51. Notable are the presence of proteins for metabotropic glutamate receptors (class I, II, and III), G-protein signaling, ionotropic glutamate receptors, and neurodegenerative disease pathways including Alzheimer's disease, Huntington's disease, and Parkinson's disease. After the initial analyses confirmed the presence of neuronal proteins, a further in depth analysis of individual proteins was performed to ensure that cytoplasmic and synaptic components were also present.

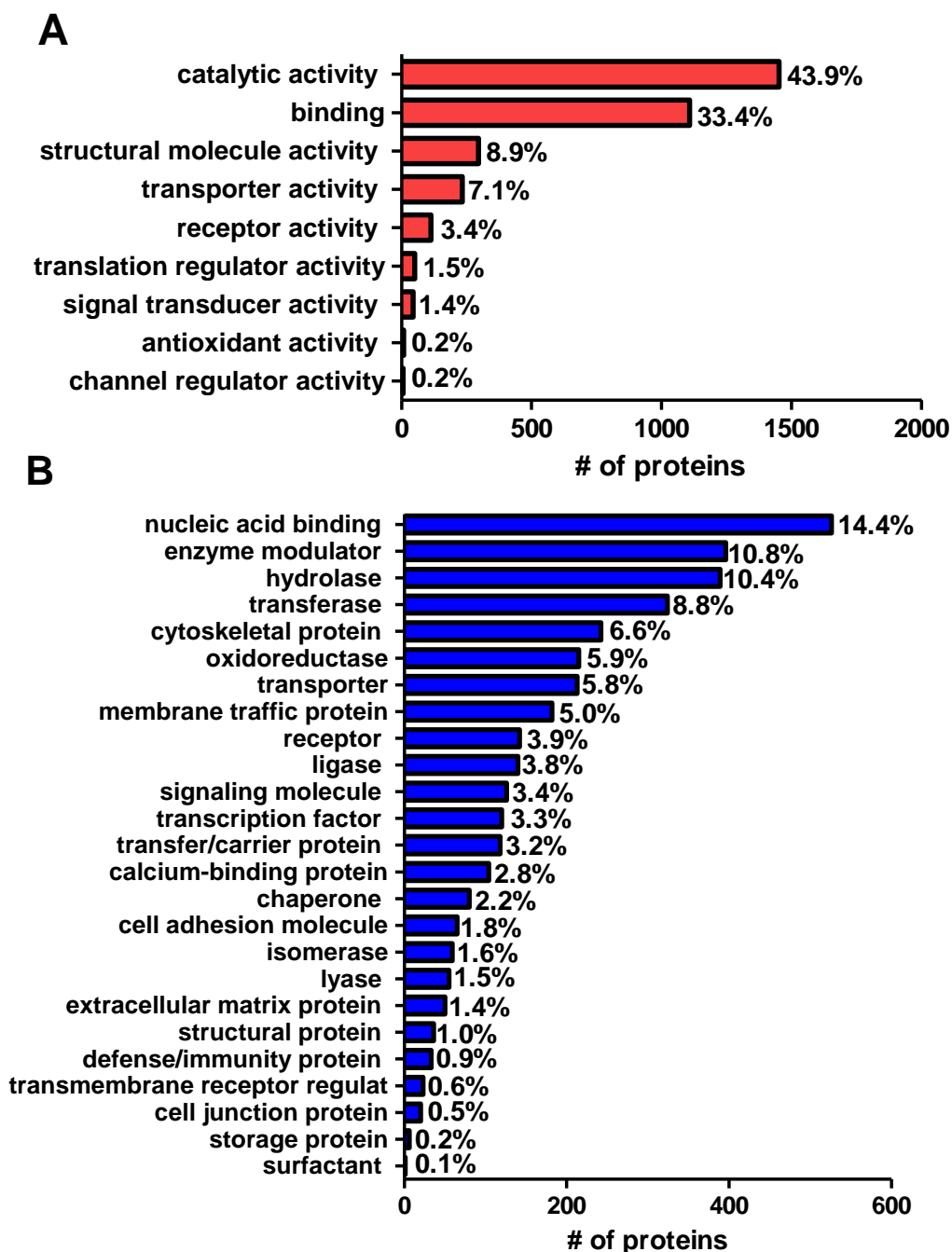


Figure 50. Protein profile of primary hippocampal neurons from miR-128-3p gain of function experiments. A) Molecular functions (red bars) and B) Protein classification (blue bars) with number of proteins involved on the X axis. Data generated querying PANTHER with 4,063 proteins detected in samples and of those 4,012 protein IDs mapping. The percentages identify the gene hits against the total number of potential molecular function or protein classification hits.

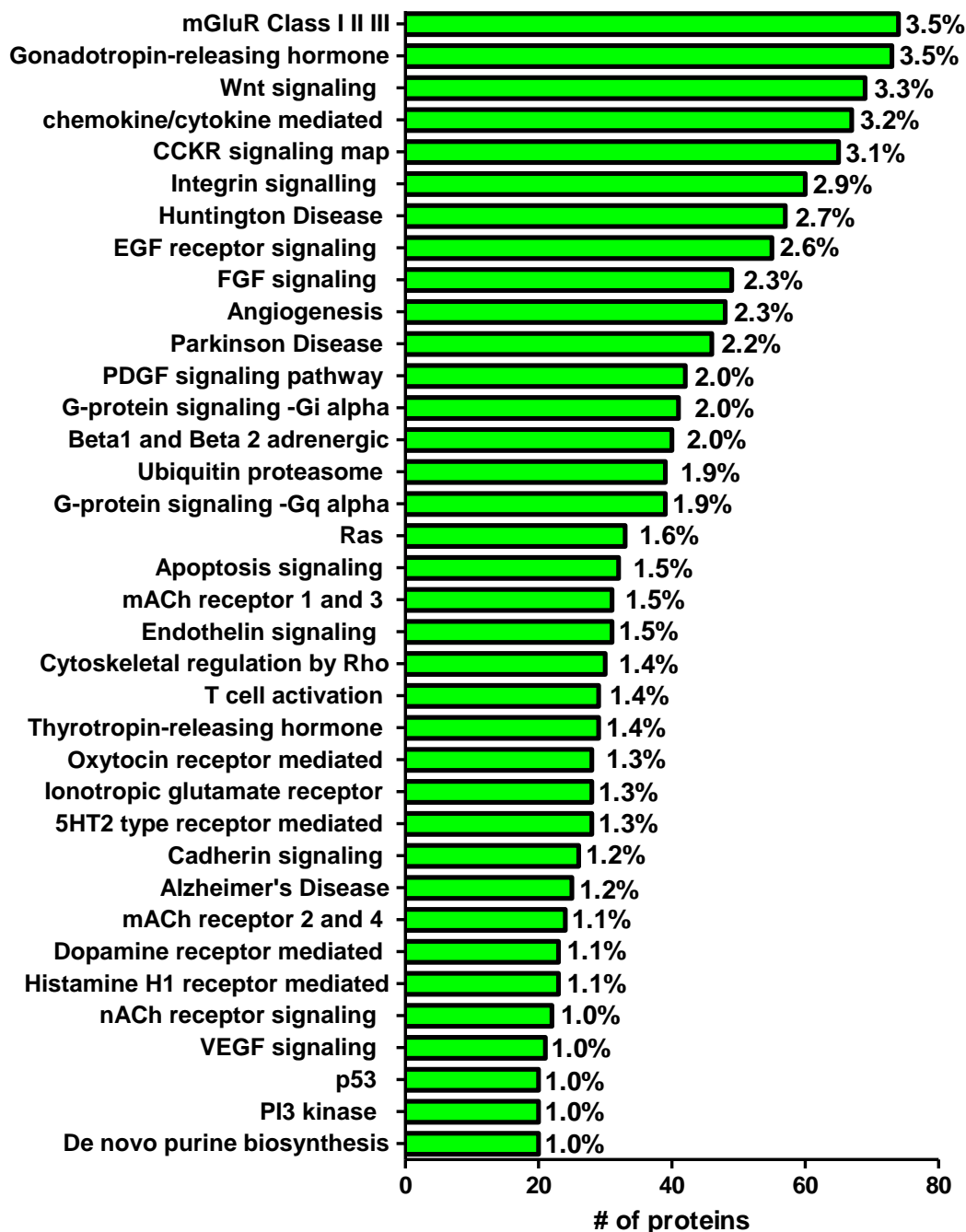


Figure 51. Pathways identified in the proteins derived from primary hippocampal neurons from the miR-128-3p gain of function experiments. The pathways that included 20 or more proteins are reported, although a total of 151 pathways were identified from the 4,012 mapped IDs in PANTHER. The percentages represent the gene hits against the total number of potential pathway hits.

The samples included many neuronal specific proteins such as synaptic and membrane proteins with a select few highlighted in Table 19. Some of these were previously identified in synaptosomes of CA3-CA1 hippocampal neurons from rodents (Corti et al. 2008) including α -synuclein, synapsin-3, syntaxin, and synaptophysin. Other neuronal proteins detected were MAP2, neuronal specific septin-3, neuronal cell adhesion molecule, and neuronal growth regulator 1. Excitatory neurotransmitter receptors were well represented including NMDARs, kainate, and AMPA (GRIA1-4), and mGluRs 2, 3, 5, and 7. The NMDAR2D protein was not detected in any samples, although the NMDAR2B and mGluR5 proteins pertaining to the miR-128-3p targeting hypothesis were. The inhibitory GABA receptors were present including α and β subunits. The mass spectrometer did indeed successfully detect neuronal transmembrane and synaptic proteins.

4.5.6 Slit homolog 3 protein was downregulated when miR-128-3p was increased in primary hippocampal neurons

To determine differential expression, the protein data was then subject to statistical testing in the Q+ section of Scaffold 4. To detect significant differences among treatments three Mann-Whitney U tests were performed which do not assume Gaussian distributions, between 1) vehicle only and scramble treated, 2) vehicle only and miR-128-3p treated, and 3) scramble and miR-128-3p treated. The p-value was set to < 0.05 with a Benjamini-Hochberg correction for multiple hypothesis testing which resulted in adjusted p-values of < 0.00006 to < 0.00004 .

Table 19. A select list of neuronal proteins found in the miR-128-3p gain of function protein lysates from primary hippocampal neurons as detected by mass spectrometry. The accession ID, protein name, exclusive unique peptides and spectra, total spectra and % coverage are indicated. There are two rows for each protein representing the two separate runs that were performed on the mass spectrometer.

| Uniprot Accession ID | Protein | exclusive unique peptides | exclusive unique spectra | total spectra | % coverage |
|-----------------------------|--|----------------------------------|---------------------------------|----------------------|-------------------|
| SYUA_MOUSE | α -synuclein | 7 | 14 | 53 | 81 |
| | | 7 | 15 | 62 | 86 |
| GRIK2_MOUSE [2] | Cluster of Glutamate receptor ionotropic, kainate 2 | 3 | 4 | 4 | 4 |
| | | 2 | 3 | 3 | 3 |
| GBRA1_MOUSE | Gamma-aminobutyric acid receptor subunit α -1 | 1 | 1 | 7 | 6 |
| | | 0 | 0 | 6 | 6 |
| GBRA2_MOUSE | Gamma-aminobutyric acid receptor subunit α -2 | 5 | 6 | 9 | 13 |
| | | 5 | 8 | 16 | 15 |
| GBRA3_MOUSE | Gamma-aminobutyric acid receptor subunit α -3 | 2 | 2 | 2 | 4 |
| | | 2 | 2 | 4 | 6 |
| GBRA5_MOUSE | Gamma-aminobutyric acid receptor subunit α -5 | 2 | 3 | 6 | 7 |
| | | 4 | 6 | 7 | 12 |

| | | | | | |
|-------------|--|----|----|----|----|
| GBRB1_MOUSE | Gamma-aminobutyric acid receptor subunit β -1 | 4 | 6 | 9 | 18 |
| | | 4 | 6 | 11 | 19 |
| GBRB2_MOUSE | Gamma-aminobutyric acid receptor subunit β -2 | 3 | 3 | 6 | 15 |
| | | 1 | 2 | 7 | 10 |
| GBRB3_MOUSE | Gamma-aminobutyric acid receptor subunit β -3 | 2 | 2 | 4 | 12 |
| | | 5 | 6 | 9 | 17 |
| GBRG2_MOUSE | Gamma-aminobutyric acid receptor subunit γ -2 | 5 | 7 | 7 | 11 |
| | | 5 | 5 | 5 | 13 |
| GRIA1_MOUSE | Glutamate receptor 1 | 15 | 18 | 28 | 23 |
| | | 16 | 20 | 33 | 26 |
| GRIA2_MOUSE | Glutamate receptor 2 | 16 | 20 | 32 | 29 |
| | | 20 | 25 | 42 | 35 |
| GRIA3_MOUSE | Glutamate receptor 3 | 5 | 6 | 14 | 12 |
| | | 6 | 7 | 14 | 12 |
| GRIA4_MOUSE | Glutamate receptor 4 | 2 | 2 | 11 | 10 |
| | | 3 | 3 | 11 | 9 |
| GRID1_MOUSE | Glutamate receptor ionotropic, delta-1 | 4 | 4 | 4 | 5 |
| | | 5 | 5 | 5 | 6 |

| | | | | | |
|-------------|---|----|-----|-----|----|
| NMDZ1_MOUSE | Glutamate receptor ionotropic, NMDA1 | 8 | 8 | 8 | 10 |
| | | 18 | 20 | 25 | 19 |
| NMDE1_MOUSE | Glutamate receptor ionotropic, NMDA2A | 1 | 1 | 2 | 2 |
| NMDE2_MOUSE | Glutamate receptor ionotropic, NMDA2B | 1 | 1 | 2 | 2 |
| | | 7 | 7 | 9 | 6 |
| NMDE3_MOUSE | Glutamate receptor ionotropic, NMDA2C | 12 | 12 | 15 | 9 |
| | | 1 | 1 | 2 | 1 |
| GRM2_MOUSE | Metabotropic glutamate receptor 2 | 1 | 1 | 3 | 2 |
| | | 4 | 4 | 5 | 7 |
| GRM3_MOUSE | Metabotropic glutamate receptor 3 | 4 | 5 | 5 | 5 |
| | | 5 | 5 | 5 | 6 |
| GRM5_MOUSE | Metabotropic glutamate receptor 5 | 3 | 3 | 3 | 4 |
| | | 17 | 18 | 19 | 14 |
| GRM7_MOUSE | Metabotropic glutamate receptor 7 | 14 | 16 | 21 | 15 |
| | | 10 | 12 | 12 | 14 |
| MTAP2_MOUSE | Microtubule- associated protein 2 | 11 | 13 | 13 | 15 |
| | | 77 | 145 | 292 | 47 |

| | | | | | |
|-------------|--|----|-----|-----|----|
| NCS1_MOUSE | Neuronal calcium sensor 1 | 80 | 139 | 272 | 51 |
| | | 4 | 4 | 5 | 26 |
| NRCAM_MOUSE | Neuronal cell adhesion molecule | 5 | 5 | 7 | 33 |
| | | 9 | 10 | 12 | 8 |
| NEGR1_MOUSE | Neuronal growth regulator 1 | 16 | 22 | 30 | 17 |
| | | 7 | 10 | 13 | 24 |
| DCX_MOUSE | Neuronal migration protein doublecortin | 9 | 14 | 21 | 32 |
| | | 11 | 16 | 29 | 42 |
| NPTXR_MOUSE | Neuronal pentraxin receptor | 14 | 21 | 34 | 58 |
| | | 7 | 10 | 15 | 17 |
| SEPT3_MOUSE | Neuronal-specific septin-3 | 10 | 14 | 21 | 24 |
| | | 12 | 18 | 30 | 41 |
| NSMF_MOUSE | NMDA receptor synaptonuclear signaling and neuronal migration factor | 14 | 23 | 42 | 47 |
| | | 3 | 4 | 4 | 8 |
| SYN3_MOUSE | Synapsin-3 | 5 | 7 | 7 | 12 |
| | | 3 | 4 | 9 | 10 |
| SYPH_MOUSE | Synaptophysin | 6 | 6 | 10 | 15 |
| | | 3 | 9 | 15 | 11 |
| STX16_MOUSE | Syntaxin-16 | 4 | 8 | 27 | 13 |
| | | 6 | 9 | 9 | 20 |

After the initial analysis, the list of differentially expressed proteins between vehicle only and miR-128-3p was examined against Scramble and miR-128-3p. The resulting Venn diagram demonstrates that 1 protein was changed in the miR-128-3p treated samples compared to both controls, Slit homolog 3 protein (SLIT3) (Figure 52A). The SLIT3 had at least 3 exclusive peptides that covered the protein and the protein probability was 100%, it was decreased by -1.09fold (p-value <0.0001) in the miR-128-3p treated neurons (Figure 52B). When comparing between Scramble and miR-128-3p treated, two other proteins were significantly downregulated, CAMK2 α (KCC2A) by -1.06fold and Splicing factor 3A subunit 3 (SF3A3) by -1.09fold (p-value < 0.0001). Although the fold changes are small, these were not unexpected as others have found that the fold changes in protein resulting from miR increases are small (Selbach et al. 2008). The mRNA encoding these three proteins was examined in TargetScan Human and RNA22 for miR-128-3p predicted binding sites, and SLIT3 was the only one predicted by RNA22 to have 2 binding sites. Although the miR-128-3p protein targets that were part of the hypothesis, NMDAR2B and mGluR5, did not demonstrate significant changes, a summary of the fold changes can be seen in Figure 53. As mentioned, NMDAR2D was not detected by the mass spectrometer in any of the 12 samples.

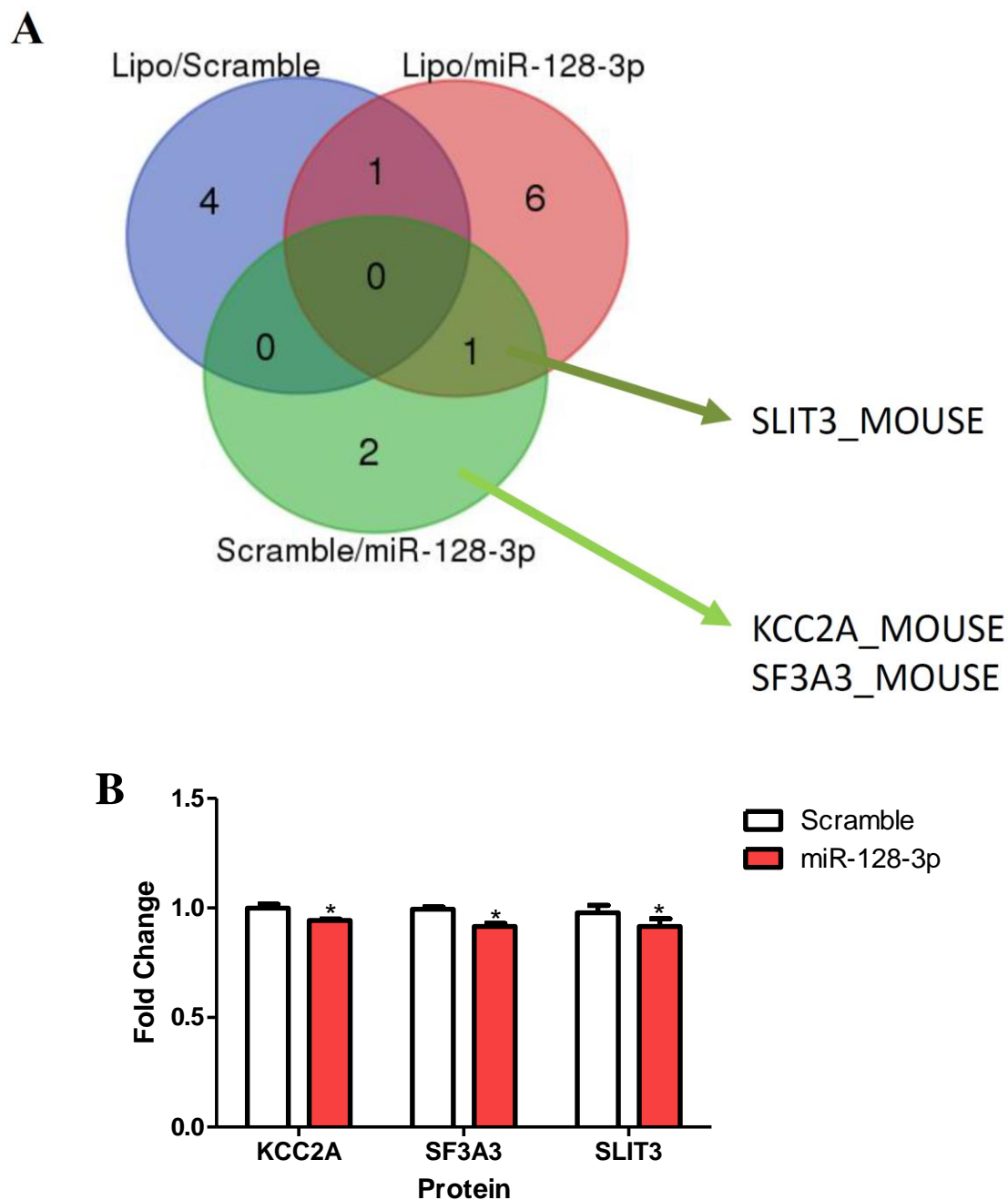


Figure 52. Identification of proteins that were significantly different in primary hippocampal neurons in miR-128-3p gain of function experiments. A) Venn diagram depicting proteins that were differentially expressed between vehicle only (Lipo), miR-scramble (Scramble) and miR-128-3p treated neurons, B) Fold change in KCC2A, SLIT3, and SF3A3p when compared to Scramble. Error bars represent SEM.

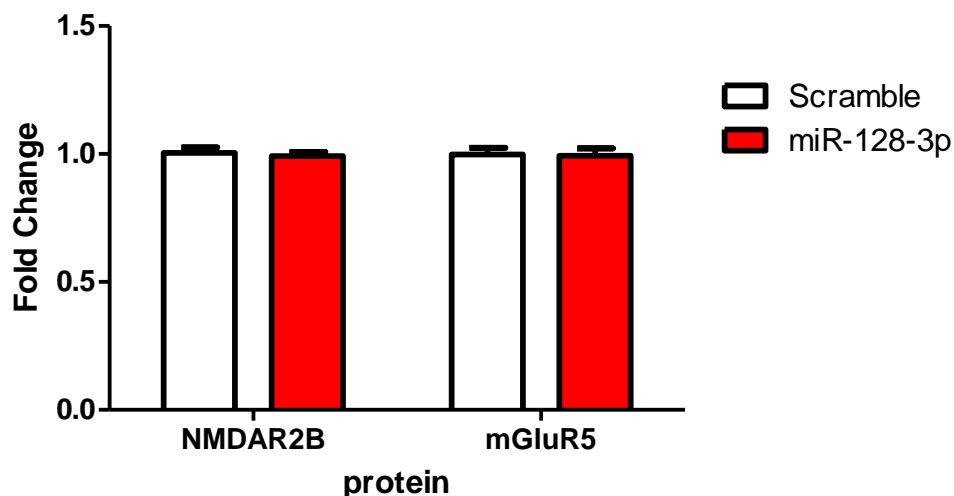


Figure 53. Protein levels of NMDAR2B and mGluR5 were unaltered in primary hippocampal neurons in miR-128-3p gain of function experiments. The protein fold change in miR-scramble (Scramble, white bar) and miR-128-3p (red bar) treated neurons as detected by TMT mass spectrometry from 4 independent experiments, fold changes were determined using vehicle only as the baseline of expression in Scaffold 4 Q+. Significance testing indicated no significant differences between treatments, error bars represent SEM.

5. Discussion

5.1 Summary

It has been well established that miR-128-3p is deregulated in the brain at terminal stages of neurodegenerative disease including Prion disease (Saba et al. 2008, Montag et al. 2009), Alzheimer's disease (Lukiw 2007, Alexandrov et al. 2012, Muller et al. 2014, Chen et al. 2016a), and Huntington's disease (Marti et al. 2010, Lee et al. 2011, Kocerha et al. 2014). However, not much detail surrounding miR-128-3p deregulation during early stages of neurodegeneration, its cell specificity nor its gene targets is known. To contribute to this lack of information, the main aim of this thesis was to determine the neuronal specific levels of miR-128-3p in the CA1 neuronal cell bodies, a subpopulation of neurons in the hippocampus in which PrP^{Sc} has been detected as replicating during early disease, and also in the hippocampal synapses, the subcellular communicative units between neuronal cells. Increased levels of miR-128-3p were detected in both the CA1 neuronal cell bodies and the hippocampal synapses, 3fold and 1.8fold respectively, at early, asymptomatic stages of prion disease in the RML scrapie prion mouse model when total RNA was examined by RT-qPCR. The neuronal related targets of miR-128-3p were predicted by the TargetScan algorithm and a select few were validated using Luciferase Reporter plasmids, which contained the 3' UTRs of glutamate receptor subunit genes of *GRIN2B*, *GRIN2D*, and *GRM5*. Following this, glutamate signaling pathways were induced in neurons cultured from the hippocampi of embryonic mice in order to evaluate changes in miR-128-3p during neuroprotective and excitotoxic glutamate signaling, with the finding that miR-128-3p was reduced after prolonged signaling of each type. The final

aim was to tie in changes at the protein level of the NMDAR2B, NMDAR2D, and mGluR5 subunits attributable to miR-128-3p by increasing miR-128-3p levels in cultured hippocampal neurons and determining global protein changes by mass spectrometry. Although no changes were detected in either of the three protein subunits, there were small but significant changes to SLIT3, KCC2A, and SF3A3 proteins.

The relevance of these results to human disease is that there is now supportive evidence for the increased levels of miR-128-3p specifically in neurons and synapses during early stages of neurodegenerative disease when no outward symptoms are apparent. This increase is occurring during a timeframe when the rescue of synaptic connections can restore behavioural and cognitive ability in prion infected mice (reviewed in Mallucci 2009). The data contained in this thesis suggest that miR-128-3p could be targeted therapeutically with the hopes of restoring synaptic connections and/or glutamate signaling that is potentially lost during neurodegenerative disease. Further work could elucidate whether to increase or decrease miR-128-3p during early disease to help in potentially restoring this synaptic function and/or loss. Ultimately, this could also be applied to other neurodegenerative diseases if careful experimentation in these diseases reveals similar changes.

The use of miRs to ameliorate disease conditions such as cancer are currently in clinical trials (reviewed in (Rupaimoole, Slack 2017)). These include the use of anti-miR against miR-122 for liver cancer and increasing miR-16 or miR-9 in other cancers. In CNS diseases, no clinical trials are in place for miRs, however viral vectors have been used to deliver dopamine by deep brain injection for Parkinson's patients (reviewed in (Boese et al. 2013)). These viral vectors have also been used in animal models to deliver miRs using viral subtypes that can cross the blood brain barrier when injected intravenously. These

provide future possibilities for the delivery of miR-128-3p for neurodegenerative disease therapy after its efficacy has been assessed further. The limitations of this thesis are discussed in section 7, Future Directions.

5.2 RML scrapie prion mouse model

The RML scrapie infection in mice provided a model that represented many aspects of the disease that are seen in human patients. These include accumulation of aggregates of misfolded prion protein, neurodegeneration, neuroinflammation, and clinical signs including behavioural changes, weight loss and ataxia that progressively increase in severity. Animals reached terminal stages of illness at 177 +/- 11 dpi, which is consistent with the literature describing this model (Thackray, Klein & Bujdoso 2003). An intraperitoneal inoculation, rather than intracerebral, was used to mimic a natural route of infection of acquired disease that included neuroinvasion of the CNS through the periphery (Bett et al. 2012). This strain of prion has been reported as replicating within the hippocampus during early stages of infection (Bruce et al. 1991) and PrP^{Sc} was indeed detected in the hippocampus at 90 dpi and colocalized with CA1 neuron cell bodies by 110 dpi, a time at which CA1 presynaptic terminals are being lost (Cunningham et al. 2003). This was during the early stages of disease when densely packed neuronal cell bodies within the CA1 region were still intact and infiltration of activated glia had not yet occurred. This meant that cutting out neuronal cells with a laser resulted in a very high ratio of neuronal cells to glia which provided a robust indication of neuronal levels of miR-128-3p during prion infection. At later stages of disease, especially by EP, the composition of the CA1 could not be described as neuronal only as it contained glial infiltration.

5.3 CA1 profile of miR-128-3p

This is the first report to show that miR-128-3p is changed specifically in a neuronal population during early RML scrapie prion infection in mice. The levels of miR-128-3p levels are increased in the CA1 during early disease and are then reduced at later stages of disease (Figure 54). During early disease, the increase of miR-128-3p is occurring at a time when PrP^{Sc} is not yet detected in the cell bodies but is in the synapses. At later, clinical stages of disease, the decrease of miR-128-3p, strikingly at the EP of infection, could be caused by a number of factors such as downregulation of transcription, the loss of neurons, and the influence of a relative increase in proportion of activated glia and astrocytes. Indeed, miR-128-3p is enriched in neurons and expressed at much lower levels in astrocytes (Smirnova et al. 2005). The elevation of miR-128-3p at early stages of RML scrapie prion infection could be also due to increased transcription of the two genes that contain this miR on their introns, *R3HDM1* or *ARPP21*. These two were deregulated by 2.5fold or more during at least one timepoint during RML scrapie infection in the CA1 (Majer et al. 2012), which gives some supporting evidence for this hypothesis. The miR-128-3p isoform that is predominant (80%) in the brains of mice is encoded by the *ARPP21* gene, which is a cAMP regulated phosphoprotein. There is experimental evidence that miR-128-3p can target the long isoform of *ARPP21* and that this gene is differentially expressed in Alzheimer's disease patients (Megraw et al. 2010, Hipfel et al. 2006). Perhaps this could be occurring in prion disease as well.

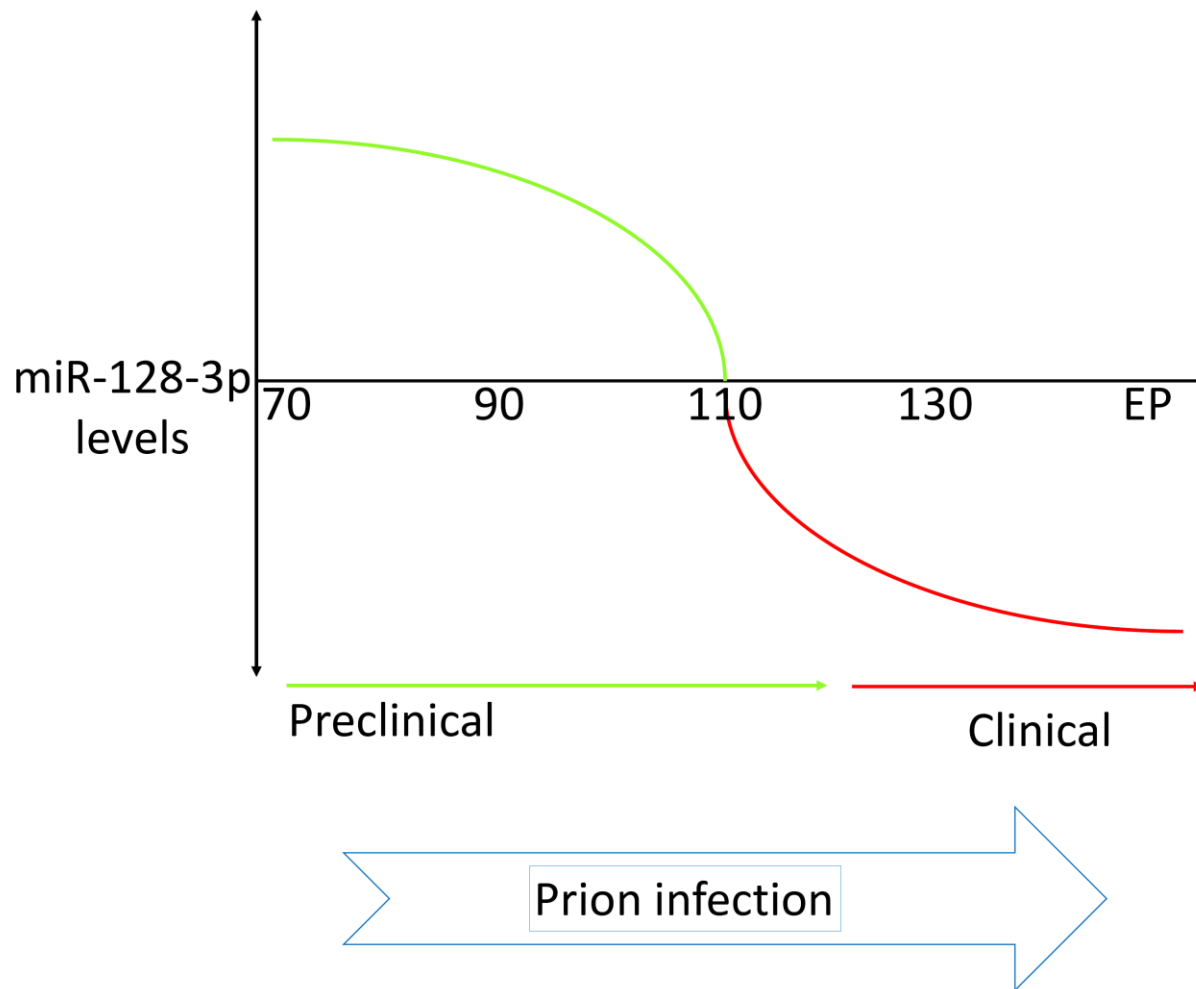


Figure 54. Diagram depicting change in the levels of miR-128-3p in CA1 neurons over the time course of RML scrapie prion infection in mice. The levels of miR-128-3p are increased at early, preclinical stages of infection in CA1 cell bodies, return to baseline, and are then reduced at clinical to terminal stages of infection.

The independent transcription of miR-128-3p outside its associated genes could be happening as there is evidence of a promoter that drives miR-128-3p expression independently of at least one of its host genes (Monteys et al. 2010). Additionally, there are transcriptional enhancers, epigenetic modifications, and other modifying factors that could also lead to altered miR expression and/or stability (reviewed in (Ha, Kim 2014a)). For example, during inflammatory processes increased transcriptional expression of miR-146a and miR-155 was promoted by NF- κ B coupled with bromodomain and extra terminal proteins (Duan et al. 2016). In addition, post-transcriptional modification by methylation of pre-miRs can lead to decreased affinity for DICER processing resulting in pre-miR decay (Xhemalce, Robson & Kouzarides 2012) or the tailing of primary miR transcripts through uridylation or adenylation to improve miR stability (Kawahara et al. 2007). The influence of these in relation to miR-128-3p in RML scrapie prion infection requires further exploration in the context of miR-128-3p in the brain. Particularly as this information regarding miR-128-3p is absent in the literature. Although no studies to determine miR levels in human prion infected brain have been performed it is notable that miR-128-3p has been determined to exhibit altered levels in the hippocampus of Alzheimer's disease patients. Interestingly, miR-128-3p was upregulated in the hippocampus of patients when tau tangle involvement was restricted to the hippocampus but in contrast was decreased in the hippocampus in those that had tau tangles spread into the cortex as well as the hippocampus.

In addition to transcriptional events, there are many instances in which miR-128-3p has been reported to have altered expression within the CNS, both normal and disease related. For example, miR-128-3p levels increase during the differentiation of neurons from progenitors (Zhang et al. 2016, Zare et al. 2015, Santos et al. 2016), and the

introduction of miR-128-3p into pluripotent stem cells causes differentiation and an increase in neuronal markers (Zare et al. 2015). Furthermore, increasing miR-128-3p in SH-SY5Y cells results in increased proliferation and differentiation of these immortalized neurons into mature neurons (Guidi et al. 2010). As synapses are starting to be lost during the early stage of prion disease, it is a possibility that miR-128-3p elevation is a host response to counter the loss of synaptic connections. The increase in miR-128-3p could be an attempt to reprogram neurons to produce new connections as a feedback loop for those that are lost. This would suggest that miR-128-3p is potentially responding in a positive way to stress or damage caused by prion replication in the brain. Another indication for a neuroprotective role for miR-128-3p is that when introduced exogenously into neuroblastoma cells, the levels of anti-apoptotic BCL2 rise, pointing towards neuroprotection against apoptosis (Guidi et al. 2010).

Behavioural experiments in rodents have demonstrated that miR-128-3p increases during fear conditioning experiments (Lin et al. 2011, Kye et al. 2011). How this fits into prion disease is not clear, however the fear conditioning was due to NMDAR activation (Kye et al. 2011). The neuroprotective gene program detected at early stages of RML scrapie infection is due to synaptic NMDAR signaling in the CA1. Also, excitotoxicity through NMDARs may be occurring during prion and Alzheimer's diseases. There are neurological conditions which cause the increase of miR-128-3p as well. In rodent models of epilepsy, the use of MK-801 to block NMDARs results in increased miR-128-3p in the hippocampus (Alsharafi, Xiao & Li 2016). Also, the antipsychotic drug haloperidol, which is used to treat schizophrenia, causes the increase of miR-128-3p in the cortex of rodents although the mechanism is not clear (Perkins et al. 2007).

Another explanation for the early increase in miR-128-3p could be related to the decay time of the mature miR affecting its accumulation within the CA1 region during infection. Studies have demonstrated that miRs have various half-lives dependent on modifications and that target directed degradation of miRs occurs as well (Marzi et al. 2016). The kinetics of miR-128-3p is not well described at this time and further studies are required to determine its half-life in neurons. If altered decay rate is the case in RML scrapie prion infection, it returns to baseline by the end of the asymptomatic stage of disease (110 dpi). This indicates that some event occurring at the transition between preclinical disease and clinical disease returns miR-128-3p levels to control until later stages of infection when it suddenly becomes reduced.

At the clinical stages of disease, the reduction of miR-128-3p could be largely in neurons but glial infiltration is a component of the input sample RNA, particularly at terminal disease. Therefore, the reduction cannot be attributed solely to neurons. In Huntington's disease, it has been demonstrated that there is an overall decrease of miR-128-3p in the striatum and cortex of non-human primate models and human patients, and this decrease in the primate model starts during embryonic development. Perhaps prion disease, at its end stages, emulates these features of Huntington's disease due to an increased accumulation of misfolded protein aggregates. As there are polyglutamine expansions in Huntington's, the accumulation of misfolded α -synuclein is occurring throughout development, whereas in prion disease the accumulation of PrP^{Sc} is progressive after a long incubation period. The reduction of miR-128-3p could be a cellular response to the advanced, increased aggregation of misfolded proteins. However the main caveat in the comparison to Huntington's disease is that the reduction of miR-128-3p arose from a heterogeneous cell mixture of brain sub region homogenates. In addition, the Alzheimer's

patients with widespread tau tangles also displayed a decrease in miR-128-3p in the hippocampus at terminal disease indicating that when the misfolded aggregates have become widespread there is a tendency in miR-128-3p reduction in the hippocampus.

There is ample evidence of a neuronal decrease of miR-128-3p contributing to disease processes *in vivo* including in epilepsy (Bot, Debski & Lukasiuk 2013, Araujo et al. 2016). In epilepsy, miR-128-3p knockdown mice have seizures from birth that ultimately result in fatality, this is cured through the administration of the anti-convulsant drug, Valproate or by restoring miR-128-3p levels to baseline (Tan et al. 2013a). Experimentation with neurons from miR-128-3p knockdown mice indicate an increase in excitability of neurons (McSweeney et al. 2016, Tan et al. 2013a). Although prion infected mice do not display epileptic symptoms, PrP^C knockout mice have increased excitability of *in vivo* derived neuron cultures (Khosravani et al. 2008a), which may correlate to a presumed loss of PrP^C during prion infection as PrP^{Sc} converts it.

Upon systemic kainic acid challenge in wild-type rats, miR-128-3p levels decreased in the hippocampal synapses (Pichardo-Casas et al. 2012). The kainate receptors are a class of ionotropic glutamate receptors similar to NMDARs and it is interesting to note that their activation led to the decrease of miR-128-3p *in vivo*. This could correlate to the chronic activation of synaptic NMDARs seen in early prion disease in the CA1, or perhaps to excitotoxic events that may be occurring during later stages of prion disease. Another explanation for the reduction in miR-128-3p at later stages of infection could be due to global DNA transcription being shut off due to cell death, as some neuronal death was seen at terminal stages with FluoroJade C staining.

Another explanation for miR-128-3p decrease at terminal disease could be due to glial infiltration at that time. The glial cells, astrocytes in particular have lower levels of

miR-128-3p compared to neurons (Smirnova et al. 2005). These cells are contributing to the RNA pool from the CA1 neurons and this could explain the reduction detected within this region compared to mock infected animals. Finally, the changes in miR-128-3p levels need further investigation into whether detection through qPCR is due to mature forms or primary transcripts. Both can form part of the amplicon that is produced. New PCR technologies now exist that can help differentiate the mature from primary forms. In addition, Northern Blots, which were difficult to conduct due to safety regulations at the NML could demonstrate these differences in miR processing.

5.4 Targets of miR-128-3p found through computational biology

The TargetScan tool was used to predict gene targets for miR-128-3p. The resulting list comprised 55% of genes that are expressed in the brain as determined by various large-scale studies to delineate tissue-specific gene expression. In addition, many of the predicted targets had multiple binding sites within the 3' UTR, suggesting multiple access points for miR-128-3p to initiate binding and suppress protein translation. It has been shown that the presence of multiple sites increases the likelihood that a gene is a genuine target of a particular miR (Fang, Rajewsky 2011). Most genes were evolutionarily conserved between mouse and human suggesting an adaptive pressure for miR-128-3p regulation in the mammalian CNS. Since the majority of predicted targets were expressed in the CNS and that miR-128-3p is primarily expressed in the CNS, an important role in the regulation of gene expression by miR-128-3p seems highly likely. The TargetScan program is not designed to stratify targets into tissue or cellular subtypes, therefore the predicted targets were compared to the forebrain CAMK2 α neuron dataset. The CAMK2 α neuron dataset consisted of targets pulled down from the forebrain CAMK2 α expressing neurons which

are glutamatergic and comprise ~30% of the total neurons of the forebrain (Wang et al. 2013). The targets were obtained using next generation sequencing and the resulting dataset was matched to the seed sequence of miR-128-3p to give its targets that are active in RISC targeting.

Almost a quarter of the predicted targets were present in the CAMK2 α neuron targets. Of these, pathways important to synaptic signaling were represented including inhibitory GABA_B receptor signaling and ionotropic glutamate receptor signaling as well as others. It was interesting to note that *GRIN2D* formed part of the targets that overlapped with CAMK2 α /miR-128-3p derived neurons while *GRIN2B* and *GRM5* did not. This could indicate that in the adult mouse CAMK2 α neurons, *GRIN2D* subunits are under tight regulation by miR-128-3p. This makes sense as *GRIN2D* gene expression is highly restricted in the adult CNS of rodents, and is particularly low in the forebrain (Standaert et al. 1996).

The lack of *GRM5* and *GRIN2B* transcripts in the CAMK2 α dataset was somewhat surprising. However, it is possible that these two are not under as tight of regulation as *GRIN2D* and serve an important role in forebrain CAMK2 α neurons, which is why they are not found in the RISC complex of these neurons. In addition, the NMDAR2D protein subunit was found in one of the forebrain synaptoneurosome protein samples by mass spectrometry but was absent in the proteome of the cultured hippocampal neurons. The differential regulation of targets could be occurring in different brain regions and in neuronal subtypes. Indeed, the majority of the targets that did not overlap between TargetScan and CAMK2 α neurons have demonstrated gene expression in the brain and a literature search showed that many of the targets absent in CAMK2 α neurons had been

described as having a functional role in neurons. The *CAMK2 α* dataset has other limitations in that a previous analysis demonstrated that it did not capture a number of neuronal published targets of miR-128-3p (Ching, Ahmad-Annur 2015). Obtaining further brain region specific neuronal datasets would provide clarity on this front, particularly target data from RISC pull down to generate biologically relevant data for miR-128-3p.

5.5 Validation of glutamate receptor subunit genes as miR-128-3p targets

Binding of miR-128-3p to the 3' UTRs of *GRIN2B*, *GRIN2D*, and *GRM5* was shown experimentally through Luciferase Reporter Assay. Previously, *GRM5* had been reported as a target of miR-128-3p (Kocerha et al. 2014), which corroborated the results in this thesis. At one concentration of miR tested, 10 nM, no binding with the *GRM5* 3' UTR was apparent. This could be due to the fact that the luciferase assay is an indirect measurement of luciferase activity and elements within cells can affect its expression. In addition, cells do endogenously express miR-128-3p, which could have been interfering at this specific concentration. This could be explained by a dose dependent concentration for miR-128-3p to bind the mRNA of *GRM5*, or perhaps that the mRNA levels within the cells interfered with the luciferase reporter assay. However, at 3 of 4 concentrations tested, there was significant binding and the fact that another group also found binding between miR-128-3p and *GRM5* 3' UTR suggests this target to be valid.

A decrease in luciferase activity was seen for all concentrations of miR-128-3p tested against the *GRIN2B* 3' UTR confirming binding capability. Although miR-128-3p has not previously been reported in relation to the regulation of *GRIN2B*, other miRs have. MiR-19a and miR-539 have previously been shown to regulate *GRIN2B* during neuronal

differentiation (Corbel et al. 2015) and in addition, miR-223, which concurrently regulates the GluR2 glutamate receptor transcript (Harrasz et al. 2012). It is known that during early RML scrapie prion infection in the CA1 region, the *GRIN2B* transcript is decreased (Majer et al. 2012). It is possible that increased miR-128-3p could be downregulating *GRIN2B* by transcript degradation. The protein level of NMDAR2B has not been determined within the CA1 to date. It is, however, entirely possible that miR-128-3p works in conjunction with other miRs in order to regulate *GRIN2B*, particularly in the hippocampus.

The *GRIN2D* subunit had the strongest binding by miR-128-3p, suppressing luciferase activity by at least 61%. In relation to prion disease, this is interesting because in neurons cultured from PrP^C knockout mice, NMDAR2D is increased (Khosravani et al. 2008a) and hippocampal neurons from these mice are more prone to excitotoxicity by NMDA. The mechanism of regulation by PrP^C is suggested to be by copper binding and S-nitrosylation of NMDARs (Gasperini et al. 2015). It could be hypothesized that NMDAR2D is increased during prion disease through loss of PrP^C function due to conversion to PrP^{Sc}. The increase of miR-128-3p detected at early stages of disease could be a feedback mechanism to bring the regulation of the NMDAR2D receptor under control, particularly if PrP^{Sc} is commencing conversion of PrP^C and is dysfunctional in the regulation of NMDAR2D. However, this remains to be tested as previous data concerning NMDAR2D in prion disease is lacking.

As miR-128-3p can target multiple glutamate receptor subunits, it makes sense that if multiple glutamate receptors are deregulated simultaneously during prion infection, miR-128-3p may be involved either to bring them back to homeostatic levels, or to protect the neuron by targeting them for translational repression. It is often the case that miRs have

been demonstrated to be feedback inhibitors, thus regulating homeostasis. One well-documented example is the role of miR-132 as a feedback inhibitor through repression of methyl CpG-binding protein 2 and brain-derived neurotrophic factor (Klein et al. 2007). In addition, miR-128-3p has a demonstrated role in nonsense mediated decay, where its increase leads to the repression of nonsense mediated decay resulting in the increase of vital neuronal proteins (Bruno et al. 2011). This could result in improving neuronal health but requires further testing in order to determine the validity of miR-128-3p in a neuroprotective role during prion disease. In Figure 55, the summary of findings from this chapter can be visualized and demonstrate that not only are mRNA transcripts involved during RML scrapie prion infection but the function of PrP^C protein at the cell surface with the NMDAR and mGluR5 could also be a factor during disease.

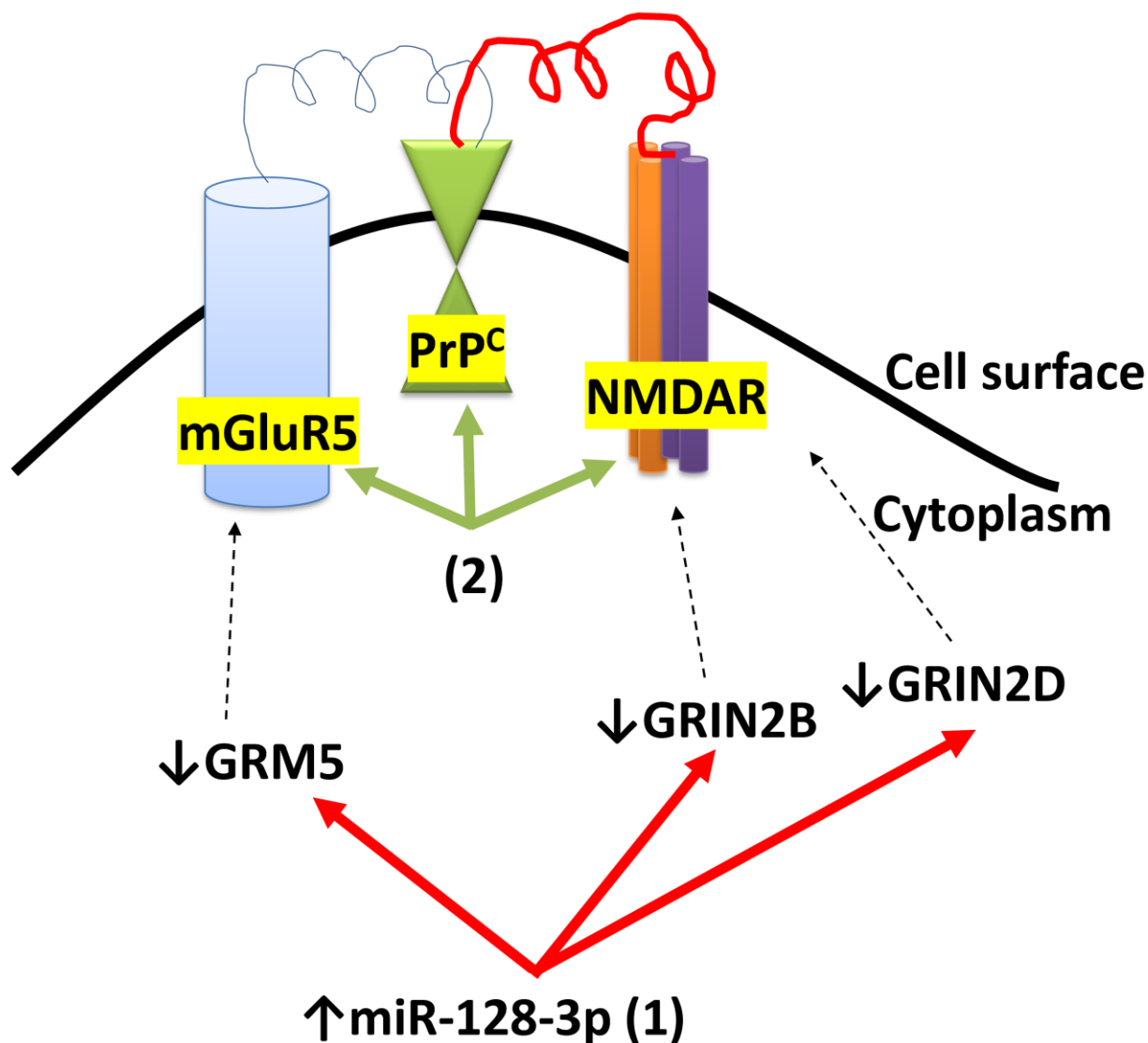


Figure 55. The proposed relationship between miR-128-3p, NMDARs, mGluR5, and PrP^C at early stages of prion infection. The first layer of regulation is that 1) the increase in miR-128-3p in *CA1* neurons during prion disease leads to the downregulation of the glutamate receptor subunits *GRM5*, *GRIN2B*, and *GRIN2D* mRNA by translational repression/degradation and 2) the mGluR5, PrP^C, and NMDARs regulate each other functionally at the cell surface.

5.6 Synaptoneurosome profiling of miRs in RML scrapie

As the increase in miR-128-3p was previously determined in isolated neuronal cell bodies, it was of interest to determine its levels at the subcellular synaptic locale as this is where pathology is first observed during asymptomatic prion disease. This was the first report isolating synaptoneurosomes in prion disease and one of the first miR isolations for synaptoneurosomes in neurodegenerative disease. There have been transcriptomic and proteomic analyses of synapses from post-mortem brain tissues in Alzheimer's disease but no miRs described. Isolated synaptoneurosomes were consistent with published reports by electron microscopy analysis and the content of their proteome. They included presynaptic vesicles, post-synaptic densities, and mitochondria (Saba et al. 2012, Rao, Steward 1991). The neuronal specificity was indicated by the presence of synapsin and PSD-95 proteins while astrocytes were largely absent, as synaptic astrocytes become excluded when the crude synaptoneurosome pellet is purified. The miR complement of the synaptoneurosomes was similar to what has already been described in wild-type rodents (Pichardo-Casas et al. 2012). This was also true of the synaptoneurosomes obtained from RML scrapie prion infected mice that had minimal astrocyte contribution even at late stage samples. This indicates that miRs found in synaptoneurosomes from prion infected animals disease remained neuronal in composition. Importantly, the contribution of post-synaptic dendrites to synaptoneurosome composition may have decreased during later stages of disease as the loss of PSD-95, a marker of post-synapses, was detected through Western Blot at the late stage of infection.

An increase in miR-128-3p levels was detected (1.8fold) in the hippocampal synapses at preclinical stages of disease although the statistical significance could not be assessed. At a similar timepoint of 105 dpi, miR-128-3p levels in the CA1 were similar to

mock infected indicating a potentially synaptic specific increase. This implies that miR-128-3p could be relevant in synaptic response during early stages of prion infection. As miR-128-3p is indicated through this thesis in the regulation of glutamate receptor genes, it could be performing in this capacity at the hippocampal synapses although further work is required to establish this hypothesis. As PrP^{Sc} was detected in the hippocampus by the early time point, the increase in miR-128-3p could be launched due to this cell stressor when synaptic connections are becoming lost. Perhaps miR-128-3p is promoting neuritogenesis in response to infection in the hippocampal neurons, as it is known to have this role in wild-type cortical neurons. Further investigation into the processes affecting hippocampal synapses are required in order to determine conditions during which miR-128-3p could become elevated.

Indeed, information pertaining to miR-128-3p at the hippocampal synapse is currently lacking. However, it includes that decreased levels are detected in hippocampal synaptoneuroosomes when rats are given systemic injections of kainic acid (Pichardo-Casas et al. 2012). An interesting thing about that study is that the levels of miR-128-3p were concomitantly increased in the forebrain synapses thus implying sub region specific synaptic response. If the decrease of miR-128-3p in the synapses of the hippocampus is seen during overexcitation of the excitatory kainate receptors, perhaps the increase seen during early RML scrapie prion infection is due to neuroprotective mechanisms. The fact that transcripts of *GRIN2B*, *GRIN2D*, and *GRM5*, which were demonstrated to bind miR-128-3p through Luciferase Reporter assay, were ‘present’ in the hippocampal synapses suggests they could be under the regulation of miR-128-3p during infection. However, the information concerning the levels of these genes and their protein component/functionality at the synapse needs to be identified during disease in order to answer this question. It

would indeed be interesting to do further experimentation with Ago2 pulldown of the synaptic fractions to determine which targets are being actively targeted by miR-128-3p during prion infection.

Although the levels of miR-128-3p were unchanged in the forebrain synaptoneuroosomes at either early or late stages in RML scrapie prion infected mice, there were many proteins found within the forebrain synaptic compartment that could be under the regulation of miR-128-3p. During the kainic experiments in rodents mentioned previously, miR-128-3p played a different role in the synapses of the forebrain compared to the hippocampus. Therefore, it was not entirely surprising that the miR-128-3p levels remained stable in the forebrain during RML scrapie prion infection but were changed in the hippocampus. In addition, there is very limited data concerning miR-128-3p at the synapse in terms of decay or turnover and its trafficking from the soma to the synapse, leaving much to be discovered. As novel synaptic functions for miRs are elucidated with time, they may provide further clues to sub region specific synaptic functions of miR-128-3p during neurodegenerative disease.

The synaptoneuroosomes obtained from the RML scrapie prion infected mouse forebrain and hippocampus contained many miRs that are enriched at the synapse (Pichardo-Casas et al. 2012). This indicates that the synaptic miR complement was largely intact. In the hippocampal synapses, the presence of miR-324-5p, which has been demonstrated as specific to synapses in this region was one of the miRs most increased in abundance. Similar to miR-128-3p, this miR has been reported to be involved in epileptic activity in rodents (Gross et al. 2016). The fact that this miR is altered indicates that there is likely a major change occurring in hippocampal synaptic function during early RML scrapie prion infection, particularly at this time when PrP^{Sc} replication is occurring in the

hippocampus. The mode of action of miR-324-5p is not currently known, but in other tissue types, it is involved in maintaining proper mitochondrial morphology (Wang et al. 2015) as well as macrophage function (Chen et al. 2014). As mitochondria form part of the synapse, it could be affected by the rise of miR-324-5p therein, further information regarding its targets at the synapse are required to demonstrate this.

It was interesting to find that miR-132-5p was not changed in levels in any of the synaptoneuroosomes, as this miR is one of the most well researched in terms of synaptic remodeling. This could be due to increased turnover or altered transport, particularly as this miR was increased in the *CA1* during early stages of disease. It is also possible this miR is functioning normally, at least in the hippocampal and forebrain synapses, even though it was deregulated in the *CA1* neurons during RML scrapie prion infection. However, discrepancies can exist between the cell bodies and the synaptic compartment when it comes to miR levels as indicated by a study of pilocarpine induced epilepsy in rats (Risbud, Porter 2013). This could also explain why the miRs found to be changed in the hippocampal synaptoneuroosomes were not in common with those found altered in the *CA1* cell bodies during RML scrapie prion infection. However, the hippocampal synaptoneuroosomes were not restricted to only the *CA1* region and as the various layers of the hippocampus have different inputs and outputs, it is entirely possible that their miR composition is different.

Overall, there were many more changes in miR levels in the synapses derived from the hippocampus compared to the forebrain. Some of the miRs found in the synaptic hippocampal samples were found to be deregulated during prion disease including miR-136-5p (*CA1*), miR-381-5p, miR-451a (*CA1*), miR-96-5p, miR-200a, miR-200b, miR-200c, miR-182-5p, and miR-183-5p among others. Perhaps the deregulation of so many

miRs in the hippocampus during early prion infection is not surprising as this region is affected early through loss of pre-synaptic terminals (Cunningham et al. 2003), which likely leads to alterations of synapses and remodeling when connections are broken. Since miRs are known to be involved in synaptic plasticity, it could be possible that the miRs identified play such a role. There were some miRs that were in common between early hippocampal synapses and early forebrain samples, including elevated levels of miR-136-5p and miR-376a-3p. The concurrent deregulation in these two miRs could be affecting a similar important process during the early stage of disease. Further work into the targets of these miRs at the synapse could perhaps elucidate common pathways they are regulating together.

The late forebrain synapses demonstrated a reduction of some miRs similar to early hippocampal changes including miR-451a, miR-141-5p, miR-182-5p, and the miR-200 family. It is interesting to note that many of these miRs including the miR-200 family were reduced at late stages of infection in the forebrains of mice that were independently inoculated with 3 different strains of scrapie namely 139A, ME7, and S15 (Gao et al. 2016). The fact that these were detected as reduced in the early hippocampal synapses but not until the late stages in the forebrain, perhaps suggests that the hippocampus is more sensitive to PrP^{Sc} replication during the early phase of disease and that these changes occur at later stages in the forebrain when the disease has spread further in the brain. In wild-type rats, the miR-200 family is not detected in the synapses of the hippocampus or forebrain but is restricted to the olfactory bulb (Pichardo-Casas et al. 2012), implying that it has a highly specialized synaptic function. Indeed, the increased reduction of these miRs during RML scrapie prion infection is implying that the function of these miRs is being downplayed further in mitigating prion infection. The decrease of this family of miRs

including miR-200, miR-182, and miR-183, has been seen in conditions such as mammalian hibernation induced torpor (Lee, Johnson & Hallenbeck 2012), and infection with West Nile virus (Kumar, Nerurkar 2014). This gives some evidence that when neurons are under stress it leads to the reduction in this miR family. Similarly, in prion disease, it is possible that the downregulation of these miRs is helping neurons respond to the stress induced by PrP^{Sc} replication.

Another miR that was found altered at the synapse was miR-146a-5p. This miR has previously been detected at late stages of infection from 4 different prion strain infections in mice (Saba et al. 2008, Montag et al. 2009, Gao et al. 2016), including in the CA1 region (Majer et al. 2012) and is associated with Alzheimer's disease (Cui et al. 2010). Polymorphisms in miR-146a-5p resulting in an increased risk of Alzheimer's disease have also been reported (Cui et al. 2014, Zhang et al. 2015). In finding this miR altered at the synapse implies importance in synaptic function during disease, particularly as this miR has been previously demonstrated as enriched in the synaptic compartment (Pichardo-Casas et al. 2012). The miR-146a-5p has a confirmed role in dendrite remodeling in neurons through regulation of microtubule-associated protein 1B (MAP1B) (Chen, Shen 2013). In the MAP1B study, the upregulation of miR-146a-5p resulted in the loss of dendrites through direct reduction of MAP1B and evidence from MAP1B knockout mice points towards the reduction of dendrite spine density (Tortosa et al. 2011). This is indicative that the miR-146a-5p increase detected in forebrain synapses at late stages of prion disease could contribute to dendrite loss, as this loss was noted through the reduction of PSD-95 at that time.

Some of the other miRs detected as changed in the synaptoneuroosomes include miR-142-3p at end stages, which was also detected in the CA1 previously, and miR-150-

5p. The increase of miR-142-3p has been identified during multiple sclerosis (Gandhi et al. 2013) and neuroAIDS (Chaudhuri et al. 2013) where it affects communication between neurons. The miR-150-5p is increased during ataxia in the genetic spinocerebellar ataxia 1, which results from polyglutamine expansions in ataxin-1 (Rodriguez-Lebron et al. 2013), as is miR-143-3p. Since there are some intact mitochondria present in the synaptoneurosome fractions, it is possible that some miRs, particularly miR-146a-5p, miR-142-3p, and miR-150-5p, which were shown in synaptic mitochondria in the hippocampus of rats during traumatic brain injury could be contributing to the changes detected (Wang et al. 2015). Taken together, this demonstration of miR alterations at the synapses of forebrain and hippocampal neurons during RML scrapie prion infection indicates potential mechanisms of synaptic function which are altered during neurodegenerative disease. Future work into the synapses may help reveal potential applications in modulating synaptic miRs with the goal of preventing disease related synaptic loss.

5.7 Primary hippocampal culture

The cultured neurons behaved similar to what others have observed as the neurons matured the dendrites increased and branched out towards other neurons forming synaptic connections by 8 DIV as demonstrated by immunostaining of the MAP2 protein, a dendrite marker (Kosik, Finch 1987). The expression of the glutamate receptor genes determined by RT-qPCR analysis including *GRM5*, *GRIN2D*, and *GRIN2B*, all increased as the neurons matured, plateauing at 8 DIV. Indeed, the *GRIN2B* gene has been shown to peak at one week in cultured hippocampal neurons from rats (Corbel et al. 2015), which supported these results.

As far as I am aware, the gene expression patterns of *GRIN2D* and *GRM5* obtained by RT-qPCR from total RNA are first reported here for cultured hippocampal neurons from mice. It was somewhat surprising that the *GRIN2D* gene increased during neuronal maturation as this subunit has been considered largely embryonic in the brain (Moriyoshi et al. 1991) with a small subset of neurons in the hippocampus demonstrating expression in adult rodents (Standaert et al. 1996). However, the levels of protein were not measured due to lack of detection by the commercially available antibodies, and the functional relevance of increased levels of *GRIN2D* gene expression in the maturing hippocampal neurons remains to be determined. The gene levels of *GRM5* increased the most which corroborates the *in vivo* situation as this gene displays high expression in the hippocampus of rodents (Catania et al. 1994). The high level of *GRM5* gene expression in the hippocampal neurons could be important during disease as it behaves as a co-receptor with PrP^C in binding not only laminin in the wild-type situation but toxic β oligomers in Alzheimer's *in vitro* models (Beraldo et al. 2016). Although knocking out mGluR5 in prion disease did not increase survival, it did improve cognitive symptoms in mice (Beraldo et al. 2016). Additionally, knocking out *GRM5* or targeting mGluR5 using the drug CTEP in a genetic Alzheimer's disease mouse model reversed amyloid β pathology and improved memory and cognition (Hamilton et al. 2014, Hamilton et al. 2016). Therefore, these hippocampal neurons could be a useful tool in studying the underlying mechanisms and signaling pathways for miRs in PrP^C-mGluR5 signaling.

The steady increase of miR-128-3p during the maturation of primary hippocampal neurons is supported by increases detected during differentiation of cortical neural progenitor stem cells into post-mitotic neurons (Zhang et al. 2016). The same is seen in immortalized neurons when retinoic acid is applied to differentiate them into mature

dendrite-containing neurons which also display a concomitant increase of miR-128-3p expression (Evangelisti et al. 2009). Coincidentally, the retinoic acid pathway is downregulated in Huntington's Disease (Niewiadomska-Cimicka et al. 2016), a disease where miR-128-3p is decreased in the CNS as well (Kocerha et al. 2014). In addition to increasing during cortical neuronal dendritic arborisation, miR-128-3p is critical in the proper migration of cortical neurons during development (Franzoni et al. 2015). The precursor form of miR-128-3p is expressed during early migration and the mature form is found after neurons have reached their destination. If the mature form is expressed early or repressed at later stages, then the neurons migrate abnormally. These data from cortical and immortalized neurons suggest that the increase of miR-128-3p detected during the development of neurons cultured from the hippocampus display a similar role and that miR-128-3p is important in mature neurons.

5.8 Glutamate signaling relationship to miR-128-3p

The expression of glutamate receptor genes and miR-128-3p in the mature neurons provided a platform to examine glutamate signaling in relation to miR-128-3p induction or repression. It was surprising that the action potential bursting pathway did not lead to the induction of miR-128-3p in the neurons, since it was this genetic program that was detected in the CA1 neurons due to early RML scrapie prion infection at which time miR-128-3p levels were tripled. The lack of miR-128-3p induction through this pathway suggests that miR-128-3p increase during early infection is through a different mechanism. It likely is a more complicated event *in vivo* that cannot be accounted for solely by this signaling but could be in concert with other pathways becoming activated during response to prion infection. It could also be a miR decay effect as mentioned for the CA1.

However, prolonged activation of synaptic NMDARs did result in trend towards a decrease of miR-128-3p, suggesting its involvement in some fashion. This could be due to decreased transcription of the *ARPP21* or *R3HDM1* genes on which miR-128-3p is encoded, or a feedback mechanism which turns off miR-128-3p during chronic Ca^{2+} influx. It is possible that chronic activation of signaling through this neuroprotective pathway is not ultimately sustainable and results in cell damage or death. If this is the case, it could partially explain the switch between neuroprotection being on and then off seen in the progression to symptomatic stages of RML scrapie prion infection in the *CA1*.

Further supporting evidence for this comes from the reduction of miR-128-3p detected during excitotoxic glutamate signaling. The excitotoxic reduction of miR-128-3p could be explained due to gene transcription shut off during cell death. This reduction was abolished by blocking the NMDARs, indicating a relationship specifically with this glutamate receptor. Further experimentation during earlier stages of excitotoxic glutamate signaling could ascertain miR-128-3p involvement.

Although the toxic levels of glutamate led to decreased miR-128-3p, which is against the working hypothesis that miR-128-3p targets these receptor subunits during disease, the induction of miR-128-3p seen at early stages of clinical disease is not accounted for by these experiments. That miR-128-3p was reduced during excitotoxicity, which can be a feature of late stages of neurodegeneration, demonstrates a partial explanation of late stages of disease. Modeling of glutamate receptor signaling and perhaps other stress related pathways that are induced at early disease in the *CA1* may provide clarity with regards to the reason for miR-128-3p induction during early disease.

The NMDAR subunit genes were similarly reduced when miR-128-3p was, both in the action potential bursting experiment as well as the excitotoxic signaling. The levels by

which these genes decreased were quite different in the two experiments. For action potential bursting, the levels decreased by 1.6-2.2fold whereas in the excitotoxic signaling they were decreased by more than 5fold. This could be due to a strong response to high levels of glutamate versus a slow activation of receptors due to synaptic NMDAR signaling. Perhaps the action potential bursting was leading to a minimal, progressive toxicity due to Ca^{2+} influx whereas the excitotoxic signaling was an intense early burst. It may well be that in prion disease progression, the switch from neuroprotective to neurotoxicity is a slow response due to multiple factors including increased cellular stress due to the replication of PrP^{Sc} in addition to the effects of prolonged neuroprotective mechanisms that cannot be sustained.

Glutamate can indeed activate many different receptors including the mGluR5, and other metabotropic and ionotropic receptors that are present in hippocampal neurons. When NMDARs only were activated in cultured rat hippocampal neurons, miR-128-3p was not detected through microarray analysis (van Spronsen et al. 2013). However, their culture contained many more astrocytes and glial cells at the stages of neuronal growth tested compare to the mouse hippocampal neurons in this thesis. Although the authors isolated NMDARs, it is possible that endogenous glutamate has different effects on miR-128-3p in concert with other effectors. Another caveat to this study is that microarray analysis is not as sensitive as PCR in detecting miRs (Mestdagh et al. 2014), therefore it is possible that miR-128-3p was simply not detected through their methodology. Signaling experiments may highlight these differences, and in addition elucidate processes in cultured rat versus mouse hippocampal neurons. An important aspect to consider in the glutamate/miR-128-3p relationship is whether miR mature levels are affected or whether transcription has changed. The detection of primary miR transcripts can help resolve this question. The

technologies to quantify changes between mature and primary transcripts of miRs were lacking but are becoming more readily available. Determining changes in miR-128-3p transcriptional versus recycling/degradation events will help reveal the nature of the relationship between it and glutamate signaling.

It has been demonstrated that β oligomers cause the release of glutamate into the extracellular space in cultured hippocampal neurons (Brito-Moreira et al. 2011). This could be a mechanism affecting glutamate receptor signaling in Alzheimer's disease, particularly as miR-128-3p is increased in the hippocampus of afflicted patients (Lukiw 2007). It would be interesting to determine whether glutamate release from neurons is affected by miR-128-3p, giving it another layer of regulation in glutamate signaling. A mixed culture setting where astrocytes help alleviate glutamate spillover may also help resolve this question.

The main findings from the relationship between glutamate signaling and miR-128-3p are summarized in Figure 56, miR-128-3p is reduced during prolonged activation of synaptic NMDARs as well as excitotoxic chronic glutamate receptor activation, presumably through extrasynaptic activation. In the excitotoxic conditions, the NMDAR inhibitors MK-801 or PPDA prevent NMDAR Ca^{2+} influx, and return the levels of miR-128-3p to baseline.

5.9 Increased levels and knockdown of miR-128-3p in primary hippocampal neurons

Raising the levels of miR-128-3p in primary hippocampal neurons resulted in decreased *GRM5* and *GRIN2D* mRNA, suggesting that the miR did target and likely degrade rather than simply repress the translation of these two transcripts. For the other transcripts such as *GRIN2B* that were not changed, it is possible that targeting is still

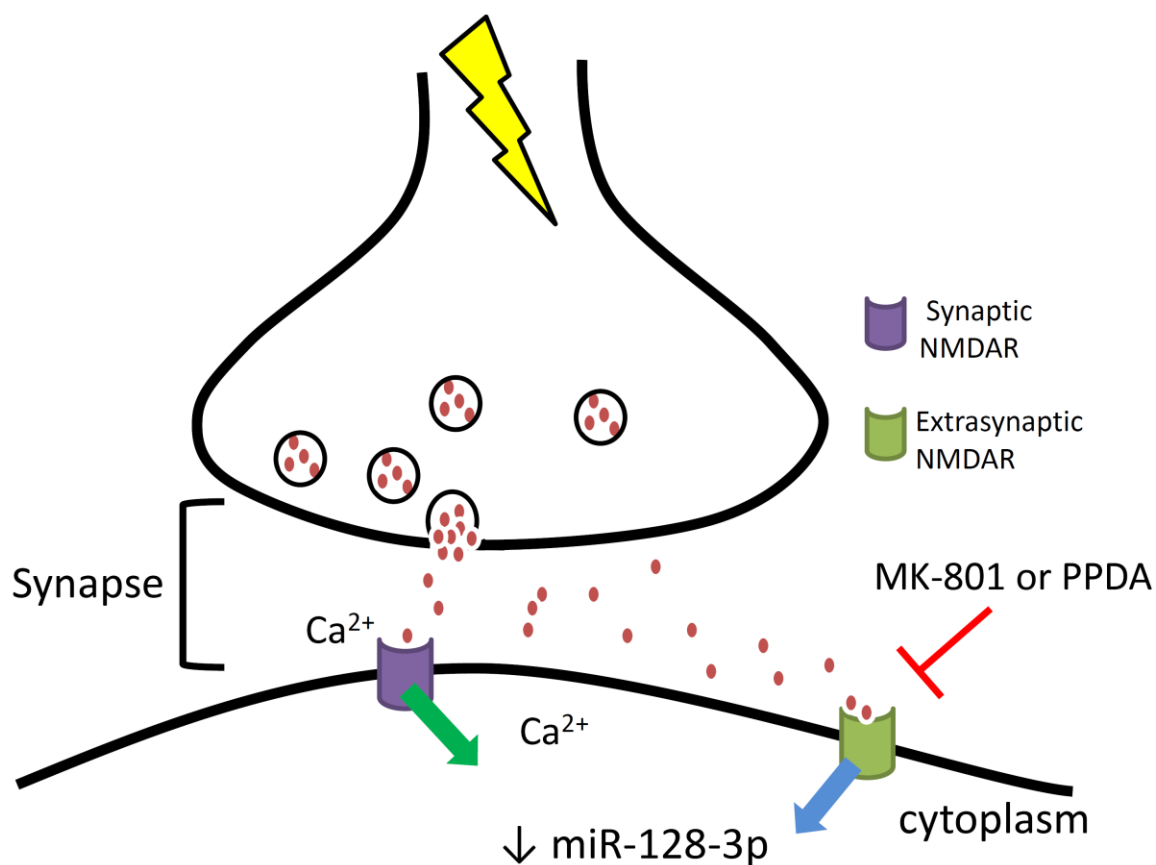


Figure 56. The relationship between miR-128-3p and glutamate/NMDAR signaling as discovered through the experimentation performed in cultured hippocampal neurons. Both chronic synaptic and extrasynaptic activation of NMDARs led to a downregulation of mature miR-128-3p levels. However, when NMDARs are blocked, by either MK-801 or PPDA, the downregulation of miR-128-3p by excitotoxic glutamate returns miR-128-3p levels to baseline.

occurring but that the transcript is sequestered rather than degraded. This would account for the same 'levels' being detected for these transcripts as control. Another method such as Ago2 pulldown of transcripts is required to determine if they were actively targeted and/or repressed by the RISC complex. These findings do suggest that miR-128-3p is strongly binding to and regulating *GRM5* and *GRIN2D* in cultured hippocampal neurons.

This is interesting in that compared to forebrain *CAMK2 α* neurons, the regulation of *GRM5* may be of higher functional significance in the hippocampus versus forebrain, as the *GRM5* mRNA was not detected in the Ago2 pulldown of forebrain neurons. In the primary hippocampal neuron miR-128-3p knockdown experiments, despite the high level of miR-128-3p knockdown achieved, no changes were apparent in any of the NMDAR genes including *GRIN2D*. However, in a miR-128-3p knockdown study in mice only 15% of gene targets were affected (Malmevik et al. 2015), perhaps indicating that changes in levels due to knockdown are not readily discernible. The combination of knocking down miR-128-3p alongside the activation of a pathway may lead to identification of affected targets that are impaired during knockdown. In addition, more time could have been required to detect changes in mRNA transcripts in the knockdown experiment. Perhaps the copy numbers of these genes remained stable leading to no net increase in transcripts due to miR-128-3p being blocked from functioning. Other potential explanations are that transcriptional events could have been affected by the introduction of the anti-miR, or that another miR could have taken up the miR-128-3p's role in regulating these transcripts, resulting in no changes in mRNA levels. This is possible as *GRIN2B* has at least 3 miRs outside of miR-128-3p that target it for repression, less is known about *GRM5* and *GRIN2D*.

Perhaps the other methods used to knockdown miRs may provide a better strategy than using anti-miRs. These strategies would include the miR sponges or TuDs, which bind multiple miRs at a time and render them inert. However, the level of knockdown that was achieved through anti-miRs were quite high and it could be that knockdown is not sufficient to see changes at the mRNA level, especially in mature post-mitotic neurons.

5.10 Protein targets of miR-128-3p

Previous studies that increased miR to examine protein changes have demonstrated small changes in protein abundances in immortalized cell lines such as HeLa using SILAC based mass spectrometry (Baek et al. 2008, Selbach et al. 2008). In SILAC, heavy isotopes are in the media surrounding cells and these isotopes are incorporated into proteins as they are translated (Ong et al. 2002). This allows for the detection of newly synthesized proteins after experimental miR manipulation. This was done to detect miR-128-3p protein targets in a cancerous glial cell line (Yang et al. 2015) but not yet for neurons. However, the SILAC method does not allow for quantification for more than 3 samples, which becomes difficult when examining multiple treatments.

In the TMT labelled mass spectrometry experiments used herein, the mass spectrometer was successful in obtaining proteome information for the primary hippocampal neurons. The detection and analysis of 4,000 proteins in the sample were wide ranging in molecular function and protein class. Within these, pathways of relevance to neurodegenerative disease were detected including Alzheimer's and Huntington's diseases, suggesting these neurons were a good model to examine functional changes for

these diseases. The glutamate receptor pathways including both metabotropic and ionotropic were identified in the neurons as well.

Published findings suggest that protein regulation by a miR is more likely to be detected by mass spectrometry analysis if there is a miR binding site located in the gene's 3' UTR (Baek et al. 2008). Therefore, as *GRM5*, *GRIN2B*, and *GRIN2D* 3' UTRs were all validated to contain miR-128-3p binding sites, it was surprising that changes were not detected in their protein counterparts by the differential mass spectrometry experiment. Therefore, in these experiments, I was unable to assess the functional regulatory capacity of miR-128-3p on the glutamate receptor subunits at a protein level. For NMDAR2D, the reason was due to lack of detection in any of the samples put forth, therefore it was not possible to know if it was under regulation through this experiment and other means are required to test quantitative effects on this NMDAR if they exist. Another method such as coimmunoprecipitation or isolation of membrane proteins may be required to concentrate the NMDAR2D protein from the hippocampal neurons as it was not detected in the whole cell protein lysates.

For the NMDAR2B and mGluR5 proteins, a number of reasons could explain why changes were not apparent. It could simply be that miR-128-3p does not result in functional changes to these proteins. Or that the timepoint of the experiment, which was 24 hours after miR-128-3p was increased was not sufficient to detect quantitative changes to these particular proteins. In this regard, it is possible that the protein degradation and recycling rates prevented a noticeable change in these two proteins. Protein turnover rates are particularly slow in mature neurons compared to younger neurons, for example GluR1 has a half-life of 12 hours in 4 DIV spinal neurons compared to 31 hours in 11 DIV (reviewed in (Alvarez-Castelao, Schuman 2015)). In addition, novel protein synthesis requires at least

72 hours as demonstrated by the lentiviral transduction of cultured neurons to express genetically engineered GFP. As miR targets the mRNA and may repress protein synthesis, more time may be required experimentally in order to see a quantitative change in the proteins present in the system. There is some evidence indicating that the protein half-life for the NMDAR2B subunit *in vitro* in dendrites is 1.8 days, which would not be sufficient in the timeframe I sampled for the proteins already in the cells to be degraded in order to detect quantitative changes (reviewed in (Hanus, Schuman 2013)). Alternative timeframes would need to be examined, perhaps for the NMDAR2B, examining protein at least 4 days post-transfection may yield changes to protein levels with the assumption that the pre-miR remains active for that long. For the mGluR5 protein, the timeframe would need to be experimentally determined to find an optimal timepoint to sample.

Furthermore, the dynamics of receptor recycling for these two proteins is not well known. If the receptor is sequestered and tagged for degradation then it may still be present in the cell and not quantified as 'lower' than the control set. The functionality of the receptor may be something that could be regulated by miR-128-3p rather than its quantity. The use of mass spectrometry was an attempt to identify global changes, but it needs further refinement in terms of experimental conditions for mGluR5 and the NMDARs. Indeed, further testing of the protein through a more sensitive detection system such as Western blot could potentially identify protein changes. In addition, the examination of receptor functionality by electrophysiology could demonstrate fine tuning effects that that miRs are known for. Since miR-128-3p knockdown leads to increased excitability of cortical neurons, examining these effects in hippocampal neurons with increased or decreased miR-128-3p levels would give some insight into this aspect in hippocampal neurons. Further

work is thus required to determine functional effects, if they exist, of miR-128-3p in hippocampal neurons.

In the proteome dataset, there were a few very small changes in proteins that passed the significance testing threshold. This is not surprising as other studies have found very few proteins to be changed when they introduced the foreign brain miR-124 into immortalized HeLas (Baek et al. 2008). In that case, a dilution effect on target changes was seen as the immortalized cells were actively dividing leaving only half of the cells with the transfected miR intact when protein content was sampled. Although a typical threshold is 2fold change or more, the biological relevance of even a 10% change in protein could be considered important, particularly in highly specialized neuronal cells. As mature hippocampal neurons display very slow protein turnover rates (Alvarez-Castelao, Schuman 2015), a small change could have a large impact on cellular functionality. Of the 3 proteins that were decreased, SLIT3, KCC2A, and SF3A3, due to experimentally increasing miR-128-3p in the cultured hippocampal neurons, none were predicted by TargetScan.

The SLIT3 protein was present in one of the synaptic protein fractions from adult forebrain, suggesting it could be regulated locally by miR-128-3p. This protein could have been decreased due to an upstream protein or gene being affected by increased levels of miR-128-3p. The SLIT3 gene is known to be highly expressed in the hippocampus (Bak et al. 2008). Studies into SLIT3 function have demonstrated that it is involved in suppression of neurite outgrowth through the roundabout receptors (Lin, Isacson 2006) and that it has an additional role in axonal guidance (Kramer et al. 2001). Although SLIT3 gene deregulation was not seen in the CA1 during prion infection, the related SLIT2 was deregulated. These initial results suggest that miR-128-3p targeting of SLIT3 could potentially be promoting neuritogenesis in the cultured hippocampal neurons. These data

would fit in with another published target of miR-128-3p, Reelin, which is also known to suppress neuritogenesis (Evangelisti et al. 2009). Perhaps the targeting of these two neurite suppressing genes is a pathway by which miR-128-3p promotes neurite outgrowth. The axonal guidance pathway which included SLIT3 was affected during sporadic early onset Alzheimer's disease as well during genetic Alzheimer's study by GWAS (Antonell et al. 2013). In another GWAS study, SNPs in SLIT3 led to a higher susceptibility for Parkinson's disease (reviewed in (Lin et al. 2009)). Experiments into the exposure of immortalized SH-SY5Y neurons to the toxic PrP^C 106-126 fragment resulted in a slight increase of SLIT3 mRNA (Martinez, Pascual 2007). In CNS disorders, changes in SLIT3 DNA are linked to depressive disorder (Glessner et al. 2010) and schizophrenia (Shi et al. 2004).

The protein KCC2A is encoded by the *CAMK2 α* gene, and is a member of the Calcium/calmodulin-dependent protein kinases, it is one of the proteins that has been identified as being locally synthesized at the synapse, specifically in dendrites (Alvarez-Castelao, Schuman 2015). This kinase interacts with NMDA receptors, specifically the NMDAR2B containing type (Robison et al. 2005). It is interesting that this protein was altered in the miR-128-3p increased neurons, especially as its downstream signaling pathway involves various glutamate receptors including mGluR5 and NMDAR2D (Figure 57). The loss of *CAMK2 α* neurons in the CA1 of the hippocampus has been noted in Alzheimer's disease brain (Wang et al. 2005). Studies into the synaptic compartments in the CA1 have demonstrated that *CAMK2 α* mRNA is localized there and that depletion of the mRNA leads to over 85% loss of its protein (Cajigas et al. 2012). The presence of SNPs in the *CAMK2 α* gene in humans leads to deficits in working memory in adolescents (Easton et al. 2013), and memory impairment occurs in neurodegenerative disease. The Creb1

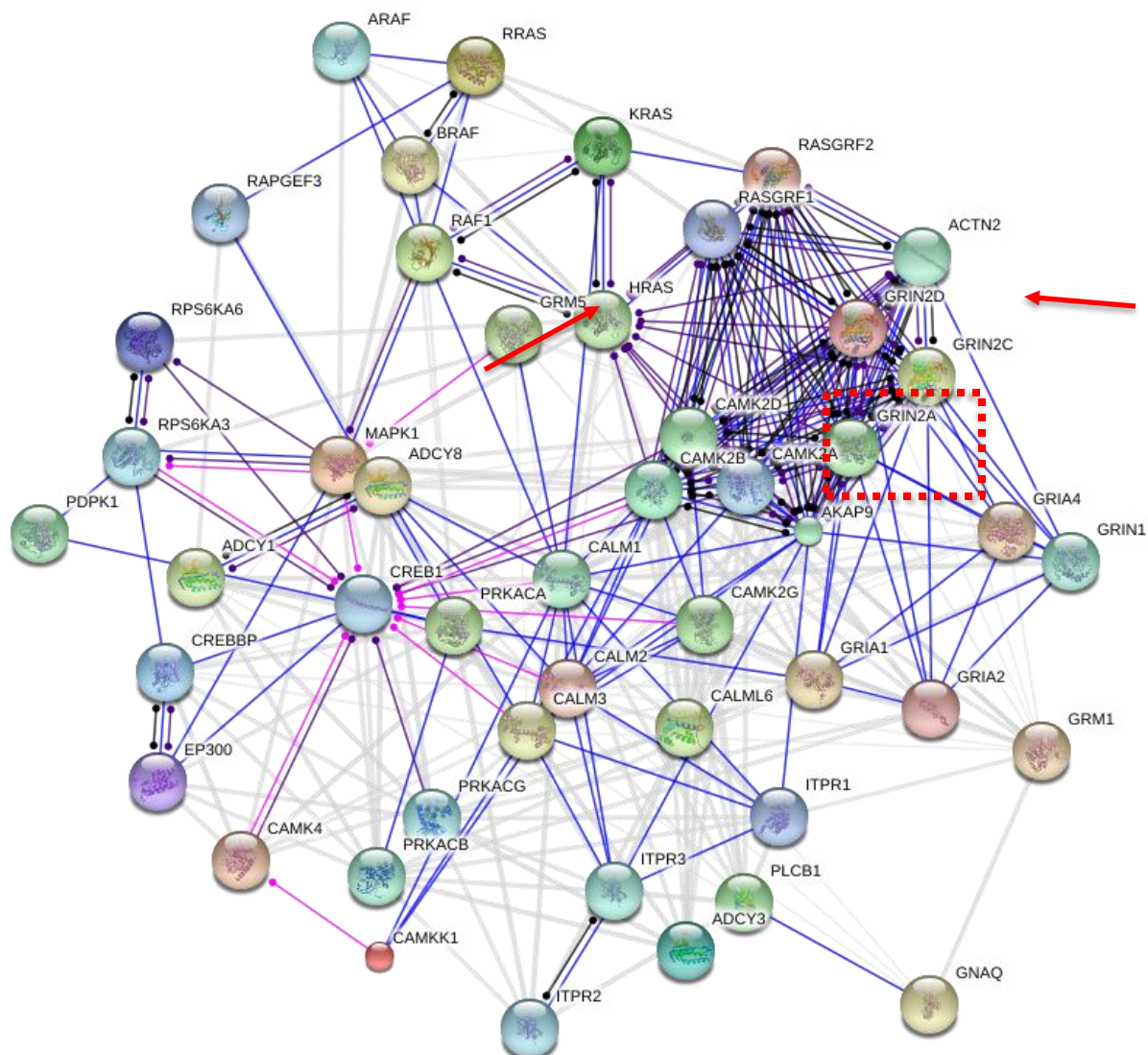


Figure 57. The string interaction network of post NMDAR activation events. Note that CAMK2 α (CAMK2A, red dashed box) is linked to GRM5 and NMDAR subunits (red arrows) alongside other glutamate subunits. Adapted from Pathcards (Belinky et al. 2015).

knockout mouse, of which $CAMK2\alpha$ also has interactions, results in a postnatal knockout phenotype that is reminiscent of Huntington's disease with a progressive loss of hippocampal neurons (Mantamadiotis et al. 2002).

The least information regarding brain related function is from the SF3A3 protein, although it demonstrates similar expression in neuronal cells as glial (Zhang, Barres 2013). It forms part of the trimeric SF3A spliceosome complex which is part of the mRNA splicing pathway. One of its functions is the correct splicing of the pre-mRNA for small nuclear ribonucleoprotein U2. Further experimentation is required to elucidate the potential contribution of miR-128-3p regulation of SF3A3.

6. Conclusions

- Analysis of miR-128-3p in the RML scrapie prion infected mouse model revealed it was increased at asymptomatic stages of disease
- miR-128-3p was reduced at the commencement of symptomatic disease and this reduction persisted at terminal disease
- At early disease miR-128-3p was increased in hippocampal synaptoneuroosomes, suggesting potential regulation of synaptic elements by miR-128-3p during neurodegenerative disease
- Although miR-128-3p was not, a number of other miRs were altered in abundance in synaptoneuroosomes derived from the forebrain at early and late stages of disease
- Synaptoneuroosomes from the hippocampus, a specialized structure that is affected during prion disease, contained the most changes in miR abundance while the forebrain demonstrated few changes at early, asymptomatic disease which increased by symptomatic, terminal stage
- miR changes in forebrain synaptoneuroosomes at terminal disease largely matched those previously found in whole brain homogenates at end stages of disease
- Exploration of miR-128-3p targets through computational biology revealed many predicted gene targets were CNS expressed with some previously identified as dysregulated during neurodegenerative disease
- 3 predicted glutamate receptor genes were validated as containing binding sites within their 3' UTR and included *GRIN2B*, *GRIN2D*, and *GRM5*

- Both *GRIN2D* and *GRM5* decreased in miR-128-3p gain of function studies in cultured hippocampal neurons, suggesting that these transcripts are targeted and likely degraded in hippocampal derived pyramidal neurons
- Evidence for the involvement of miR-128-3p in regulating glutamate signaling in hippocampal neurons was indicated by the reduction of miR-128-3p after prolonged action potential bursting or bath application of excitotoxic glutamate
- The proteome changes identified by miR-128-3p gain of function experiments in primary hippocampal neurons using mass spectrometry revealed no changes to mGluR5 or NMDAR2B, while NMDAR2D was not detected
- Three proteins were decreased albeit with very small changes, SLIT3, KCC2A, and SF3A3, whereas SLIT3 and KCC2A have been identified as important in neuronal function and KCC2A forms part of glutamate signaling pathways
- Further work is required to determine whether functional outcomes on NMDAR2B, NMDAR2D, and mGluR5 proteins are a feature of miR-128-3p regulation

7. Future Directions

There are a number of limitations in this study that could be addressed by future experimentation. For the work on the *CA1*, it would be ideal to tease apart the involvement of primary versus mature miR transcripts. The miR assay employed with TaqMan probes can include both primary and mature miR-128-3p sequences, but a Northern Blot could help to elucidate the two based on size. In addition, newer RT-qPCR assays can detect primary transcripts from total RNA and these could be employed to at least determine some of the contribution of the primary transcripts. Another issue would be to improve *CA1* sampling of miR-128-3p from individual animals to ascribe statistical significance to the effects seen. It would be interesting to characterize miR-128-3p in the different hippocampal layers including the *CA2*, *CA3*, and dentate gyrus, however these areas are not as homogeneous as the *CA1* therefore could be more heterogeneous than the *CA1*.

The modeling of miR-128-3p in other neurodegenerative diseases particularly in Alzheimer's disease in neuronal *CA1* cell bodies of rodent models could be useful in determining if it has the same features as RML scrapie prion infection. The involvement of a neuronal population could be performed for Huntington's animal models as they mimic human disease fairly well, however in that case perhaps neurons in the striatum could be isolated as hippocampal involvement is not typically indicated.

The prediction analysis and validation of targets by Luciferase reporter assay provided strong evidence that miR-128-3p has binding capability within *GRIN2B*, *GRIN2D*, and *GRM5* 3' UTRs. Although it would be difficult and costly to undertake, to truly validate the specific binding sites site-directed mutation in the seed sequence binding sites on the 3' UTR would be necessary to demonstrate which sites are important. For

GRM5 this was previously demonstrated by another group, leaving *GRIN2B* and *GRIN2D*. The main difficulty in performing this site directed study is that there are so many binding sites in both of these 3' UTRs, with 8 sites in human multiplied by 6 seed sequence nucleotides, resulting in 48 individual plasmid constructs for one gene. If the goal is to characterize the 3' UTR this would be a necessity but may not be needed to identify therapeutic qualities for miR-128-3p.

In the synaptoneurosome studies, future experiments to determine the statistical significance of the miR-128-3p increase seen in the hippocampus from the RML scrapie infected mice would be ideal by increasing sample size. Although there are other methods that maximize the amount of synaptoneurosome that can be obtained from the hippocampus, they are not as pure as subjecting them to the Ficoll gradient, which is where the pooling of tissues becomes necessary. Since this is the first study to directly examine the miR complement during neurodegenerative disease, it would be interesting to apply these same methods to other models of neurodegenerative disease such as Alzheimer's or Huntington's. In addition, though the data may limit therapeutic intervention for early stages of disease, the synaptic miR levels could be determined from brain samples from Alzheimer's patients brain banks to further understanding of synaptic miR alterations during disease. This is especially possible as synaptoneurosome were previously obtained from frozen Alzheimer's post-mortem brain tissues to describe mRNA and protein changes.

Since miR-128-3p demonstrated the targeting of multiple glutamate receptor subunits in hippocampal neurons but only at the mRNA level, the assessment of this effect in terms of protein function would be relevant to elucidate, especially at the synapse. Indeed, its differential modulation in forebrain versus hippocampal synapses during kainic

acid challenge in rodents indicates that it has different roles in different regional synapses. The increased excitability of cortical neurons during knockdown of miR-128-3p needs to be determined in hippocampal neurons. These functional changes could be determined by measuring electrophysiological changes in glutamate receptor response when challenged with glutamate or NMDA in hippocampal neurons that have miR-128-3p knocked down either experimentally or cultured from knockout mice.

The studies of primary hippocampal culture were largely based on gene expression as examined through PCR of total RNA and measuring the increase in the genetic component suggests that these are likely being translated into protein but it is indirect evidence. Determining the protein levels of mGluR5 and the NMDARs through Western blot or ELISA would give further insight into their properties during the maturation of hippocampal neurons. The functional component could be examined through activating the neuroprotective or excitotoxic glutamate pathways and examining protein for changes. On top of examining the levels of the mGluR5 and NMDAR proteins, the proteins and phosphorylation of proteins from the glutamate signaling pathway could help to elucidate the activation intracellular signaling pathways.

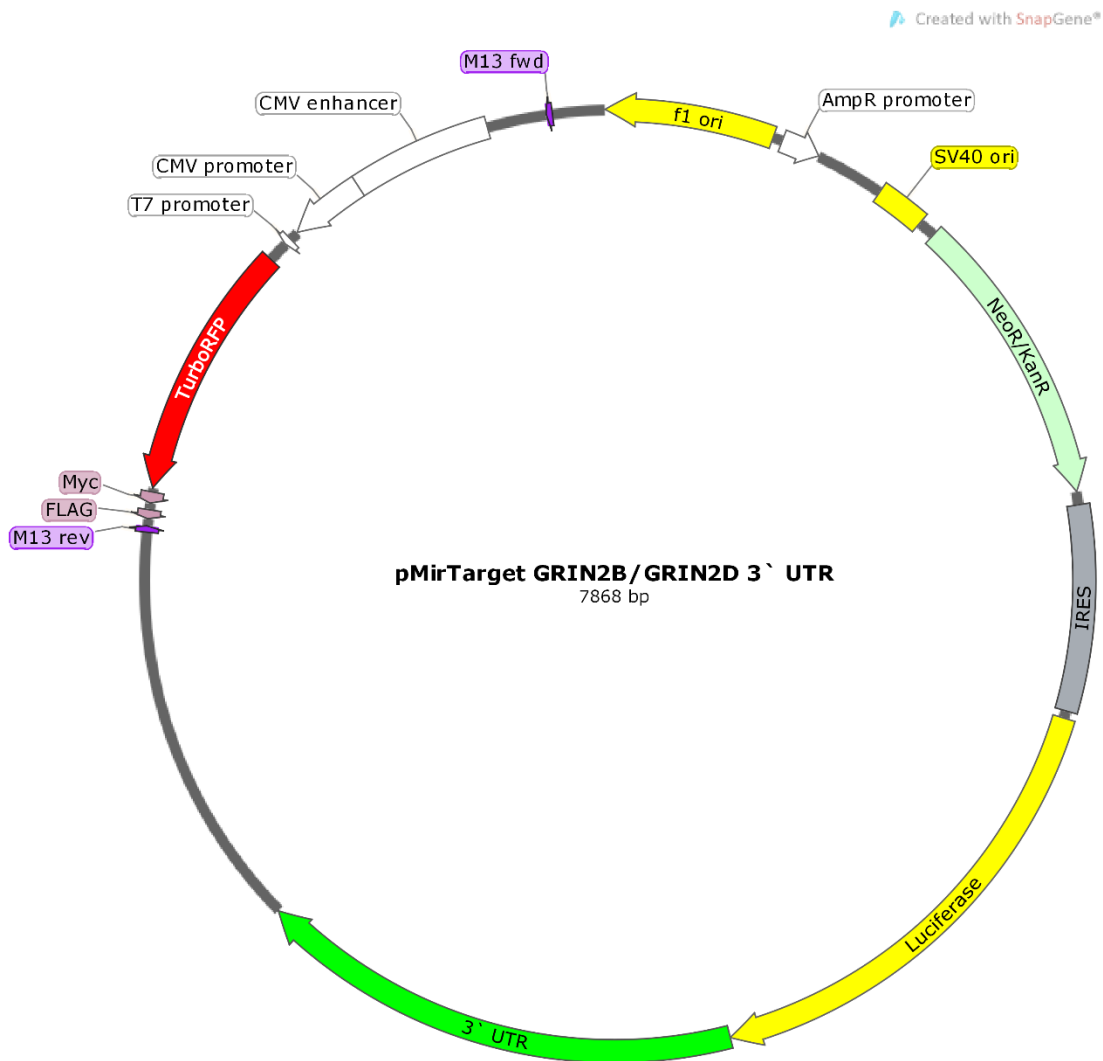
An area that needs exploration is the structural properties of neurons during miR-128-3p gain of function and loss of function in hippocampal neurons. Since miR-128-3p has been identified in neuritogenesis and migration of cortical neurons, these properties need to be described in relation to neurons from the hippocampus. In addition, the use of pre-miRs or anti-miRs with fluorescent tags or alternatively lentiviral or adeno-associated viral vectors that express GFP miR-128-3p could be used to determine these properties using Sholl analysis of dendrite arborisation, measuring the axon, or spine analysis.

The gain of function protein studies were limited in that the timeframe selected was likely not ideal for the protein half-lives and receptor recycling rates for NMDAR or mGluR5. Future experiments which allow more time for the proteins to be processed and/or degraded are needed, especially for detection by mass spectrometry. A better timeframe would likely be at least 4 days after introducing the pre-miR. However, the activity of pre-miRs for a lengthier time period need to be evaluated. Another system such as plasmid expression could also be employed to constitutively express the miR-128-3p with genetic engineering to ensure the antisense strand is degraded.

The end goal of examining miR-128-3p in neurodegenerative disease is to determine if it could serve as a therapeutic target during disease. Since it is upregulated in early disease here in the RML scrapie prion model and then reduced at later stages, and is associated with mature neurons, it could serve as such a target. However, further details surrounding its role at the synaptic structure need elucidation in order to assess this potential. Its modulation whether increasing it at later stages of disease or knocking it down at early stages of disease needs further work in order to delineate the possibility of synapse function rescue. There are currently a number of miRs in clinical trials for other diseases indicating a future endeavour for neurodegenerative disease particularly as other therapies for prion or Alzheimer's disease have failed. In addition, the use of lentiviral mediated gene therapeutics is currently in clinical trial for Parkinson's disease indicating the possibility of using these vectors for the delivery of miRs. Indeed, these vectors have been used to successfully deliver miRs in animal models (reviewed in (Boese et al. 2013)).

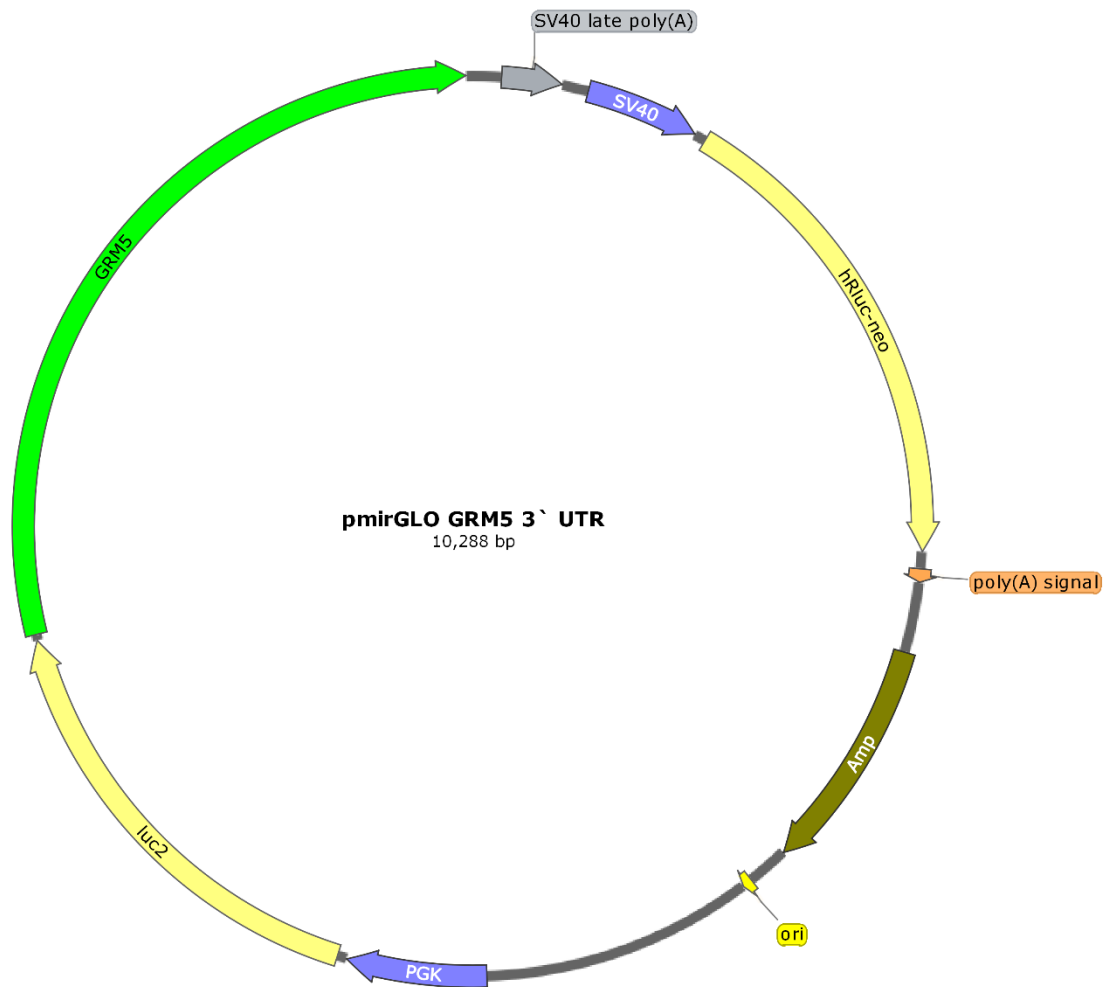
8. Appendices

Appendix 1. pMirTarget plasmid map. Luciferase gene in front of the 3' UTR (Green) of *GRIN2B* or *GRIN2D* under the IRES promoter while the normalizing RFP is under the CMV promoter (Origene). Drawn using SnapGene software (from GSL Biotech; available at snapgene.com).



Appendix 2. pmirGLO plasmid map. The firefly luciferase (*luc2*) gene followed by the human GRM5 3' UTR both under the PGK promoter while the normalizing gene of *Renilla* luciferase (*Rluc-neo*) is under the SV40 promoter. Plasmid map produced using SnapGene software (from GSL Biotech; available at snapgene.com).

Created with SnapGene®



Appendix 3. Copyright permissions

Copyright permission ■ Inbox x



Amrit Boese [REDACTED]

to anna.majer ▾

Dear Dr. Majer,

I am writing to you to ask for your permission to include figures from your Doctoral thesis entitled "Temporal Dereglulation of Genes and MicroRNAs in Ne

I will cite your publication appropriately and would appreciate the use of your figures, thank you for your consideration,

Amrit Boese



Anna Majer

to me ▾

Dear Amrit,

You have my permission to include information from my publication in your Doctoral thesis.

All the best,

Anna



Title: MicroRNA abundance is altered in synaptoneuroosomes during prion disease

Author: Amrit S. Boese, Reuben Saba, Kristyn Campbell, Anna Majer, Sarah Medina, Lynn Burton, Timothy F. Booth, Patrick Chong, Garrett Westmacott, Sucharita M. Dutta, Julian A. Saba, Stephanie A. Booth

Publication: Molecular and Cellular Neuroscience

Publisher: Elsevier

Date: March 2016

Crown copyright © 2015 Published by Elsevier Inc.

LOGIN

If you're a copyright.com user, you can login to RightsLink using your copyright.com credentials. Already a RightsLink user or want to [learn more?](#)

Creative Commons Attribution-NonCommercial-No Derivatives License (CC BY NC ND)

This article is published under the terms of the [Creative Commons Attribution-NonCommercial-No Derivatives License \(CC BY NC ND\)](#).

For non-commercial purposes you may copy and distribute the article, use portions or extracts from the article in other works, and text or data mine the article, provided you do not alter or modify the article without permission from Elsevier. You may also create adaptations of the article for your own personal use only, but not distribute these to others. You must give appropriate credit to the original work, together with a link to the formal publication through the relevant DOI, and a link to the Creative Commons user license above. If changes are permitted, you must indicate if any changes are made but not in any way that suggests the licensor endorses you or your use of the work.

Permission is not required for this non-commercial use. For commercial use please continue to request permission via Rightslink.

BACK

CLOSE WINDOW



Creative Commons Legal Code

Attribution 4.0 International

Official translations of this license are available [in other languages](#).



Creative Commons Corporation (“Creative Commons”) is not a law firm and does not provide legal services or legal advice. Distribution of Creative Commons public licenses does not create a lawyer-client or other relationship. Creative Commons makes its licenses and related information available on an “as-is” basis. Creative Commons gives no warranties regarding its licenses, any material licensed under their terms and conditions, or any related information. Creative Commons disclaims all liability for damages resulting from their use to the fullest extent possible.

Using Creative Commons Public Licenses

Creative Commons public licenses provide a standard set of terms and conditions that creators and other rights holders may use to share original works of authorship and other material subject to copyright and certain other rights specified in the public license below. The following considerations are for informational purposes only, are not exhaustive, and do not form part of our licenses.

Considerations for licensors: *Our public licenses are intended for use by those authorized to give the public permission to use material in ways otherwise restricted by copyright and certain other rights. Our licenses are irrevocable. Licensors should read and understand the terms and conditions of the license they choose before applying it. Licensors should also secure all rights necessary before applying our licenses so that the public can reuse the material as expected. Licensors should clearly mark any material not subject to the license. This includes other CC-licensed material, or material used under an exception or limitation to copyright. [More considerations for licensors.](#)*

Considerations for the public: *By using one of our public licenses, a licensor grants the public permission to use the licensed material under specified terms and conditions. If the licensor's permission is not necessary for any reason—for example, because of any applicable exception or limitation to copyright—then that use is not regulated by the license. Our licenses grant only permissions under copyright and certain other rights that a licensor has authority to grant. Use of the licensed material may still be restricted for other reasons, including because others have copyright or other rights in the material. A licensor may make special requests, such as asking that all changes be marked or described. Although not required by our licenses, you are encouraged to respect those requests where reasonable. [More considerations for the public.](#)*

Creative Commons Attribution 4.0 International Public License

By exercising the Licensed Rights (defined below), You accept and agree to be bound by the terms and conditions of this Creative Commons Attribution 4.0 International Public License (“Public License”). To the extent this Public License may be interpreted as a contract, You are granted the Licensed Rights in consideration of Your acceptance of these terms and conditions, and the Licensor grants You such rights in consideration of benefits the Licensor receives from making the Licensed Material available under these terms and conditions.

Section 1 – Definitions.

- a. **Adapted Material** means material subject to Copyright and Similar Rights that is derived from or based upon the Licensed Material and in which the Licensed Material is translated, altered, arranged, transformed, or otherwise modified in a manner requiring permission under the Copyright and Similar Rights held by the Licensor. For purposes of this Public License, where the Licensed Material is a musical work, performance, or sound recording, Adapted Material is always produced where the Licensed Material is synched in timed relation with a moving image.
- b. **Adapter's License** means the license You apply to Your Copyright and Similar Rights in Your contributions to Adapted Material in accordance with the terms and conditions of this Public License.
- c. **Copyright and Similar Rights** means copyright and/or similar rights closely related to copyright including, without limitation, performance, broadcast, sound recording, and Sui Generis Database Rights, without regard to how the rights are labeled or categorized. For purposes of this Public License, the rights specified in Section [2\(b\)\(1\)-\(2\)](#) are not Copyright and Similar Rights.
- d. **Effective Technological Measures** means those measures that, in the absence of proper authority, may not be circumvented under laws fulfilling obligations under Article 11 of the WIPO Copyright Treaty adopted on December 20, 1996, and/or similar international agreements.
- e. **Exceptions and Limitations** means fair use, fair dealing, and/or any other exception or limitation to Copyright and Similar Rights that applies to Your use of the Licensed Material.
- f. **Licensed Material** means the artistic or literary work, database, or other material to which the Licensor applied this Public License.
- g. **Licensed Rights** means the rights granted to You subject to the terms and conditions of this Public License, which are limited to all Copyright and Similar Rights that apply to Your use of the Licensed Material and that the Licensor has authority to license.
- h. **Licensor** means the individual(s) or entity(ies) granting rights under this Public License.
- i. **Share** means to provide material to the public by any means or process that requires permission under the Licensed Rights, such as reproduction, public display, public performance, distribution, dissemination, communication, or importation, and to make material available to the public including in ways that members of the public may access the material from a place and at a time individually chosen by them.
- j. **Sui Generis Database Rights** means rights other than copyright resulting from Directive 96/9/EC of the European Parliament and of the Council of 11 March 1996 on the legal protection of databases, as amended and/or succeeded, as well as other essentially equivalent rights anywhere in the world.
- k. **You** means the individual or entity exercising the Licensed Rights under this Public License. **Your** has a corresponding meaning.

Section 2 – Scope.

a. License grant.

1. Subject to the terms and conditions of this Public License, the Licensor hereby grants You a worldwide, royalty-free, non-sublicensable, non-exclusive, irrevocable license to exercise the Licensed Rights in the Licensed Material to:
 - A. reproduce and Share the Licensed Material, in whole or in part; and
 - B. produce, reproduce, and Share Adapted Material.
2. **Exceptions and Limitations.** For the avoidance of doubt, where Exceptions and Limitations apply to Your use, this Public License does not apply, and You do not need to comply with its terms and conditions.
3. **Term.** The term of this Public License is specified in Section [6\(a\)](#).
4. **Media and formats; technical modifications allowed.** The Licensor authorizes You to exercise the Licensed Rights in all media and formats whether now known or hereafter created, and to make technical modifications necessary to do so. The Licensor waives and/or agrees not to assert any right or authority to forbid You from making technical modifications necessary to exercise the Licensed Rights, including technical modifications necessary to circumvent Effective Technological Measures. For purposes of this Public License, simply making modifications authorized by this Section [2\(a\)\(4\)](#) never produces Adapted Material.
5. **Downstream recipients.**
 - A. **Offer from the Licensor – Licensed Material.** Every recipient of the Licensed Material automatically receives an offer from the Licensor to exercise the Licensed Rights under the terms and conditions of this Public License.
 - B. **No downstream restrictions.** You may not offer or impose any additional or different terms or conditions on, or apply any Effective Technological Measures to, the Licensed Material if doing so restricts exercise of the Licensed Rights by any recipient of the Licensed Material.

6. **No endorsement.** Nothing in this Public License constitutes or may be construed as permission to assert or imply that You are, or that Your use of the Licensed Material is, connected with, or sponsored, endorsed, or granted official status by, the Licensor or others designated to receive attribution as provided in Section [3\(a\)\(1\)\(A\)\(i\)](#).

b. Other rights.

1. Moral rights, such as the right of integrity, are not licensed under this Public License, nor are publicity, privacy, and/or other similar personality rights; however, to the extent possible, the Licensor waives and/or agrees not to assert any such rights held by the Licensor to the limited extent necessary to allow You to exercise the Licensed Rights, but not otherwise.
2. Patent and trademark rights are not licensed under this Public License.
3. To the extent possible, the Licensor waives any right to collect royalties from You for the exercise of the Licensed Rights, whether directly or through a collecting society under any voluntary or waivable statutory or compulsory licensing scheme. In all other cases the Licensor expressly reserves any right to collect such royalties.

Section 3 – License Conditions.

Your exercise of the Licensed Rights is expressly made subject to the following conditions.

a. Attribution.

1. If You Share the Licensed Material (including in modified form), You must:
 - A. retain the following if it is supplied by the Licensor with the Licensed Material:
 - i. identification of the creator(s) of the Licensed Material and any others designated to receive attribution, in any reasonable manner requested by the Licensor (including by pseudonym if designated);
 - ii. a copyright notice;
 - iii. a notice that refers to this Public License;
 - iv. a notice that refers to the disclaimer of warranties;
 - v. a URI or hyperlink to the Licensed Material to the extent reasonably practicable;
 - B. indicate if You modified the Licensed Material and retain an indication of any previous modifications; and
 - C. indicate the Licensed Material is licensed under this Public License, and include the text of, or the URI or hyperlink to, this Public License.
2. You may satisfy the conditions in Section [3\(a\)\(1\)](#) in any reasonable manner based on the medium, means, and context in which You Share the Licensed Material. For example, it may be reasonable to satisfy the conditions by providing a URI or hyperlink to a resource that includes the required information.
3. If requested by the Licensor, You must remove any of the information required by Section [3\(a\)\(1\)\(A\)](#) to the extent reasonably practicable.
4. If You Share Adapted Material You produce, the Adapter's License You apply must not prevent recipients of the Adapted Material from complying with this Public License.

Section 4 – Sui Generis Database Rights.

Where the Licensed Rights include Sui Generis Database Rights that apply to Your use of the Licensed Material:

- a. for the avoidance of doubt, Section [2\(a\)\(1\)](#) grants You the right to extract, reuse, reproduce, and Share all or a substantial portion of the contents of the database;
- b. if You include all or a substantial portion of the database contents in a database in which You have Sui Generis Database Rights, then the database in which You have Sui Generis Database Rights (but not its individual contents) is Adapted Material; and
- c. You must comply with the conditions in Section [3\(a\)](#) if You Share all or a substantial portion of the contents of the database.

For the avoidance of doubt, this Section [4](#) supplements and does not replace Your obligations under this Public License where the Licensed Rights include other Copyright and Similar Rights.

Section 5 – Disclaimer of Warranties and Limitation of Liability.

- a. Unless otherwise separately undertaken by the Licensor, to the extent possible, the Licensor offers the Licensed Material as-is and as-available, and makes no representations or warranties of any kind concerning the Licensed Material, whether express, implied, statutory, or other. This includes, without limitation, warranties of title, merchantability, fitness for a particular purpose, non-infringement, absence of latent or other defects, accuracy, or the presence or absence of errors, whether or not known or discoverable. Where disclaimers of warranties are not allowed in full or in part, this disclaimer may not apply to You.
- b. To the extent possible, in no event will the Licensor be liable to You on any legal theory (including, without limitation, negligence) or otherwise for any direct, special, indirect, incidental, consequential, punitive, exemplary, or other losses, costs, expenses, or damages arising out of this Public License or use of the Licensed Material, even if the Licensor has been advised of the possibility of such losses, costs, expenses, or damages. Where a limitation of liability is not allowed in full or in part, this limitation may not apply to You.
- c. The disclaimer of warranties and limitation of liability provided above shall be interpreted in a manner that, to the extent possible, most closely approximates an absolute disclaimer and waiver of all liability.

Section 6 – Term and Termination.

- a. This Public License applies for the term of the Copyright and Similar Rights licensed here. However, if You fail to comply with this Public License, then Your rights under this Public License terminate automatically.
- b. Where Your right to use the Licensed Material has terminated under Section [6\(a\)](#), it reinstates:
 - 1. automatically as of the date the violation is cured, provided it is cured within 30 days of Your discovery of the violation; or
 - 2. upon express reinstatement by the Licensor.
 For the avoidance of doubt, this Section [6\(b\)](#) does not affect any right the Licensor may have to seek remedies for Your violations of this Public License.
- c. For the avoidance of doubt, the Licensor may also offer the Licensed Material under separate terms or conditions or stop distributing the Licensed Material at any time; however, doing so will not terminate this Public License.
- d. Sections [1](#), [5](#), [6](#), [7](#), and [8](#) survive termination of this Public License.

Section 7 – Other Terms and Conditions.

- a. The Licensor shall not be bound by any additional or different terms or conditions communicated by You unless expressly agreed.
- b. Any arrangements, understandings, or agreements regarding the Licensed Material not stated herein are separate from and independent of the terms and conditions of this Public License.

Section 8 – Interpretation.

- a. For the avoidance of doubt, this Public License does not, and shall not be interpreted to, reduce, limit, restrict, or impose conditions on any use of the Licensed Material that could lawfully be made without permission under this Public License.
- b. To the extent possible, if any provision of this Public License is deemed unenforceable, it shall be automatically reformed to the minimum extent necessary to make it enforceable. If the provision cannot be reformed, it shall be severed from this Public License without affecting the enforceability of the remaining terms and conditions.
- c. No term or condition of this Public License will be waived and no failure to comply consented to unless expressly agreed to by the Licensor.
- d. Nothing in this Public License constitutes or may be interpreted as a limitation upon, or waiver of, any privileges and immunities that apply to the Licensor or You, including from the legal processes of any jurisdiction or authority.

Creative Commons is not a party to its public licenses. Notwithstanding, Creative Commons may elect to apply one of its public licenses to material it publishes and in those instances will be considered the "Licensor." The text of the Creative Commons public licenses is dedicated to the public domain under the [CC0 Public Domain Dedication](#). Except for the limited purpose of indicating that material is shared

4/20/2017

Creative Commons — Attribution 4.0 International — CC BY 4.0

under a Creative Commons public license or as otherwise permitted by the Creative Commons policies published at creativecommons.org/policies. Creative Commons does not authorize the use of the trademark “Creative Commons” or any other trademark or logo of Creative Commons without its prior written consent including, without limitation, in connection with any unauthorized modifications to any of its public licenses or any other arrangements, understandings, or agreements concerning use of licensed material. For the avoidance of doubt, this paragraph does not form part of the public licenses.

Creative Commons may be contacted at creativecommons.org.

Additional languages available: [Bahasa Indonesia](#), [Deutsch](#), [hrvatski](#), [Nederlands](#), [norsk](#), [polski](#), [suomeksi](#), [svenska](#), [te reo Māori](#), [українська](#), [العربية](#), [日本語](#). Please read the [FAQ](#) for more information about official translations.

9. References

- Adlakha, Y.K. & Saini, N. 2014, "Brain microRNAs and insights into biological functions and therapeutic potential of brain enriched miRNA-128", *Molecular cancer*, vol. 13, pp. 33-4598-13-33.
- Agarwal, V., Bell, G.W., Nam, J.W. & Bartel, D.P. 2015, "Predicting effective microRNA target sites in mammalian mRNAs", *eLife*, vol. 4, pp. 10.7554/eLife.05005.
- Ahn, I. & Son, H.S. 2007, "Comparative bioinformatics analysis of prion proteins isolated from reptile, rodent, ruminant, and human species", *Experimental & molecular medicine*, vol. 39, no. 6, pp. 769-777.
- Alexandrov, P.N., Dua, P., Hill, J.M., Bhattacharjee, S., Zhao, Y. & Lukiw, W.J. 2012, "microRNA (miRNA) speciation in Alzheimer's disease (AD) cerebrospinal fluid (CSF) and extracellular fluid (ECF)", *International journal of biochemistry and molecular biology*, vol. 3, no. 4, pp. 365-373.
- Alsharafi, W.A., Xiao, B. & Li, J. 2016, "MicroRNA-139-5p negatively regulates NR2A-containing NMDA receptor in the rat pilocarpine model and patients with temporal lobe epilepsy", *Epilepsia*, vol. 57, no. 11, pp. 1931-1940.
- Altschul, S.F., Gish, W., Miller, W., Myers, E.W. & Lipman, D.J. 1990, "Basic local alignment search tool", *Journal of Molecular Biology*, vol. 215, no. 3, pp. 403-410.
- Alvarez-Castelao, B. & Schuman, E.M. 2015, "The Regulation of Synaptic Protein Turnover", *The Journal of biological chemistry*, vol. 290, no. 48, pp. 28623-28630.
- Alzheimer's Association 2016, "2016 Alzheimer's disease facts and figures", *Alzheimer's & dementia : the journal of the Alzheimer's Association*, vol. 12, no. 4, pp. 459-509.
- Amadoro, G., Ciotti, M.T., Costanzi, M., Cestari, V., Calissano, P. & Canu, N. 2006, "NMDA receptor mediates tau-induced neurotoxicity by calpain and ERK/MAPK activation", *Proceedings of the National Academy of Sciences of the United States of America*, vol. 103, no. 8, pp. 2892-2897.
- Antonell, A., Llado, A., Altirriba, J., Botta-Orfila, T., Balasa, M., Fernandez, M., Ferrer, I., Sanchez-Valle, R. & Molinuevo, J.L. 2013, "A preliminary study of the whole-genome expression profile of sporadic and monogenic early-onset Alzheimer's disease", *Neurobiology of aging*, vol. 34, no. 7, pp. 1772-1778.
- Araujo, M.A., Marques, T.E., Octacilio-Silva, S., Arroxelas-Silva, C.L., Pereira, M.G., Peixoto-Santos, J.E., Kandratavicius, L., Leite, J.P., Garcia-Cairasco, N., Castro, O.W., Duzzioni, M., Passos, G.A., Paco-Larson, M.L. & Goes Gitai, D.L. 2016, "Identification of microRNAs with Dysregulated Expression in Status Epilepticus Induced Epileptogenesis", *PloS one*, vol. 11, no. 10, pp. e0163855.

- Arias, C., Arrieta, I. & Tapia, R. 1995, "beta-Amyloid peptide fragment 25-35 potentiates the calcium-dependent release of excitatory amino acids from depolarized hippocampal slices", *Journal of neuroscience research*, vol. 41, no. 4, pp. 561-566.
- Arjona, F.J., de Baaij, J.H., Schlingmann, K.P., Lameris, A.L., van Wijk, E., Flik, G., Regele, S., Korenke, G.C., Neophytou, B., Rust, S., Reintjes, N., Konrad, M., Bindels, R.J. & Hoenderop, J.G. 2014, "CNNM2 mutations cause impaired brain development and seizures in patients with hypomagnesemia", *PLoS genetics*, vol. 10, no. 4, pp. e1004267.
- Asante, E.A., Smidak, M., Grimshaw, A., Houghton, R., Tomlinson, A., Jeelani, A., Jakubcova, T., Hamdan, S., Richard-Londt, A., Linehan, J.M., Brandner, S., Alpers, M., Whitfield, J., Mead, S., Wadsworth, J.D. & Collinge, J. 2015, "A naturally occurring variant of the human prion protein completely prevents prion disease", *Nature*, vol. 522, no. 7557, pp. 478-481.
- Ashraf, S.I., McLoon, A.L., Sclarsic, S.M. & Kunes, S. 2006, "Synaptic protein synthesis associated with memory is regulated by the RISC pathway in *Drosophila*", *Cell*, vol. 124, no. 1, pp. 191-205.
- Baek, D., Villen, J., Shin, C., Camargo, F.D., Gygi, S.P. & Bartel, D.P. 2008, "The impact of microRNAs on protein output", *Nature*, vol. 455, no. 7209, pp. 64-71.
- Baig, S.S., Strong, M. & Quarrell, O.W. 2016, "The global prevalence of Huntington's disease: a systematic review and discussion", *Neurodegenerative disease management*, vol. 6, no. 4, pp. 331-343.
- Bak, M., Silahatoglu, A., Moller, M., Christensen, M., Rath, M.F., Skryabin, B., Tommerup, N. & Kauppinen, S. 2008, "MicroRNA expression in the adult mouse central nervous system", *RNA (New York, N.Y.)*, vol. 14, no. 3, pp. 432-444.
- Baker, H.F., Ridley, R.M., Duchen, L.W., Crow, T.J. & Bruton, C.J. 1994, "Induction of beta (A4)-amyloid in primates by injection of Alzheimer's disease brain homogenate. Comparison with transmission of spongiform encephalopathy", *Molecular neurobiology*, vol. 8, no. 1, pp. 25-39.
- Baron, A., Montagne, A., Casse, F., Launay, S., Maubert, E., Ali, C. & Vivien, D. 2010, "NR2D-containing NMDA receptors mediate tissue plasminogen activator-promoted neuronal excitotoxicity", *Cell death and differentiation*, vol. 17, no. 5, pp. 860-871.
- Barry, A.E., Klyubin, I., Mc Donald, J.M., Mably, A.J., Farrell, M.A., Scott, M., Walsh, D.M. & Rowan, M.J. 2011, "Alzheimer's disease brain-derived amyloid-beta-mediated inhibition of LTP in vivo is prevented by immunotargeting cellular prion protein", *The Journal of neuroscience : the official journal of the Society for Neuroscience*, vol. 31, no. 20, pp. 7259-7263.
- Bartel, D.P. 2009, "MicroRNAs: target recognition and regulatory functions", *Cell*, vol. 136, no. 2, pp. 215-233.
- Basler, K., Oesch, B., Scott, M., Westaway, D., Walchli, M., Groth, D.F., McKinley, M.P., Prusiner, S.B. & Weissmann, C. 1986, "scrapie and cellular PrP isoforms are encoded by the same chromosomal gene", *Cell*, vol. 46, no. 3, pp. 417-428.

- Basu, U., Lozynska, O., Moorwood, C., Patel, G., Wilton, S.D. & Khurana, T.S. 2011, "Translational regulation of utrophin by miRNAs", *PLoS one*, vol. 6, no. 12, pp. e29376.
- Belinky, F., Nativ, N., Stelzer, G., Zimmerman, S., Iny Stein, T., Safran, M. & Lancet, D. 2015, "PathCards: multi-source consolidation of human biological pathways", *Database : the journal of biological databases and curation*, vol. 2015, pp. 10.1093/database/bav006. Print 2015.
- Bell, J.E. & Ironside, J.W. 1993, "Neuropathology of spongiform encephalopathies in humans", *British medical bulletin*, vol. 49, no. 4, pp. 738-777.
- Benestad, S.L., Mitchell, G., Simmons, M., Ytrehus, B. & Vikoren, T. 2016, "First case of chronic wasting disease in Europe in a Norwegian free-ranging reindeer", *Veterinary research*, vol. 47, no. 1, pp. 88-016-0375-4.
- Beraldo, F.H., Arantes, C.P., Santos, T.G., Machado, C.F., Roffe, M., Hajj, G.N., Lee, K.S., Magalhaes, A.C., Caetano, F.A., Mancini, G.L., Lopes, M.H., Americo, T.A., Magdesian, M.H., Ferguson, S.S., Linden, R., Prado, M.A. & Martins, V.R. 2011, "Metabotropic glutamate receptors transduce signals for neurite outgrowth after binding of the prion protein to laminin gamma1 chain", *FASEB journal : official publication of the Federation of American Societies for Experimental Biology*, vol. 25, no. 1, pp. 265-279.
- Beraldo, F.H., Ostapchenko, V.G., Caetano, F.A., Guimaraes, A.L., Ferretti, G.D., Daude, N., Bertram, L., Nogueira, K.O., Silva, J.L., Westaway, D., Cashman, N.R., Martins, V.R., Prado, V.F. & Prado, M.A. 2016, "Regulation of Amyloid beta oligomer binding to neurons and neurotoxicity by the complex prion protein/mGluR5", *The Journal of biological chemistry*, .
- Bett, C., Joshi-Barr, S., Lucero, M., Trejo, M., Liberski, P., Kelly, J.W., Masliah, E. & Sigurdson, C.J. 2012, "Biochemical properties of highly neuroinvasive prion strains", *PLoS pathogens*, vol. 8, no. 2, pp. e1002522.
- Bicker, S., Lackinger, M., Weiss, K. & Schrott, G. 2014, "MicroRNA-132, -134, and -138: a microRNA troika rules in neuronal dendrites", *Cellular and molecular life sciences : CMLS*, vol. 71, no. 20, pp. 3987-4005.
- Boese, A.S., Majer, A., Saba, R. & Booth, S.A. 2013, "Small RNA drugs for prion disease: a new frontier", *Expert opinion on drug discovery*, vol. 8, no. 10, pp. 1265-1284.
- Boese, A.S., Saba, R., Campbell, K., Majer, A., Medina, S., Burton, L., Booth, T.F., Chong, P., Westmacott, G., Dutta, S.M., Saba, J.A. & Booth, S.A. 2015, "MicroRNA abundance is altered in synaptoneuroosomes during prion disease", *Molecular and cellular neurosciences*, vol. 71, pp. 13-24.
- Bone, I., Belton, L., Walker, A.S. & Darbyshire, J. 2008, "Intraventricular pentosan polysulphate in human prion diseases: an observational study in the UK", *European journal of neurology*, vol. 15, no. 5, pp. 458-464.
- Bot, A.M., Debski, K.J. & Lukasiuk, K. 2013, "Alterations in miRNA levels in the dentate gyrus in epileptic rats", *PLoS one*, vol. 8, no. 10, pp. e76051.

- Boutla, A., Delidakis, C. & Tabler, M. 2003, "Developmental defects by antisense-mediated inactivation of micro-RNAs 2 and 13 in *Drosophila* and the identification of putative target genes", *Nucleic acids research*, vol. 31, no. 17, pp. 4973-4980.
- Bremer, J., Baumann, F., Tiberi, C., Wessig, C., Fischer, H., Schwarz, P., Steele, A.D., Toyka, K.V., Nave, K.A., Weis, J. & Aguzzi, A. 2010, "Axonal prion protein is required for peripheral myelin maintenance", *Nature neuroscience*, vol. 13, no. 3, pp. 310-318.
- Brewer, G.J., Torricelli, J.R., Evege, E.K. & Price, P.J. 1993, "Optimized survival of hippocampal neurons in B27-supplemented Neurobasal, a new serum-free medium combination", *Journal of neuroscience research*, vol. 35, no. 5, pp. 567-576.
- Brito-Moreira, J., Paula-Lima, A.C., Bomfim, T.R., Oliveira, F.B., Sepulveda, F.J., De Mello, F.G., Aguayo, L.G., Panizzutti, R. & Ferreira, S.T. 2011, "Abeta oligomers induce glutamate release from hippocampal neurons", *Current Alzheimer research*, vol. 8, no. 5, pp. 552-562.
- Brown, D.R., Qin, K., Herms, J.W., Madlung, A., Manson, J., Strome, R., Fraser, P.E., Kruck, T., von Bohlen, A., Schulz-Schaeffer, W., Giese, A., Westaway, D. & Kretzschmar, H. 1997, "The cellular prion protein binds copper in vivo", *Nature*, vol. 390, no. 6661, pp. 684-687.
- Bruce, M.E., McConnell, I., Fraser, H. & Dickinson, A.G. 1991, "The disease characteristics of different strains of scrapie in Sinc congenic mouse lines: implications for the nature of the agent and host control of pathogenesis", *The Journal of general virology*, vol. 72 (Pt 3), no. Pt 3, pp. 595-603.
- Bruno, I.G., Karam, R., Huang, L., Bhardwaj, A., Lou, C.H., Shum, E.Y., Song, H.W., Corbett, M.A., Gifford, W.D., Gecz, J., Pfaff, S.L. & Wilkinson, M.F. 2011, "Identification of a microRNA that activates gene expression by repressing nonsense-mediated RNA decay", *Molecular cell*, vol. 42, no. 4, pp. 500-510.
- Bueler, H., Aguzzi, A., Sailer, A., Greiner, R.A., Autenried, P., Aguet, M. & Weissmann, C. 1993, "Mice devoid of PrP are resistant to scrapie", *Cell*, vol. 73, no. 7, pp. 1339-1347.
- Butovsky, O., Jedrychowski, M.P., Moore, C.S., Cialic, R., Lanser, A.J., Gabriely, G., Koeglsperger, T., Dake, B., Wu, P.M., Doykan, C.E., Fanek, Z., Liu, L., Chen, Z., Rothstein, J.D., Ransohoff, R.M., Gygi, S.P., Antel, J.P. & Weiner, H.L. 2014, "Identification of a unique TGF-beta-dependent molecular and functional signature in microglia", *Nature neuroscience*, vol. 17, no. 1, pp. 131-143.
- Cajigas, I.J., Tushev, G., Will, T.J., tom Dieck, S., Fuerst, N. & Schuman, E.M. 2012, "The local transcriptome in the synaptic neuropil revealed by deep sequencing and high-resolution imaging", *Neuron*, vol. 74, no. 3, pp. 453-466.
- Capellari, S., Strammiello, R., Saverioni, D., Kretzschmar, H. & Parchi, P. 2011, "Genetic Creutzfeldt-Jakob disease and fatal familial insomnia: insights into phenotypic variability and disease pathogenesis", *Acta Neuropathologica*, vol. 121, no. 1, pp. 21-37.

- Carleton, A., Tremblay, P., Vincent, J.D. & Lledo, P.M. 2001, "Dose-dependent, prion protein (PrP)-mediated facilitation of excitatory synaptic transmission in the mouse hippocampus", *Pflugers Archiv : European journal of physiology*, vol. 442, no. 2, pp. 223-229.
- Carroll, J.A., Striebel, J.F., Rangel, A., Woods, T., Phillips, K., Peterson, K.E., Race, B. & Chesebro, B. 2016, "Prion Strain Differences in Accumulation of PrP^{Sc} on Neurons and Glia Are Associated with Similar Expression Profiles of Neuroinflammatory Genes: Comparison of Three Prion Strains", *PLoS pathogens*, vol. 12, no. 4, pp. e1005551.
- Castellani, R.J., Siedlak, S.L., Perry, G. & Smith, M.A. 2000, "Sequestration of iron by Lewy bodies in Parkinson's disease", *Acta Neuropathologica*, vol. 100, no. 2, pp. 111-114.
- Catania, M.V., Landwehrmeyer, G.B., Testa, C.M., Standaert, D.G., Penney, J.B., Jr & Young, A.B. 1994, "Metabotropic glutamate receptors are differentially regulated during development", *Neuroscience*, vol. 61, no. 3, pp. 481-495.
- Caughey, B.W., Dong, A., Bhat, K.S., Ernst, D., Hayes, S.F. & Caughey, W.S. 1991, "Secondary structure analysis of the scrapie-associated protein PrP 27-30 in water by infrared spectroscopy", *Biochemistry*, vol. 30, no. 31, pp. 7672-7680.
- Chandler, R.L. 1961, "Encephalopathy in mice produced by inoculation with scrapie brain material", *Lancet (London, England)*, vol. 1, no. 7191, pp. 1378-1379.
- Chaudhuri, A.D., Yelamanchili, S.V., Marcondes, M.C. & Fox, H.S. 2013, "Up-regulation of microRNA-142 in simian immunodeficiency virus encephalitis leads to repression of sirtuin1", *FASEB journal : official publication of the Federation of American Societies for Experimental Biology*, vol. 27, no. 9, pp. 3720-3729.
- Chen, J., Li, W., Li, Y., He, S., Li, L., Liang, L., Song, Y., Qin, D. & Zheng, H. 2016a, "MicroRNA-128-3p impaired water maze learning by suppressing Doublecortin expression in both wild type and Abeta-42 infused mice", *Neuroscience letters*, vol. 626, pp. 79-85.
- Chen, J., Li, W., Li, Y., He, S., Li, L., Liang, L., Song, Y., Qin, D. & Zheng, H. 2016b, "MicroRNA-128-3p impaired water maze learning by suppressing Doublecortin expression in both wild type and Abeta-42 infused mice", *Neuroscience letters*, vol. 626, pp. 79-85.
- Chen, S., Mange, A., Dong, L., Lehmann, S. & Schachner, M. 2003, "Prion protein as trans-interacting partner for neurons is involved in neurite outgrowth and neuronal survival", *Molecular and cellular neurosciences*, vol. 22, no. 2, pp. 227-233.
- Chen, Y., Wang, S.X., Mu, R., Luo, X., Liu, Z.S., Liang, B., Zhuo, H.L., Hao, X.P., Wang, Q., Fang, D.F., Bai, Z.F., Wang, Q.Y., Wang, H.M., Jin, B.F., Gong, W.L., Zhou, T., Zhang, X.M., Xia, Q. & Li, T. 2014, "Dysregulation of the miR-324-5p-CUEDC2 axis leads to macrophage dysfunction and is associated with colon cancer", *Cell reports*, vol. 7, no. 6, pp. 1982-1993.

- Chen, Y.L. & Shen, C.K. 2013, "Modulation of mGluR-dependent MAP1B translation and AMPA receptor endocytosis by microRNA miR-146a-5p", *The Journal of neuroscience : the official journal of the Society for Neuroscience*, vol. 33, no. 21, pp. 9013-9020.
- Chi, S.W., Hannon, G.J. & Darnell, R.B. 2012, "An alternative mode of microRNA target recognition", *Nature structural & molecular biology*, vol. 19, no. 3, pp. 321-327.
- Ching, A.S. & Ahmad-Annur, A. 2015, "A Perspective on the Role of microRNA-128 Regulation in Mental and Behavioral Disorders", *Frontiers in cellular neuroscience*, vol. 9, pp. 465.
- Chiti, Z., Knutsen, O.M., Betmouni, S. & Greene, J.R. 2006, "An integrated, temporal study of the behavioural, electrophysiological and neuropathological consequences of murine prion disease", *Neurobiology of disease*, vol. 22, no. 2, pp. 363-373.
- Cingaram, P.K., Nyeste, A., Dondapati, D.T., Fodor, E. & Welker, E. 2015, "Prion Protein Does Not Confer Resistance to Hippocampus-Derived Zpl Cells against the Toxic Effects of Cu²⁺, Mn²⁺, Zn²⁺ and Co²⁺ Not Supporting a General Protective Role for PrP in Transition Metal Induced Toxicity", *PloS one*, vol. 10, no. 10, pp. e0139219.
- Colby, D.W. & Prusiner, S.B. 2011, "Prions", *Cold Spring Harbor perspectives in biology*, vol. 3, no. 1, pp. a006833.
- Cole, S. & Kimberlin, R.H. 1985, "Pathogenesis of mouse scrapie: dynamics of vacuolation in brain and spinal cord after intraperitoneal infection", *Neuropathology and applied neurobiology*, vol. 11, no. 3, pp. 213-227.
- Collinge, J., Gorham, M., Hudson, F., Kennedy, A., Keogh, G., Pal, S., Rossor, M., Rudge, P., Siddique, D., Spyer, M., Thomas, D., Walker, S., Webb, T., Wroe, S. & Darbyshire, J. 2009, "Safety and efficacy of quinacrine in human prion disease (PRION-1 study): a patient-preference trial", *The Lancet.Neurology*, vol. 8, no. 4, pp. 334-344.
- Collinge, J., Jaunmuktane, Z., Mead, S., Rudge, P. & Brandner, S. 2016, "Collinge et al. reply", *Nature*, vol. 535, no. 7611, pp. E2-3.
- Collinge, J., Palmer, M.S. & Dryden, A.J. 1991, "Genetic predisposition to iatrogenic Creutzfeldt-Jakob disease", *Lancet (London, England)*, vol. 337, no. 8755, pp. 1441-1442.
- Collinge, J., Whittington, M.A., Sidle, K.C., Smith, C.J., Palmer, M.S., Clarke, A.R. & Jefferys, J.G. 1994, "Prion protein is necessary for normal synaptic function", *Nature*, vol. 370, no. 6487, pp. 295-297.
- Cooper, A., Grigoryan, G., Guy-David, L., Tsoory, M.M., Chen, A. & Reuveny, E. 2012, "Trisomy of the G protein-coupled K⁺ channel gene, Kcnj6, affects reward mechanisms, cognitive functions, and synaptic plasticity in mice", *Proceedings of the National Academy of Sciences of the United States of America*, vol. 109, no. 7, pp. 2642-2647.
- Corbel, C., Hernandez, I., Wu, B. & Kosik, K.S. 2015, "Developmental attenuation of N-methyl-D-aspartate receptor subunit expression by microRNAs", *Neural development*, vol. 10, pp. 20-015-0047-5.

- Corti, V., Sanchez-Ruiz, Y., Piccoli, G., Bergamaschi, A., Cannistraci, C.V., Pattini, L., Cerutti, S., Bachi, A., Alessio, M. & Malgaroli, A. 2008, "Protein fingerprints of cultured CA3-CA1 hippocampal neurons: comparative analysis of the distribution of synaptosomal and cytosolic proteins", *BMC neuroscience*, vol. 9, pp. 36-2202-9-36.
- Costa, B.M., Feng, B., Tsintsadze, T.S., Morley, R.M., Irvine, M.W., Tsintsadze, V., Lozovaya, N.A., Jane, D.E. & Monaghan, D.T. 2009, "N-methyl-D-aspartate (NMDA) receptor NR2 subunit selectivity of a series of novel piperazine-2,3-dicarboxylate derivatives: preferential blockade of extrasynaptic NMDA receptors in the rat hippocampal CA3-CA1 synapse", *The Journal of pharmacology and experimental therapeutics*, vol. 331, no. 2, pp. 618-626.
- Cui, J.G., Li, Y.Y., Zhao, Y., Bhattacharjee, S. & Lukiw, W.J. 2010, "Differential regulation of interleukin-1 receptor-associated kinase-1 (IRAK-1) and IRAK-2 by microRNA-146a and NF-kappaB in stressed human astroglial cells and in Alzheimer disease", *The Journal of biological chemistry*, vol. 285, no. 50, pp. 38951-38960.
- Cui, L., Li, Y., Ma, G., Wang, Y., Cai, Y., Liu, S., Chen, Y., Li, J., Xie, Y., Liu, G., Zhao, B. & Li, K. 2014, "A functional polymorphism in the promoter region of microRNA-146a is associated with the risk of Alzheimer disease and the rate of cognitive decline in patients", *PloS one*, vol. 9, no. 2, pp. e89019.
- Cunningham, C., Deacon, R., Wells, H., Boche, D., Waters, S., Diniz, C.P., Scott, H., Rawlins, J.N. & Perry, V.H. 2003, "Synaptic changes characterize early behavioural signs in the ME7 model of murine prion disease", *The European journal of neuroscience*, vol. 17, no. 10, pp. 2147-2155.
- Cunningham, F., Amode, M.R., Barrell, D., Beal, K., Billis, K., Brent, S., Carvalho-Silva, D., Clapham, P., Coates, G., Fitzgerald, S., Gil, L., Giron, C.G., Gordon, L., Hourlier, T., Hunt, S.E., Janacek, S.H., Johnson, N., Juettemann, T., Kahari, A.K., Keenan, S., Martin, F.J., Maurel, T., McLaren, W., Murphy, D.N., Nag, R., Overduin, B., Parker, A., Patricio, M., Perry, E., Pignatelli, M., Riat, H.S., Sheppard, D., Taylor, K., Thormann, A., Vullo, A., Wilder, S.P., Zadissa, A., Aken, B.L., Birney, E., Harrow, J., Kinsella, R., Muffato, M., Ruffier, M., Searle, S.M., Spudich, G., Trevanion, S.J., Yates, A., Zerbino, D.R. & Flicek, P. 2015, "Ensembl 2015", *Nucleic acids research*, vol. 43, no. Database issue, pp. D662-9.
- Dalby, B., Cates, S., Harris, A., Ohki, E.C., Tilkins, M.L., Price, P.J. & Ciccarone, V.C. 2004, "Advanced transfection with Lipofectamine 2000 reagent: primary neurons, siRNA, and high-throughput applications", *Methods (San Diego, Calif.)*, vol. 33, no. 2, pp. 95-103.
- Dayon, L., Hainard, A., Licker, V., Turck, N., Kuhn, K., Hochstrasser, D.F., Burkhard, P.R. & Sanchez, J.C. 2008, "Relative quantification of proteins in human cerebrospinal fluids by MS/MS using 6-plex isobaric tags", *Analytical Chemistry*, vol. 80, no. 8, pp. 2921-2931.
- De Simone, A., Kitchen, C., Kwan, A.H., Sunde, M., Dobson, C.M. & Frenkel, D. 2012, "Intrinsic disorder modulates protein self-assembly and aggregation", *Proceedings of*

- the National Academy of Sciences of the United States of America*, vol. 109, no. 18, pp. 6951-6956.
- Deriziotis, P. & Tabrizi, S.J. 2008, "Prions and the proteasome", *Biochimica et biophysica acta*, vol. 1782, no. 12, pp. 713-722.
- Devanathan, V., Jakovcevski, I., Santuccione, A., Li, S., Lee, H.J., Peles, E., Leshchyn'ska, I., Sytnyk, V. & Schachner, M. 2010, "Cellular form of prion protein inhibits Reelin-mediated shedding of Caspr from the neuronal cell surface to potentiate Caspr-mediated inhibition of neurite outgrowth", *The Journal of neuroscience : the official journal of the Society for Neuroscience*, vol. 30, no. 27, pp. 9292-9305.
- Doi-Yi, R., Kitamoto, T. & Tateishi, J. 1991, "Immunoreactivity of cerebral amyloidosis is enhanced by protein denaturation treatments", *Acta Neuropathologica*, vol. 82, no. 4, pp. 260-265.
- Dong, J., Atwood, C.S., Anderson, V.E., Siedlak, S.L., Smith, M.A., Perry, G. & Carey, P.R. 2003, "Metal binding and oxidation of amyloid-beta within isolated senile plaque cores: Raman microscopic evidence", *Biochemistry*, vol. 42, no. 10, pp. 2768-2773.
- Duan, Q., Mao, X., Xiao, Y., Liu, Z., Wang, Y., Zhou, H., Zhou, Z., Cai, J., Xia, K., Zhu, Q., Qi, J., Huang, H., Plutzky, J. & Yang, T. 2016, "Super enhancers at the miR-146a and miR-155 genes contribute to self-regulation of inflammation", *Biochimica et biophysica acta*, vol. 1859, no. 4, pp. 564-571.
- Duursma, A.M., Kedde, M., Schrier, M., le Sage, C. & Agami, R. 2008, "miR-148 targets human DNMT3b protein coding region", *RNA (New York, N.Y.)*, vol. 14, no. 5, pp. 872-877.
- Easton, A.C., Lourdasamy, A., Loth, E., Toro, R., Giese, K.P., Kornhuber, J., de Quervain, D.J., Papassotiropoulos, A., Fernandes, C., Muller, C.P. & Schumann, G. 2013, "CAMK2A polymorphisms predict working memory performance in humans", *Molecular psychiatry*, vol. 18, no. 8, pp. 850-852.
- Ebert, M.S., Neilson, J.R. & Sharp, P.A. 2007, "MicroRNA sponges: competitive inhibitors of small RNAs in mammalian cells", *Nature methods*, vol. 4, no. 9, pp. 721-726.
- Eisele, Y.S., Bolmont, T., Heikenwalder, M., Langer, F., Jacobson, L.H., Yan, Z.X., Roth, K., Aguzzi, A., Staufenbiel, M., Walker, L.C. & Jucker, M. 2009, "Induction of cerebral beta-amyloidosis: intracerebral versus systemic Abeta inoculation", *Proceedings of the National Academy of Sciences of the United States of America*, vol. 106, no. 31, pp. 12926-12931.
- Elder, G.A., Gama Sosa, M.A. & De Gasperi, R. 2010, "Transgenic mouse models of Alzheimer's disease", *The Mount Sinai journal of medicine, New York*, vol. 77, no. 1, pp. 69-81.
- Enright, A.J., John, B., Gaul, U., Tuschl, T., Sander, C. & Marks, D.S. 2003, "MicroRNA targets in Drosophila", *Genome biology*, vol. 5, no. 1, pp. R1.
- Esposito, Z., Belli, L., Toniolo, S., Sancesario, G., Bianconi, C. & Martorana, A. 2013, "Amyloid beta, glutamate, excitotoxicity in Alzheimer's disease: are we on the right track?", *CNS neuroscience & therapeutics*, vol. 19, no. 8, pp. 549-555.

- Evangelisti, C., Florian, M.C., Massimi, I., Dominici, C., Giannini, G., Galardi, S., Bue, M.C., Massalini, S., McDowell, H.P., Messi, E., Gulino, A., Farace, M.G. & Ciafre, S.A. 2009, "MiR-128 up-regulation inhibits Reelin and DCX expression and reduces neuroblastoma cell motility and invasiveness", *FASEB journal : official publication of the Federation of American Societies for Experimental Biology*, vol. 23, no. 12, pp. 4276-4287.
- Fang, Z. & Rajewsky, N. 2011, "The impact of miRNA target sites in coding sequences and in 3'UTRs", *PloS one*, vol. 6, no. 3, pp. e18067.
- Feeney, C., Scott, G.P., Cole, J.H., Sastre, M., Goldstone, A.P. & Leech, R. 2016, "Seeds of neuroendocrine doubt", *Nature*, vol. 535, no. 7611, pp. E1-2.
- Feng, B., Tse, H.W., Skifter, D.A., Morley, R., Jane, D.E. & Monaghan, D.T. 2004, "Structure-activity analysis of a novel NR2C/NR2D-preferring NMDA receptor antagonist: 1-(phenanthrene-2-carbonyl) piperazine-2,3-dicarboxylic acid", *British journal of pharmacology*, vol. 141, no. 3, pp. 508-516.
- Franzoni, E., Booker, S.A., Parthasarathy, S., Rehfeld, F., Grosser, S., Srivatsa, S., Fuchs, H.R., Tarabykin, V., Vida, I. & Wulczyn, F.G. 2015, "miR-128 regulates neuronal migration, outgrowth and intrinsic excitability via the intellectual disability gene Phf6", *eLife*, vol. 4, pp. 10.7554/eLife.04263.
- Freeman, O.J. & Mallucci, G.R. 2016, "The UPR and synaptic dysfunction in neurodegeneration", *Brain research*, .
- Fujita, K., Harada, M., Sasaki, M., Yuasa, T., Sakai, K., Hamaguchi, T., Sanjo, N., Shiga, Y., Satoh, K., Atarashi, R., Shirabe, S., Nagata, K., Maeda, T., Murayama, S., Izumi, Y., Kaji, R., Yamada, M. & Mizusawa, H. 2012, "Multicentre multiobserver study of diffusion-weighted and fluid-attenuated inversion recovery MRI for the diagnosis of sporadic Creutzfeldt-Jakob disease: a reliability and agreement study", *BMJ open*, vol. 2, no. 1, pp. e000649-2011-000649. Print 2012.
- Gadotti, V.M., Bonfield, S.P. & Zamponi, G.W. 2012, "Depressive-like behaviour of mice lacking cellular prion protein", *Behavioural brain research*, vol. 227, no. 2, pp. 319-323.
- Gadotti, V.M. & Zamponi, G.W. 2011, "Cellular prion protein protects from inflammatory and neuropathic pain", *Molecular pain*, vol. 7, pp. 59-8069-7-59.
- Gandhi, R., Healy, B., Gholipour, T., Egorova, S., Musallam, A., Hussain, M.S., Nejad, P., Patel, B., Hei, H., Khoury, S., Quintana, F., Kivisakk, P., Chitnis, T. & Weiner, H.L. 2013, "Circulating microRNAs as biomarkers for disease staging in multiple sclerosis", *Annals of Neurology*, vol. 73, no. 6, pp. 729-740.
- Gao, C., Wei, J., Zhang, B.Y., Shi, Q., Chen, C., Wang, J., Shi, Q. & Dong, X.P. 2016, "MiRNA expression profiles in the brains of mice infected with scrapie agents 139A, ME7 and S15", *Emerging microbes & infections*, vol. 5, no. 11, pp. e115.
- Gao, Y., Su, J., Guo, W., Polich, E.D., Magyar, D.P., Xing, Y., Li, H., Smrt, R.D., Chang, Q. & Zhao, X. 2015, "Inhibition of miR-15a Promotes BDNF Expression and Rescues

- Dendritic Maturation Deficits in MeCP2-Deficient Neurons", *Stem cells (Dayton, Ohio)*, vol. 33, no. 5, pp. 1618-1629.
- Garza-Manero, S., Pichardo-Casas, I., Arias, C., Vaca, L. & Zepeda, A. 2014, "Selective distribution and dynamic modulation of miRNAs in the synapse and its possible role in Alzheimer's Disease", *Brain research*, vol. 1584, pp. 80-93.
- Gasperini, L., Meneghetti, E., Pastore, B., Benetti, F. & Legname, G. 2015, "Prion protein and copper cooperatively protect neurons by modulating NMDA receptor through S-nitrosylation", *Antioxidants & redox signaling*, vol. 22, no. 9, pp. 772-784.
- Geng, D., Kang, L., Su, Y., Jia, J., Ma, J., Li, S., Du, J. & Cui, H. 2013, "Protective effects of EphB2 on Abeta1-42 oligomer-induced neurotoxicity and synaptic NMDA receptor signaling in hippocampal neurons", *Neurochemistry international*, vol. 63, no. 4, pp. 283-290.
- Geschwind, M.D., Kuo, A.L., Wong, K.S., Haman, A., Devereux, G., Raudabaugh, B.J., Johnson, D.Y., Torres-Chae, C.C., Finley, R., Garcia, P., Thai, J.N., Cheng, H.Q., Neuhaus, J.M., Forner, S.A., Duncan, J.L., Possin, K.L., Dearmond, S.J., Prusiner, S.B. & Miller, B.L. 2013, "Quinacrine treatment trial for sporadic Creutzfeldt-Jakob disease", *Neurology*, vol. 81, no. 23, pp. 2015-2023.
- Glessner, J.T., Wang, K., Sleiman, P.M., Zhang, H., Kim, C.E., Flory, J.H., Bradfield, J.P., Imielinski, M., Frackelton, E.C., Qiu, H., Mentch, F., Grant, S.F. & Hakonarson, H. 2010, "Duplication of the SLIT3 locus on 5q35.1 predisposes to major depressive disorder", *PloS one*, vol. 5, no. 12, pp. e15463.
- Goebel, D.J. & Poosch, M.S. 2001, "Transient down-regulation of NMDA receptor subunit gene expression in the rat retina following NMDA-induced neurotoxicity is attenuated in the presence of the non-competitive NMDA receptor antagonist MK-801", *Experimental eye research*, vol. 72, no. 5, pp. 547-558.
- Goldschmidt, L., Teng, P.K., Riek, R. & Eisenberg, D. 2010, "Identifying the amyloids, proteins capable of forming amyloid-like fibrils", *Proceedings of the National Academy of Sciences of the United States of America*, vol. 107, no. 8, pp. 3487-3492.
- Gross, C., Yao, X., Engel, T., Tiwari, D., Xing, L., Rowley, S., Danielson, S.W., Thomas, K.T., Jimenez-Mateos, E.M., Schroeder, L.M., Pun, R.Y., Danzer, S.C., Henshall, D.C. & Bassell, G.J. 2016, "MicroRNA-Mediated Downregulation of the Potassium Channel Kv4.2 Contributes to Seizure Onset", *Cell reports*, vol. 17, no. 1, pp. 37-45.
- Guidi, M., Muinos-Gimeno, M., Kagerbauer, B., Marti, E., Estivill, X. & Espinosa-Parrilla, Y. 2010, "Overexpression of miR-128 specifically inhibits the truncated isoform of NTRK3 and upregulates BCL2 in SH-SY5Y neuroblastoma cells", *BMC molecular biology*, vol. 11, pp. 95-2199-11-95.
- Guo, B.B., Bellingham, S.A. & Hill, A.F. 2016, "Stimulating the Release of Exosomes Increases the Intercellular Transfer of Prions", *The Journal of biological chemistry*, vol. 291, no. 10, pp. 5128-5137.
- Ha, M. & Kim, V.N. 2014a, "Regulation of microRNA biogenesis", *Nature reviews.Molecular cell biology*, vol. 15, no. 8, pp. 509-524.

- Ha, M. & Kim, V.N. 2014b, "Regulation of microRNA biogenesis", *Nature reviews.Molecular cell biology*, vol. 15, no. 8, pp. 509-524.
- Haas, L.T., Kostylev, M.A. & Strittmatter, S.M. 2014, "Therapeutic molecules and endogenous ligands regulate the interaction between brain cellular prion protein (PrPC) and metabotropic glutamate receptor 5 (mGluR5)", *The Journal of biological chemistry*, vol. 289, no. 41, pp. 28460-28477.
- Haas, L.T., Salazar, S.V., Kostylev, M.A., Um, J.W., Kaufman, A.C. & Strittmatter, S.M. 2016, "Metabotropic glutamate receptor 5 couples cellular prion protein to intracellular signalling in Alzheimer's disease", *Brain : a journal of neurology*, vol. 139, no. Pt 2, pp. 526-546.
- Hadlow, W.J. 1995, "Neuropathology and the scrapie-kuru connection", *Brain pathology (Zurich, Switzerland)*, vol. 5, no. 1, pp. 27-31.
- Haik, S., Marcon, G., Mallet, A., Tettamanti, M., Welaratne, A., Giaccone, G., Azimi, S., Pietrini, V., Fabreguettes, J.R., Imperiale, D., Cesaro, P., Buffa, C., Aucan, C., Lucca, U., Peckeu, L., Suardi, S., Tranchant, C., Zerr, I., Houillier, C., Redaelli, V., Vespignani, H., Campanella, A., Sellal, F., Krasnianski, A., Seilhean, D., Heinemann, U., Sedel, F., Canovi, M., Gobbi, M., Di Fede, G., Laplanche, J.L., Pocchiari, M., Salmona, M., Forloni, G., Brandel, J.P. & Tagliavini, F. 2014, "Doxycycline in Creutzfeldt-Jakob disease: a phase 2, randomised, double-blind, placebo-controlled trial", *The Lancet.Neurology*, vol. 13, no. 2, pp. 150-158.
- Haley, N.J. & Hoover, E.A. 2015, "Chronic wasting disease of cervids: current knowledge and future perspectives", *Annual review of animal biosciences*, vol. 3, pp. 305-325.
- Hamilton, A., Esseltine, J.L., DeVries, R.A., Cregan, S.P. & Ferguson, S.S. 2014, "Metabotropic glutamate receptor 5 knockout reduces cognitive impairment and pathogenesis in a mouse model of Alzheimer's disease", *Molecular brain*, vol. 7, pp. 40-6606-7-40.
- Hamilton, A., Vasefi, M., Vander Tuin, C., McQuaid, R.J., Anisman, H. & Ferguson, S.S. 2016, "Chronic Pharmacological mGluR5 Inhibition Prevents Cognitive Impairment and Reduces Pathogenesis in an Alzheimer Disease Mouse Model", *Cell reports*, vol. 15, no. 9, pp. 1859-1865.
- Hamilton, A., Zamponi, G.W. & Ferguson, S.S. 2015, "Glutamate receptors function as scaffolds for the regulation of beta-amyloid and cellular prion protein signaling complexes", *Molecular brain*, vol. 8, pp. 18-015-0107-0.
- Hammell, M., Long, D., Zhang, L., Lee, A., Carmack, C.S., Han, M., Ding, Y. & Ambros, V. 2008, "mirWIP: microRNA target prediction based on microRNA-containing ribonucleoprotein-enriched transcripts", *Nature methods*, vol. 5, no. 9, pp. 813-819.
- Hanus, C. & Schuman, E.M. 2013, "Proteostasis in complex dendrites", *Nature reviews.Neuroscience*, vol. 14, no. 9, pp. 638-648.
- Haraguchi, T., Ozaki, Y. & Iba, H. 2009, "Vectors expressing efficient RNA decoys achieve the long-term suppression of specific microRNA activity in mammalian cells", *Nucleic acids research*, vol. 37, no. 6, pp. e43.

- Hardingham, G.E. 2006, "Pro-survival signalling from the NMDA receptor", *Biochemical Society transactions*, vol. 34, no. Pt 5, pp. 936-938.
- Hardingham, G.E., Arnold, F.J. & Bading, H. 2001, "Nuclear calcium signaling controls CREB-mediated gene expression triggered by synaptic activity", *Nature neuroscience*, vol. 4, no. 3, pp. 261-267.
- Hardy, R.J. 1998, "QKI expression is regulated during neuron-glia cell fate decisions", *Journal of neuroscience research*, vol. 54, no. 1, pp. 46-57.
- Harraz, M.M., Eacker, S.M., Wang, X., Dawson, T.M. & Dawson, V.L. 2012, "MicroRNA-223 is neuroprotective by targeting glutamate receptors", *Proceedings of the National Academy of Sciences of the United States of America*, vol. 109, no. 46, pp. 18962-18967.
- Herculano-Houzel, S. & Lent, R. 2005, "Isotropic fractionator: a simple, rapid method for the quantification of total cell and neuron numbers in the brain", *The Journal of neuroscience : the official journal of the Society for Neuroscience*, vol. 25, no. 10, pp. 2518-2521.
- Herring, A., Donath, A., Steiner, K.M., Widera, M.P., Hamzehian, S., Kanakis, D., Kolble, K., ElAli, A., Hermann, D.M., Paulus, W. & Keyvani, K. 2012, "Reelin depletion is an early phenomenon of Alzheimer's pathology", *Journal of Alzheimer's disease : JAD*, vol. 30, no. 4, pp. 963-979.
- Herrmann, U.S., Schutz, A.K., Shirani, H., Huang, D., Saban, D., Nuvolone, M., Li, B., Ballmer, B., Aslund, A.K., Mason, J.J., Rushing, E., Budka, H., Nystrom, S., Hammarstrom, P., Bockmann, A., Caflisch, A., Meier, B.H., Nilsson, K.P., Hornemann, S. & Aguzzi, A. 2015, "Structure-based drug design identifies polythiophenes as antiprion compounds", *Science translational medicine*, vol. 7, no. 299, pp. 299ra123.
- Hill, A.F., Desbruslais, M., Joiner, S., Sidle, K.C., Gowland, I., Collinge, J., Doey, L.J. & Lantos, P. 1997, "The same prion strain causes vCJD and BSE", *Nature*, vol. 389, no. 6650, pp. 448-50, 526.
- Hipfel, R., Hanes, J., Von Der Kammer, H. & Pohlner, J. 2006, *Camp-regulated phosphoprotein for diagnostic and therapeutic use in neurodegenerative diseases*, Google Patents.
- Holman, R.C., Khan, A.S., Belay, E.D. & Schonberger, L.B. 1996, "Creutzfeldt-Jakob disease in the United States, 1979-1994: using national mortality data to assess the possible occurrence of variant cases", *Emerging infectious diseases*, vol. 2, no. 4, pp. 333-337.
- Hornshaw, M.P., McDermott, J.R. & Candy, J.M. 1995, "Copper binding to the N-terminal tandem repeat regions of mammalian and avian prion protein", *Biochemical and biophysical research communications*, vol. 207, no. 2, pp. 621-629.
- Hsu, P.W., Huang, H.D., Hsu, S.D., Lin, L.Z., Tsou, A.P., Tseng, C.P., Stadler, P.F., Washietl, S. & Hofacker, I.L. 2006, "miRNAMap: genomic maps of microRNA genes

- and their target genes in mammalian genomes", *Nucleic acids research*, vol. 34, no. Database issue, pp. D135-9.
- Hu, N.W., Nicoll, A.J., Zhang, D., Mably, A.J., O'Malley, T., Purro, S.A., Terry, C., Collinge, J., Walsh, D.M. & Rowan, M.J. 2014, "mGlu5 receptors and cellular prion protein mediate amyloid-beta-facilitated synaptic long-term depression in vivo", *Nature communications*, vol. 5, pp. 3374.
- Huang da, W., Sherman, B.T. & Lempicki, R.A. 2009a, "Bioinformatics enrichment tools: paths toward the comprehensive functional analysis of large gene lists", *Nucleic acids research*, vol. 37, no. 1, pp. 1-13.
- Huang da, W., Sherman, B.T. & Lempicki, R.A. 2009b, "Systematic and integrative analysis of large gene lists using DAVID bioinformatics resources", *Nature protocols*, vol. 4, no. 1, pp. 44-57.
- Imai, Y., Ibata, I., Ito, D., Ohsawa, K. & Kohsaka, S. 1996, "A novel gene *iba1* in the major histocompatibility complex class III region encoding an EF hand protein expressed in a monocytic lineage", *Biochemical and biophysical research communications*, vol. 224, no. 3, pp. 855-862.
- Imarisio, S., Carmichael, J., Korolchuk, V., Chen, C.W., Saiki, S., Rose, C., Krishna, G., Davies, J.E., Ttofi, E., Underwood, B.R. & Rubinsztein, D.C. 2008, "Huntington's disease: from pathology and genetics to potential therapies", *The Biochemical journal*, vol. 412, no. 2, pp. 191-209.
- Imran, M. & Mahmood, S. 2011, "An overview of animal prion diseases", *Virology journal*, vol. 8, pp. 493-422X-8-493.
- Ivanov, A., Pellegrino, C., Rama, S., Dumalska, I., Salyha, Y., Ben-Ari, Y. & Medina, I. 2006, "Opposing role of synaptic and extrasynaptic NMDA receptors in regulation of the extracellular signal-regulated kinases (ERK) activity in cultured rat hippocampal neurons", *The Journal of physiology*, vol. 572, no. Pt 3, pp. 789-798.
- Jabaudon, D., Shnider, S.J., Tischfield, D.J., Galazo, M.J. & Macklis, J.D. 2012, "RORbeta induces barrel-like neuronal clusters in the developing neocortex", *Cerebral cortex (New York, N.Y.: 1991)*, vol. 22, no. 5, pp. 996-1006.
- Jaunmuktane, Z., Mead, S., Ellis, M., Wadsworth, J.D., Nicoll, A.J., Kenny, J., Launchbury, F., Linehan, J., Richard-Loendt, A., Walker, A.S., Rudge, P., Collinge, J. & Brandner, S. 2015, "Evidence for human transmission of amyloid-beta pathology and cerebral amyloid angiopathy", *Nature*, vol. 525, no. 7568, pp. 247-250.
- Jespersen, A., Tajima, N., Fernandez-Cuervo, G., Garnier-Amblard, E.C. & Furukawa, H. 2014, "Structural insights into competitive antagonism in NMDA receptors", *Neuron*, vol. 81, no. 2, pp. 366-378.
- Jones, E.G., Huntley, G.W. & Benson, D.L. 1994, "Alpha calcium/calmodulin-dependent protein kinase II selectively expressed in a subpopulation of excitatory neurons in monkey sensory-motor cortex: comparison with GAD-67 expression", *The Journal of neuroscience : the official journal of the Society for Neuroscience*, vol. 14, no. 2, pp. 611-629.

- Jovicic, A., Zaldivar Jolissaint, J.F., Moser, R., Silva Santos Mde, F. & Luthi-Carter, R. 2013, "MicroRNA-22 (miR-22) overexpression is neuroprotective via general anti-apoptotic effects and may also target specific Huntington's disease-related mechanisms", *PloS one*, vol. 8, no. 1, pp. e54222.
- Kawahara, Y., Zinshteyn, B., Chendrimada, T.P., Shiekhattar, R. & Nishikura, K. 2007, "RNA editing of the microRNA-151 precursor blocks cleavage by the Dicer-TRBP complex", *EMBO reports*, vol. 8, no. 8, pp. 763-769.
- Khawaled, R., Bruening-Wright, A., Adelman, J.P. & Maylie, J. 1999, "Bicuculline block of small-conductance calcium-activated potassium channels", *Pflugers Archiv : European journal of physiology*, vol. 438, no. 3, pp. 314-321.
- Khosravani, H., Zhang, Y., Tsutsui, S., Hameed, S., Altier, C., Hamid, J., Chen, L., Villemaire, M., Ali, Z., Jirik, F.R. & Zamponi, G.W. 2008a, "Prion protein attenuates excitotoxicity by inhibiting NMDA receptors", *The Journal of cell biology*, vol. 181, no. 3, pp. 551-565.
- Khosravani, H., Zhang, Y., Tsutsui, S., Hameed, S., Altier, C., Hamid, J., Chen, L., Villemaire, M., Ali, Z., Jirik, F.R. & Zamponi, G.W. 2008b, "Prion protein attenuates excitotoxicity by inhibiting NMDA receptors", *The Journal of general physiology*, vol. 131, no. 6, pp. i5.
- Khudayberdiev, S.A., Zampa, F., Rajman, M. & Schrott, G. 2013, "A comprehensive characterization of the nuclear microRNA repertoire of post-mitotic neurons", *Frontiers in molecular neuroscience*, vol. 6, pp. 43.
- Kimberlin, R.H. & Walker, C.A. 1982, "Pathogenesis of mouse scrapie: patterns of agent replication in different parts of the CNS following intraperitoneal infection", *Journal of the Royal Society of Medicine*, vol. 75, no. 8, pp. 618-624.
- Klein, M.E., Liroy, D.T., Ma, L., Impey, S., Mandel, G. & Goodman, R.H. 2007, "Homeostatic regulation of MeCP2 expression by a CREB-induced microRNA", *Nature neuroscience*, vol. 10, no. 12, pp. 1513-1514.
- Klyubin, I., Nicoll, A.J., Khalili-Shirazi, A., Farmer, M., Canning, S., Mably, A., Linehan, J., Brown, A., Wakeling, M., Brandner, S., Walsh, D.M., Rowan, M.J. & Collinge, J. 2014, "Peripheral administration of a humanized anti-PrP antibody blocks Alzheimer's disease A β synaptotoxicity", *The Journal of neuroscience : the official journal of the Society for Neuroscience*, vol. 34, no. 18, pp. 6140-6145.
- Kocerha, J., Xu, Y., Prucha, M.S., Zhao, D. & Chan, A.W. 2014, "microRNA-128a dysregulation in transgenic Huntington's disease monkeys", *Molecular brain*, vol. 7, pp. 46-6606-7-46.
- Koffie, R.M., Hyman, B.T. & Spires-Jones, T.L. 2011, "Alzheimer's disease: synapses gone cold", *Molecular neurodegeneration*, vol. 6, no. 1, pp. 63-1326-6-63.
- Komori, T., Doi, A., Nosaka, T., Furuta, H., Akamizu, T., Kitamura, T., Senba, E. & Morikawa, Y. 2012, "Regulation of AMP-activated protein kinase signaling by AFF4 protein, member of AF4 (ALL1-fused gene from chromosome 4) family of

- transcription factors, in hypothalamic neurons", *The Journal of biological chemistry*, vol. 287, no. 24, pp. 19985-19996.
- Kos, A., Olde Loohuis, N., Meinhardt, J., van Bokhoven, H., Kaplan, B.B., Martens, G.J. & Aschrafi, A. 2016, "MicroRNA-181 promotes synaptogenesis and attenuates axonal outgrowth in cortical neurons", *Cellular and molecular life sciences : CMLS*, vol. 73, no. 18, pp. 3555-3567.
- Kosik, K.S. & Finch, E.A. 1987, "MAP2 and tau segregate into dendritic and axonal domains after the elaboration of morphologically distinct neurites: an immunocytochemical study of cultured rat cerebrum", *The Journal of neuroscience : the official journal of the Society for Neuroscience*, vol. 7, no. 10, pp. 3142-3153.
- Kozomara, A. & Griffiths-Jones, S. 2014, "miRBase: annotating high confidence microRNAs using deep sequencing data", *Nucleic acids research*, vol. 42, no. Database issue, pp. D68-73.
- Kralovicova, S., Fontaine, S.N., Alderton, A., Alderman, J., Ragnarsdottir, K.V., Collins, S.J. & Brown, D.R. 2009, "The effects of prion protein expression on metal metabolism", *Molecular and cellular neurosciences*, vol. 41, no. 2, pp. 135-147.
- Kramer, S.G., Kidd, T., Simpson, J.H. & Goodman, C.S. 2001, "Switching repulsion to attraction: changing responses to slit during transition in mesoderm migration", *Science (New York, N.Y.)*, vol. 292, no. 5517, pp. 737-740.
- Krishnan, K., Steptoe, A.L., Martin, H.C., Wani, S., Nones, K., Waddell, N., Mariasegaram, M., Simpson, P.T., Lakhani, S.R., Gabrielli, B., Vlassov, A., Cloonan, N. & Grimmond, S.M. 2013, "MicroRNA-182-5p targets a network of genes involved in DNA repair", *RNA (New York, N.Y.)*, vol. 19, no. 2, pp. 230-242.
- Krutzfeldt, J., Kuwajima, S., Braich, R., Rajeev, K.G., Pena, J., Tuschl, T., Manoharan, M. & Stoffel, M. 2007, "Specificity, duplex degradation and subcellular localization of antagomirs", *Nucleic acids research*, vol. 35, no. 9, pp. 2885-2892.
- Kuffer, A., Lakkaraju, A.K., Mogha, A., Petersen, S.C., Airich, K., Doucerain, C., Marpakwar, R., Bakirci, P., Senatore, A., Monnard, A., Schiavi, C., Nuvolone, M., Grosshans, B., Hornemann, S., Bassilana, F., Monk, K.R. & Aguzzi, A. 2016, "The prion protein is an agonistic ligand of the G protein-coupled receptor Adgrg6", *Nature*, vol. 536, no. 7617, pp. 464-468.
- Kumar, M. & Nerurkar, V.R. 2014, "Integrated analysis of microRNAs and their disease related targets in the brain of mice infected with West Nile virus", *Virology*, vol. 452-453, pp. 143-151.
- Kye, M.J., Liu, T., Levy, S.F., Xu, N.L., Groves, B.B., Bonneau, R., Lao, K. & Kosik, K.S. 2007, "Somatodendritic microRNAs identified by laser capture and multiplex RT-PCR", *RNA (New York, N.Y.)*, vol. 13, no. 8, pp. 1224-1234.
- Kye, M.J., Neveu, P., Lee, Y.S., Zhou, M., Steen, J.A., Sahin, M., Kosik, K.S. & Silva, A.J. 2011, "NMDA mediated contextual conditioning changes miRNA expression", *PloS one*, vol. 6, no. 9, pp. e24682.

- Lal, A., Kim, H.H., Abdelmohsen, K., Kuwano, Y., Pullmann, R., Jr, Srikantan, S., Subrahmanyam, R., Martindale, J.L., Yang, X., Ahmed, F., Navarro, F., Dykxhoorn, D., Lieberman, J. & Gorospe, M. 2008, "p16(INK4a) translation suppressed by miR-24", *PloS one*, vol. 3, no. 3, pp. e1864.
- Landgraf, P., Rusu, M., Sheridan, R., Sewer, A., Iovino, N., Aravin, A., Pfeffer, S., Rice, A., Kamphorst, A.O., Landthaler, M., Lin, C., Socci, N.D., Hermida, L., Fulci, V., Chiaretti, S., Foa, R., Schliwka, J., Fuchs, U., Novosel, A., Muller, R.U., Schermer, B., Bissels, U., Inman, J., Phan, Q., Chien, M., Weir, D.B., Choksi, R., De Vita, G., Frezzetti, D., Trompeter, H.I., Hornung, V., Teng, G., Hartmann, G., Palkovits, M., Di Lauro, R., Wernet, P., Macino, G., Rogler, C.E., Nagle, J.W., Ju, J., Papavasiliou, F.N., Benzing, T., Lichter, P., Tam, W., Brownstein, M.J., Bosio, A., Borkhardt, A., Russo, J.J., Sander, C., Zavolan, M. & Tuschl, T. 2007, "A mammalian microRNA expression atlas based on small RNA library sequencing", *Cell*, vol. 129, no. 7, pp. 1401-1414.
- Lauren, J., Gimbel, D.A., Nygaard, H.B., Gilbert, J.W. & Strittmatter, S.M. 2009, "Cellular prion protein mediates impairment of synaptic plasticity by amyloid-beta oligomers", *Nature*, vol. 457, no. 7233, pp. 1128-1132.
- Le Pichon, C.E., Valley, M.T., Polymenidou, M., Chesler, A.T., Sagdullaev, B.T., Aguzzi, A. & Firestein, S. 2009, "Olfactory behavior and physiology are disrupted in prion protein knockout mice", *Nature neuroscience*, vol. 12, no. 1, pp. 60-69.
- Lee, S.T., Chu, K., Im, W.S., Yoon, H.J., Im, J.Y., Park, J.E., Park, K.H., Jung, K.H., Lee, S.K., Kim, M. & Roh, J.K. 2011, "Altered microRNA regulation in Huntington's disease models", *Experimental neurology*, vol. 227, no. 1, pp. 172-179.
- Lee, Y.J. & Baskakov, I.V. 2014, "The cellular form of the prion protein guides the differentiation of human embryonic stem cells into neuron-, oligodendrocyte-, and astrocyte-committed lineages", *Prion*, vol. 8, no. 3, pp. 266-275.
- Lee, Y.J., Johnson, K.R. & Hallenbeck, J.M. 2012, "Global protein conjugation by ubiquitin-like-modifiers during ischemic stress is regulated by microRNAs and confers robust tolerance to ischemia", *PloS one*, vol. 7, no. 10, pp. e47787.
- Lewis, B.P., Burge, C.B. & Bartel, D.P. 2005, "Conserved seed pairing, often flanked by adenosines, indicates that thousands of human genes are microRNA targets", *Cell*, vol. 120, no. 1, pp. 15-20.
- Li, D., Yuan, H., Ortiz-Gonzalez, X.R., Marsh, E.D., Tian, L., McCormick, E.M., Kosobucki, G.J., Chen, W., Schulien, A.J., Chiavacci, R., Tankovic, A., Naase, C., Brueckner, F., von Stulpnagel-Steinbeis, C., Hu, C., Kusumoto, H., Hedrich, U.B., Elsen, G., Hortnagel, K., Aizenman, E., Lemke, J.R., Hakonarson, H., Traynelis, S.F. & Falk, M.J. 2016, "GRIN2D Recurrent De Novo Dominant Mutation Causes a Severe Epileptic Encephalopathy Treatable with NMDA Receptor Channel Blockers", *American Journal of Human Genetics*, .

- Li, X.F. & Lytton, J. 2014, "An essential role for the K⁺-dependent Na⁺/Ca²⁺-exchanger, NCKX4, in melanocortin-4-receptor-dependent satiety", *The Journal of biological chemistry*, vol. 289, no. 37, pp. 25445-25459.
- Liebert, A., Bicknell, B. & Adams, R. 2014, "Prion Protein Signaling in the Nervous System - A Review and Perspective", vol. 3, pp. 11.
- Lin, L. & Isacson, O. 2006, "Axonal growth regulation of fetal and embryonic stem cell-derived dopaminergic neurons by Netrin-1 and Slits", *Stem cells (Dayton, Ohio)*, vol. 24, no. 11, pp. 2504-2513.
- Lin, L., Lesnick, T.G., Maraganore, D.M. & Isacson, O. 2009, "Axon guidance and synaptic maintenance: preclinical markers for neurodegenerative disease and therapeutics", *Trends in neurosciences*, vol. 32, no. 3, pp. 142-149.
- Lin, Q., Wei, W., Coelho, C.M., Li, X., Baker-Andresen, D., Dudley, K., Ratnu, V.S., Boskovic, Z., Kobor, M.S., Sun, Y.E. & Bredy, T.W. 2011, "The brain-specific microRNA miR-128b regulates the formation of fear-extinction memory", *Nature neuroscience*, vol. 14, no. 9, pp. 1115-1117.
- Liu, T., Li, R., Pan, T., Liu, D., Petersen, R.B., Wong, B.S., Gambetti, P. & Sy, M.S. 2002, "Intercellular transfer of the cellular prion protein", *The Journal of biological chemistry*, vol. 277, no. 49, pp. 47671-47678.
- Livak, K.J. & Schmittgen, T.D. 2001, "Analysis of relative gene expression data using real-time quantitative PCR and the 2(-Delta Delta C(T)) Method", *Methods (San Diego, Calif.)*, vol. 25, no. 4, pp. 402-408.
- Loher, P. & Rigoutsos, I. 2012, "Interactive exploration of RNA22 microRNA target predictions", *Bioinformatics (Oxford, England)*, vol. 28, no. 24, pp. 3322-3323.
- Lorenz, R., Bernhart, S.H., Honer Zu Siederdisen, C., Tafer, H., Flamm, C., Stadler, P.F. & Hofacker, I.L. 2011, "ViennaRNA Package 2.0", *Algorithms for molecular biology : AMB*, vol. 6, pp. 26-7188-6-26.
- Lovell, M.A., Robertson, J.D., Teesdale, W.J., Campbell, J.L. & Markesbery, W.R. 1998, "Copper, iron and zinc in Alzheimer's disease senile plaques", *Journal of the neurological sciences*, vol. 158, no. 1, pp. 47-52.
- Lugli, G., Larson, J., Demars, M.P. & Smalheiser, N.R. 2012, "Primary microRNA precursor transcripts are localized at post-synaptic densities in adult mouse forebrain", *Journal of neurochemistry*, vol. 123, no. 4, pp. 459-466.
- Lugli, G., Larson, J., Martone, M.E., Jones, Y. & Smalheiser, N.R. 2005, "Dicer and eIF2c are enriched at postsynaptic densities in adult mouse brain and are modified by neuronal activity in a calpain-dependent manner", *Journal of neurochemistry*, vol. 94, no. 4, pp. 896-905.
- Lugli, G., Torvik, V.I., Larson, J. & Smalheiser, N.R. 2008, "Expression of microRNAs and their precursors in synaptic fractions of adult mouse forebrain", *Journal of neurochemistry*, vol. 106, no. 2, pp. 650-661.
- Lukiw, W.J. 2007, "Micro-RNA speciation in fetal, adult and Alzheimer's disease hippocampus", *Neuroreport*, vol. 18, no. 3, pp. 297-300.

- Lytle, J.R., Yario, T.A. & Steitz, J.A. 2007, "Target mRNAs are repressed as efficiently by microRNA-binding sites in the 5' UTR as in the 3' UTR", *Proceedings of the National Academy of Sciences of the United States of America*, vol. 104, no. 23, pp. 9667-9672.
- Magill, S.T., Cambronne, X.A., Luikart, B.W., Lioy, D.T., Leighton, B.H., Westbrook, G.L., Mandel, G. & Goodman, R.H. 2010, "microRNA-132 regulates dendritic growth and arborization of newborn neurons in the adult hippocampus", *Proceedings of the National Academy of Sciences of the United States of America*, vol. 107, no. 47, pp. 20382-20387.
- Majer, A., Medina, S.J., Niu, Y., Abrenica, B., Manguiat, K.J., Frost, K.L., Philipson, C.S., Sorensen, D.L. & Booth, S.A. 2012, "Early mechanisms of pathobiology are revealed by transcriptional temporal dynamics in hippocampal CA1 neurons of prion infected mice", *PLoS pathogens*, vol. 8, no. 11, pp. e1003002.
- Mallucci, G.R. 2009, "Prion neurodegeneration: starts and stops at the synapse", *Prion*, vol. 3, no. 4, pp. 195-201.
- Mallucci, G.R., White, M.D., Farmer, M., Dickinson, A., Khatun, H., Powell, A.D., Brandner, S., Jefferys, J.G. & Collinge, J. 2007, "Targeting cellular prion protein reverses early cognitive deficits and neurophysiological dysfunction in prion-infected mice", *Neuron*, vol. 53, no. 3, pp. 325-335.
- Malmevik, J., Petri, R., Klussendorf, T., Knauff, P., Akerblom, M., Johansson, J., Soneji, S. & Jakobsson, J. 2015, "Identification of the miRNA targetome in hippocampal neurons using RIP-seq", *Scientific reports*, vol. 5, pp. 12609.
- Mantamadiotis, T., Lemberger, T., Bleckmann, S.C., Kern, H., Kretz, O., Martin Villalba, A., Tronche, F., Kellendonk, C., Gau, D., Kapfhammer, J., Otto, C., Schmid, W. & Schutz, G. 2002, "Disruption of CREB function in brain leads to neurodegeneration", *Nature genetics*, vol. 31, no. 1, pp. 47-54.
- Mao, G., Ren, P., Wang, G., Yan, F. & Zhang, Y. 2017, "MicroRNA-128-3p Protects Mouse Against Cerebral Ischemia Through Reducing p38alpha Mitogen-Activated Protein Kinase Activity", *Journal of molecular neuroscience : MN*, vol. 61, no. 2, pp. 152-158.
- Marti, E., Pantano, L., Banez-Coronel, M., Llorens, F., Minones-Moyano, E., Porta, S., Sumoy, L., Ferrer, I. & Estivill, X. 2010, "A myriad of miRNA variants in control and Huntington's disease brain regions detected by massively parallel sequencing", *Nucleic acids research*, vol. 38, no. 20, pp. 7219-7235.
- Martinez, T. & Pascual, A. 2007, "Identification of genes differentially expressed in SH-SY5Y neuroblastoma cells exposed to the prion peptide 106-126", *The European journal of neuroscience*, vol. 26, no. 1, pp. 51-59.
- Marzi, M.J., Ghini, F., Cerruti, B., de Pretis, S., Bonetti, P., Giacomelli, C., Gorski, M.M., Kress, T., Pelizzola, M., Muller, H., Amati, B. & Nicassio, F. 2016, "Degradation dynamics of microRNAs revealed by a novel pulse-chase approach", *Genome research*, vol. 26, no. 4, pp. 554-565.

- Mathews, J.D., Glasse, R. & Lindenbaum, S. 1968, "Kuru and cannibalism", *Lancet (London, England)*, vol. 2, no. 7565, pp. 449-452.
- Mathiason, C.K., Powers, J.G., Dahmes, S.J., Osborn, D.A., Miller, K.V., Warren, R.J., Mason, G.L., Hays, S.A., Hayes-Klug, J., Seelig, D.M., Wild, M.A., Wolfe, L.L., Spraker, T.R., Miller, M.W., Sigurdson, C.J., Telling, G.C. & Hoover, E.A. 2006, "Infectious prions in the saliva and blood of deer with chronic wasting disease", *Science (New York, N.Y.)*, vol. 314, no. 5796, pp. 133-136.
- Matta, J.A., Ashby, M.C., Sanz-Clemente, A., Roche, K.W. & Isaac, J.T. 2011, "mGluR5 and NMDA receptors drive the experience- and activity-dependent NMDA receptor NR2B to NR2A subunit switch", *Neuron*, vol. 70, no. 2, pp. 339-351.
- McKay, S., Bengtson, C.P., Bading, H., Wyllie, D.J. & Hardingham, G.E. 2013, "Recovery of NMDA receptor currents from MK-801 blockade is accelerated by Mg²⁺ and memantine under conditions of agonist exposure", *Neuropharmacology*, vol. 74, pp. 119-125.
- McSweeney, K.M., Gussow, A.B., Bradrick, S.S., Dugger, S.A., Gelfman, S., Wang, Q., Petrovski, S., Frankel, W.N., Boland, M.J. & Goldstein, D.B. 2016, "Inhibition of microRNA 128 promotes excitability of cultured cortical neuronal networks", *Genome research*, vol. 26, no. 10, pp. 1411-1416.
- Megraw, M., Sethupathy, P., Gumireddy, K., Jensen, S.T., Huang, Q. & Hatzigeorgiou, A.G. 2010, "**Isoform specific gene auto-regulation via miRNAs: a case study on miR-128b and ARPP-21**", *Theoretical Chemistry Accounts*, vol. 125, no. 3, pp. 593.
- Mestdagh, P., Hartmann, N., Baeriswyl, L., Andreasen, D., Bernard, N., Chen, C., Cheo, D., D'Andrade, P., DeMayo, M., Dennis, L., Derveaux, S., Feng, Y., Fulmer-Smentek, S., Gerstmayer, B., Gouffon, J., Grimley, C., Lader, E., Lee, K.Y., Luo, S., Mouritzen, P., Narayanan, A., Patel, S., Peiffer, S., Ruberg, S., Schroth, G., Schuster, D., Shaffer, J.M., Shelton, E.J., Silveria, S., Ulmanella, U., Veeramachaneni, V., Staedtler, F., Peters, T., Guettouche, T., Wong, L. & Vandesompele, J. 2014, "Evaluation of quantitative miRNA expression platforms in the microRNA quality control (miRQC) study", *Nature methods*, vol. 11, no. 8, pp. 809-815.
- Meunier, J., Lemoine, F., Soumillon, M., Liechti, A., Weier, M., Guschanski, K., Hu, H., Khaitovich, P. & Kaessmann, H. 2013, "Birth and expression evolution of mammalian microRNA genes", *Genome research*, vol. 23, no. 1, pp. 34-45.
- Meyer-Luehmann, M., Coomaraswamy, J., Bolmont, T., Kaeser, S., Schaefer, C., Kilger, E., Neuenschwander, A., Abramowski, D., Frey, P., Jaton, A.L., Vigouret, J.M., Paganetti, P., Walsh, D.M., Mathews, P.M., Ghiso, J., Staufenbiel, M., Walker, L.C. & Jucker, M. 2006, "Exogenous induction of cerebral beta-amyloidogenesis is governed by agent and host", *Science (New York, N.Y.)*, vol. 313, no. 5794, pp. 1781-1784.
- Mi, H., Huang, X., Muruganujan, A., Tang, H., Mills, C., Kang, D. & Thomas, P.D. 2017, "PANTHER version 11: expanded annotation data from Gene Ontology and Reactome

- pathways, and data analysis tool enhancements", *Nucleic acids research*, vol. 45, no. D1, pp. D183-D189.
- Miller, L.M., Wang, Q., Telivala, T.P., Smith, R.J., Lanzirrotti, A. & Miklossy, J. 2006, "Synchrotron-based infrared and X-ray imaging shows focalized accumulation of Cu and Zn co-localized with beta-amyloid deposits in Alzheimer's disease", *Journal of structural biology*, vol. 155, no. 1, pp. 30-37.
- Minikel, E.V., Vallabh, S.M., Lek, M., Estrada, K., Samocha, K.E., Sathirapongsasuti, J.F., McLean, C.Y., Tung, J.Y., Yu, L.P., Gambetti, P., Blevins, J., Zhang, S., Cohen, Y., Chen, W., Yamada, M., Hamaguchi, T., Sanjo, N., Mizusawa, H., Nakamura, Y., Kitamoto, T., Collins, S.J., Boyd, A., Will, R.G., Knight, R., Ponto, C., Zerr, I., Kraus, T.F., Eigenbrod, S., Giese, A., Calero, M., de Pedro-Cuesta, J., Haik, S., Laplanche, J.L., Bouaziz-Amar, E., Brandel, J.P., Capellari, S., Parchi, P., Poggi, A., Ladogana, A., O'Donnell-Luria, A.H., Karczewski, K.J., Marshall, J.L., Boehnke, M., Laakso, M., Mohlke, K.L., Kahler, A., Chambert, K., McCarroll, S., Sullivan, P.F., Hultman, C.M., Purcell, S.M., Sklar, P., van der Lee, S.J., Rozemuller, A., Jansen, C., Hofman, A., Kraaij, R., van Rooij, J.G., Ikram, M.A., Uitterlinden, A.G., van Duijn, C.M., Exome Aggregation Consortium (ExAC), Daly, M.J. & MacArthur, D.G. 2016, "Quantifying prion disease penetrance using large population control cohorts", *Science translational medicine*, vol. 8, no. 322, pp. 322ra9.
- Miranda, K.C., Huynh, T., Tay, Y., Ang, Y.S., Tam, W.L., Thomson, A.M., Lim, B. & Rigoutsos, I. 2006, "A pattern-based method for the identification of MicroRNA binding sites and their corresponding heteroduplexes", *Cell*, vol. 126, no. 6, pp. 1203-1217.
- Mohammadi, E. & Bigdeli, M.R. 2014, "Time course of neuroprotection induced by normobaric hyperoxia and NCX1 expression", *Brain injury*, vol. 28, no. 8, pp. 1127-1134.
- Mok, T., Jaunmuktane, Z., Joiner, S., Campbell, T., Morgan, C., Wakerley, B., Golestani, F., Rudge, P., Mead, S., Jager, H.R., Wadsworth, J.D., Brandner, S. & Collinge, J. 2017, "Variant Creutzfeldt-Jakob Disease in a Patient with Heterozygosity at PRNP Codon 129", *The New England journal of medicine*, vol. 376, no. 3, pp. 292-294.
- Montag, J., Hitt, R., Opitz, L., Schulz-Schaeffer, W.J., Hunsmann, G. & Motzkus, D. 2009, "Upregulation of miRNA hsa-miR-342-3p in experimental and idiopathic prion disease", *Molecular neurodegeneration*, vol. 4, pp. 36.
- Monteys, A.M., Spengler, R.M., Wan, J., Tecedor, L., Lennox, K.A., Xing, Y. & Davidson, B.L. 2010, "Structure and activity of putative intronic miRNA promoters", *RNA (New York, N.Y.)*, vol. 16, no. 3, pp. 495-505.
- Moreno, J.A., Halliday, M., Molloy, C., Radford, H., Verity, N., Axten, J.M., Ortori, C.A., Willis, A.E., Fischer, P.M., Barrett, D.A. & Mallucci, G.R. 2013, "Oral treatment targeting the unfolded protein response prevents neurodegeneration and clinical disease in prion-infected mice", *Science translational medicine*, vol. 5, no. 206, pp. 206ra138.

- Moriyoshi, K., Masu, M., Ishii, T., Shigemoto, R., Mizuno, N. & Nakanishi, S. 1991, "Molecular cloning and characterization of the rat NMDA receptor", *Nature*, vol. 354, no. 6348, pp. 31-37.
- Muller, M., Kuiperij, H.B., Claassen, J.A., Kusters, B. & Verbeek, M.M. 2014, "MicroRNAs in Alzheimer's disease: differential expression in hippocampus and cell-free cerebrospinal fluid", *Neurobiology of aging*, vol. 35, no. 1, pp. 152-158.
- Naslund, J., Haroutunian, V., Mohs, R., Davis, K.L., Davies, P., Greengard, P. & Buxbaum, J.D. 2000, "Correlation between elevated levels of amyloid beta-peptide in the brain and cognitive decline", *Jama*, vol. 283, no. 12, pp. 1571-1577.
- Nesler, K.R., Starke, E.L., Boin, N.G., Ritz, M. & Barbee, S.A. 2016, "Presynaptic CamKII regulates activity-dependent axon terminal growth", *Molecular and cellular neurosciences*, vol. 76, pp. 33-41.
- Niewiadomska-Cimicka, A., Krzyzosiak, A., Ye, T., Podlesny-Drabiniok, A., Dembele, D., Dolle, P. & Krezel, W. 2016, "Genome-wide Analysis of RARbeta Transcriptional Targets in Mouse Striatum Links Retinoic Acid Signaling with Huntington's Disease and Other Neurodegenerative Disorders", *Molecular neurobiology*, .
- Nowak, L.M., Young, A.B. & Macdonald, R.L. 1982, "GABA and bicuculline actions on mouse spinal cord and cortical neurons in cell culture", *Brain research*, vol. 244, no. 1, pp. 155-164.
- Ohki, E.C., Tilkins, M.L., Ciccarone, V.C. & Price, P.J. 2001, "Improving the transfection efficiency of post-mitotic neurons", *Journal of neuroscience methods*, vol. 112, no. 2, pp. 95-99.
- Ong, S.E., Blagoev, B., Kratchmarova, I., Kristensen, D.B., Steen, H., Pandey, A. & Mann, M. 2002, "Stable isotope labeling by amino acids in cell culture, SILAC, as a simple and accurate approach to expression proteomics", *Molecular & cellular proteomics : MCP*, vol. 1, no. 5, pp. 376-386.
- Otto, M., Cepek, L., Ratzka, P., Doehlinger, S., Boekhoff, I., Wiltfang, J., Irle, E., Pergande, G., Ellers-Lenz, B., Windl, O., Kretschmar, H.A., Poser, S. & Prange, H. 2004, "Efficacy of flupirtine on cognitive function in patients with CJD: A double-blind study", *Neurology*, vol. 62, no. 5, pp. 714-718.
- Palay, S.L. 1956, "Synapses in the central nervous system", *The Journal of biophysical and biochemical cytology*, vol. 2, no. 4 Suppl, pp. 193-202.
- Pall, H.S., Williams, A.C., Blake, D.R., Lunec, J., Gutteridge, J.M., Hall, M. & Taylor, A. 1987, "Raised cerebrospinal-fluid copper concentration in Parkinson's disease", *Lancet (London, England)*, vol. 2, no. 8553, pp. 238-241.
- Palmer, M.S., Dryden, A.J., Hughes, J.T. & Collinge, J. 1991, "Homozygous prion protein genotype predisposes to sporadic Creutzfeldt-Jakob disease", *Nature*, vol. 352, no. 6333, pp. 340-342.
- Pan, K.M., Baldwin, M., Nguyen, J., Gasset, M., Serban, A., Groth, D., Mehlhorn, I., Huang, Z., Fletterick, R.J. & Cohen, F.E. 1993, "Conversion of alpha-helices into beta-sheets features in the formation of the scrapie prion proteins", *Proceedings of the*

National Academy of Sciences of the United States of America, vol. 90, no. 23, pp. 10962-10966.

- Perez-Palma, E., Bustos, B.I., Villaman, C.F., Alarcon, M.A., Avila, M.E., Ugarte, G.D., Reyes, A.E., Opazo, C., De Ferrari, G.V., Alzheimer's Disease Neuroimaging Initiative & NIA-LOAD/NCRAD Family Study Group 2014, "Overrepresentation of glutamate signaling in Alzheimer's disease: network-based pathway enrichment using meta-analysis of genome-wide association studies", *PloS one*, vol. 9, no. 4, pp. e95413.
- Perkins, D.O., Jeffries, C.D., Jarskog, L.F., Thomson, J.M., Woods, K., Newman, M.A., Parker, J.S., Jin, J. & Hammond, S.M. 2007, "microRNA expression in the prefrontal cortex of individuals with schizophrenia and schizoaffective disorder", *Genome biology*, vol. 8, no. 2, pp. R27.
- Peters, P.J., Mironov, A., Jr, Peretz, D., van Donselaar, E., Leclerc, E., Erpel, S., DeArmond, S.J., Burton, D.R., Williamson, R.A., Vey, M. & Prusiner, S.B. 2003, "Trafficking of prion proteins through a caveolae-mediated endosomal pathway", *The Journal of cell biology*, vol. 162, no. 4, pp. 703-717.
- Pichardo-Casas, I., Goff, L.A., Swerdel, M.R., Athie, A., Davila, J., Ramos-Brossier, M., Lapid-Volosin, M., Friedman, W.J., Hart, R.P. & Vaca, L. 2012, "Expression profiling of synaptic microRNAs from the adult rat brain identifies regional differences and seizure-induced dynamic modulation", *Brain research*, vol. 1436, pp. 20-33.
- Pirooznia, M., Nagarajan, V. & Deng, Y. 2007, "GeneVenn - A web application for comparing gene lists using Venn diagrams", *Bioinformatics*, vol. 1, no. 10, pp. 420-422.
- Pirttimaki, T.M., Codadu, N.K., Awni, A., Pratik, P., Nagel, D.A., Hill, E.J., Dineley, K.T. & Parri, H.R. 2013, "alpha7 Nicotinic receptor-mediated astrocytic gliotransmitter release: A beta effects in a preclinical Alzheimer's mouse model", *PloS one*, vol. 8, no. 11, pp. e81828.
- Poggiolini, I., Saverioni, D. & Parchi, P. 2013, "Prion protein misfolding, strains, and neurotoxicity: an update from studies on Mammalian prions", *International journal of cell biology*, vol. 2013, pp. 910314.
- Poulin, J.F., Tasic, B., Hjerling-Lefler, J., Trimarchi, J.M. & Awatramani, R. 2016, "Disentangling neural cell diversity using single-cell transcriptomics", *Nature neuroscience*, vol. 19, no. 9, pp. 1131-1141.
- Premzl, M., Gready, J.E., Jermini, L.S., Simonic, T. & Marshall Graves, J.A. 2004, "Evolution of vertebrate genes related to prion and Shadoo proteins--clues from comparative genomic analysis", *Molecular biology and evolution*, vol. 21, no. 12, pp. 2210-2231.
- Prusiner, S.B. 2013, "Biology and genetics of prions causing neurodegeneration", *Annual Review of Genetics*, vol. 47, pp. 601-623.
- Prusiner, S.B. 1982, "Novel proteinaceous infectious particles cause scrapie", *Science (New York, N.Y.)*, vol. 216, no. 4542, pp. 136-144.

- Puoti, G., Bizzi, A., Forloni, G., Safar, J.G., Tagliavini, F. & Gambetti, P. 2012, "Sporadic human prion diseases: molecular insights and diagnosis", *The Lancet.Neurology*, vol. 11, no. 7, pp. 618-628.
- Pushie, M.J., Pickering, I.J., Martin, G.R., Tsutsui, S., Jirik, F.R. & George, G.N. 2011, "Prion protein expression level alters regional copper, iron and zinc content in the mouse brain", *Metallomics : integrated biometal science*, vol. 3, no. 2, pp. 206-214.
- Qiao, Q., Bowman, G.R. & Huang, X. 2013, "Dynamics of an intrinsically disordered protein reveal metastable conformations that potentially seed aggregation", *Journal of the American Chemical Society*, vol. 135, no. 43, pp. 16092-16101.
- Rajewsky, N. 2006, "microRNA target predictions in animals", *Nature genetics*, vol. 38 Suppl, pp. S8-13.
- Rangel, A., Madronal, N., Gruart, A., Gavin, R., Llorens, F., Sumoy, L., Torres, J.M., Delgado-Garcia, J.M. & Del Rio, J.A. 2009, "Regulation of GABA(A) and glutamate receptor expression, synaptic facilitation and long-term potentiation in the hippocampus of prion mutant mice", *PloS one*, vol. 4, no. 10, pp. e7592.
- Rao, A. & Steward, O. 1991, "Evidence that protein constituents of postsynaptic membrane specializations are locally synthesized: analysis of proteins synthesized within synaptosomes", *The Journal of neuroscience : the official journal of the Society for Neuroscience*, vol. 11, no. 9, pp. 2881-2895.
- Rauniyar, N. & Yates, J.R., 3rd 2014, "Isobaric labeling-based relative quantification in shotgun proteomics", *Journal of proteome research*, vol. 13, no. 12, pp. 5293-5309.
- Reddy, P.H., Mani, G., Park, B.S., Jacques, J., Murdoch, G., Whetsell, W., Jr, Kaye, J. & Manczak, M. 2005, "Differential loss of synaptic proteins in Alzheimer's disease: implications for synaptic dysfunction", *Journal of Alzheimer's disease : JAD*, vol. 7, no. 2, pp. 103-17; discussion 173-80.
- Ren, J., Sun, J., Zhang, Y., Liu, T., Ren, Q., Li, Y. & Guo, A. 2012, "Down-regulation of Decapping Protein 2 mediates chronic nicotine exposure-induced locomotor hyperactivity in Drosophila", *PloS one*, vol. 7, no. 12, pp. e52521.
- Riek, R., Hornemann, S., Wider, G., Billeter, M., Glockshuber, R. & Wuthrich, K. 1996, "NMR structure of the mouse prion protein domain PrP(121-231)", *Nature*, vol. 382, no. 6587, pp. 180-182.
- Riemer, C., Burwinkel, M., Schwarz, A., Gultner, S., Mok, S.W., Heise, I., Holtkamp, N. & Baier, M. 2008, "Evaluation of drugs for treatment of prion infections of the central nervous system", *The Journal of general virology*, vol. 89, no. Pt 2, pp. 594-597.
- Rigoutsos, I. & Floratos, A. 1998, "Combinatorial pattern discovery in biological sequences: The TEIRESIAS algorithm", *Bioinformatics (Oxford, England)*, vol. 14, no. 1, pp. 55-67.
- Risbud, R.M. & Porter, B.E. 2013, "Changes in microRNA expression in the whole hippocampus and hippocampal synaptoneurosome fraction following pilocarpine induced status epilepticus", *PloS one*, vol. 8, no. 1, pp. e53464.

- Ritchie, W., Flamant, S. & Rasko, J.E. 2009, "Predicting microRNA targets and functions: traps for the unwary", *Nature methods*, vol. 6, no. 6, pp. 397-398.
- Robertson, C., Booth, S.A., Beniac, D.R., Coulthart, M.B., Booth, T.F. & McNicol, A. 2006, "Cellular prion protein is released on exosomes from activated platelets", *Blood*, vol. 107, no. 10, pp. 3907-3911.
- Robinson, S.W., Nugent, M.L., Dinsdale, D. & Steinert, J.R. 2014, "Prion protein facilitates synaptic vesicle release by enhancing release probability", *Human molecular genetics*, vol. 23, no. 17, pp. 4581-4596.
- Robison, A.J., Bartlett, R.K., Bass, M.A. & Colbran, R.J. 2005, "Differential modulation of Ca²⁺/calmodulin-dependent protein kinase II activity by regulated interactions with N-methyl-D-aspartate receptor NR2B subunits and alpha-actinin", *The Journal of biological chemistry*, vol. 280, no. 47, pp. 39316-39323.
- Rodriguez-Lebron, E., Liu, G., Keiser, M., Behlke, M.A. & Davidson, B.L. 2013, "Altered Purkinje cell miRNA expression and SCA1 pathogenesis", *Neurobiology of disease*, vol. 54, pp. 456-463.
- Rosas, H.D., Liu, A.K., Hersch, S., Glessner, M., Ferrante, R.J., Salat, D.H., van der Kouwe, A., Jenkins, B.G., Dale, A.M. & Fischl, B. 2002, "Regional and progressive thinning of the cortical ribbon in Huntington's disease", *Neurology*, vol. 58, no. 5, pp. 695-701.
- Rudy, C.C., Hunsberger, H.C., Weitzner, D.S. & Reed, M.N. 2015, "The role of the tripartite glutamatergic synapse in the pathophysiology of Alzheimer's disease", *Aging and disease*, vol. 6, no. 2, pp. 131-148.
- Saba, R., Goodman, C.D., Huzarewich, R.L., Robertson, C. & Booth, S.A. 2008, "A miRNA signature of prion induced neurodegeneration", *PLoS ONE*, vol. 3, no. 11, pp. e3652.
- Saba, R., Medina, S.J. & Booth, S.A. 2014, "A functional SNP catalog of overlapping miRNA-binding sites in genes implicated in prion disease and other neurodegenerative disorders", *Human mutation*, vol. 35, no. 10, pp. 1233-1248.
- Saba, R., Storchel, P.H., Aksoy-Aksel, A., Kepura, F., Lippi, G., Plant, T.D. & Schrott, G.M. 2012, "Dopamine-regulated microRNA MiR-181a controls GluA2 surface expression in hippocampal neurons", *Molecular and cellular biology*, vol. 32, no. 3, pp. 619-632.
- Sanchez-Juan, P., Bishop, M.T., Kovacs, G.G., Calero, M., Aulchenko, Y.S., Ladogana, A., Boyd, A., Lewis, V., Ponto, C., Calero, O., Poleggi, A., Carracedo, A., van der Lee, S.J., Strobel, T., Rivadeneira, F., Hofman, A., Haik, S., Combarros, O., Berciano, J., Uitterlinden, A.G., Collins, S.J., Budka, H., Brandel, J.P., Laplanche, J.L., Pocchiari, M., Zerr, I., Knight, R.S., Will, R.G. & van Duijn, C.M. 2015, "A genome wide association study links glutamate receptor pathway to sporadic Creutzfeldt-Jakob disease risk", *PLoS one*, vol. 10, no. 4, pp. e0123654.
- Santos, M.C., Tegge, A.N., Correa, B.R., Mahesula, S., Kohnke, L.Q., Qiao, M., Ferreira, M.A., Kokovay, E. & Penalva, L.O. 2016, "miR-124, -128, and -137 Orchestrate

- Neural Differentiation by Acting on Overlapping Gene Sets Containing a Highly Connected Transcription Factor Network", *Stem cells (Dayton, Ohio)*, vol. 34, no. 1, pp. 220-232.
- Santos, T.G., Silva, I.R., Costa-Silva, B., Lepique, A.P., Martins, V.R. & Lopes, M.H. 2011, "Enhanced neural progenitor/stem cells self-renewal via the interaction of stress-inducible protein 1 with the prion protein", *Stem cells (Dayton, Ohio)*, vol. 29, no. 7, pp. 1126-1136.
- Santuccione, A., Sytnyk, V., Leshchyns'ka, I. & Schachner, M. 2005, "Prion protein recruits its neuronal receptor NCAM to lipid rafts to activate p59fyn and to enhance neurite outgrowth", *The Journal of cell biology*, vol. 169, no. 2, pp. 341-354.
- Schmued, L.C., Stowers, C.C., Scallet, A.C. & Xu, L. 2005, "Fluoro-Jade C results in ultra high resolution and contrast labeling of degenerating neurons", *Brain research*, vol. 1035, no. 1, pp. 24-31.
- Schratt, G.M., Tuebing, F., Nigh, E.A., Kane, C.G., Sabatini, M.E., Kiebler, M. & Greenberg, M.E. 2006, "A brain-specific microRNA regulates dendritic spine development", *Nature*, vol. 439, no. 7074, pp. 283-289.
- Searle, B.C. 2010, "Scaffold: a bioinformatic tool for validating MS/MS-based proteomic studies", *Proteomics*, vol. 10, no. 6, pp. 1265-1269.
- Seibenhener, M.L. & Wooten, M.W. 2012, "Isolation and culture of hippocampal neurons from prenatal mice", *Journal of visualized experiments : JoVE*, vol. (65). pii: 3634. doi, no. 65, pp. 10.3791/3634.
- Selbach, M., Schwanhauser, B., Thierfelder, N., Fang, Z., Khanin, R. & Rajewsky, N. 2008, "Widespread changes in protein synthesis induced by microRNAs", *Nature*, vol. 455, no. 7209, pp. 58-63.
- Shi, Y., Zhao, X., Yu, L., Tao, R., Tang, J., La, Y., Duan, Y., Gao, B., Gu, N., Xu, Y., Feng, G., Zhu, S., Liu, H., Salter, H. & He, L. 2004, "Genetic structure adds power to detect schizophrenia susceptibility at SLIT3 in the Chinese Han population", *Genome research*, vol. 14, no. 7, pp. 1345-1349.
- Shott, R.H., Majer, A., Frost, K.L., Booth, S.A. & Schang, L.M. 2014, "Activation of pro-survival CaMK4beta/CREB and pro-death MST1 signaling at early and late times during a mouse model of prion disease", *Virology journal*, vol. 11, pp. 160-422X-11-160.
- Shyng, S.L., Heuser, J.E. & Harris, D.A. 1994, "A glycolipid-anchored prion protein is endocytosed via clathrin-coated pits", *The Journal of cell biology*, vol. 125, no. 6, pp. 1239-1250.
- Siegert, S., Seo, J., Kwon, E.J., Rudenko, A., Cho, S., Wang, W., Flood, Z., Martorell, A.J., Ericsson, M., Mungenast, A.E. & Tsai, L.H. 2015, "The schizophrenia risk gene product miR-137 alters presynaptic plasticity", *Nature neuroscience*, vol. 18, no. 7, pp. 1008-1016.

- Smirnova, L., Grafe, A., Seiler, A., Schumacher, S., Nitsch, R. & Wulczyn, F.G. 2005, "Regulation of miRNA expression during neural cell specification", *The European journal of neuroscience*, vol. 21, no. 6, pp. 1469-1477.
- Smith, C.M., Finger, J.H., Hayamizu, T.F., McCright, I.J., Xu, J., Berghout, J., Campbell, J., Corbani, L.E., Forthofer, K.L., Frost, P.J., Miers, D., Shaw, D.R., Stone, K.R., Eppig, J.T., Kadin, J.A., Richardson, J.E. & Ringwald, M. 2014, "The mouse Gene Expression Database (GXD): 2014 update", *Nucleic acids research*, vol. 42, no. Database issue, pp. D818-24.
- Smith, S.M., Kimyon, R.S. & Watters, J.J. 2014, "Cell-type-specific Jumonji histone demethylase gene expression in the healthy rat CNS: detection by a novel flow cytometry method", *ASN neuro*, vol. 6, no. 3, pp. 193-207.
- Soto, C. 2004, "Diagnosing prion diseases: needs, challenges and hopes", *Nature reviews.Microbiology*, vol. 2, no. 10, pp. 809-819.
- Spielhauer, C. & Schatzl, H.M. 2001, "PrPC directly interacts with proteins involved in signaling pathways", *The Journal of biological chemistry*, vol. 276, no. 48, pp. 44604-44612.
- Stahl, N., Baldwin, M.A., Teplow, D.B., Hood, L., Gibson, B.W., Burlingame, A.L. & Prusiner, S.B. 1993, "Structural studies of the scrapie prion protein using mass spectrometry and amino acid sequencing", *Biochemistry*, vol. 32, no. 8, pp. 1991-2002.
- Standaert, D.G., Landwehrmeyer, G.B., Kerner, J.A., Penney, J.B., Jr & Young, A.B. 1996, "Expression of NMDAR2D glutamate receptor subunit mRNA in neurochemically identified interneurons in the rat neostriatum, neocortex and hippocampus", *Brain research.Molecular brain research*, vol. 42, no. 1, pp. 89-102.
- Steele, A.D., Emsley, J.G., Ozdinler, P.H., Lindquist, S. & Macklis, J.D. 2006, "Prion protein (PrPc) positively regulates neural precursor proliferation during developmental and adult mammalian neurogenesis", *Proceedings of the National Academy of Sciences of the United States of America*, vol. 103, no. 9, pp. 3416-3421.
- Steele, A.D., Lindquist, S. & Aguzzi, A. 2007, "The prion protein knockout mouse: a phenotype under challenge", *Prion*, vol. 1, no. 2, pp. 83-93.
- Stegmuller, J., Huynh, M.A., Yuan, Z., Konishi, Y. & Bonni, A. 2008, "TGFbeta-Smad2 signaling regulates the Cdh1-APC/SnoN pathway of axonal morphogenesis", *The Journal of neuroscience : the official journal of the Society for Neuroscience*, vol. 28, no. 8, pp. 1961-1969.
- Steinhoff, B.J., Zerr, I., Glatting, M., Schulz-Schaeffer, W., Poser, S. & Kretzschmar, H.A. 2004, "Diagnostic value of periodic complexes in Creutzfeldt-Jakob disease", *Annals of Neurology*, vol. 56, no. 5, pp. 702-708.
- Steinkraus, B.R., Toegel, M. & Fulga, T.A. 2016, "Tiny giants of gene regulation: experimental strategies for microRNA functional studies", *Wiley interdisciplinary reviews.Developmental biology*, vol. 5, no. 3, pp. 311-362.

- Stevens, D.J., Walter, E.D., Rodriguez, A., Draper, D., Davies, P., Brown, D.R. & Millhauser, G.L. 2009, "Early onset prion disease from octarepeat expansion correlates with copper binding properties", *PLoS pathogens*, vol. 5, no. 4, pp. e1000390.
- Steward, O. & Levy, W.B. 1982, "Preferential localization of polyribosomes under the base of dendritic spines in granule cells of the dentate gyrus", *The Journal of neuroscience : the official journal of the Society for Neuroscience*, vol. 2, no. 3, pp. 284-291.
- Stohr, J., Weinmann, N., Wille, H., Kaimann, T., Nagel-Steger, L., Birkmann, E., Panza, G., Prusiner, S.B., Eigen, M. & Riesner, D. 2008, "Mechanisms of prion protein assembly into amyloid", *Proceedings of the National Academy of Sciences of the United States of America*, vol. 105, no. 7, pp. 2409-2414.
- Suyama, S., Kodaira-Hirano, M., Otgon-Uul, Z., Ueta, Y., Nakata, M. & Yada, T. 2016, "Fasted/fed states regulate postsynaptic hub protein DYNLL2 and glutamatergic transmission in oxytocin neurons in the hypothalamic paraventricular nucleus", *Neuropeptides*, vol. 56, pp. 115-123.
- Tackenberg, C., Grinschgl, S., Trutzel, A., Santuccione, A.C., Frey, M.C., Konietzko, U., Grimm, J., Brandt, R. & Nitsch, R.M. 2013, "NMDA receptor subunit composition determines beta-amyloid-induced neurodegeneration and synaptic loss", *Cell death & disease*, vol. 4, pp. e608.
- Taganov, K.D., Boldin, M.P., Chang, K.J. & Baltimore, D. 2006, "NF-kappaB-dependent induction of microRNA miR-146, an inhibitor targeted to signaling proteins of innate immune responses", *Proceedings of the National Academy of Sciences of the United States of America*, vol. 103, no. 33, pp. 12481-12486.
- Talantova, M., Sanz-Blasco, S., Zhang, X., Xia, P., Akhtar, M.W., Okamoto, S., Dziejczapolski, G., Nakamura, T., Cao, G., Pratt, A.E., Kang, Y.J., Tu, S., Molokanova, E., McKercher, S.R., Hires, S.A., Sason, H., Stouffer, D.G., Buczynski, M.W., Solomon, J.P., Michael, S., Powers, E.T., Kelly, J.W., Roberts, A., Tong, G., Fang-Newmeyer, T., Parker, J., Holland, E.A., Zhang, D., Nakanishi, N., Chen, H.S., Wolosker, H., Wang, Y., Parsons, L.H., Ambasudhan, R., Masliah, E., Heinemann, S.F., Pina-Crespo, J.C. & Lipton, S.A. 2013, "Abeta induces astrocytic glutamate release, extrasynaptic NMDA receptor activation, and synaptic loss", *Proceedings of the National Academy of Sciences of the United States of America*, vol. 110, no. 27, pp. E2518-27.
- Tan, C.L., Plotkin, J.L., Veno, M.T., von Schimmelmann, M., Feinberg, P., Mann, S., Handler, A., Kjemis, J., Surmeier, D.J., O'Carroll, D., Greengard, P. & Schaefer, A. 2013a, "MicroRNA-128 governs neuronal excitability and motor behavior in mice", *Science (New York, N.Y.)*, vol. 342, no. 6163, pp. 1254-1258.
- Tan, C.L., Plotkin, J.L., Veno, M.T., von Schimmelmann, M., Feinberg, P., Mann, S., Handler, A., Kjemis, J., Surmeier, D.J., O'Carroll, D., Greengard, P. & Schaefer, A. 2013b, "MicroRNA-128 governs neuronal excitability and motor behavior in mice", *Science (New York, N.Y.)*, vol. 342, no. 6163, pp. 1254-1258.

- Tao-Cheng, J.H., Toy, D., Winters, C.A., Reese, T.S. & Dosemeci, A. 2016, "Zinc Stabilizes Shank3 at the Postsynaptic Density of Hippocampal Synapses", *PloS one*, vol. 11, no. 5, pp. e0153979.
- Tay, Y., Zhang, J., Thomson, A.M., Lim, B. & Rigoutsos, I. 2008, "MicroRNAs to Nanog, Oct4 and Sox2 coding regions modulate embryonic stem cell differentiation", *Nature*, vol. 455, no. 7216, pp. 1124-1128.
- Taylor, D.R. & Hooper, N.M. 2006, "The prion protein and lipid rafts", *Molecular membrane biology*, vol. 23, no. 1, pp. 89-99.
- Telling, G.C., Parchi, P., DeArmond, S.J., Cortelli, P., Montagna, P., Gabizon, R., Mastrianni, J., Lugaresi, E., Gambetti, P. & Prusiner, S.B. 1996, "Evidence for the conformation of the pathologic isoform of the prion protein enciphering and propagating prion diversity", *Science (New York, N.Y.)*, vol. 274, no. 5295, pp. 2079-2082.
- Thackray, A.M., Hopkins, L., Klein, M.A. & Bujdoso, R. 2007, "Mouse-adapted ovine scrapie prion strains are characterized by different conformers of PrP^{Sc}", *Journal of virology*, vol. 81, no. 22, pp. 12119-12127.
- Thackray, A.M., Klein, M.A. & Bujdoso, R. 2003, "Subclinical prion disease induced by oral inoculation", *Journal of virology*, vol. 77, no. 14, pp. 7991-7998.
- Thakur, R., Vincent, Y.M. & Chaturvedi, S. 2002, "Human prion diseases", *The National medical journal of India*, vol. 15, no. 6, pp. 339-345.
- The Huntington's Disease Collaborative Research Group 1993, "A novel gene containing a trinucleotide repeat that is expanded and unstable on Huntington's disease chromosomes.", *Cell*, vol. 72, no. 6, pp. 971-983.
- Thompson, A., Schafer, J., Kuhn, K., Kienle, S., Schwarz, J., Schmidt, G., Neumann, T., Johnstone, R., Mohammed, A.K. & Hamon, C. 2003, "Tandem mass tags: a novel quantification strategy for comparative analysis of complex protein mixtures by MS/MS", *Analytical Chemistry*, vol. 75, no. 8, pp. 1895-1904.
- Tibbs, G.R., Barrie, A.P., Van Mieghem, F.J., McMahon, H.T. & Nicholls, D.G. 1989, "Repetitive action potentials in isolated nerve terminals in the presence of 4-aminopyridine: effects on cytosolic free Ca²⁺ and glutamate release", *Journal of neurochemistry*, vol. 53, no. 6, pp. 1693-1699.
- Tobler, I., Deboer, T. & Fischer, M. 1997, "Sleep and sleep regulation in normal and prion protein-deficient mice", *The Journal of neuroscience : the official journal of the Society for Neuroscience*, vol. 17, no. 5, pp. 1869-1879.
- Tobler, I., Gaus, S.E., Deboer, T., Achermann, P., Fischer, M., Rulicke, T., Moser, M., Oesch, B., McBride, P.A. & Manson, J.C. 1996, "Altered circadian activity rhythms and sleep in mice devoid of prion protein", *Nature*, vol. 380, no. 6575, pp. 639-642.
- Tonges, L., Lingor, P., Egle, R., Dietz, G.P., Fahr, A. & Bahr, M. 2006, "Stearylated octaarginine and artificial virus-like particles for transfection of siRNA into primary rat neurons", *RNA (New York, N.Y.)*, vol. 12, no. 7, pp. 1431-1438.

- Tortosa, E., Montenegro-Venegas, C., Benoist, M., Hartel, S., Gonzalez-Billault, C., Esteban, J.A. & Avila, J. 2011, "Microtubule-associated protein 1B (MAP1B) is required for dendritic spine development and synaptic maturation", *The Journal of biological chemistry*, vol. 286, no. 47, pp. 40638-40648.
- Traynelis, S.F., Wollmuth, L.P., McBain, C.J., Menniti, F.S., Vance, K.M., Ogden, K.K., Hansen, K.B., Yuan, H., Myers, S.J. & Dingledine, R. 2010, "Glutamate receptor ion channels: structure, regulation, and function", *Pharmacological reviews*, vol. 62, no. 3, pp. 405-496.
- Tsuboi, Y., Doh-Ura, K. & Yamada, T. 2009, "Continuous intraventricular infusion of pentosan polysulfate: clinical trial against prion diseases", *Neuropathology : official journal of the Japanese Society of Neuropathology*, vol. 29, no. 5, pp. 632-636.
- Um, J.W., Kaufman, A.C., Kostylev, M., Heiss, J.K., Stagi, M., Takahashi, H., Kerrisk, M.E., Vortmeyer, A., Wisniewski, T., Koleske, A.J., Gunther, E.C., Nygaard, H.B. & Strittmatter, S.M. 2013, "Metabotropic glutamate receptor 5 is a coreceptor for Alzheimer abeta oligomer bound to cellular prion protein", *Neuron*, vol. 79, no. 5, pp. 887-902.
- Urban, E.T., 3rd, Bury, S.D., Barbay, H.S., Guggenmos, D.J., Dong, Y. & Nudo, R.J. 2012, "Gene expression changes of interconnected spared cortical neurons 7 days after ischemic infarct of the primary motor cortex in the rat", *Molecular and cellular biochemistry*, vol. 369, no. 1-2, pp. 267-286.
- van Eitzen, U., Egensperger, R., Kosel, S., Grasbon-Frodl, E.M., Imai, Y., Bise, K., Kohsaka, S., Mehraein, P. & Graeber, M.B. 1998, "Microglia and the development of spongiform change in Creutzfeldt-Jakob disease", *Journal of neuropathology and experimental neurology*, vol. 57, no. 3, pp. 246-256.
- van Spronsen, M., van Battum, E.Y., Kuijpers, M., Vangoor, V.R., Rietman, M.L., Pothof, J., Gumy, L.F., van Ijcken, W.F., Akhmanova, A., Pasterkamp, R.J. & Hoogenraad, C.C. 2013, "Developmental and activity-dependent miRNA expression profiling in primary hippocampal neuron cultures", *PLoS one*, vol. 8, no. 10, pp. e74907.
- Vazquez-Fernandez, E., Vos, M.R., Afanasyev, P., Cebey, L., Sevillano, A.M., Vidal, E., Rosa, I., Renault, L., Ramos, A., Peters, P.J., Fernandez, J.J., van Heel, M., Young, H.S., Requena, J.R. & Wille, H. 2016, "The Structural Architecture of an Infectious Mammalian Prion Using Electron Cryomicroscopy", *PLoS pathogens*, vol. 12, no. 9, pp. e1005835.
- Vella, L.J., Sharples, R.A., Lawson, V.A., Masters, C.L., Cappai, R. & Hill, A.F. 2007, "Packaging of prions into exosomes is associated with a novel pathway of PrP processing", *The Journal of pathology*, vol. 211, no. 5, pp. 582-590.
- Verity, M.A. 1972, "Cation modulation of synaptosomal respiration", *Journal of neurochemistry*, vol. 19, no. 5, pp. 1305-1317.
- Vo, N., Klein, M.E., Varlamova, O., Keller, D.M., Yamamoto, T., Goodman, R.H. & Impey, S. 2005, "A cAMP-response element binding protein-induced microRNA

- regulates neuronal morphogenesis", *Proceedings of the National Academy of Sciences of the United States of America*, vol. 102, no. 45, pp. 16426-16431.
- Walter, E.D., Stevens, D.J., Visconte, M.P. & Millhauser, G.L. 2007, "The prion protein is a combined zinc and copper binding protein: Zn²⁺ alters the distribution of Cu²⁺ coordination modes", *Journal of the American Chemical Society*, vol. 129, no. 50, pp. 15440-15441.
- Wang, K., Zhang, D.L., Long, B., An, T., Zhang, J., Zhou, L.Y., Liu, C.Y. & Li, P.F. 2015, "NFAT4-dependent miR-324-5p regulates mitochondrial morphology and cardiomyocyte cell death by targeting Mtf1", *Cell death & disease*, vol. 6, pp. e2007.
- Wang, W., Crandall, J.E., Litwack, E.D., Gronostajski, R.M. & Kilpatrick, D.L. 2010, "Targets of the nuclear factor I regulon involved in early and late development of postmitotic cerebellar granule neurons", *Journal of neuroscience research*, vol. 88, no. 2, pp. 258-265.
- Wang, W.X., Visavadiya, N.P., Pandya, J.D., Nelson, P.T., Sullivan, P.G. & Springer, J.E. 2015, "Mitochondria-associated microRNAs in rat hippocampus following traumatic brain injury", *Experimental neurology*, vol. 265, pp. 84-93.
- Wang, X., Zhang, C., Szabo, G. & Sun, Q.Q. 2013, "Distribution of CaMKIIalpha expression in the brain in vivo, studied by CaMKIIalpha-GFP mice", *Brain research*, vol. 1518, pp. 9-25.
- Wang, Y., Su, B. & Xia, Z. 2006, "Brain-derived neurotrophic factor activates ERK5 in cortical neurons via a Rap1-MEKK2 signaling cascade", *The Journal of biological chemistry*, vol. 281, no. 47, pp. 35965-35974.
- Wang, Y.J., Chen, G.H., Hu, X.Y., Lu, Y.P., Zhou, J.N. & Liu, R.Y. 2005, "The expression of calcium/calmodulin-dependent protein kinase II-alpha in the hippocampus of patients with Alzheimer's disease and its links with AD-related pathology", *Brain research*, vol. 1031, no. 1, pp. 101-108.
- Watt, N.T., Taylor, D.R., Kerrigan, T.L., Griffiths, H.H., Rushworth, J.V., Whitehouse, I.J. & Hooper, N.M. 2012, "Prion protein facilitates uptake of zinc into neuronal cells", *Nature communications*, vol. 3, pp. 1134.
- Wiersma, V.I., van Hecke, W., Scheper, W., van Osch, M.A., Hermsen, W.J., Rozemuller, A.J. & Hoozemans, J.J. 2016, "Activation of the unfolded protein response and granulovacuolar degeneration are not common features of human prion pathology", *Acta neuropathologica communications*, vol. 4, no. 1, pp. 113.
- Wille, H., Bian, W., McDonald, M., Kendall, A., Colby, D.W., Bloch, L., Ollesch, J., Borovinskiy, A.L., Cohen, F.E., Prusiner, S.B. & Stubbs, G. 2009, "Natural and synthetic prion structure from X-ray fiber diffraction", *Proceedings of the National Academy of Sciences of the United States of America*, vol. 106, no. 40, pp. 16990-16995.
- Williams, C., Mehrian Shai, R., Wu, Y., Hsu, Y.H., Sitzer, T., Spann, B., McCleary, C., Mo, Y. & Miller, C.A. 2009, "Transcriptome analysis of synaptoneuroosomes identifies

- neuroplasticity genes overexpressed in incipient Alzheimer's disease", *PloS one*, vol. 4, no. 3, pp. e4936.
- Wong, E.H., Kemp, J.A., Priestley, T., Knight, A.R., Woodruff, G.N. & Iversen, L.L. 1986, "The anticonvulsant MK-801 is a potent N-methyl-D-aspartate antagonist", *Proceedings of the National Academy of Sciences of the United States of America*, vol. 83, no. 18, pp. 7104-7108.
- Wong, R.K. & Prince, D.A. 1979, "Dendritic mechanisms underlying penicillin-induced epileptiform activity", *Science (New York, N.Y.)*, vol. 204, no. 4398, pp. 1228-1231.
- Xhemalce, B., Robson, S.C. & Kouzarides, T. 2012, "Human RNA methyltransferase BCDIN3D regulates microRNA processing", *Cell*, vol. 151, no. 2, pp. 278-288.
- Xia, P., Chen, H.S., Zhang, D. & Lipton, S.A. 2010, "Memantine preferentially blocks extrasynaptic over synaptic NMDA receptor currents in hippocampal autapses", *The Journal of neuroscience : the official journal of the Society for Neuroscience*, vol. 30, no. 33, pp. 11246-11250.
- Yang, B., Wang, S., Zeng, J., Zhang, Y., Ruan, X., Han, W., Yin, B., Yuan, J., Qiang, B., Ying, W., Qian, X. & Peng, X. 2015, "Proteomic screening and identification of microRNA-128 targets in glioma cells", *Proteomics*, vol. 15, no. 15, pp. 2602-2617.
- You, H., Tsutsui, S., Hameed, S., Kannanayakal, T.J., Chen, L., Xia, P., Engbers, J.D., Lipton, S.A., Stys, P.K. & Zamponi, G.W. 2012, "Abeta neurotoxicity depends on interactions between copper ions, prion protein, and N-methyl-D-aspartate receptors", *Proceedings of the National Academy of Sciences of the United States of America*, vol. 109, no. 5, pp. 1737-1742.
- Zahn, R., Liu, A., Luhrs, T., Riek, R., von Schroetter, C., Lopez Garcia, F., Billeter, M., Calzolari, L., Wider, G. & Wuthrich, K. 2000, "NMR solution structure of the human prion protein", *Proceedings of the National Academy of Sciences of the United States of America*, vol. 97, no. 1, pp. 145-150.
- Zare, M., Soleimani, M., Akbarzadeh, A., Bakhshandeh, B., Aghaee-Bakhtiari, S.H. & Zarghami, N. 2015, "A Novel Protocol to Differentiate Induced Pluripotent Stem Cells by Neuronal microRNAs to Provide a Suitable Cellular Model", *Chemical biology & drug design*, vol. 86, no. 2, pp. 232-238.
- Zerr, I., Bodemer, M., Gefeller, O., Otto, M., Poser, S., Wiltfang, J., Windl, O., Kretzschmar, H.A. & Weber, T. 1998, "Detection of 14-3-3 protein in the cerebrospinal fluid supports the diagnosis of Creutzfeldt-Jakob disease", *Annals of Neurology*, vol. 43, no. 1, pp. 32-40.
- Zhang, B., Wang, A., Xia, C., Lin, Q. & Chen, C. 2015, "A single nucleotide polymorphism in primary-microRNA-146a reduces the expression of mature microRNA-146a in patients with Alzheimer's disease and is associated with the pathogenesis of Alzheimer's disease", *Molecular medicine reports*, vol. 12, no. 3, pp. 4037-4042.
- Zhang, H.Y., Zheng, S.J., Zhao, J.H., Zhao, W., Zheng, L.F., Zhao, D., Li, J.M., Zhang, X.F., Chen, Z.B. & Yi, X.N. 2011, "MicroRNAs 144, 145, and 214 are down-regulated

- in primary neurons responding to sciatic nerve transection", *Brain research*, vol. 1383, pp. 62-70.
- Zhang, S.J., Steijaert, M.N., Lau, D., Schutz, G., Delucinge-Vivier, C., Descombes, P. & Bading, H. 2007, "Decoding NMDA receptor signaling: identification of genomic programs specifying neuronal survival and death", *Neuron*, vol. 53, no. 4, pp. 549-562.
- Zhang, S.J., Zou, M., Lu, L., Lau, D., Ditzel, D.A., Delucinge-Vivier, C., Aso, Y., Descombes, P. & Bading, H. 2009, "Nuclear calcium signaling controls expression of a large gene pool: identification of a gene program for acquired neuroprotection induced by synaptic activity", *PLoS genetics*, vol. 5, no. 8, pp. e1000604.
- Zhang, W., Kim, P.J., Chen, Z., Lokman, H., Qiu, L., Zhang, K., Rozen, S.G., Tan, E.K., Je, H.S. & Zeng, L. 2016, "MiRNA-128 regulates the proliferation and neurogenesis of neural precursors by targeting PCM1 in the developing cortex", *eLife*, vol. 5, pp. 10.7554/eLife.11324.
- Zhang, Y. & Barres, B.A. 2013, "A smarter mouse with human astrocytes", *BioEssays : news and reviews in molecular, cellular and developmental biology*, vol. 35, no. 10, pp. 876-880.